2020

Spectroscopic Investigation Into The Heme Binding And The Heme Degradation By Mycobacterium Tuberculosis Mhud

Biswash Thakuri
University of Vermont

SPECTROSCOPIC INVESTIGATION INTO THE HEME BINDING AND THE HEME DEGRADATION BY *MYCOBACTERIUM TUBERCULOSIS* MHUD

A Dissertation Presented

by

Biswash Thakuri

to

The Faculty of Graduate College

Of

The University of Vermont

In Partial Fulfilment of the Requirements
for the Degree of Doctor of Philosophy
Specializing in Chemistry

October, 2020

Defense Date: August 13th, 2020
Dissertation Examination Committee:

Matthew D. Liptak, Ph.D., Advisor
Christopher D. Francklyn, Ph.D., Chairperson
Rory Waterman, Ph.D.
Giuseppe A. Petrucci, Ph.D.
Cynthia J. Forehand, Ph.D., Dean of the Graduate College

ABSTRACT

MhuD is a heme degrading enzyme found across mycobacteria. In the heme uptake machinery of *Mycobacterium Tuberculosis*, MhuD is a heme oxygenase (HO) involved in catalyzing the degradation of heme. Canonical HOs, such as human HO, have been shown to degrade heme to non-heme iron, carbon monoxide (CO) and biliverdin. However, MhuD has been demonstrated to degrade heme to non-heme iron and mycobilin without the release of CO. Formation of a novel chromophore by MhuD revealed that it follows a unique heme degradation mechanism compared to that of canonical HOs. Binding of heme to MhuD is the first step in the degradation process and previous studies have reported the binding affinity of heme to MhuD to be micromolar. This would mean that MhuD may be an inefficient HO *in vivo*, especially at the recently measured cytosolic labile heme concentration of 20-40 nM. Therefore, heme binding to MhuD was re-investigated using fluorescence spectroscopy. Based on a recently developed fluorescence-based assay, the K_{d1} for heme-bound MhuD (MhuD—heme) was determined to be 7.6 ± 0.8 nM. In addition, a UV/Vis absorption-based assay was developed to measure the K_{d2} for heme dissociation from diheme-bound MhuD (MhuD—diheme), which was determined to be 3.3 ± 1.1 μM. These data strongly suggest that MhuD is a competent heme oxygenase *in vivo.*

Next, heme degradation by MhuD was investigated, which is shown to proceed via formation of a *meso*-hydroxyheme intermediate. Time-resolved and tandem mass spectrometry (MS) identified formation of both mycobilin (major product) and biliverdin (minor product) by wild type (WT) MhuD. This interesting discovery warranted further investigation. Heme bound to the MhuD active site undergoes a dynamic distortion between two substrate conformations. Thus, we hypothesized that the conformation of heme may be responsible for the product identity, and that both heme conformations may be required for an efficient enzymatic activity of MhuD. To test these hypothesis, different variants of MhuD were investigated. F23W MhuD has been shown to stabilize more ruffled heme and W66F MhuD has been shown to stabilize less ruffled heme than WT. MS studies of these variants identified mycobilin and biliverdin as the major products for F23W and W66F MhuD, respectively. Thus, suggesting that the heme confirmation plays a role in product identity. Also, the biliverdin formation by WT and F23W MhuD lacked regioselectivity, which suggests that its formation proceeds via a non-enzymatic pathway. In addition, UV/Vis study identified *meso*-hydroxyheme intermediate for the heme degradation by F23W MhuD. Kinetic analysis of the reaction catalyzed by F23W MhuD revealed that the *meso*-hydroxyheme dioxygenation rate is considerably slower for this variant. In summary, these data strongly suggest that heme degradation product of MhuD depends upon the degree of heme ruffling induced by the active site and that dynamic heme is essential for MhuD.

DEDICATION

I dedicate this dissertation to my loving wife, parents, brother, family and friends, for providing me constant support, love and encouragement.

ACKNOWLEDGEMENTS

I would like to express my sincere gratitude to my advisor Prof. Matthew D. Liptak for his constant support, patience, and encouragement throughout my Ph.D. studies. I would like to thank him for being very helpful, approachable and always willing to discuss whenever I needed his guidance. His technical and editorial advice has helped me a great deal and taught valuable lessons throughout my studies.

I would also like to thank the members of my committee, Dr. Rory Waterman and Dr. Giuseppe Petrucci, and my committee chair Dr. Christopher Francklyn, for their constant support during graduate school.

Finally, I am very grateful for being part of the Liptak Group, as both previous and current group members were always there to help and support. Thank you for the great memories.

TABLE OF CONTENTS

Page

LIST OF TABLES

Table Page

LIST OF FIGURES

Figure Page

LIST OF ABBREVIATIONS

Abs	UV/Vis absorption
Arg	Arginine
CD	Circular dichroism
CO	Carbon monoxide
EIC	Extracted ion chromatogram
ESI-MS	Electrospray ionization mass spectrometry
FPLC	Fast protein liquid chromatography
hDME	Heme dimethyl ester
HO	Heme oxygenase
HOMO	Highest occupied molecular orbital
IsdG	Iron surface determinant G
IsdG–heme	Heme-bound IsdG
k_1	Rate of heme monooxygenation
k_2	Rate of *meso*-hydroxyheme dioxygenation
KCN	Potassium cyanide
K_{d1}	Equilibrium dissociation constant of binding first heme
K_{d2}	Equilibrium dissociation constant of binding second heme
KPi	Potassium phosphate buffer
LUMO	Lowest unoccupied molecular orbital
MCD	Magnetic circular dichroism
meso-bPPIX-DME	*meso*-benzoyloxyprotoporphyrin IX dimethyl ester
MhuD	Mycobacterium heme utilization degrader

$MhuD_{CH}$	His-tag cleaved MhuD
MhuD–diheme	Diheme bound MhuD
MhuD–heme	Heme bound MhuD
MhuD–heme–CN	Cyanide-inhibited, heme bound MhuD
MmPL	Membrane protein large
Mtb	Mycobacterium tuberculosis
NaPi	Sodium phosphate buffer
NMR	Nuclear magnetic resonance
Phe	Phenylalanine
SDS-PAGE	Sodium dodecyl sulfate–polyacrylamide gel electrophoresis
Ser	Serine
Super-WEFT	Super water elimination Fourier transform
TB	Tuberculosis
TEV	Tobacco etch virus
Trp	Tryptophan
VTVH	Variable-temperature variable-field
WT	Wild type
μ-oxo-bis(hDME)	μ-oxo-bis(heme dimethyl ester).

CHAPTER 1: HEME DEGRADATION CATABOLIZED BY MYCOBACTERIUM TUBERCULOSIS MHUD

1.1 GLOBAL TUBERCULOSIS IMPACT

Tuberculosis (TB) is one of the deadliest and most infectious diseases, which is caused by an airborne pathogen called *Mycobacterium Tuberculosis*. In 2019, WHO estimated that around 10 million people were infected with TB that resulted in about 1.2 million deaths worldwide.[1] TB is the leading killer of people positive with HIV due to the compromised immune system, and has a higher death rate compared to HIV negative patients. In addition, drug-resistant TB is a serious public health threat. WHO reported that in 2018, there were about half a million cases of rifampicin-resistant tuberculosis, of which 78% were multidrug-resistant TB. Therefore, with the emergence of the drug-resistant TB, the need to develop novel anti-TB therapeutics is critical.

1.2 IRON ACQUITISION PATHWAY OF MYCOBACTERIUM TUBERCULOSIS

Iron is an essential nutrient that is utilized by *M. tuberculosis* (Mtb) for growth and survival. Iron in the human body is found in the heme or nonheme (will be called just "iron" hereafter) form.[2, 3] The majority of the iron is in the ferric form and complexed with transferrin and lactoferrin. The two siderophores; mycobactin and carboxymycobactin are proposed to be involved in the iron uptake pathway of Mtb[2, 4] by scavenging iron from transferrin and lactoferrin. Mycobactin is insoluble in water and thus is tethered to the Mtb outer membrane and the cell-wall environments. On the other hand, carboxymycobactins are relatively soluble, thus, are involved in scavenging iron from transferrin and lactoferrin. Also, they are imported into the Mtb cytoplasm by IrtA/IrtB protein, where the iron in ferric carboxymycobactin is reduced and then

released.[3, 5] However, the most abundant form of iron in the human body is heme, and it is mostly bound to hemoglobin. Thus, Mtb also contains a heme uptake pathway.[6]

1.3 HEME ACQUITISION PATHWAY OF MYCOBACTERIUM TUBERCULOSIS

Several proteins have been identified for the acquisition of heme into the Mtb cytosol. Rv0203 was identified and was proposed to be an extracellular heme binding

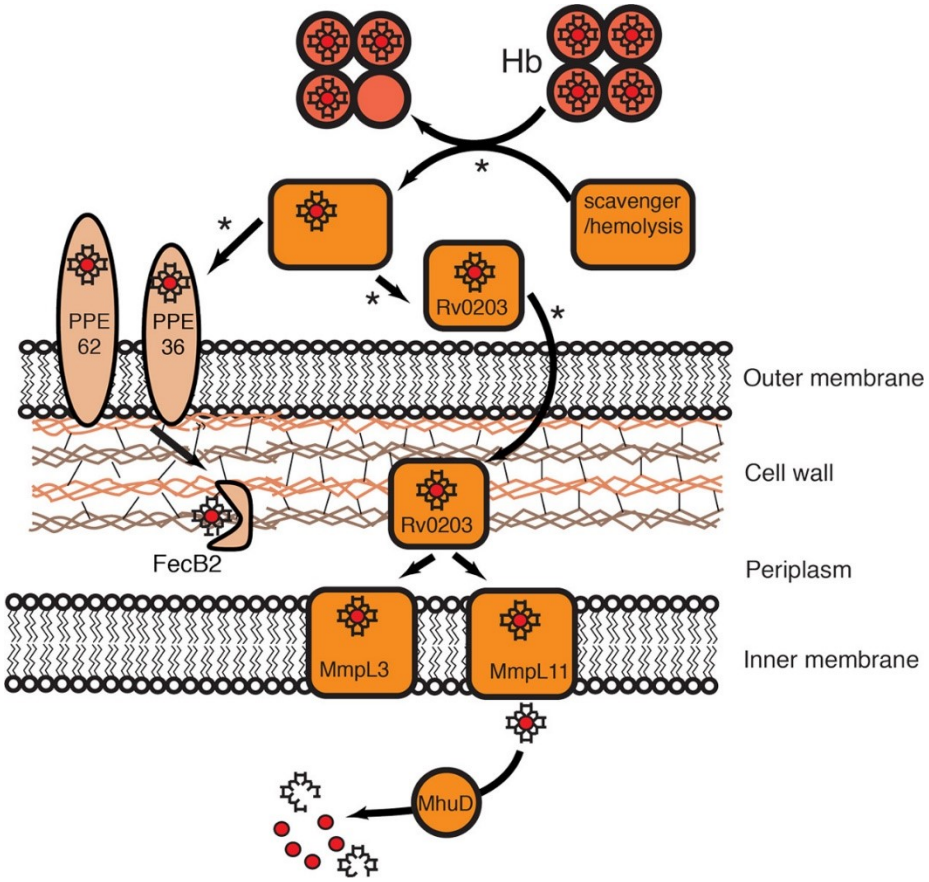

Figure 1. 1. Mtb heme uptake pathway. Two pathways involved in heme uptake are colored orange and light orange. In the first pathway, Rv0203, MmPL3 and MmPL11 and MhuD are identified to be involved in transport and degradation of heme. In the second pathway, so far PPE36, PPE62 and FecB2 are proposed to be involved in binding and shuttling heme through Mtb periplasm. Figure taken from reference 6.

protein.[7] The relatively weak ability of Rv0203 to bind heme[8] suggested that another unknown protein may be involved in stealing heme from hemoglobin through protein-protein interaction. Thus, it was proposed that Rv0203 binds free heme and shuttles it through the outer membrane to the inner membrane MmpL (mycobacteriual membrane protein large) proteins: MmpL3 and MmpL11 (Figure 1.1).[9] However, MmpL3 has been shown to act as a flippase for mycolics acids[10] and also to export tryhalose monomycolate[11], and MmpL11 has been shown to export lipids.[12] Therefore, these studies suggest MmpL3 and MmpL11 may have other roles beside transporting heme into the cytosol. Mycobacterium heme utilization Degrader (MhuD) is the final enzyme involved in the heme update pathway of Mtb, and it is involved in degradation of heme to release iron (Figure 1.1).

Anti-TB drugs can be developed targeting these enzymes along the heme updake pathway using a Trojan horse strategy. Previous study using Gallium Protoporphyrin IX demonstrated that it was toxic against *M. smegmatis.*[13] A study performed using Tin Protoporphyrin IX (SnPPIX) showed that it inhibited human HO-1 and significantly reduced bacterial load in Mtb infected mice when treated in combination with the anti-TB medicine. However, the SnPPIX failed to inhibit MhuD or the Mtb growth *in vitro*.[14] This may seem like a viable strategy, but the problem with this is that all human and bacterial heme dependent enzymes may incorporate the mismetallated heme, thereby inactivating these enzymes *in vivo*. For MhuD, a potential inhibitor does not exist yet, but the inhibitor needs to be selective enough to bind and disrupt the activity of MhuD and not of human HO. Also, MhuD is an important enzyme that is found across mycobacteria,

which means that development of a potential MhuD inhibitor may be utilized for other nontuberculous mycobacteria as well.

1.4 HEME DEGRADATION MECHANISM

For developing a potential selective inhibitor, detailed understanding regarding heme binding and its degradation by MhuD is essential. An original study has demonstrated that MhuD binds heme with a micromolar affinity.[20] This is in contrast with the binding affinity calculated for other heme oxygenases,[15-17] which are nanomolar. In addition, cytosolic labile heme pool was determined to be 20-40 nM.[18, 19] Based on these data, it calls into question whether MhuD would be an efficient HO *in vivo.* An interesting aspect of MhuD is that it can bind two hemes in its active site.[20] However, binding the second heme inactivates the enzyme itself.

Following heme binding, the next step in the heme acquisition process in MhuD-mediated heme degradation. The canonical HO enzymes present in the bacterial pathogens and in mammals have a very similar overall α-helical structural fold.[21-23] In the active site of canonical HO, the heme is sandwiched in between proximal and distal helices.[24] The heme in the active site of these enzymes are coordinated through a histidine residue on the proximal side and is observed to be in planar conformation. A conserved and ordered water network is also present on the distal side of the heme (Figure 1.2). In contrast, the non-canonical HOs, such as *Staphylococcus aureus* IsdG/IsdI and *Mycobacterium tuberculosis* MhuD share high sequence and structural homology with each other, however, they are quite distinct compared to canonical HOs. The non-canonical HOs are homodimers that have ferredoxin like α+β fold, which form a β-barrel in between the homodimer.[23, 25, 26] The heme in the active site makes

interactions with various hydrophobic amino acids. Similar to HO, the heme is coordinated through a histidine residue on the proximal side, however due to the presence of hydrophobic amino acid residues, it lacks water network on the distal side.[25, 26] The heme in the active site of these enzymes features out-of-plane distortions, and the most prominent distortion is ruffling. The degree of heme ruffling observed for IsdI, IsdG and MhuD is 1.9, 2.3 and 1.4 Å, respectively.[25, 27]

The non-canonical HOs, such as *Staphylococcus Aureus* IsdG and *Mycobacterium tuberculosis* MhuD, degrade heme to non-biliverdin products. IsdG-mediated heme degradation releases iron and formaldehyde towards formation of staphylobilin (Figure 1.2, bottom).[28-30] While MhuD-mediated heme degradation releases iron and mycobilin, where the *meso*-carbon is retained as an aldehyde group at the α-*meso* position (Figure 1.2, middle).[31, 32] This is distinct from canonical HOs, which degrade heme to biliverdin, by releasing iron and carbon monoxide (CO) (Figure 1.2, top).[33] This means that MhuD and IsdG carryout heme degradation through distinct mechanistic pathways from canonical HOs. Therefore, detailed understanding of the mechanistic steps towards formation of mycobilin by MhuD is essential.

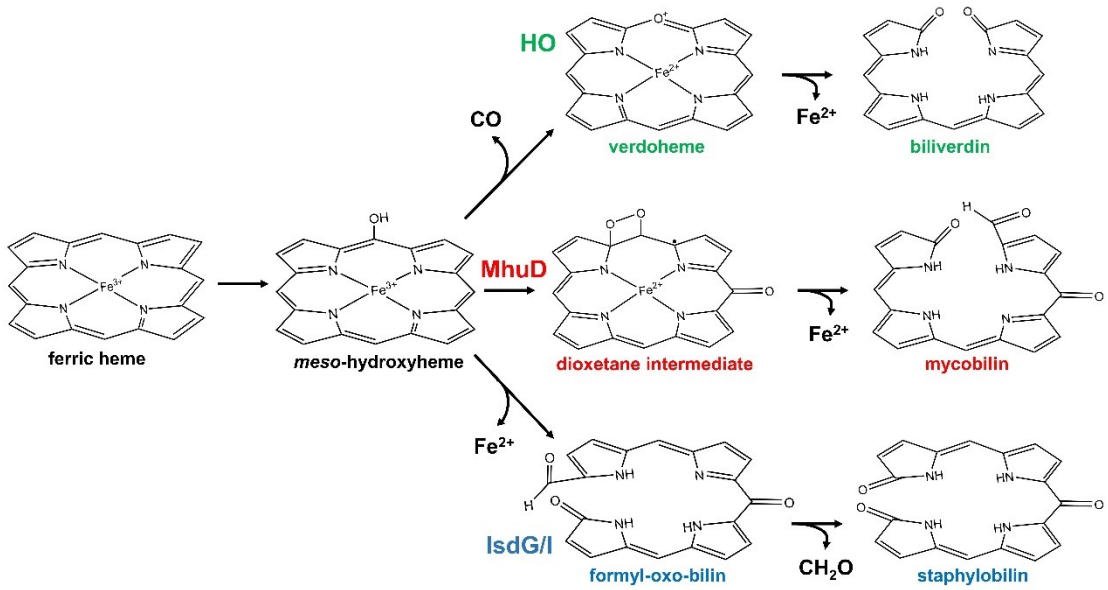

Figure 1. 2. HO degrades heme to for biliverdin by releasing iron and CO (*top*). MhuD degrades heme to generate mycobilin, with the release of iron (*middle*). Staphylobilin is generated, with the release of iron and formaldehyde during heme degradation by IsdG (*bottom*).

A previous biochemical study investigating heme degradation by MhuD has identified intermediates along the pathway.[32] Initial monooxygenation during heme degradation by MhuD occurs at the β/δ-*meso*-carbon to produce β/δ-*meso*–hydroxyheme intermediate (Figure 1.2, middle). The Electron Paramagnetic Resonance (EPR) study of the β/δ-*meso*–hydroxyheme bound to MhuD showed a radical species, probably due to its ferrous neutral radical form. On the other hand, the regiochemistry of the initial monooxygenation step is distinct in MhuD vs canonical HOs. The canonical HOs degrade heme to biliverdin through an α-*meso*–hydroxyheme intermediate (Figure 1.2, top).[34] A QM/MM study suggested that the ordered hydrogen bonding network present in canonical HOs is responsible for guiding the transient HO radical to attack the α-*meso*-carbon to produce an α-*meso*–hydroxyheme intermediate.[35] However, this water network

is absent in the non-canonical HOs,[27] such as MhuD.[25] Thus, the initial monooxygenation may proceed via a different mechanism. Next, the conversion of β/δ-*meso*–hydroxyheme proceeds via dioxygenation and cleavage at α-*meso*-carbon position and has been proposed to proceed via a dioxetane intermediate (Figure 1.2, middle).[32]

Previous studies have suggested that dynamic ruffling of heme, which is absent in canonical HOs, may be essential in conversion of heme to mycobilin by MhuD. As mentioned above, the heme substrate is relatively planar for canonical HO; however, the active site of non-canonical HOs induces an out-of-plane ruffling deformation of the heme substrate. A spectroscopic study of MhuD, suggested that the heme substrate in MhuD has a $^2B_{2g}$ ground state (ruffled) with a $(d_{xz},d_{yz})^4 (d_{xy})^1$ electronic configuration and a thermally accessible ^2E_g excited state (planar) with a $(d_{xy})^2 (d_{xz},d_{yz})^3$ electronic configuration.[25] A computational study predicted a double well potential along the heme ruffling coordinate, which suggested that heme in MhuD can interchange between ruffled and planar conformations.[36] The ruffled heme conformation has been shown to place spin density onto the *meso* carbons, which may direct a regiospecific attack on the *meso* carbons for the conversion of heme to *meso*-hydroxyheme.[37, 38] Indeed, the ruffling of heme has been proposed to modulate the reactivity by changing the electronic configuration of MhuD-*meso*-hydroxyheme complex, thus leading to CO suppressed mechanism to produce mycobilin.[29]

Crystallographic study has shown that the heme is ruffled for MhuD, and various amino acids make several interactions with heme in its active site (Figure 1.3). Second-sphere amino acid residues Phe23 and Trp66 makes hydrophobic interaction with the heme in the active site of MhuD (Figure 1.3). Site-directed mutagenesis study on Phe23 and Trp66 residue has shown that the heme ruffling deformation can be controlled by altering the steric interaction of the residues at 23 and 66 position.[36, 39] Increasing the steric bulk of Phe23 to Trp resulted in increased heme ruffling compared to WT. On the other hand, decreasing the steric bulk of Trp66 to Phe resulted in decreased heme ruffling than WT. In addition, these substitutions also led to decreased enzymatic activity by

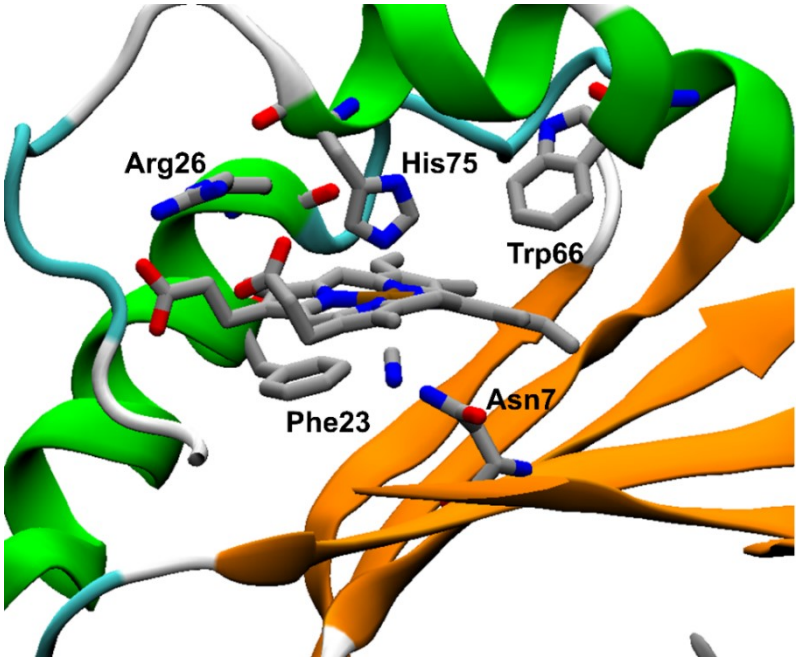

Figure 1. 3. Crystal structure of MhuD−heme−CN (PDB ID 4NL5) showing active site amino acid residue along with the heme substrate. Trp66 and Phe23 makes hydrophobic interaction with heme. Asn7 is hydrogen bonded to the distal cyanide ligand, and Arg26 makes salt bridge interaction with propionate group of heme.

MhuD. Moreover, Asn7 has a hydrogen bonding interaction with the distal cyanide (CN) ligand, while Arg26 makes a salt bridge interaction with the propionate group (Figure 1.3). A study probing the role of Arg26 demonstrated that disrupting the salt-bridge interaction through the mutation of Arg26 to Ser changed the product identity of heme degradation from mycobilin to biliverdin.[40]

Various studies on MhuD have answered several questions regarding its electronic structure, role of second-sphere amino acids on heme distortion and its degradation, the presence of intermediates on the heme degradation mechanism, etc. However, there are various questions that are still untested experimentally. First, the ability of MhuD to be a competent HO *in vivo* is in question due to its weaker affinity towards heme. Moreover, the MhuD has an ability to incorporate a dynamic heme in its active site, which may be essential for its activity. Also, R26S MhuD has been demonstrated to degrade heme to biliverdin, however a small amount of mycobilin was also observed.[40] Thus, it is possible that the presence of two different conformations of heme in the active site of MhuD may lead to different products. These questions and hypotheses will be explored in this dissertation. Initially, the binding affinity of MhuD to heme and diheme will be reinvestigated. Next, the heme degradation mechanism by R26S MhuD will be investigated utilizing various spectroscopic techniques to elucidate the electronic structure of heme bound R26S MhuD. Also, kinetic studies will be performed to elucidate the role of dynamic heme for the enzymatic activity of MhuD. Finally, biochemical studies will be performed to assess the role of heme conformation on product formation by MhuD.

1.5 EXPERIMENTAL APPROACHES TO STUDY MHUD

A fluorescence assay had been developed previously to measure the heme dissociation constant.[17] Fluorescence spectroscopy takes advantage of intrinsic fluorescence of tryptophan, which will be quenched with the addition of heme substrate through Förster resonance energy transfer (FRET). MhuD has a Trp66 residue in the active site within 4 Å of the heme substrate (Figure 1.3, PDB ID 4NL5).[25] Thus, the fluorescence assay developed for heme-bound *S. aureus* IsdG and IsdI can be used for MhuD. The fluorescence spectroscopy is sensitive enough to work with proteins at nanomolar concentrations, and thus the change in fluorescence intensity upon heme addition can be quantified to extract the dissociation constant of first heme binding to MhuD (K_{d1}). An interesting thing about MhuD is it can bind second heme in its active site and will be investigated. Abs spectroscopy has been utilized previously to study heme binding.[16] The Abs spectra of heme, heme-bound and diheme-bound MhuD are distinct. The different spectral feature of these species in solution can be utilized to study the binding of second heme to the active site of MhuD. Titration of heme to the apo protein can be monitored using Abs spectroscopy and the distinct spectral features of free heme, heme-bound and diheme-bound MhuD can be quantified to extract the binding constant for MhuD–diheme. Since, the binding constant for the first heme to MhuD can be extracted using fluorescence spectroscopy, this value can be used as a constant to extract the second dissociation constant (K_{d2}). However, Abs spectroscopy hasn't been previously utilized to study the binding of two heme substrates. Therefore, a new fitting model will be developed to study the second binding event.

Abs spectroscopy has been previously used to probe the electronic structure and to subsequently determine the ruffling of the heme macrocycle compared to WT MhuD.[39] The Abs spectra observed in porphyrins has been explained through Gouterman's four orbital (Figure 1.4a).[41, 42] The Abs spectra arises from the $\pi \rightarrow \pi^*$ transition from the two highest occupied molecular orbitals (HOMOs); a_{1u} and a_{2u} to the two lowest unoccupied molecular orbitals (LUMOs); degenerate e_g^*. Transitions between these orbitals give rise to two excited states, both with ^1E_u character. Orbital mixing between the excited states splits these states through configuration interaction, giving rise to a higher energy Soret band and a lower energy Q-band (Figure 1.4b). Heme ruffling has been shown to alter the energy gap between the filled a_{1u}/a_{2u} orbitals and the unoccupied e_g^* orbitals. A DFT study has demonstrated that Q-band energy remains unchanged up to1.0 Å heme ruffling,

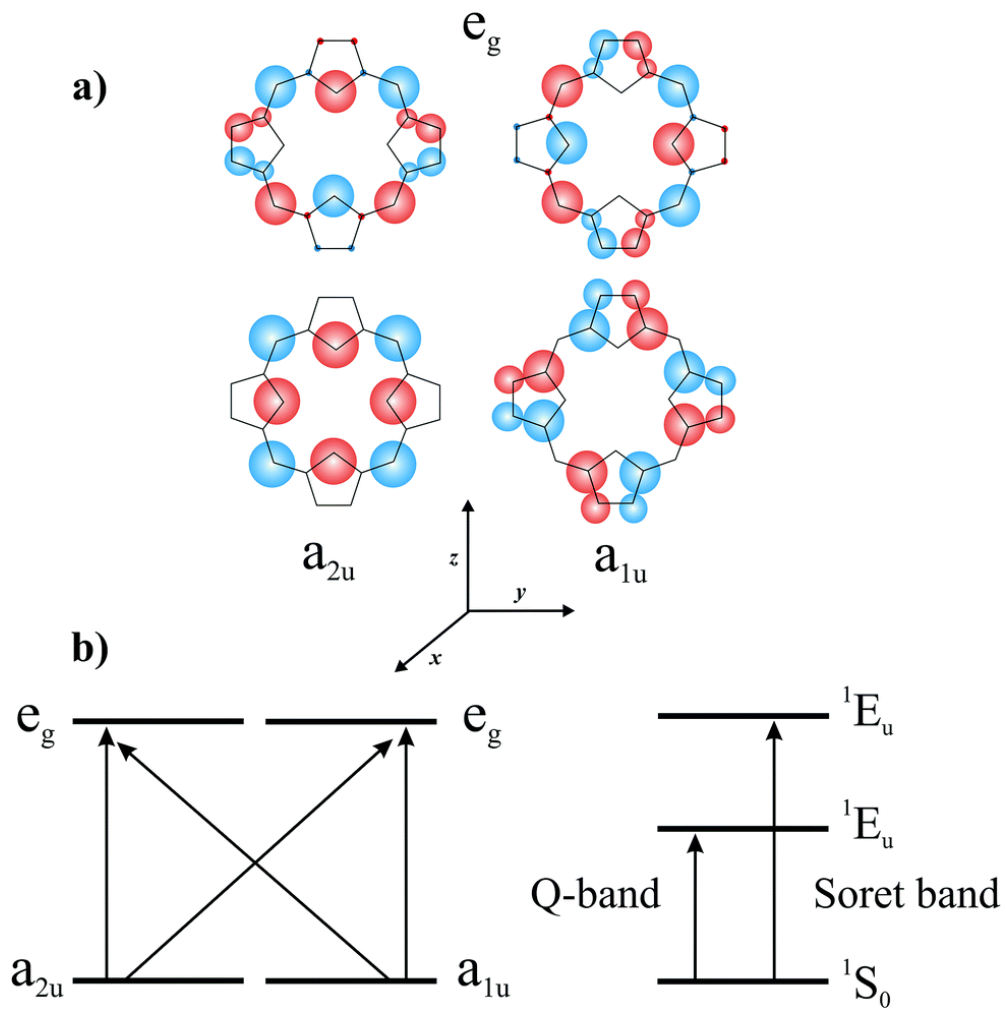

Figure 1. 4. Gouterman's four orbitals involved in the Abs spectra of a porphyrin (a) and energy levels responsible for electronic transitions in the porphyrin system (b). Figure taken from reference 38.[43]

however, the Abs spectra then red shifts with distortion above 1.0 Å. Similarly, the Soret band energy is blue shifted up to 1.0 Å ruffling, then red-shifts from 1.0 – 2.3 Å.[39] The change in heme ruffling due to second-sphere amino acid substitution has been studied in the past.[36, 39, 44] Therefore, ruffling distortion of heme substrate due to Arg26 mutation to Ser for MhuD and Phe23 mutation to Trp for IsdG will be investigated using Abs spectroscopy.

Magnetic Circular Dichroism (MCD) spectroscopy can be utilized to probe the electronic structure changes caused by the second-sphere amino acid substitutions in the heme bound enzyme.[45] MCD measures the difference between the absorption of left- and right-circularly polarized light. The MCD spectrum is taken as a function of the wavelength in the presence of a magnetic field that is applied parallel to the direction of propagation of the light beam. The MCD spectrum arises from the transition from a ground to an excited state and depends on three Faraday terms: A, B and C-term. An A-term arises from a transition from a non-degenerate ground state to orbitally degenerate excited state. The degeneracy of the excited state is split in the presence of a magnetic field due to Zeeman effect. Therefore, the transition would be temperature-independent, and the spectrum would be a derivative shaped (Figure 1.5). The B-term arises from the field-induced mixing between different states. The resulting MCD spectrum is absorption-shaped and is temperature-independent. The C-term contribution to the MCD spectrum arises due to the transition from the degenerate ground state to the non-degenerate excited state. Thus, resulting in absorption-shaped temperature-dependent MCD spectrum (Figure 1.5).[46] Optical transitions such as d→d charge transfer, metal to ligand charge transfer and vice-versa, can be observed for a low spin ferric heme with an unpaired electron in its ground state. The states arising from these configurations can mix through spin-orbit coupling and give rise to temperature dependent C-terms, which dominate the MCD spectra of heme proteins.

Variable field variable temperature (VTVH) MCD spectra can reveal information regarding ground electronic state of paramagnetic systems. The Soret band is dominated by the C-term, which at a fixed temperature increases linearly in the presence of low

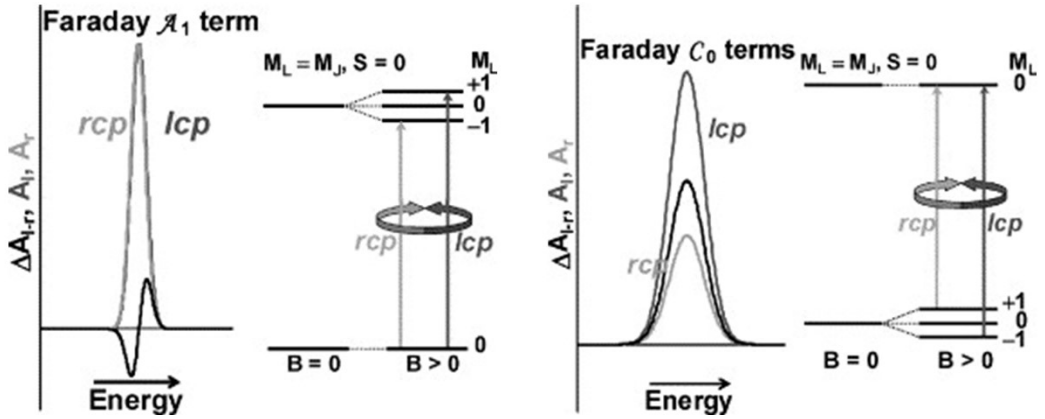

Figure 1. 5. A- and C-term MCD spectra origin. A-term arises from transition from non-degenerate ground state to degenerate excited state, whereas C-term arises from a transition from degenerate ground state to non-degenerate excited state. In the presence of a magnetic field, the degeneracy is lifted due to Zeeman Splitting. Adapted from reference 42.[47]

field. However, at higher fields, the intensity starts to saturate due to Zeeman splitting, as the lowest electronic state is populated due to Boltzmann distribution. In hemoproteins, the Soret-Band is dominated by xy-polarized transitions, which means that the initial slope of the saturation magnetization curves depends on the g_z value. This will help provide insights into the ground electronic state. Therefore, the change in the ground electronic state due to second-sphere substitution can be probed using VTVH MCD.

Nuclear magnetic resonance (NMR) spectroscopy has been utilized for a low spin ferric heme system to determine the ground electronic configuration. Generally, ^{1}H NMR spectra of a diamagnetic sample are observed from 0 – 10 ppm. However, in the presence of an unpaired electron, these chemical shifts are hyperfine shifted either upfield or downfield. Two electronic structures are possible for low spin ferric heme: $(d_{xy})^2 (d_{xz},$

$d_{yz})^3$ and (d_{xz}, $d_{yz})^4$ ($d_{xy})^1$. When the unpaired electron is in the d_{xy} orbital, the *meso*-protons will experience spin polarization through *meso* carbons and shift upfield. On the other hand, when the unpaired electron is in the d_{xz} or d_{yz} orbital the spin density is delocalized onto the pyrrole rings and spin polarization is experienced by the methyl protons resuling in a downfield shift. Previous ^{1}H NMR studies have determined the ground state as ($d_{xy})^2$ (d_{xz}, $d_{yz})^3$ for HO-heme-CN,[48-50] and as (d_{xz}, $d_{yz})^4$ ($d_{xy})^1$ for IsdG-heme-CN[51] and MhuD-heme-CN.[25] ^{1}H NMR spectroscopy was also utilized to investigate the change in ground electronic structure induced by the second-sphere amino acid substitution in MhuD.[36, 39] A Curie plot of the hyperfine-shifted resonances as an inverse function of temperature can be plotted to investigate their linear dependence.[52] Linear dependence would mean a Curie behavior, and would suggest presence of single electronic state. However, non-linear dependence would mean a non-Curie behavior, and would suggest presence of thermally accessible excited state. Therefore, ^{1}H NMR spectroscopy can be utilized to gain insights onto the ground electronic state and its change induced by second-sphere amino acid substitution.

1.6 CHAPTER 1 REFERENCES

1. World Health Organization. Grobal Tuberculosis Report. 2019.

2. De Voss, J. J.; Rutter, K.; Schroeder, B. G.; Barry, C. E., 3rd, Iron acquisition and metabolism by mycobacteria. *J. Bacteriol.*, 1999, *181* (15), 4443-51.

3. Rodriguez, G. M.; Smith, I., Identification of an ABC transporter required for iron acquisition and virulence in Mycobacterium tuberculosis. *J. Bacteriol.*, 2006, *188* (2), 424-30.

4. Ratledge, C.; Dover, L. G., Iron metabolism in pathogenic bacteria. *Annu. Rev. Microbiol.*, 2000, *54*, 881-941.

5. Ryndak, M. B.; Wang, S.; Smith, I.; Rodriguez, G. M., The Mycobacterium tuberculosis high-affinity iron importer, IrtA, contains an FAD-binding domain. *J. Bacteriol.*, 2010, *192* (3), 861-9.

6. Chao, A.; Sieminski, P. J.; Owens, C. P.; Goulding, C. W., Iron Acquisition in Mycobacterium tuberculosis. *Chem. Rev.*, 2019, *119* (2), 1193-1220.

7. Tullius, M. V.; Harmston, C. A.; Owens, C. P.; Chim, N.; Morse, R. P.; McMath, L. M.; Iniguez, A.; Kimmey, J. M.; Sawaya, M. R.; Whitelegge, J. P.; Horwitz, M. A.; Goulding, C. W., Discovery and characterization of a unique mycobacterial heme acquisition system. *Proc. Natl. Acad. Sci.*, 2011, *108* (12), 5051-5056.

8. Owens, C. P.; Du, J.; Dawson, J. H.; Goulding, C. W., Characterization of heme ligation properties of Rv0203, a secreted heme binding protein involved in Mycobacterium tuberculosis heme uptake. *Biochemistry*, 2012, *51* (7), 1518-31.

9. Owens, C. P.; Chim, N.; Graves, A. B.; Harmston, C. A.; Iniguez, A.; Contreras, H.; Liptak, M. D.; Goulding, C. W., The Mycobacterium tuberculosis secreted protein Rv0203 transfers heme to membrane proteins MmpL3 and MmpL11. *J. Biol. Chem.*, 2013, *288* (30), 21714-28.

10. Xu, Z. J.; Meshcheryakov, V. A.; Poce, G.; Chng, S. S., MmpL3 is the flippase for mycolic acids in mycobacteria. *Proc. Natl. Acad. Sci.*, 2017, *114* (30), 7993-7998.

11. Grzegorzewicz, A. E.; Pham, H.; Gundi, V. A. K. B.; Scherman, M. S.; North, E. J.; Hess, T.; Jones, V.; Gruppo, V.; Born, S. E. M.; Kordulakova, J.; Chavadi, S. S.; Morisseau, C.; Lenaerts, A. J.; Lee, R. E.; McNeil, M. R.; Jackson, M., Inhibition of mycolic acid transport across the Mycobacterium tuberculosis plasma membrane. *Nat. Chem. Biol.*, 2012, *8* (4), 334-341.

12. Pacheco, S. A.; Hsu, F. F.; Powers, K. M.; Purdy, G. E., MmpL11 Protein Transports Mycolic Acid-containing Lipids to the Mycobacterial Cell Wall and Contributes to Biofilm Formation in Mycobacterium smegmatis. *J. Biol. Chem.*, 2013, *288* (33), 24213-24222.

13. Stojiljkovic, I.; Kumar, V.; Srinivasan, N., Non-iron metalloporphyrins: potent antibacterial compounds that exploit haem/Hb uptake systems of pathogenic bacteria. *Mol. Microbiol.*, 1999, *31* (2), 429-42.

14. Costa, D. L.; Namasivayam, S.; Amaral, E. P.; Arora, K.; Chao, A.; Mittereder, L. R.; Maiga, M.; Boshoff, H. I.; Barry, C. E., 3rd; Goulding, C. W.; Andrade, B. B.; Sher, A., Pharmacological Inhibition of Host Heme Oxygenase-1 Suppresses Mycobacterium tuberculosis Infection In Vivo by a Mechanism Dependent on T Lymphocytes. *Mbio*, 2016, *7* (5).

15. Koga, S.; Yoshihara, S.; Bando, H.; Yamasaki, K.; Higashimoto, Y.; Noguchi, M.; Sueda, S.; Komatsu, H.; Sakamoto, H., Development of a heme sensor using fluorescently labeled heme oxygenase-1. *Anal. Biochem.*, 2013, *433* (1), 2-9.

16. Fleischhacker, A. S.; Sharma, A.; Choi, M.; Spencer, A. M.; Bagai, I.; Hoffman, B. M.; Ragsdale, S. W., The C-Terminal Heme Regulatory Motifs of Heme Oxygenase-2 Are Redox-Regulated Heme Binding Sites. *Biochemistry*, 2015, *54* (17), 2709-2718.

17. Conger, M. A.; Pokhrel, D.; Liptak, M. D., Tight binding of heme to Staphylococcus aureus IsdG and IsdI precludes design of a competitive inhibitor. *Metallomics*, 2017, *9* (5), 556-563.

18. Song, Y.; Yang, M.; Wegner, S. V.; Zhao, J.; Zhu, R.; Wu, Y.; He, C.; Chen, P. R., A Genetically Encoded FRET Sensor for Intracellular Heme. *ACS Chem. Biol.*, 2015, *10* (7), 1610-5.

19. Hanna, D. A.; Harvey, R. M.; Martinez-Guzman, O.; Yuan, X.; Chandrasekharan, B.; Raju, G.; Outten, F. W.; Hamza, I.; Reddi, A. R., Heme dynamics and trafficking factors revealed by genetically encoded fluorescent heme sensors. *Proc. Natl. Acad. Sci.*, 2016, *113* (27), 7539-44.

20. Chim, N.; Iniguez, A.; Nguyen, T. Q.; Goulding, C. W., Unusual diheme conformation of the heme-degrading protein from Mycobacterium tuberculosis. *J. Mol. Bio.*, 2010, *395* (3), 595-608.

21. Matsui, T.; Iwasaki, M.; Sugiyama, R.; Unno, M.; Ikeda-Saito, M., Dioxygen Activation for the Self-Degradation of Heme: Reaction Mechanism and Regulation of Heme Oxygenase. *Inorg. Chem.*, 2010, *49* (8), 3602-3609.

22. Lad, L.; Friedman, J.; Li, H.; Bhaskar, B.; Ortiz de Montellano, P. R.; Poulos, T. L., Crystal structure of human heme oxygenase-1 in a complex with biliverdin. *Biochemistry*, 2004, *43* (13), 3793-801.

23. Wilks, A.; Ikeda-Saito, M., Heme Utilization by Pathogenic Bacteria: Not All Pathways Lead to Biliverdin. *Acc. Chem. Res.*, 2014, *47* (8), 2291-2298.

24. Schuller, D. J.; Wilks, A.; Ortiz de Montellano, P. R.; Poulos, T. L., Crystal structure of human heme oxygenase-1. *Nat. Struct. Biol.*, 1999, *6* (9), 860-7.

25. Graves, A. B.; Morse, R. P.; Chao, A.; Iniguez, A.; Goulding, C. W.; Liptak, M. D., Crystallographic and spectroscopic insights into heme degradation by Mycobacterium tuberculosis MhuD. *Inorg. Chem.*, 2014, *53* (12), 5931-40.

26. Wu, R. Y.; Skaar, E. P.; Zhang, R. G.; Joachimiak, G.; Gornicki, P.; Schneewind, O.; Joachimiak, A., Staphylococcus aureus IsdG and IsdI, heme-degrading enzymes with structural similarity to monooxygenases. *J. Biol. Chem.*, 2005, *280* (4), 2840-2846.

27. Lee, W. C.; Reniere, M. L.; Skaar, E. P.; Murphy, M. E., Ruffling of metalloporphyrins bound to IsdG and IsdI, two heme-degrading enzymes in Staphylococcus aureus. *J. Biol. Chem.*, 2008, *283* (45), 30957-63.

28. Skaar, E. P.; Gaspar, A. H.; Schneewind, O., IsdG and IsdI, heme-degrading enzymes in the cytoplasm of Staphylococcus aureus. *J. Biol. Chem.*, 2004, *279* (1), 436-43.

29. Matsui, T.; Nambu, S.; Ono, Y.; Goulding, C. W.; Tsumoto, K.; Ikeda-Saito, M., Heme degradation by Staphylococcus aureus IsdG and IsdI liberates formaldehyde rather than carbon monoxide. *Biochemistry*, 2013, *52* (18), 3025-7.

30. Reniere, M. L.; Ukpabi, G. N.; Harry, S. R.; Stec, D. F.; Krull, R.; Wright, D. W.; Bachmann, B. O.; Murphy, M. E.; Skaar, E. P., The IsdG-family of haem oxygenases degrades haem to a novel chromophore. *Mol. Microbiol.*, 2010, *75* (6), 1529-38.

31. Nambu, S.; Matsui, T.; Goulding, C. W.; Takahashi, S.; Ikeda-Saito, M., A new way to degrade heme: the Mycobacterium tuberculosis enzyme MhuD catalyzes heme degradation without generating CO. *J. Biol. Chem.*, 2013, *288* (14), 10101-9.

32. Matsui, T.; Nambu, S.; Goulding, C. W.; Takahashi, S.; Fujii, H.; Ikeda-Saito, M., Unique coupling of mono- and dioxygenase chemistries in a single active site promotes heme degradation. *Proc. Natl. Acad. Sci.*, 2016, *113* (14), 3779-84.

33. Tenhunen, R.; Marver, H. S.; Schmid, R., Microsomal heme oxygenase. Characterization of the enzyme. *J. Biol. Chem.*, 1969, *244* (23), 6388-94.

34. Matsui, T.; Unno, M.; Ikeda-Saito, M., Heme oxygenase reveals its strategy for catalyzing three successive oxygenation reactions. *Acc. Chem. Res.*, 2010, *43* (2), 240-7.

35. Chen, H.; Moreau, Y.; Derat, E.; Shaik, S., Quantum mechanical/molecular mechanical study of mechanisms of heme degradation by the enzyme heme oxygenase: the strategic function of the water cluster. *J. Am. Chem. Soc.*, 2008, *130* (6), 1953-65.

36. Graves, A. B.; Horak, E. H.; Liptak, M. D., Dynamic ruffling distortion of the heme substrate in non-canonical heme oxygenase enzymes. *Dalton Trans.*, 2016, *45* (24), 10058-67.

37. Rivera, M.; Caignan, G. A.; Astashkin, A. V.; Raitsimring, A. M.; Shokhireva, T.; Walker, F. A., Models of the low-spin iron(III) hydroperoxide intermediate of

heme oxygenase: magnetic resonance evidence for thermodynamic stabilization of the d(xy) electronic state at ambient temperatures. *J. Am. Chem. Soc.*, 2002, *124* (21), 6077-89.

38. Kleingardner, J. G.; Bowman, S. E.; Bren, K. L., The influence of heme ruffling on spin densities in ferricytochromes c probed by heme core 13C NMR. *Inorg. Chem.*, 2013, *52* (22), 12933-46.

39. Graves, A. B.; Graves, M. T.; Liptak, M. D., Measurement of Heme Ruffling Changes in MhuD Using UV-vis Spectroscopy. *J. Phys. Chem. B*, 2016, *120* (16), 3844-53.

40. Chao, A.; Goulding, C. W., A Single Mutation in the Mycobacterium tuberculosis Heme-Degrading Protein, MhuD, Results in Different Products. *Biochemistry*, 2019, *58* (6), 489-492.

41. Gouterman, M., Spectra of Porphyrins. *J. Mol. Spectrosc.*, 1961, *6*, 138-163.

42. Gouterman, M., Study of the Effects of Substitution on the Absorption Spectra of Porphin. *J. Chem. Phys.*, 1959, *30*, 1139 - 1161.

43. Namuangruk, S.; Sirithip, K.; Rattanatwan, R.; Keawin, T.; Kungwan, N.; Sudyodsuk, T.; Promarak, V.; Surakhot, Y.; Jungsuttiwong, S., Theoretical investigation of the charge-transfer properties in different meso-linked zinc porphyrins for highly efficient dye-sensitized solar cells. *Dalton Trans.*, 2014, *43* (24), 9166-9176.

44. Schuelke-Sanchez, A. E. Spectroscopic Study of the Formation and Degradation of Metalated Tetrapyrroles by the Enzymes CfbA, IsdG, and MhuD. Dissertation and Theses, University of Vermont, 2019.

45. Cheesman, M. R.; Greenwood, C.; Thomson, A. J., Magnetic Circular-Dichroism of Hemoproteins. *Adv. Inorg. Chem.*, 1991, *36*, 201-255.

46. Solomon, E. I.; Pavel, E. G.; Loeb, K. E.; Campochiaro, C., Magnetic Circular-Dichroism Spectroscopy as a Probe of the Geometric and Electronic-Structure of Nonheme Ferrous Enzymes. *Coord. Chem. Rev.*, 1995, *144*, 369-460.

47. Mack, J.; Stillman, M. J.; Kobayashi, N., Application of MCD spectroscopy to porphyrinoids. *Coord. Chem. Rev.*, 2007, *251* (3-4), 429-453.

48. Caignan, G. A.; Deshmukh, R.; Wilks, A.; Zeng, Y. H.; Huang, H. W.; Moenne-Loccoz, P.; Bunce, R. A.; Eastman, M. A.; Rivera, M., Oxidation of heme to beta- and delta-biliverdin by Pseudomonas aeruginosa heme oxygenase as a consequence of an unusual seating of the heme. *J. Am. Chem. Soc.*, 2002, *124* (50), 14879-14892.

49. Gorst, C. M.; Wilks, A.; Yeh, D. C.; de Montellano, P. R. O.; La Mar, G. N., Solution H-1 NMR investigation of the molecular and electronic structure of the active site of substrate-bound human heme oxygenase: the nature of the distal hydrogen bond donor to bound ligands. *J. Am. Chem. Soc.*, 1998, *120* (34), 8875-8884.

50. Ogura, H.; Evans, J. P.; Peng, D. G.; Satterlee, J. D.; de Montellano, P. R. O.; La Mar, G. N., The Orbital Ground State of the Azide-Substrate Complex of Human Heme Oxygenase Is an Indicator of Distal H-Bonding: Implications for the Enzyme Mechanism. *Biochemistry*, 2009, *48* (14), 3127-3137.

51. Takayama, S. J.; Ukpabi, G.; Murphy, M. E.; Mauk, A. G., Electronic properties of the highly ruffled heme bound to the heme degrading enzyme IsdI. *Proc. Natl. Acad. Sci.*, 2011, *108* (32), 13071-6.

52. Shokhirev, N. V.; Walker, F. A., Analysis of the temperature dependence of the H-1 contact shifts in low-spin Fe(III) model hemes and heme proteins: Explanation of "Curie" and "anti-Curie" behavior within the same molecule. *J. Phys. Chem.*, 1995, *99* (50), 17795-17804.

CHAPTER 2: THE AFFINITY OF MHUD FOR HEME IS CONSISTENT WITH A HEME DEGRADING FUNCTION *IN VIVO*.

Material in this dissertation chapter is an adaptation of the Metallomics manuscript shown below:

Thakuri, B.; Graves, A. B.; Chao, A.; Johansen, S. L.; Goulding, C. W.; Liptak, M. D., The affinity of MhuD for heme is consistent with a heme degrading function in vivo. Metallomics 2018, 10 (11), 1560-1563

2.1 INTRODUCTION

Mycobacterial infections are responsible for a range of human diseases, including two ancient ones: tuberculosis (Mycobacterium tuberculosis infection)[1] and leprosy (Mycobacterium leprae infection).[2] This genus has a unique heme acquisition pathway that is at least partially responsible for supplying a critical nutrient during infection by harvesting iron from hemoglobin and perhaps other host heme-containing proteins.[3, 4] Since bacteria require micromolar iron for growth,[5] and the proteins of this pathway are unique to mycobacteria, the proteins of the mycobacterial heme acquisition system are promising drug targets.[6, 7] Currently, this heme iron acquisition pathway is thought to begin with Rv0203, a secreted heme binding protein that could transport extracellular heme to the mycobacterial cell surface.[8] Next, heme is transferred from Rv0203 to the periplasmic domains of inner membrane proteins MmpL3 or MmpL11.[9] Finally, heme is degraded to non-heme iron and mycobilin by cytosolic MhuD.[10-12] However, the precise mechanism of mycobacterial heme acquisition and the identities of the protein components are still poorly understood.

MhuD is a non-canonical heme oxygenase that is functionally distinct from both eukaryotic heme oxygenases and IsdG heme oxygenases.[13-15] This enzyme catalyzes the monooxygenation of heme to meso-hydroxyheme, followed by dioxygenation of this intermediate to the mycobilin product.[11, 16] Detailed crystallographic and spectroscopic characterization, coupled with computational modeling, have revealed that an out-of-plane ruffling distortion of the heme substrate is critical for the monooxygenation reaction.[17, 18] However, the dissociation constant for heme-bound MhuD (MhuD–heme) has been reported to be in the micromolar range in the original study,[10] which is

inconsistent with the nanomolar values reported for four other heme oxygenases: HO-1[19], HO-2[20], IsdG[21] and IsdI.[21] Furthermore, the reported heme dissociation constant for MhuD–diheme is also micromolar,[10] implying that there is only a narrow labile heme concentration range where the enzymatically-active MhuD–heme species can be formed. These observations call into question whether MhuD is a competent heme oxygenase *in vivo*. In addition, two recent studies have established that the concentration of the cytosolic labile heme pool in Homo sapiens and Saccharomyces cerevisiae is 20-40 nM,[22, 23] and if the only source of heme for MhuD is this labile heme pool, the micromolar heme affinity is insufficient as only 1% of MhuD would be heme loaded. A recent reinvestigation of the heme dissociation constants for *Staphylococcus aureus* IsdG and IsdI revealed that the previously reported values were two to three orders of magnitude too large due to inherent sensitivity limitations of an assay that requires micromolar protein samples.[21] Thus, a reinvestigation of the MhuD–heme dissociation constant previously measured in the original study using isothermal titration calorimetery (ITC) and micromolar protein samples with a more sensitive spectroscopic technique is warranted in order to determine whether MhuD is a competent heme oxygenase *in vivo*.

MhuD is unique among heme oxygenases in the fact that it can bind two heme molecules per protein monomer. The X-ray crystal structure of diheme-bound MhuD (MhuD–diheme, PDB ID 3HX9) revealed that the two hemes are stacked with nearly parallel porphyrin planes (Figure 1.1).[10] The MhuD–diheme form of the enzyme does not degrade heme, which has led to speculation regarding the function of this species. Initially, it was proposed that the MhuD–diheme form enables MhuD to function as a heme storage protein, mitigating the toxicity of heme at high concentrations,[24] and

provide a heme reservoir under heme-deplete conditions. However, as noted above, MhuD catalyzes a unique multi-step oxygenation of heme to mycobilin,[11, 16] which requires that MhuD has an active site distinct from other heme-dependent proteins (PDB ID 4NL5).[17] Thus, the MhuD–diheme form may be an *in vitro* artifact arising from the combination of a unique active site and an excess of exogenous heme. For these reasons, a reinvestigation of the dissociation constant for the second heme bound to MhuD–diheme was also undertaken.

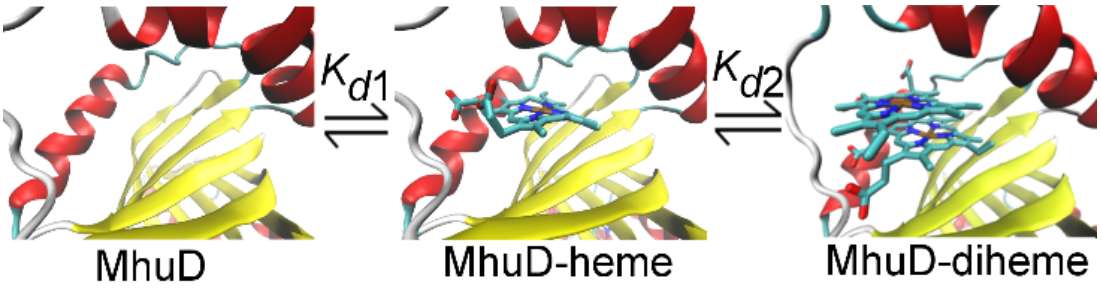

Figure 2. 1. MhuD is a non-canonical heme oxygenase found in mycobacteria (PDB IDs 3HX9 and 4NL5).[10, 17] Heme-bound MhuD (MhuD–heme) is converted to iron and mycobilin, but diheme-bound MhuD (MhuD–diheme) is enzymatically inactive. Dissociation constants can be defined for dissociation of heme from MhuD–heme (K_{d1}) and MhuD–diheme (K_{d2}).

This study reports dissociation constant measurements for heme dissociation from MhuD–heme and MhuD–diheme based upon fluorescence and UV/Vis absorption (Abs) spectroscopy-based assays. A previously described fluorescence assay was used to measure the dissociation constant for MhuD–heme (K_{d1}),[21] and an Abs assay was developed to measure heme dissociation from MhuD–diheme (K_{d2}). Critical analyses of the fits of these mathematical models to the experimental data suggested that the C-

terminal His_6 tag interferes with heme binding despite the fact that no interaction between heme and the His_6 tag was observed in the X-ray crystal structures of MhuD–heme (PDB ID 4NL5) or MhuD–diheme (PDB ID 3HX9).[10, 17] For this reason, a form of MhuD with an enterokinase-cleavable N-terminal His_6-tag was prepared. Fluorescence- and Abs-detected titrations of heme into this form of MhuD were well fit by the mathematical models yielding nanomolar and micromolar dissociation constants for MhuD–heme and MhuD–diheme, respectively. The implications of these data for the biological functions of MhuD–heme and MhuD–diheme are discussed.

2.2 EXPERIMENTAL

All materials were purchased from Fisher Scientific and used without further purification unless otherwise noted. All water was obtained from a Synergy water purification system (Millipore).

Cloning, Expression, and Purification. The cloning and expression of MhuD (Rv3592) with a C-terminal His_6 tag into pET-22b (Amp^r, Novagen) has been previously described.[10] The MhuD gene was recloned into a pET30a vector to encode a protein with an enterokinase cleavable N-terminal His_6 tag, which results in encoded full-length MhuD with an additional N-terminal Ala ($MhuD_{CH}$). The *M. tuberculosis* MhuD gene (Rv3592) was PCR amplified from the pET22a plasmid noted above using KOD-Hot Start DNA Polymerase (Novagen) with primers (5’ – GGC CAT GGC CCC AGT GGT GAA GAT CAA CGC AAT CGA GGT GCC CGC C – 3’) and (5’ – GGA AGC TTA TTA TGC AGT CTT GCC GGT CCC ACC GAC GTC AAG CAC GAC – 3’) containing the restriction sites NcoI and HindIII, respectively. The PCR product was gel purified (Qiagen) and ligated into a linearized blunt vector, pCR-BluntII-TOPO

(Invitrogen), and transformed into One-Shot TOP10 Escherichia coli cells (Invitrogen). Restriction enzymes NcoI and HindIII were used to excise the MhuD insert from pCR-BluntII-TOPO as well as cut the empty pET30a (Kan^r) vector. The excised MhuD insert and cut pET30a were ligated together using T4 DNA ligase (New England Biolabs). The resulting DNA construct was verified by DNA sequencing (Retrogen).

Cells containing recombinant MhuD were lysed as described previously,[17] and the filtered supernatant was loaded onto a 5 mL Ni(II)-charged HiTrap chelating HP column (GE Healthcare) equilibrated with 50 mM Tris pH 7.8, 350 mM NaCl using an ÄKTA pure 25 L fast protein liquid chromatography (FPLC) system (GE Healthcare). The column was washed with a 2 mM/mL linear gradient from 0 to 100 mM imidazole in 50 mM Tris pH 7.8, 350 mM NaCl at a flow rate of 5.0 mL/min. Pure MhuD eluted during a subsequent 1.6 mM/mL linear gradient from 100 to 300 mM imidazole in 50 mM Tris pH 7.8, 350 mM NaCl at a flow rate of 5.0 mL/min (Figures A.1 - A.2). FPLC fractions containing pure MhuD were pooled and the sample volume was reduced to 10 mL using Amicon stirred cells with 10 kDa ultrafiltration membranes (Millipore). Following overnight dialysis against 20 mM Tris pH 8.0, 50 mM NaCl, >99% pure MhuD was obtained as assessed by SDS-PAGE gel electrophoresis (Figure A.3).

For recombinant expression of $MhuD_{CH}$, the pET30a (Kan^r) vector encoding $MhuD_{CH}$ was transformed into BL21-GOLD (DE3) cells (Stratagene). DNA sequencing at the Vermont Cancer Center DNA Analysis Facility confirmed the sequence of the $MhuD_{CH}$ gene for all cell lines used at the University of Vermont (Table A.1). E. coli cells containing pET30a were grown in Luria-Bertani medium containing 30 μg/μL kanamycin at 37 °C using a MaxQ 5000 floor-model shaker (Thermo Scientific), and

$MhuD_{CH}$ over-expression was induced with 1 mM isopropyl β-D-1-thiogalactopyranoside at an OD_{600} of 0.8 a.u. Cells were lysed in 50 mM Tris pH 7.8, 350 mM NaCl by sonication following the addition of 2.5 mg lysozyme and 0.01 M phenylmethane sulfonyl fluoride using a Branson S-450A Sonifier. The lysate was centrifuged at 15,000 x *g* for 45 mins using a Sorvall Legend XTR centrifuge (Thermo Scientific) and the supernatant was filtered through a 0.45 μm membrane (Millipore). The filtered lysate was loaded onto a 5 mL Ni(II)-charged HiTrap chelating HP column equilibrated with 50 mM Tris pH 7.8, 350 mM NaCl using an ÄKTA pure 25 L FPLC system. The column was washed with a 2.25 mM/mL linear gradient from 0 to 90 mM imidazole in 50 mM Tris pH 7.8, 350 mM NaCl at a flow rate of 5.0 mL/min. Pure, uncleaved $MhuD_{CH}$ eluted during a subsequent 1.48 mM/mL linear gradient from 90 to 275 mM imidazole in 50 mM Tris pH 7.8, 350 mM NaCl at a flow rate of 5.0 mL/min (Figures A.4 - A.5). FPLC fractions containing pure, uncleaved $MhuD_{CH}$ were pooled and the sample volume was reduced to 10 mL using Amicon stirred cells with 10 kDa ultrafiltration membranes. Uncleaved $MhuD_{CH}$ was dialyzed overnight against 20 mM Tris pH 8.0, 50 mM NaCl, 2 mM CaCl2.

The His_6 tag of $MhuD_{CH}$ was removed by adding enterokinase (New England Biolabs) in a molar ratio of 1:250,000. The mixture was stirred for 36 h at 4 °C, then loaded onto a 5 mL HiTrap Q HP column (GE Healthcare) equilibrated with 20 mM Tris pH 8.0, 10 mM NaCl using an ÄKTA pure 25 L FPLC system. Pure, cleaved $MhuD_{CH}$ eluted during a 1.0 mM/mL linear gradient from 50 to 250 mM NaCl in 20 mM Tris pH 8.0 at a flow rate of 5.0 mL/min (Figures A.6 - A.7). FPLC fractions containing pure, cleaved $MhuD_{CH}$ were pooled and the sample volume was reduced to 2.5 mL using

Amicon stirred cells with 10 kDa ultrafiltration membranes. Following exchange into 50 mM Tris pH 7.4, 150 mM NaCl using a PD-10 desalting column (GE Healthcare), >95% pure, cleaved $MhuD_{CH}$ was obtained as assessed by SDS-PAGE gel electrophoresis (Figure A.8).

Electrospray ionization mass spectrometry (ESI-MS) was used to assess the $MhuD_{CH}$ product. A 30 μM sample of cleaved $MhuD_{CH}$ in 50 mM Tris pH 7.4, 150 mM NaCl was loaded onto a C18 guard column equilibrated with 2% acetonitrile with 0.1% formic acid (v/v) in water (v/v) using a QTRAP 4000 LCMS/MS system (Sciex) with an M/z from 600-2000. The column was washed using 2% acetonitrile with 0.1% formic acid (v/v) in water (v/v) for 1 min at a flow rate of 100 μL/min. $MhuD_{CH}$ eluted during a 13.7%/min linear gradient from 2 to 98% acetonitrile with 0.1% formic acid (v/v) in water (v/v) at a flow rate of 100 μL/min. The spectrum was deconvoluted using BioAnalyst 1.5 software. The observed molecular weight of 11,327 Da was in perfect agreement with the expected molecular weight of 11,327 Da (Figure A.9).

Spectroscopic characterization. The MhuD–heme extinction coefficient was determined previously,[17] and the extinction coefficients for MhuD–diheme, heme-bound $MhuD_{CH}$ ($MhuD_{CH}$–heme), and diheme-bound $MhuD_{CH}$ ($MhuD_{CH}$–diheme) were determined using a similar procedure. Samples of MhuD–diheme, $MhuD_{CH}$–heme, and $MhuD_{CH}$–diheme were prepared in 50 mM Tris pH 7.4, 150 mM NaCl as described previously,[10] and their room temperature. Abs spectra were acquired from 900 to 200 nm with a scan rate of 600 nm/min, a 1.0 nm data interval, and a 0.1 s integration time using a Cary 100 Bio UV-Vis Spectrophotometer. The following extinction coefficients were determined using the pyridine hemochrome assay:[25] MhuD–diheme (ε_{410} = 165.3 mM^{-}

$^{1}cm^{-1}$), $MhuD_{CH}$–heme (ε_{407} = 87.9 $mM^{-1}cm^{-1}$), and $MhuD_{CH}$–diheme (ε_{395} = 162.3 $mM^{-1}cm^{-1}$).

Fluorescence-detected heme titrations into MhuD and $MhuD_{CH}$ were completed by slightly modifying a previously described procedure.[21] Briefly, 100 nM samples of MhuD and $MhuD_{CH}$, plus 17.5 μM heme solutions, were prepared in 50 mM Tris pH 7.4, 150 mM NaCl as previously described.[17] Heme was titrated into MhuD and $MhuD_{CH}$ in 16 nM increments, and allowed to equilibrate for 5 min prior to fluorescence characterization. Fluorescence emission spectra were acquired for 285 nm excitation using a Photon Technology International QuantaMaster 4 spectrofluorometer equipped with a Xenon arc lamp connected to an LPS-220b power supply, an ASOC-10 electronics interface, an MD-4000 motor driver control, and a model 814 photomultiplier detection system. Emission spectra were acquired in the 410 to 310 nm range with a step size of 1 nm, an integration time of 1 s, and slit widths of 3 nm.

Abs-detected titrations were carried out using similar protein samples. 5 μM samples of MhuD and $MhuD_{CH}$, and a 500 μM heme solution, were prepared in 50 mM Tris pH 7.4, 150 mM NaCl as described before.[17]Heme was titrated into MhuD and $MhuD_{CH}$ in 1 μM increments, and allowed to equilibrate until no further spectral changes were observed. Abs spectra were acquired using the equipment and parameters described above.

Spectral Analysis. The fluorescence-detected titrations of heme into MhuD and $MhuD_{CH}$ were analyzed in order to determine K_{d1} for MhuD and $MhuD_{CH}$. The Trp66 fluorescence intensity for a mixture of MhuD, MhuD–heme, and heme depends upon equation (2.1):

$$F = \frac{([MhuD_T] + [heme_T] + K_{d1}) - \sqrt{([MhuD_T] + [heme_T] + K_{d1})^2 - 4[MhuD_T][heme_T]}}{2} \times \left(\frac{F_{min} - F_{max}}{[MhuD_T]}\right) + F_{max} \quad (2.1)$$

where $[MhuD_T]$ is the total MhuD concentration, $[heme_T]$ is the total heme concentration, F_{max} is the fluorescence intensity in the absence of heme, and F_{min} is the fluorescence intensity for fully heme–bound MhuD. The emission intensity at 336 nm as a function of $[heme_T]$ was fit to equation (2.1) using GraphPad Prism 7.0 to determine K_{d1} and its standard error. The complete derivation of equation (2.1) has been reported previously for Staphylococcus aureus IsdG,[21] and a similar equation can be derived for $MhuD_{CH}$.

The Abs-detected titrations were analyzed to extract K_{d2} for MhuD and $MhuD_{CH}$. The Abs intensity at 410 nm for a mixture of MhuD, MhuD–diheme, MhuD–heme, and heme depends upon equation (2.2):

$$A_{410} = \frac{\varepsilon_{MhuD-diheme}[MhuD_T][heme]^2 + \varepsilon_{MhuD-heme}K_{d2}[MhuD_T][heme]}{[heme]^2 + K_{d2}[heme] + K_{d1}K_{d2}} + \frac{\varepsilon_{heme}([heme]^3 + K_{d2}[heme]^2 + K_{d1}K_{d2}[heme])}{[heme]^2 + K_{d2}[heme] + K_{d1}K_{d2}} \quad (2.2)$$

where $\varepsilon_{MhuD–diheme}$, $\varepsilon_{MhuD–heme}$, and ε_{heme} are the molar extinction coefficients for MhuD–diheme, MhuD–heme, and heme, respectively, at 410 nm. An equation for [heme] as a function of only K_{d1}, K_{d2}, $[MhuD_T]$, and $[heme_T]$ is derived in Appendix A. The Abs

intensity at 410 nm as a function of [heme$_T$] was fit to equation (2.2) using Graph Pad Prism 7.0 to determine K_{d2} and its standard error. K_{d1} was constrained to the value determined above from analysis of the fluorescence-detected titrations. A similar equation can be derived for MhuD$_{CH}$. The complete derivation of equation (2.2) is available in the Appendix A.

2.3 RESULTS

Heme binding to MhuD. Fluorescence spectroscopy was used to measure K_{d1} for heme dissociation from MhuD–heme. This was accomplished using an assay originally developed for heme-bound *S. aureus* IsdG (IsdG–heme) and IsdI (IsdI–heme),[21] which can also be used for MhuD–heme because Trp66 is within 4 Å of the heme substrate (PDB ID 4NL5).[17] For MhuD, which can sequentially bind two heme substrates,[10] the K_d value extracted from this experiment will correspond to K_{d1} because Trp66 fluorescence will be fully quenched by Förster resonance energy transfer (FRET) to the first heme molecule bound by the active site. The fluorescence-detected titrations of heme into 100 nM MhuD were fit to equation (2.1), yielding a K_{d1} of 4.2 ± 1.4 nM (Figure 1.2). This value is similar to those measured previously for IsdG–heme and IsdI–heme, but three orders of magnitude lower than the ITC-based micromolar value previously reported for MhuD–heme. However, it should be noted that the R^2 value for this fit (0.908) is significantly lower than those previously reported for IsdG–heme and IsdI–heme (0.960 and 0.955, respectively), suggesting an additional interaction between MhuD and heme is not captured by our single-site binding model. Nevertheless, the fitted curve does pass within the error bars of all experimental data points and, as a result, the MhuD

fluorescence experiments suggest that the K_d value for MhuD–heme is in the low nanomolar range.

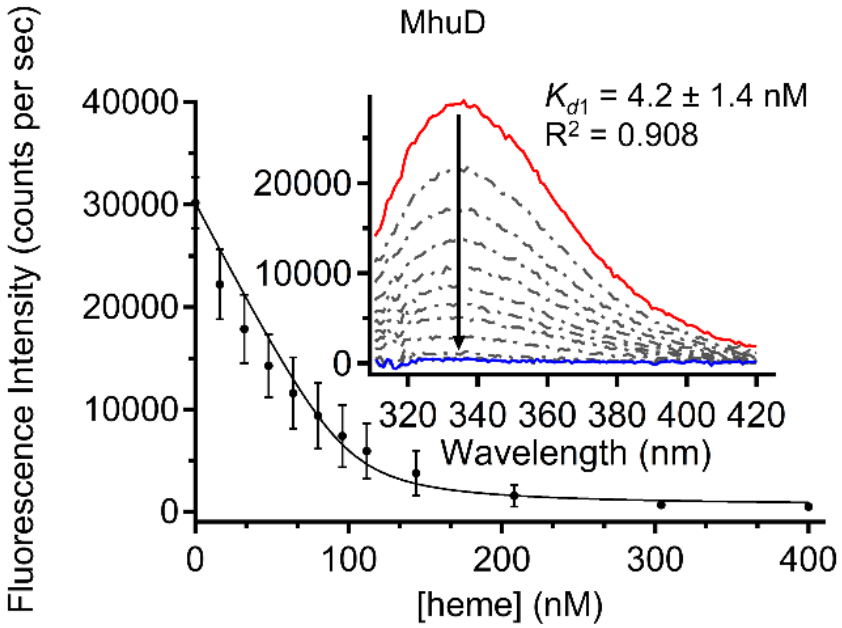

Figure 2. 2. Fluorescence-detected titration of heme into 100 nM MhuD in 50 mM Tris pH 7.4, 150 mM NaCl. The error bars represent the standard deviation of three independent trials. The emission intensity was fit to equation (2.1) yielding a K_{d1} of 4.2 ± 1.4 nM. Inset: Emission spectra with 0 (solid red), 4 (*solid blue*), and intermediate (*dashed gray*) equivalents of heme.

Formation of MhuD–diheme. Following measurement of K_{d1} for MhuD–heme using fluorescence spectroscopy, Abs spectroscopy was used to measure K_{d2} for MhuD–diheme. Abs-detected titrations of heme into 5 μM MhuD were monitored at 410 nm and fit to equation (2.2), which has been derived here as an analytical expression for sequential binding of two substrates to a single protein. As the K_{d1} for MhuD–heme measured at 100 nM is expected to be more accurate than any value measured at 5 μM,

K_{d1} was held constant at its fluorescence-measured value when fitting the Abs-detected heme titration into equation (2.2). These fits yielded a K_{d2} of 4.4 ± 7.2 nM (Figure 2.3). As was the case for the K_{d1} measured here for MhuD–heme, the K_{d2} measured for MhuD–

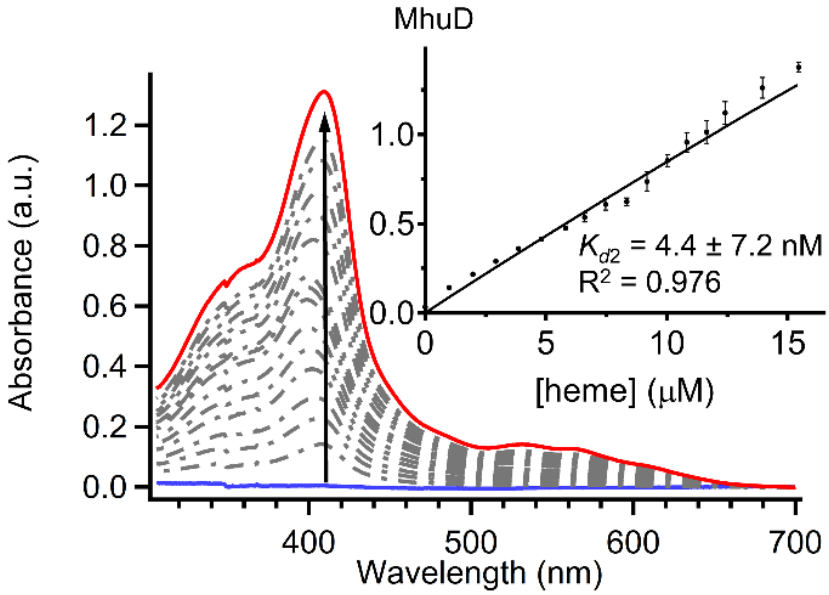

Figure 2. 3. Abs-detected heme titration into 5 μM MhuD in 50 mM Tris pH 7.4, 150 mM NaCl. The spectra represent MhuD with 0 (*solid blue*), 3 (*solid red*), and intermediate (*dashed gray*) equivalents of heme. Inset: The error bars represent the standard deviation of three independent trials. The Abs-detected heme titration was fit to equation (2.2) yielding a K_{d2} of 4.4 ± 7.2 nM.

diheme is significantly lower than that previously measured using ITC.[10] But, careful inspection of the fit to equation (2.2) reveals that the best fit line falls outside the experimental error bars for several data points. Furthermore, the Soret band initially blue-shifts by 6 nm to 401 nm upon addition of up to two equivalents of heme, then red-shifts to 410 nm upon addition of a third equivalent of heme (Table A.2). As was the case for the fluorescence-detected heme titration (Figure 2.2), these data suggest that there is an

additional interaction between MhuD and heme that is not captured by our binding models. These issues with the extraction of K_{d1} and K_{d2} values from analyses of heme titrations into MhuD motivated preparation of a His_6 tag-free version of MhuD.

Heme binding to $MhuD_{CH}$. A His_6 tag-free version of MhuD ($MhuD_{CH}$) was prepared and the K_{d1} for heme dissociation from $MhuD_{CH}$–heme was measured using fluorescence spectroscopy. A tag-free version of *M. tuberculosis* MhuD was obtained from E. coli by designing a recombinant gene for MhuD with an enterokinase cleavable N-terminal His_6 tag. A fluorescence experiment similar to that described above for MhuD–heme was used to determine K_{d1} for heme dissociation from $MhuD_{CH}$–heme. Analysis of these data resulted in a K_{d1} of 7.6 ± 0.8 nM with an R^2 of 0.985 (Figure 2.4). Thus, the K_{d1} values for heme dissociation from MhuD–heme and $MhuD_{CH}$–heme are similar, suggesting that the His_6 tag of MhuD minimally interferes with formation of the MhuD–heme complex. As noted above for MhuD–heme, the K_{d1} for $MhuD_{CH}$–heme is three orders of magnitude lower than the value previously reported for this complex based upon ITC,[10] but similar to those previously reported two other non-canonical heme oxygenases.[21] Nevertheless, since there has been an issue in the literature with the accuracy of K_d values extracted from heme titrations into heme oxygenases,[21, 26] the accuracy of the fit was further assessed.

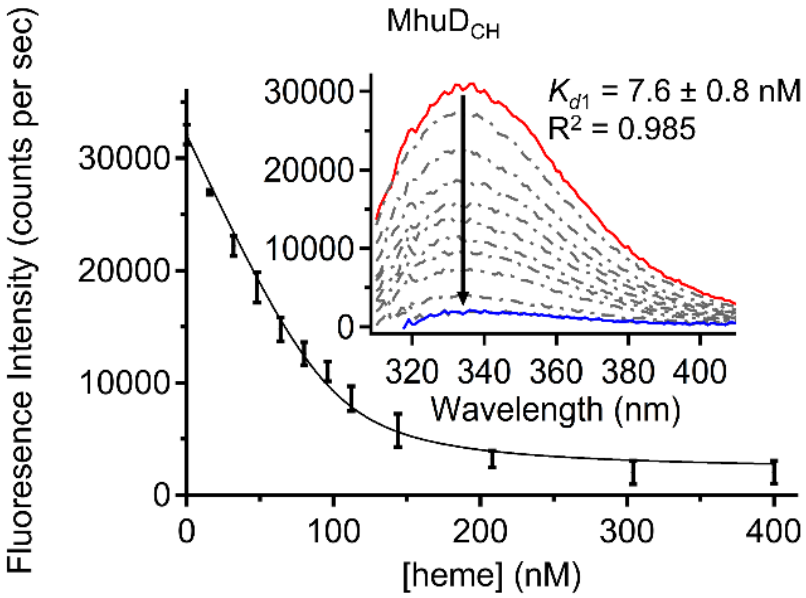

Figure 2. 4. Fluorescence-detected titration of heme into 100 nM MhuD$_{CH}$ in 50 mM Tris pH 7.4, 150 mM NaCl. The error bars represent the standard deviation of three independent trials. The emission intensity was fit to equation (1) yielding a K_{d1} of 7.6 ± 0.8 nM. Inset: Emission spectra with 0 (solid red), 4 (*solid blue*), and intermediate (*dashed gray*) equivalents of heme.

In order to assess the goodness of fit, simulated titration curves for K_{d1} values one order of magnitude smaller and larger than the best fit were compared to the experimental data for MhuD$_{CH}$–heme (Figure 2.5). Decreasing the K_{d1} value from the best fit of 7.6 nM to 0.76 nM lowered R2 from 0.985 to 0.911 and resulted in a simulated titration curve that misses the error bars for six data points. Increasing K_{d1} to 76 nM decreased R2 to 0.398 and produced a simulated curve that missed all but one of the experimental error bars. Thus, these data indicate that the nanomolar value measured here for K_{d1} is

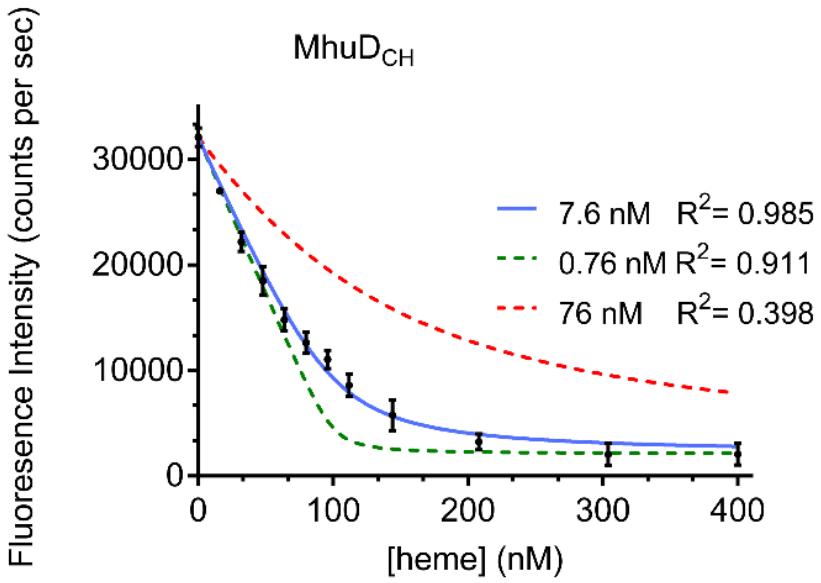

Figure 2. 5. Best fit of the fluorescence-detected heme titrations for MhuD$_{CH}$ using equation (2.1) (*solid blue*). The error bars represent the standard deviation of three independent trials. Titration curves simulated using equation (1) and K_{d1} values one order of magnitude larger (*dashed red*) or smaller (*dashed green*) than the best fit, are inconsistent with experiment.

accurate, and the micromolar value measured previously is actually an upper limit due to the micromolar protein concentration required for ITC.[10] Based upon the data presented in this manuscript, and that reported previously for IsdG–heme and IsdI–heme,[21] it is reasonable to conclude that the Kd for heme dissocation from non-canonical heme oxygenases is nanomolar.

Formation of MhuD$_{CH}$–diheme. The K_{d2} value for heme dissocation from MhuD–diheme was also reinvestigated for a form of MhuD without a His$_6$ tag (MhuD$_{CH}$). As was the case for MhuD–diheme, K_{d2} for heme dissociation from MhuD$_{CH}$–diheme was extracted from an Abs-detected heme titration monitored at 395 nm. Unlike the case

for the Abs-detected titration of heme into MhuD (Figure 2.6), the Soret band steadily blue-shifts from 408 nm to 394 nm upon addition of up to three equivalents of heme (Figure 2.6, Table A.3). Since no interaction between the His_6 tag and the active site of MhuD was observed in the X-ray crystal structure of this species (PDB ID: 3HX9),[10]

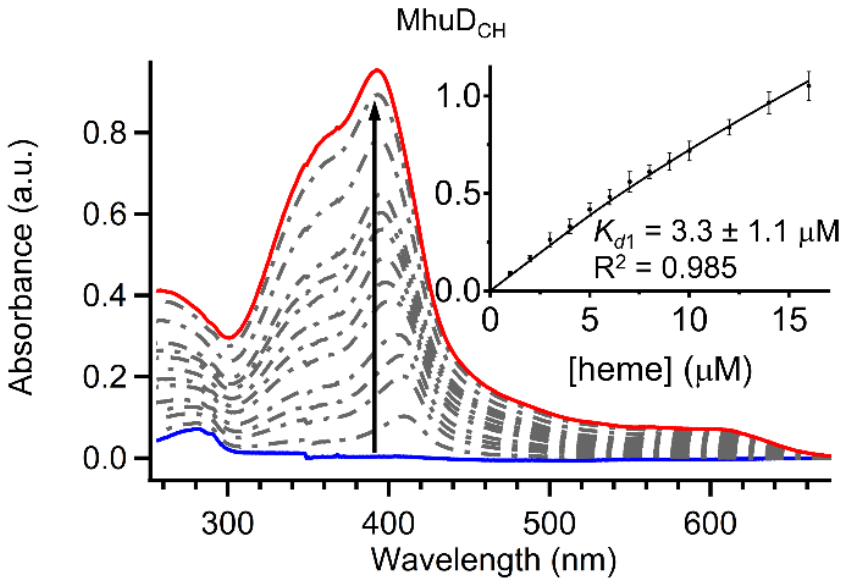

Figure 2. 6. Abs-detected titration of heme into 5 μM MhuD$_{CH}$ in 50 mM Tris pH 7.4, 150 mM NaCl. The spectra represent MhuD$_{CH}$ with 0 (*solid blue*), 3 (*solid red*), and intermediate (*dashed gray*) equivalents of heme. Inset: The error bars represent the standard deviation of three independent trials. The Abs-detected heme titration was fit to equation (2.2) yielding a K_{d2} of 3.3 ± 1.1 μM.

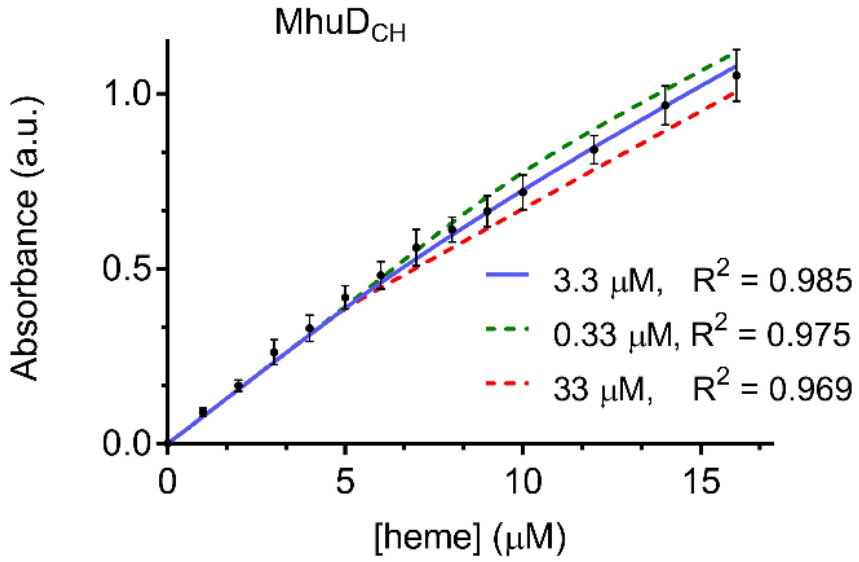

Figure 2. 7. Best fit of the Abs-detected heme titrations for MhuD$_{CH}$ using equation (2.2) (*solid blue*). The error bars represent the standard deviation of three independent trials. Titration curves simulated using equation (2.2) and K_{d2} values one order of magnitude larger (*dashed red*) or smaller (*dashed green*) than the best fit are inconsistent with experiment.

this band shift may be derived from loss of a weak interaction between the His$_6$ tag and labile heme. Analysis of the heme titration data following the methodology outlined above for MhuD–diheme resulted in a K_{d2} of 3.3 ± 1.1 μM for MhuD$_{CH}$–diheme. This value is three orders of magnitude higher than that reported here for MhuD–heme, but similar to the 5.0 ± 0.8 μM value reported previously based upon ITC. The discrepancies between the two K_{d2} values reported in this work, and the one reported in the literature, motivated a careful assessment of the accuracy of the values reported here.

Similar to the strategy described above to assess the accuracy of the fluorescence analysis, the Abs data was compared to simulated titration curves for K_{d2} values one

order of magnitude smaller and larger than the best fit (Figure 2.7). The R^2 value for the fit decreased from 0.985 to 0.975 and 0.969 when titration curves were simulated for K_{d2} values of 0.33 and 33 μM, respectively. Furthermore, the best fit titration curve passes through all experimental error bars for $MhuD_{CH}$–diheme, whereas the fits for K_{d2} values one order of magnitude smaller or larger than the best fit do not. In addition, it is worth restating that the best fit curve for heme dissociation from MhuD–diheme also does not fall within all experimental error bars (Figure 2.3). These analyses strongly suggest that the K_{d2} value reported here for $MhuD_{CH}$–diheme is accurate, and the His_6 tag interferes with measurement of this value. The fact that the K_{d2} value reported previously for MhuD–diheme based upon ITC is consistent with the accurate K_{d2} value reported here for $MhuD_{CH}$–diheme suggests that the interaction between the His_6 tag and the heme substrate has a minimal impact on the thermodynamics of heme binding. In summary, the data presented here indicate that K_{d1} for heme dissociation from $MhuD_{CH}$–heme is 7.6 ± 0.8 nM and K_{d2} for heme dissociation from $MhuD_{CH}$–diheme is 3.3 ± 1.1 μM.

2.4 DISCUSSION

Accuracy of the K_{d1} value. The data presented here strongly suggest that MhuD is a competent heme oxygenase *in vivo* with a nanomolar binding affinity to heme. This is however, three orders of magnitude lower than the reported value in both the original study using ITC,[10] and a recent study using MS.[27] Similar to the original study,[10] a recent MS study also employed micromolar protein concentration to extract the binding constant. The issue with this is that when nanomolar dissociation constant is measured using micromolar protein concentration, it becomes very hard to extract an accurate dissociation constant, as most of the heme would be bound to protein prior to

measurements. Based on the published literature, the concentration of the cytosolic labile heme in *Saccharomyces cerevisiae* and humans is in nanomolar range (20-40 nM).[22, 23] In addition, the K_{d1} value extracted in our study is consistent with those reported in the literature for the heme bound heme oxygenases.[19-21] Moreover, a recent study has reported the K_{d1} of heme binding to MhuD to be in nanomolar range.[28] Similarly, the statistical analysis of the fitting curve shown above for heme binding to MhuD (Figure 2.5) demonstrated that the fitting got worse even with an order of magnitude higher value of the fitted K_{d1}. Therefore, these observations strongly suggest that the K_{d1} for heme binding to MhuD is nanomolar and accurate.

Expected *in vivo* functions of MhuD. The relevance of the K_d values can perhaps be best understood by considering several scenarios. At sub-nanomolar concentrations of labile heme, the measured K_d values imply that MhuD–heme and MhuD–diheme complexes are not stable and will dissociate prior to enzymatic turnover (Figure 2.8), which means that any excess heme biosynthesis or acquisition relative to heme protein loading will increase the labile heme concentration.[2, 3, 29] Once nanomolar concentrations of labile heme are reached, a stable MhuD–heme complex will be formed resulting in heme degradation and a reduction of the heme concentration by one molecule per turnover.[10] In a sense, this means that MhuD can buffer the labile heme concentration at a nanomolar level within *M. tuberculosis*. As mentioned earlier, two recent studies have established that the concentration of the cytosolic labile heme pool in *Homo sapiens* and *Saccharomyces cerevisiae* is 20–40 nM,[22, 23] and notably in human IMR90 lung

fibroblasts and HEK293 cells the labile heme pool is 400–600 nM,[30] so a nanomolar concentration of labile heme within *M. tuberculosis* is conceivable implying that MhuD–

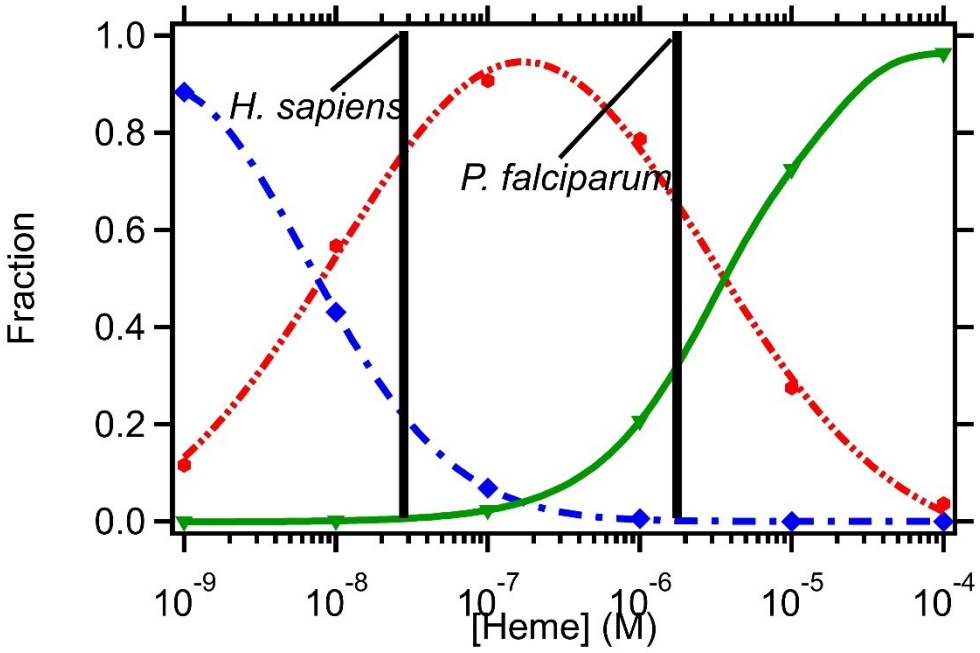

Figure 2. 8. Fractionation of MhuD as a fuction of heme concentration. The curves represent the fraction of MhuD (*dotted blue*), MhuD–heme (*dashed red*), and MhuD–diheme (s*olid green*) present for heme concentrations between 1 nM and 100 μM. Under typical conditions, the primary form of MhuD is MhuD-heme, but significant amounts of MhuD-diheme can be formed under heme replete conditions.

heme is a competent heme oxygenase *in vivo*. Despite the buffering capability of MhuD, it is conceivable that the labile heme concentration within *M. tuberculosis* could increase to micromolar levels if an inadequate amount of MhuD is present to buffer heme and/or if there is a high flux of heme into the organism via the heme acquisition system resulting in formation of a stable MhuD–diheme complex.

The biological function of MhuD–diheme is currently unknown, but here we speculate that MhuD may have a secondary function in its diheme form as a heme storage

or heme sensor/regulatory protein. The diheme form of MhuD is unique among heme oxygenases and is one feature that distinguishes the MhuD enzyme found throughout mycobacteria from the IsdG enzymes found in Gram-positive bacteria and eukaryotic green algae.[10, 26, 31-35] Mycobacteria are a diverse genus that encounter a wide range of heme replete and deplete conditions, and any one of these conditions may be the origin of the MhuD–diheme function. For example, Mycobacterium haemophilum can only utilize heme as its sole exogenous iron source and has no siderophore-dependent iron uptake mechanism;[36, 37] this is also the case for M. leprae.[38, 39] It is compelling to speculate that these two mycobacterial strains utilize MhuD to harbor a second heme molecule as a storage mechanism when faced with an abundance of host heme. Over the 100 nM to 100 μM labile heme concentration range a significant mixture of MhuD–heme and MhuD–diheme would be present, and the storage function may act to slow the rate of heme degradation in order to accommodate the rate of MhuD product utilization by downstream enzymes. Alternatively, the MhuD–diheme form may act as a sensor/regulator, as many bacterial heme uptake systems have been shown to be regulated. In fact, both the Pseudomonas aeruginosa and S. aureus heme uptake systems are regulated by their heme degrading proteins albeit through different mechanisms.[40, 41] Thus, these observations suggest that MhuD may have a dual function throughout mycobacteria, heme degradation and, possibly, heme storage or regulation.

Development of general assays to quantify tetrapyrrole binding by proteins. This work, and a recent publication,[21] describe the development of two assays that could be used to measure dissociation constants for a wide range of tetrapyrroles from a protein site. The fluorescence-based assay employed here to measure K_{d1} for MhuD–heme could

be used to measure K_d for any protein–tetrapyrrole interaction where the protein has a binding site tryptophan and the molecule is a d^1-d^9 metal tetrapyrrole. A large number of protein–cofactor interactions meet these criteria, including heme binding by a number of heme-dependent peroxidases and cytochromes P450.[42-44] The assay relies upon measuring intrinsic Trp fluorescence, which is quenched in close proximity to a d^1-d^9 metal tetrapyrrole be-cause the tetrapyrrole Abs spectrum promotes efficient FRET and the d^1-d^9 transition metal center provides efficient non-radiative relaxation pathways, as a function of tetrapyrrole con-centration. One important limitation of the fluorescence-based assay is spectral interference arising from non-binding site Trp residues and Raman scattering. Fortunately, these limitations can be overcome by subtracting the background fluorescence observed upon complete tetrapyrrole binding and adjusting the detection wavelength, respectively. In summary, this fluorescence assay can be used to quantify binding of heme, vitamin B_{12}, cofactor F_{430}, and their unnatural analogues to any protein with an active site Trp.

The Abs-based assay used here to measure K_{d2} for MhuD–diheme could be used for any protein site that binds two tetrapyrroles sequentially. This assay takes advantage of the intense Abs spectrum of tetrapyrroles,[45] but the mathematical model used for analysis must correct for the relatively unusual situation in protein-ligand binding assays where the free ligand concentration contributes directly to the experimental observable. An approximation-free model for Abs spectroscopy monitored binding of a single tetrapyrrole to a protein site has been described previously,[46] which involves solution of a quadratic polynomial. Here, an approximation-free model for sequential binding of two tetrapyrroles to a single protein site is described, which involves solution of a cubic

polynomial. A range of applications for this assay can be envisaged, including determination of whether heme stacking observed at protein dimer interfaces in several proteins involved in heme uptake by pathogens is physiologically-relevant.[9, 47-50] An important caveat is that the mathematical model described here was explicitly derived for sequential binding, and deviations of the experimental data from this model are indicative of a second binding site or non-sequential binding. In the future, approximation-free models for additional tetrapyrroles or binding sites could be derived in a manner analogous to that described here or by scripting the appropriate mechanism for a software package such as DynaFit.[51, 52]

2.5 CONCLUSION

In conclusion, a comprehensive study of heme binding by *M. tuberculosis* MhuD has been completed. Following removal of the His_6-tag, it was determined that the K_{d1} for heme dissociation from MhuD–heme is 7.6 ± 0.8 nM using a previously described fluorescence-based assay.[21] An Abs assay was developed here to measure K_{d2} for heme dissociation from MhuD–diheme, which was revealed to be 3.3 ± 1.1 μM. The low nanomolar K_{d1} value for MhuD–heme, coupled with the in vitro function of MhuD, establishes this protein as a competent heme oxygenase *in vivo*. Based upon the micromolar K_{d2} value for MhuD–diheme, we speculate that MhuD may have a secondary function as a heme storage or regulatory protein, but the biological function of MhuD–diheme remains an open question that merits further investigation. Finally, it is expected that the assays described here can be used to measure accurate dissociation constants for a wide range of tetrapyrrole-dependent proteins.

2.6 CHAPTER 2 REFERENCES

1. Lawn, S. D.; Zumla, A. I., Tuberculosis. *Lancet*, 2011, *378* (9785), 57-72.

2. Suzuki, K.; Akama, T.; Kawashima, A.; Yoshihara, A.; Yotsu, R. R.; Ishii, N., Current status of leprosy: Epidemiology, basic science and clinical perspectives. *J. Dermatol.*, 2012, *39* (2), 121-129.

3. Tullius, M. V.; Harmston, C. A.; Owens, C. P.; Chim, N.; Morse, R. P.; McMath, L. M.; Iniguez, A.; Kimmey, J. M.; Sawaya, M. R.; Whitelegge, J. P.; Horwitz, M. A.; Goulding, C. W., Discovery and characterization of a unique mycobacterial heme acquisition system. *Proc. Natl. Acad. Sci.*, 2011, *108* (12), 5051-5056.

4. Jones, C. M.; Niederweis, M., Mycobacterium tuberculosis Can Utilize Heme as an Iron Source. *J. Bacteriol.*, 2011, *193* (7), 1767-1770.

5. Weinberg, E. D., Iron and infection. *Microbiol. Rev.*, 1978, *42* (1), 45-66.

6. Owens, C. P.; Chim, N.; Goulding, C. W., Insights on how the Mycobacterium tuberculosis heme uptake pathway can be used as a drug target. *Future Med. Chem.*, 2013, *5* (12), 1391-1403.

7. McLean, K. J.; Munro, A. W., Drug targeting of heme proteins in Mycobacterium tuberculosis. *Drug Discovery Today*, 2017, *22* (3), 566-575.

8. Owens, C. P.; Du, J.; Dawson, J. H.; Goulding, C. W., Characterization of heme ligation properties of Rv0203, a secreted heme binding protein involved in Mycobacterium tuberculosis heme uptake. *Biochemistry*, 2012, *51* (7), 1518-31.

9. Owens, C. P.; Chim, N.; Graves, A. B.; Harmston, C. A.; Iniguez, A.; Contreras, H.; Liptak, M. D.; Goulding, C. W., The Mycobacterium tuberculosis secreted protein Rv0203 transfers heme to membrane proteins MmpL3 and MmpL11. *J. Biol. Chem.*, 2013, *288* (30), 21714-28.

10. Chim, N.; Iniguez, A.; Nguyen, T. Q.; Goulding, C. W., Unusual diheme conformation of the heme-degrading protein from Mycobacterium tuberculosis. *J. Mol. Bio.*, 2010, *395* (3), 595-608.

11. Nambu, S.; Matsui, T.; Goulding, C. W.; Takahashi, S.; Ikeda-Saito, M., A new way to degrade heme: the Mycobacterium tuberculosis enzyme MhuD catalyzes heme degradation without generating CO. *J. Biol. Chem.*, 2013, *288* (14), 10101-9.

12. Contreras, H.; Joens, M. S.; McMath, L. M.; Le, V. P.; Tullius, M. V.; Kimmey, J. M.; Bionghi, N.; Horwitz, M. A.; Fitzpatrick, J. A.; Goulding, C. W., Characterization of a Mycobacterium tuberculosis nanocompartment and its potential cargo proteins. *J. Biol. Chem.*, 2014, *289* (26), 18279-89.

13. Wilks, A.; Heinzl, G., Heme oxygenation and the widening paradigm of heme degradation. *Arch. Biochem. Biophys.*, 2014, *544*, 87-95.

14. Contreras, H.; Chim, N.; Credali, A.; Goulding, C. W., Heme uptake in bacterial pathogens. *Curr. Opin. Chem. Biol.*, 2014, *19*, 34-41.

15. Wilks, A.; Ikeda-Saito, M., Heme Utilization by Pathogenic Bacteria: Not All Pathways Lead to Biliverdin. *Acc. Chem. Res.*, 2014, *47* (8), 2291-2298.

16. Matsui, T.; Nambu, S.; Goulding, C. W.; Takahashi, S.; Fujii, H.; Ikeda-Saito, M., Unique coupling of mono- and dioxygenase chemistries in a single active site promotes heme degradation. *Proc. Natl. Acad. Sci.*, 2016, *113* (14), 3779-84.

17. Graves, A. B.; Morse, R. P.; Chao, A.; Iniguez, A.; Goulding, C. W.; Liptak, M. D., Crystallographic and spectroscopic insights into heme degradation by Mycobacterium tuberculosis MhuD. *Inorg. Chem.*, 2014, *53* (12), 5931-40.

18. Graves, A. B.; Graves, M. T.; Liptak, M. D., Measurement of Heme Ruffling Changes in MhuD Using UV-vis Spectroscopy. *J. Phys. Chem. B*, 2016, *120* (16), 3844-53.

19. Koga, S.; Yoshihara, S.; Bando, H.; Yamasaki, K.; Higashimoto, Y.; Noguchi, M.; Sueda, S.; Komatsu, H.; Sakamoto, H., Development of a heme sensor using fluorescently labeled heme oxygenase-1. *Anal. Biochem.*, 2013, *433* (1), 2-9.

20. Fleischhacker, A. S.; Sharma, A.; Choi, M.; Spencer, A. M.; Bagai, I.; Hoffman, B. M.; Ragsdale, S. W., The C-Terminal Heme Regulatory Motifs of Heme Oxygenase-2 Are Redox-Regulated Heme Binding Sites. *Biochemistry*, 2015, *54* (17), 2709-2718.

21. Conger, M. A.; Pokhrel, D.; Liptak, M. D., Tight binding of heme to Staphylococcus aureus IsdG and IsdI precludes design of a competitive inhibitor. *Metallomics*, 2017, *9* (5), 556-563.

22. Song, Y.; Yang, M.; Wegner, S. V.; Zhao, J.; Zhu, R.; Wu, Y.; He, C.; Chen, P. R., A Genetically Encoded FRET Sensor for Intracellular Heme. *ACS Chem. Biol.*, 2015, *10* (7), 1610-5.

23. Hanna, D. A.; Harvey, R. M.; Martinez-Guzman, O.; Yuan, X.; Chandrasekharan, B.; Raju, G.; Outten, F. W.; Hamza, I.; Reddi, A. R., Heme dynamics and trafficking factors revealed by genetically encoded fluorescent heme sensors. *Proc. Natl. Acad. Sci.*, 2016, *113* (27), 7539-44.

24. Anzaldi, L. L.; Skaar, E. P., Overcoming the heme paradox: heme toxicity and tolerance in bacterial pathogens. *Infect. Immun.*, 2010, *78* (12), 4977-89.

25. Berry, E. A.; Trumpower, B. L., Simultaneous determination of hemes a, b, and c from pyridine hemochrome spectra. *Anal. Biochem.*, 1987, *161* (1), 1-15.

26. Skaar, E. P.; Gaspar, A. H.; Schneewind, O., IsdG and IsdI, heme-degrading enzymes in the cytoplasm of Staphylococcus aureus. *J. Biol. Chem.*, 2004, *279* (1), 436-43.

27. Matthews, S.; Pacholarz, K. J.; France, A. P.; Jowitt, T. A.; Hay, S.; Barran, P.; Munro, A. W., MhuD from Mycobacterium tuberculosis: Probing a Dual Role in Heme Storage and Degradation. *ACS Infect. Dis.*, 2019, *5* (11), 1855-1866.

28. Chao, A.; Burley, K. H.; Sieminski, P. J.; de Miranda, R.; Chen, X.; Mobley, D. L.; Goulding, C. W., Structure of a Mycobacterium tuberculosis Heme-Degrading Protein, MhuD, Variant in Complex with Its Product. *Biochemistry*, 2019, *58* (46), 4610-4620.

29. Dailey, H. A.; Gerdes, S.; Dailey, T. A.; Burch, J. S.; Phillips, J. D., Noncanonical coproporphyrin-dependent bacterial heme biosynthesis pathway that does not use protoporphyrin. *Proc. Natl. Acad. Sci.*, 2015, *112* (7), 2210-2215.

30. Yuan, X.; Rietzschel, N.; Kwon, H.; Walter Nuno, A. B.; Hanna, D. A.; Phillips, J. D.; Raven, E. L.; Reddi, A. R.; Hamza, I., Regulation of intracellular heme trafficking revealed by subcellular reporters. *Proc. Natl. Acad. Sci.*, 2016, *113* (35), E5144-52.

31. Skaar, E. P.; Gaspar, A. H.; Schneewind, O., Bacillus anthracis IsdG, a heme-degrading monooxygenase. *J. Bacteriol.*, 2006, *188* (3), 1071-80.

32. Puri, S.; O'Brian, M. R., The hmuQ and hmuD genes from Bradyrhizobium japonicum encode heme-degrading enzymes. *J. Bacteriol.*, 2006, *188* (18), 6476-82.

33. Haley, K. P.; Janson, E. M.; Heilbronner, S.; Foster, T. J.; Skaar, E. P., Staphylococcus lugdunensis IsdG liberates iron from host heme. *J. Bacteriol.*, 2011, *193* (18), 4749-57.

34. Duong, T.; Park, K.; Kim, T.; Kang, S. W.; Hahn, M. J.; Hwang, H. Y.; Jang, I.; Oh, H. B.; Kim, K. K., Structural and functional characterization of an Isd-type haem-degradation enzyme from Listeria monocytogenes. *Acta Crystallogr., Sect. D: Biol. Crystallogr.*, 2014, *70* (Pt 3), 615-26.

35. Lojek, L. J.; Farrand, A. J.; Wisecaver, J. H.; Blaby-Haas, C. E.; Michel, B. W.; Merchant, S. S.; Rokas, A.; Skaar, E. P., Chlamydomonas reinhardtii LFO1 Is an IsdG Family Heme Oxygenase. *Msphere*, 2017, *2* (4).

36. Naveh, D.; Yankilewitz, T.; Lagziel, A.; Sompolinsky, D., [Skin granulomata caused by a new microorganism (Mycobacterium haemophilum sp. nov.)]. *Harefuah*, 1978, *95* (1), 5-8.

37. Tufariello, J. M.; Kerantzas, C. A.; Vilcheze, C.; Calder, R. B.; Nordberg, E. K.; Fischer, J. A.; Hartman, T. E.; Yang, E.; Driscoll, T.; Cole, L. E.; Sebra, R.; Maqbool, S. B.; Wattam, A. R.; Jacobs, W. R., The Complete Genome Sequence of the Emerging Pathogen Mycobacterium haemophilum Explains Its Unique Culture Requirements. *Mbio*, 2015, *6* (6).

38. Cole, S. T.; Eiglmeier, K.; Parkhill, J.; James, K. D.; Thomson, N. R.; Wheeler, P. R.; Honore, N.; Garnier, T.; Churcher, C.; Harris, D.; Mungall, K.; Basham, D.; Brown, D.; Chillingworth, T.; Connor, R.; Davies, R. M.; Devlin, K.; Duthoy, S.; Feltwell, T.; Fraser, A.; Hamlin, N.; Holroyd, S.; Hornsby, T.; Jagels, K.; Lacroix, C.; Maclean, J.; Moule, S.; Murphy, L.; Oliver, K.; Quail, M. A.; Rajandream, M. A.; Rutherford, K. M.; Rutter, S.; Seeger, K.; Simon, S.; Simmonds, M.; Skelton, J.; Squares, R.; Squares, S.; Stevens, K.; Taylor, K.; Whitehead, S.; Woodward, J. R.; Barrell, B. G., Massive gene decay in the leprosy bacillus. *Nature*, 2001, *409* (6823), 1007-11.

39. Singh, P.; Benjak, A.; Schuenemann, V. J.; Herbig, A.; Avanzi, C.; Busso, P.; Nieselt, K.; Krause, J.; Vera-Cabrera, L.; Cole, S. T., Insight into the evolution and origin of leprosy bacilli from the genome sequence of Mycobacterium lepromatosis. *Proc. Natl. Acad. Sci.*, 2015, *112* (14), 4459-4464.

40. Mourino, S.; Giardina, B. J.; Reyes-Caballero, H.; Wilks, A., Metabolite-driven Regulation of Heme Uptake by the Biliverdin IXbeta/delta-Selective Heme Oxygenase (HemO) of Pseudomonas aeruginosa. *J. Biol. Chem.*, 2016, *291* (39), 20503-15.

41. Videira, M. A. M.; Lobo, S. A. L.; Silva, L. S. O.; Palmer, D. J.; Warren, M. J.; Prieto, M.; Coutinho, A.; Sousa, F. L.; Fernandes, F.; Saraiva, L. M., Staphylococcus aureus haem biosynthesis and acquisition pathways are linked through haem monooxygenase IsdG. *Mol. Microbiol.*, 2018, *109* (3), 385-400.

42. Poulos, T. L., Heme Enzyme Structure and Function. *Chem. Rev.*, 2014, *114* (7), 3919-3962.

43. Huang, X. Y.; Groves, J. T., Oxygen Activation and Radical Transformations in Heme Proteins and Metalloporphyrins. *Chem. Rev.*, 2018, *118* (5), 2491-2553.

44. Moody, P. C. E.; Raven, E. L., The Nature and Reactivity of Ferryl Heme in Compounds I and II. *Acc. Chem. Res.*, 2018, *51* (2), 427-435.

45. Gouterman, M., Study of the Effects of Substitution on the Absorption Spectra of Porphin. *J. Chem. Phys.*, 1959, *30*, 1139 - 1161.

46. Yi, L.; Ragsdale, S. W., Evidence that the heme regulatory motifs in heme oxygenase-2 serve as a Thiol/Disulfide redox switch regulating heme binding. *J. Biol. Chem.*, 2007, *282* (29), 21056-21067.

47. Chan, A. C. K.; Lelj-Garolla, B.; Rosell, F. I.; Pedersen, K. A.; Mauk, A. G.; Murphy, M. E. P., Cofacial heme binding is linked to dimerization by a bacterial heme transport protein. *J. Mol. Bio.*, 2006, *362* (5), 1108-1119.

48. Aranda, R.; Worley, C. E.; Liu, M.; Bitto, E.; Cates, M. S.; Olson, J. S.; Lei, B.; Phillips, G. N., Bis-methionyl coordination in the crystal structure of the heme-binding domain of the streptococcal cell surface protein shp. *J. Mol. Bio.*, 2007, *374* (2), 374-383.

49. Watanabe, M.; Tanaka, Y.; Suenaga, A.; Kuroda, M.; Yao, M.; Watanabe, N.; Arisaka, F.; Ohta, T.; Tanaka, I.; Tsumoto, K., Structural basis for multimeric heme complexation through a specific protein-heme interaction - The case of the third neat domain of IsdH from Staphylococcus aureus. *J. Biol. Chem.*, 2008, *283* (42), 28649-28659.

50. Mattle, D.; Zeltina, A.; Woo, J. S.; Goetz, B. A.; Locher, K. P., Two Stacked Heme Molecules in the Binding Pocket of the Periplasmic Heme-Binding Protein HmuT from Yersinia pestis. *J. Mol. Bio.*, 2010, *404* (2), 220-231.

51. Kuzmic, P., Dynafit-a Software Package for Enzymology. *Method Enzymol.*, 2009, *467*, 247-280.

52. Kuzmic, P., Program DYNAFIT for the analysis of enzyme kinetic data: Application to HIV proteinase. *Anal. Biochem.*, 1996, *237* (2), 260-273.

CHAPTER 3: THE HEME DEGRADATION PRODUCT OF *MYCOBACTERIUM TUBERCULOSIS* MHUD DEPENDS UPON THE DEGREE OF HEME SUBSTRATE RUFFLING INDUCED BY THE ACTIVE SITE.

3.1 INTRODUCTION

At physiologically relevant temperatures, proteins vibrate around their equilibrium structure and these dynamic motions are often essential for their function. Sometimes dynamic motion is dramatic, as is the case for the domain rearrangements of cobalamin-dependent methionine synthase during enzymatic turnover.[1] Other times, more subtle structural changes have important functions as is the case with the allosteric changes to hemoglobin following binding of molecular oxygen.[2] In heme proteins, a source of dynamic motion is out-of-plane deformations of the heme substrate.[3] For clarity, these motions are described based upon the normal coordinates for distortion from a D_{4h} symmetric tetrapyrrole: waving (e_g), propelling (a_{1u}), doming (a_{2u}), ruffling (b_{1u}), and saddling (b_{2u}).[4] *Mycobacterium tuberculosis* MhuD is an example where a protein active site can induce a dynamic ruffling distortion of a heme substrate. A prominent example of a protein that hosts a dynamic heme is Mycobacterium tuberculosis MhuD.[5] MhuD is a non-canonical heme oxygenase (HO) whose heme substrate undergoes a dynamic ruffling deformation, but it has not you been ascertained whether the substrate dynamics have a functional role.

It has been shown that MhuD binds a dynamic heme and that MhuD degrades heme to a unique product, but a connection between heme ruffling and mycobilin production has been elusive. Magnetic measurements have shown that the large ruffling deformation observed in the X-ray crystal structure of cyanide-inhibited MhuD (MhuD–heme–CN, PDB ID 4NL5) arises from a dynamic heme substrate that is present in solution as an equilibrium mixture of planar and ruffled heme.[5, 6] The populations of these conformations can be tuned by the F23W and W66F substitutions because these

residues act like a vice on the heme substrate (Figure 3.1).[7] As alluded to above, MhuD is a non-canonical HO that degrades heme to mycobilin via a *meso*-hydroxyheme intermediate.[8, 9] Canonical HOs, which degrade heme to biliverdin, also have a *meso*-hydroxyheme intermediate, suggesting the mechanisms of the two enzymes diverge after the first oxygenation reaction.[10] These observations suggest that heme ruffling induced by the MhuD active site may be responsible for the novel trioxygenated product of this enzyme. However, no clear correlation between heme ruffling and HO degradation product has been reported.

To assess whether heme dynamics are correlated with heme degradation, we measured rate constants and identified isomeric products for MhuD-catalyzed heme trioxygenation as a function of substrate conformation. The enzyme catalyzed conversion of heme to *meso*-hydroxyheme is formally a monooxygenation,[9] and the influence of ruffling on the rate of this reaction had previously been assessed using an established assay.[11] Decreased heme ruffling in W66F MhuD is correlated with a decreased rate of MhuD-catalyzed heme monooxygenation.[7] The further oxygenation of *meso*-hydroxyheme to mycobilin is formally a dioxygenation reaction.[9] The rate of this reaction was assessed here by a novel enzyme assay. Finally, we determined the isomeric products of MhuD-catalyzed heme degradation for enzyme variants that stabilize one of two substrate conformations.[5] These experiments have provided important insight into the role of dynamic heme ruffling in the enzymatic mechanism of MhuD.

This article describes a mechanistic study of MhuD-catalyzed heme trioxygenation carried out using UV/Vis absorption (Abs) spectroscopy and mass spectrometry (MS). Using a previously described UV/Vis Abs-based assay,[11] the rates of

WT, F23W, and W66F MhuD-catalyzed heme monooxygenation were measured by monitoring the disappearance of the Soret band. Next, the rate of *meso*-hydroxyheme oxygenation was quantified by analyzing the time course of a UV/Vis Abs band in the

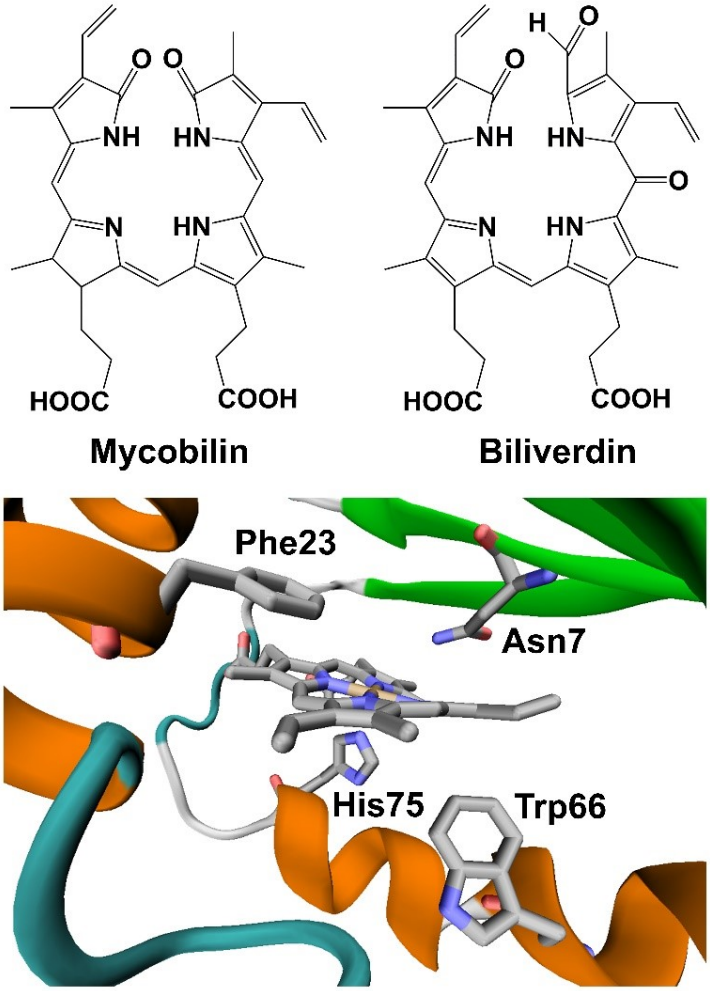

Figure 3. 1. MhuD is a non-canonical heme oxygenase whose heme degradation products and active site structure differ from canonical enzymes. MhuD produces a trioxygenated mycobilin product, whereas canonical heme oxygenases generate dioxygenated biliverdin (*top*). His75 is a first-sphere ligand to the heme substrate. Asn7, Phe23, and Trp66 are second-sphere ligands that perturb the heme substrate via non-bonding interactions (*bottom*).

red region of the spectrum. The heme degradation products of WT, F23W, and W66F MhuD were identified using electrospray ionization (ESI)-MS. Each reaction produced multiple heme degradation products, and the major product for each enzyme variant was determined by monitoring the product ratio over a 2 h time course. Finally, tandem liquid chromatography (LC)-MS was employed to determine the product isomer(s) for each reaction. These data have provided significant new insight into the enzymatic mechanism of MhuD and revealed a new example of protein function derived from protein dynamics.

3.2 EXPERIMENTAL

All reagents were purchase from Fisher Scientific and used without further purification unless noted otherwise.

Protein expression and purification. WT, F23W, and W66F MhuD were expressed as described previously. Briefly, a pET-22b (Ampr) plasmid encoding WT mhuD was a gift from Prof. Celia Goulding (University of California-Irvine).[11] The F23W and W66F mutations were introduced using QuikChange site-directed mutagenesis kits (Agilent).[5, 7] All three MhuD variants were overexpressed in BL21-GOLD (DE3) cells, grown aerobically in Luria-Bertani (LB) medium, as described previously.[11]

WT, F23W, and W66F MhuD were purified in a manner similar to that previously described for WT enzyme. WT MhuD was purified using an ÄKTA pure 25 L fast protein liquid chromatography (FPLC) system.[12] F23W MhuD was purified similarly, but a 1.3 mM/mL elution gradient was employed (Figure B.1). This procedure yielded 17.6 mg of >99% pure F23W MhuD per liter of LB medium (Figure B.2). W66F MhuD was also purified similarly to WT enzyme, but with an elution gradient of 3.3 mM/mL from

125 to 325 mM imidazole (Figure B.3). Purification of W66F MhuD yielded 14.8 mg of >99% pure protein per liter of growth medium (Figure B.4), as assessed by SDS-PAGE.

UV/Vis Abs spectroscopy. Heme degradation by MhuD variants was assayed in a manner similar to previously described experiments. WT, F23W, and W66F heme-bound MhuD (MhuD–heme) were prepared as previously described.[6, 11] UV/Vis-detected heme degradation assays were performed in a manner similar to that previously described,3 with several exceptions. Briefly, 50 μM MhuD–heme in 50 mM potassium phosphate (KPi) pH 6.0 was reacted with 5 mM ascorbic acid, 10 mM ethylenediaminetetraacetic acid (EDTA), 840 U/mL bovine catalase (Sigma-Aldrich), and 167 U/mL bovine superoxide dismutase at 37 ^{o}C and protected from light. For each enzyme variant, UV/Vis Abs spectra were acquired between 700 and 300 nm with a scan rate of 600 nm/min, a 1.0 nm data interval, and a 0.1 s integration time using a Cary 100 Bio UV-Vis spectrophotometer at 0, 5, 10, 20, 30, 60, and 120 min after mixing.

In addition, the decrease of the Soret band (412 nm) and the growth of the 620 nm feature for heme degradation by F23W MhuD was monitored by acquiring an Abs spectra of 20 μM F23W MhuD–heme in 50 mM KPi pH 6.0 reacted with 2 mM ascorbic acid, 5 mM EDTA, 840 U/mL bovine catalase (Sigma-Aldrich), and 167 U/mL bovine superoxide dismutase at room temperature protected from light. The spectra were taken every 60 s for 120 min at 600 nm/min, using a 0.1 s digital integration time, 2 nm bandwidth, and 1.0 nm data interval.

Kinetic information was extracted from the UV/Vis Abs data via non-linear least squares fitting to kinetic models. The decrease of the MhuD–heme Soret band as a function of time was fit to a pseudo-first order kinetic model:

$$A_{Soret} = \left(A_{Soret,0} - A_{Soret,\infty}\right)e^{-k_1 t} + A_{Soret,\infty} \quad (3.1)$$

where $A_{Soret,0}$ is the absorbance at 0 min, $A_{Soret,\infty}$ is the absorbance at ∞ min, and k_1 is the rate constant for heme monooxygenation. The decrease of the Soret band absorption intensity versus time was fit to equation 3.1 using GraphPad Prism 8.0 in order to extract k_1 and its standard error for each MhuD variant. For F23W MhuD, the increase of 620 nm UV/Vis Abs feature was described by the following kinetic model:

$$A_{620} = A_{620,0}\left[e^{-k_1 t} + \left(\frac{\varepsilon_{mh}}{\varepsilon_h}\right)\left(\frac{k_1}{k_2 - k_1}\right)\left(e^{-k_1 t} - e^{-k_2 t}\right)\right] \quad (3.2)$$

where $A_{620,0}$ is the absorbance at 0 min, k_1 is the rate constant for F23W MhuD-catalyze heme monooxygenation determined from fitting the Soret band decrease to equation 3.1, ε_{mh} is the molar extinction coefficient for *meso*-hydroxyheme, ε_h is the molar extinction coefficient for heme, and k_2 is the rate constant for heme dioxygenation. ε_h was determined based upon the pyridine hemochrome assay.[13] The change in absorbance at 620 nm versus time was fit to equation 3.2 using GraphPad Prism 8.0 to extract k_2, ε_{mh}, and their standard errors. Complete derivations of equations 3.1 and 3.2 are available in the Appendix B.

ESI-MS. ESI-MS was also used to monitor heme degradation for WT, F23W, and W66F MhuD as a function of time. WT, F23W, and W66F MhuD samples with partially degraded heme were prepared as described above and flash frozen in liquid nitrogen

(Airgas) after 0, 5, 10, 20, 30, 60 and 120 min of reaction time. In addition, a control experiment was performed where 50 μM hemin chloride in 50 mM KPi pH 6.0 was reacted with 5 mM ascorbic acid, 10 mM EDTA, 840 U/mL bovine catalase (Sigma-Aldrich), and 167 U/mL bovine superoxide dismutase at 37 ºC for 120 min before flash freezing the sample in liquid nitrogen. ESI-MS data was acquired using a system composed of a Shimadzu Prominence HPLC coupled to an ABI Sciex 4000 QTrap Pro hybrid triple-quadrupole/linear ion trap. All 22 reactions were loaded onto a C18 column equilibrated with 2% acetonitrile (MeCN) with 0.1% formic acid (v/v) in water (v/v), and eluted with a linear gradient from 2% to 98% MeCN with 0.1% formic acid (v/v) in water (v/v) over 50 min. ESI-MS data for 600-1500 m/z was acquired in positive ion mode.

The ESI-MS data were analyzed in order to determine the heme degradation products of WT, F23W, and W66F MhuD as a function of time. Ions with m/z of 583, 611, and 616 m/z eluted after 20.8, 22.8, and 23.8 min of the linear MeCN gradient described above. Ion chromatograms (EIC) of the target ions (m/z 583, 611 and 616) were extracted from the total ion chromatogram from each ESI-MS run using BioAnalyst 1.5. The averaged background spectra from the baseline of the chromatogram preceding each chromatographic peak in each EIC were subtracted from the averaged spectra of the chromatographic peak to produce background subtracted spectra for each target ion. The integrated peak area for each EIC of the target ions was used to calculate the relative abundances of the target ions for each time-point.

Tandem LC-MS. Tandem LC-MS experiments were employed to further characterize each of the major ions produced by the WT, F23W, and W66F MhuD-catalyzed reactions. Tandem LC-MS data were obtained for the 583, 611 and 616 m/z

parent ions with a collision energy of 44 mV using the same system described above. A third quadrupole was used as a linear ion trap to scan the fragmentation products of these parent ions. To improve chromatographic resolution of four 583 m/z isomers, ESI-MS data for a WT, F23W and W66F MhuD sample with a 120 min reaction time was eluted with a modified linear gradient from 2% to 82% MeCN with 0.1% formic acid (v/v) in water (v/v) over 38 min. The tandem LC-MS data was analyzed in order to determine the product isomer(s) for each enzyme-catalyzed reaction. Finally, tandem LC-MS data was also acquired 50 μM hemin chloride in 50 mM KPi pH 6.0. Background subtracted tandem LC-MS chromatograms were extracted using BioAnalyst 1.5 as described above for the ESI-MS data.

3.3 RESULTS

Second-sphere substitutions alter MhuD reaction mechanism. Abs spectroscopy was used to monitor the heme degradation by WT MhuD at 0, 5, 10, 15, 20, 30, 60 and 120 mins. After 0 min time-point, the intensity of the Soret band at 407 nm decreased until 30 min without the observable band shift. After 30 mins, the intensity of the Soret band further decreased, and blue shifted to 399 nm. The intensity of the Q-band peaks also decreased with time, and a peak at 540 nm was observed. As expected, these data suggest that the heme is being degraded by WT MhuD to possibly mycobilin (Figure B.5). This is similar to what has been observed in the past studies.[8]

Next, using similar reaction conditions, heme degradation by F23W MhuD was monitored using the Abs spectroscopy. During the heme degradation, the Soret band at 412 nm (0 min) decreased in intensity and blue-shifted to 407 nm (120 min) (Figure 3.2). The relative decrease of the Soret band intensity in smaller for F23W compared to WT

(Figure B.5). Also, a previous study has shown that the mycobilin bound MhuD has less intense peak in the violet region compared to the *meso*-hydroxyheme bound MhuD.[9] The Q-band at 537 and 560 nm decreased in intensity, however, the intensity of a peak at 620 nm slowly started to increase over time (Figure 3.2). The peak at 620 nm has been attributed to MhuD complexed with *meso*-hydroxyheme.[9] The 620 nm peak started to form immediately and saturated with time. Thus, this suggest a possible *meso*-hydroxyheme intermediate building up with time during the heme degradation by F23W MhuD.

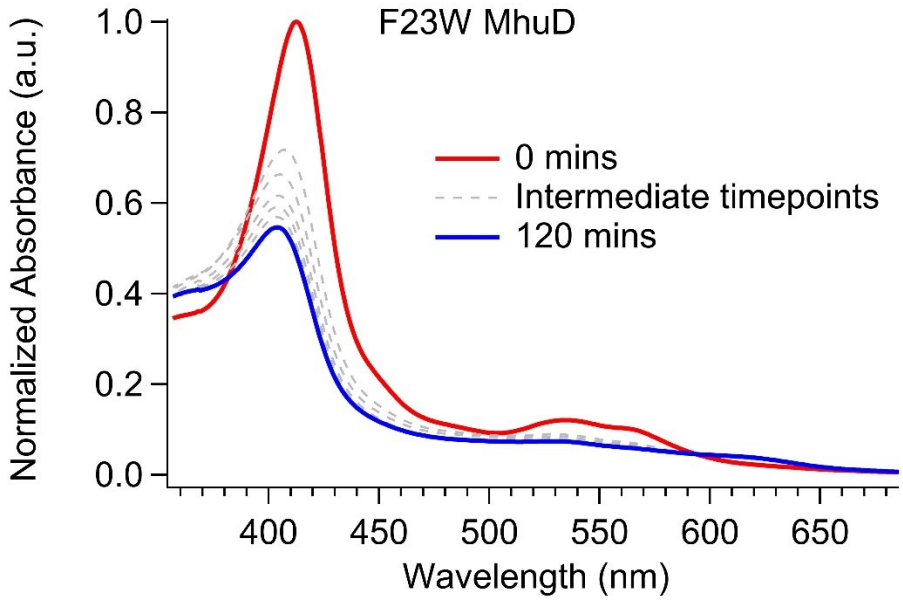

Figure 3. 2. Abs monitored heme degradation by F23W MhuD (50 μM F23W MhuD–heme, 50 mM KPi pH 6.0, 37ºC) monitored at 0 (*red trace*), 5 - 60 (d*otted gray*) and 120 mins (*blue trace*). Peak at 620 nm gradually increases with time.

Finally, using Abs spectroscopy, heme degradation by W66F MhuD was monitored. The heme degradation reaction featured a decrease in the Soret band coupled

with a red shift from 402 to 405 nm (from 0 to 120 mins) (Figure 3.3). The Soret band further red-shifted to 408 nm at 180 mins. Multiple changes were observed at the Q-band region; the 560 nm peak with a shoulder at 601 nm disappeared with time, as the peak at 536 nm with a shoulder at 560 nm grew. Most importantly, a feature at ~690 nm grew over the same time period (Figure 3.3). This would suggest a possible biliverdin formation.[14] Thus, ESI-MS study will be performed to identify possible intermediates and products of heme degradation by WT MhuD and its variants.

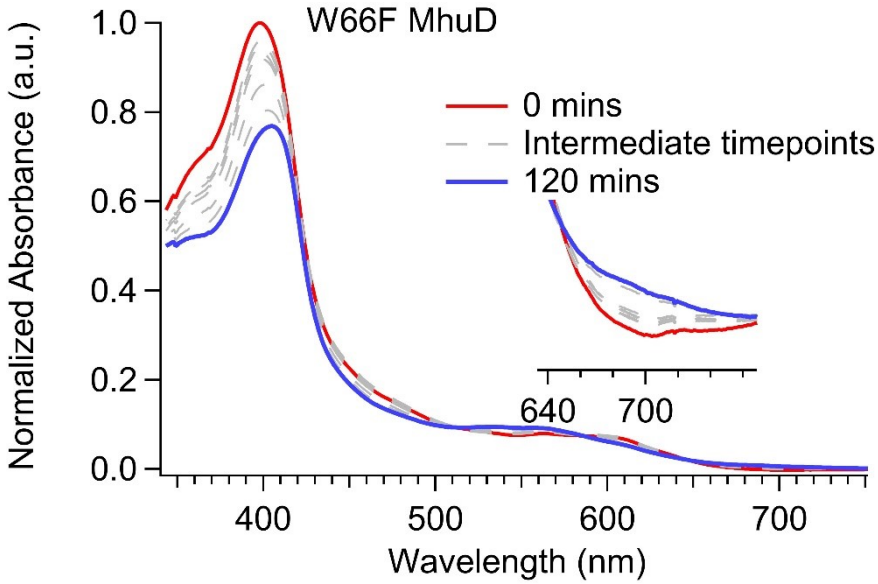

Figure 3. 3. Abs monitored heme degradation by W66F MhuD (50 μM W66F MhuD–heme, 50 mM KPi pH 6.0, 37°C) monitored at 0 (*red trace*), 5 - 60 (*dotted gray*), 120 mins (*blue trace*). Inset: Maximized spectra from 620 - 760 nm.

WT MhuD produces a mixture of mycobilin and biliverdin. The heme degradation sample by WT MhuD was analyzed using ESI-MS. The mass spectrum of the 30 min sample revealed the presence of 3 peaks with m/z 583, 611 and 616, eluting at

20.8, 22.8, and 23.8 mins respectively (Figure B.6). These peaks likely correspond to biliverdin (m/z 583), mycobilin (m/z 611) and heme (m/z 616). However, to confirm this, tandem LC-MS study on each of these peaks were performed. For, m/z 616, hemin chloride solution was analyzed. The fragmentation pattern of the m/z 616 is the same as the one observed for hemin chloride (Figure 3.4 and B.7). Major fragments observed are m/z 557 and m/z 498, corresponding to the loss of CH_2COOH and $(CH_2COOH)_2$ respectively. This implies that the m/z 616 is the undegraded heme molecule.

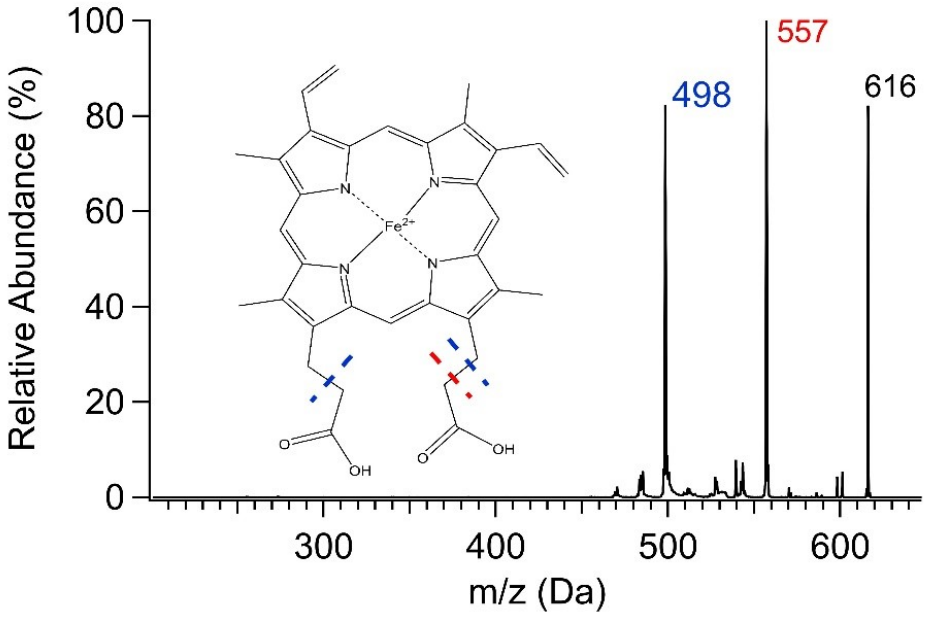

Figure 3. 4. MS/MS spectrum of m/z 616. Two major daughter fragments of m/z 557 and m/z 498 is observed corresponding to loss of CH_2COOH (*red dotted line*) and $(CH_2COOH)_2$ (*blue dotted line*) respectively. Fragment ions of m/z 616 matches up with that of hemin chloride (Figure B.7.).

Similarly, tandem LC-MS on the m/z 611 was also performed for the 30 min sample of heme degradation by WT MhuD. The m/z 611 likely corresponds to mycobilin, which has been observed in previous studies as well.[8] The fragment ions observed for MS/MS of m/z 611 are shown in the supplemental section (Figure B.8). Each of the

fragment ions are color matched to where the fragmentation occurs in the mycobilin structure. For example, the largest fragment ion corresponding to m/z 476 results from the cleavage below the δ-*meso* carbon (red dashed line, Figure B.8). In a similar way, other fragment ions can be traced back to the mycobilin structure. Therefore, the m/z 611 peak is most likely mycobilin. As expected, it has the highest relative intensity compared to other peaks (Figure B.6).

Finally, tandem LC-MS was performed on the m/z 583 peak, and a single fragment ion of m/z 297 was observed (Figure B.9). The m/z 297 is due to the fragmentation at the γ-meso carbon position. This likely suggests that m/z 583 peak corresponds to biliverdin. This is a surprising and an interesting find as biliverdin is a major product formed during the heme degradation by canonical heme oxygenase.[15] A recent study has identified biliverdin as the major product of R26S MhuD.[16] However, it is the first time it has been observed for WT MhuD. Therefore, to investigate whether this peak arises from enzymatic turnover or coupled oxidation, a control degradation assay was performed using just hemin chloride instead of heme bound MhuD. 120 min of this sample injected onto the ESI-MS showed the presence of m/z 583 in a miniscule amount (Figure B.10). The relative abundance of m/z 583 compared to the heme peak (m/z 616) is ~2%. This value is significantly lower than the value observed for the heme degradation by WT MhuD (Figure B.6). This implies that the m/z 583 peak arises from the enzymatic turnover. Therefore, these data suggest that WT MhuD is degrading heme to produce a mixture of mycobilin and biliverdin.

Second-sphere substitutions alter identity of primary reaction product. Next, to analyze the formation of mycobilin and biliverdin during the heme degradation by WT

MhuD, the reaction mixtures were monitored as a function of time using ESI-MS to get a better understanding of the product distribution (Figure 3.5). Similar to the Abs assay, the reaction was monitored at 0, 5, 10, 20, 30, 60 and 120 mins. Initially, the ratio of mycobilin to biliverdin was small but with time, the major product is clearly identified as mycobilin, and biliverdin is observed as the minor product. The amount of biliverdin formation stays consistent after 60 mins, however, the amount of mycobilin formation increases with time. One explanation on the biliverdin formation can be rationalized from the fact that MhuD can accommodate dynamic heme in its active site. Thus, the ruffled and planar heme conformation may be important in formation of different heme degradation products.

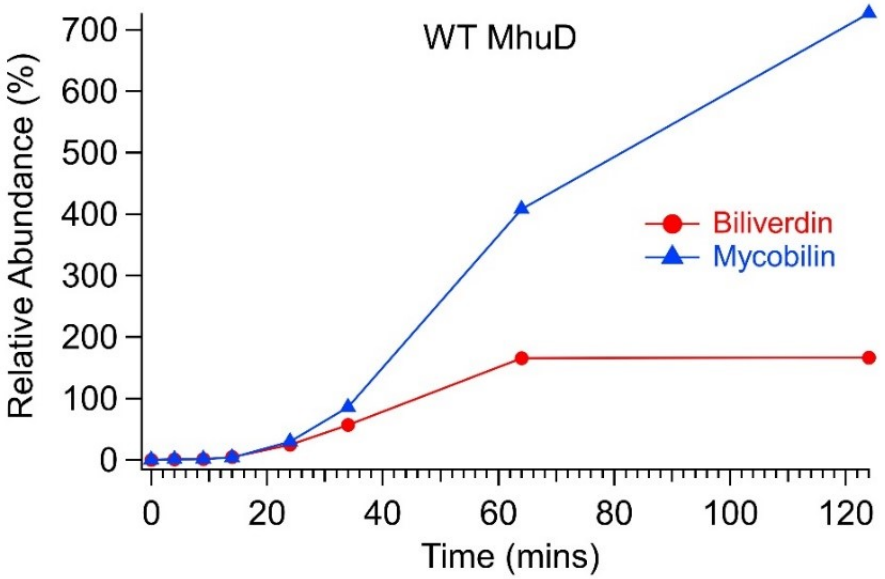

Figure 3. 5. Time-resolved ESI-MS study on heme degradation by WT MhuD. Formation of mycobilin and biliverdin is plotted as relative abundance (%) against heme as a function of time. Sample at each time-point has 4 mins delay taken up by thawing and injecting process. Thus, 0 min time-point sample is 50 μM WT MhuD–heme (50 mM KPi pH 6.0, 37°C).

Time-dependent MS study was performed on the heme degradation sample by F23W MhuD, because it has been shown that the F23W substitution induces more ruffled conformation of heme compared to WT MhuD.[5] The heme degradation study by F23W MhuD was similar to the one performed for WT MhuD. Like WT MhuD, the study on heme degradation by F23W MhuD showed mycobilin as the major product and biliverdin as the minor product (Figure 3.6). However, as expected, the enzymatic activity is slower than WT MhuD. UV/Vis assay suggested a possible *meso*-hydroxyheme intermediate being observed during the heme degradation by F23W MhuD. This may explain why there is a noticeably lag in mycobilin formation. Thus, the increased ruffling, did not change the product identity, but may have considerably slowed down the conversion of *meso*-hydroxyheme to mycobilin.

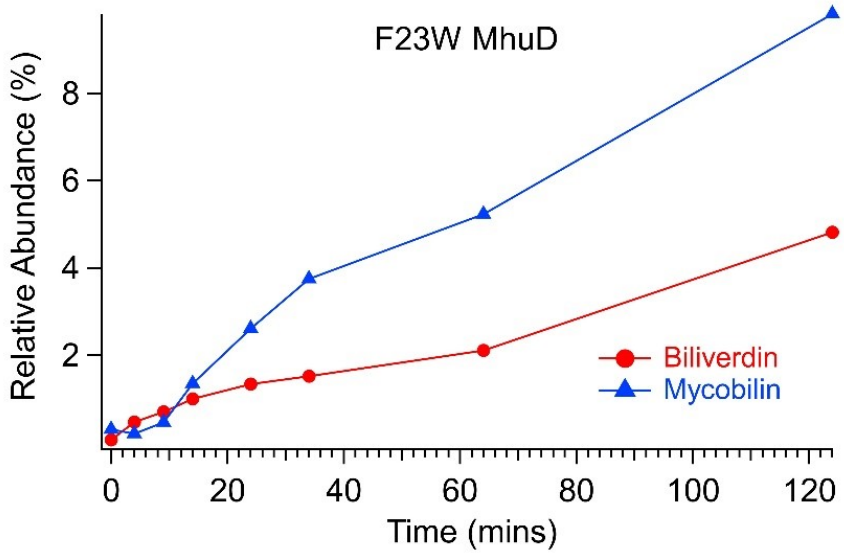

Figure 3. 6. Time-resolved ESI-MS study on heme degradation by F23W MhuD. Formation of mycobilin and biliverdin is plotted as relative abundance (%) against heme as a function of time. Sample at each time-point has 4 mins delay taken up by thawing and injecting process. Thus, 0 min time-point sample is 50 μM F23W MhuD–heme (50 mM KPi pH 6.0, 37°C).

Next, a time-dependent MS study was performed to monitor heme degradation by W66F MhuD, as it has been shown to house more planar heme in its active site than WT MhuD.[6] Unlike, WT and F23W MhuD, heme degradation by W66F MhuD showed biliverdin as the major product and mycobilin as the minor product (Figure 3.7). This confirms the earlier observation (Figure 3.3), where the increase of the feature at ~690 nm suggested biliverdin formation. The biliverdin formation also becomes more apparent at higher timepoints. R26S MhuD is the only variant that has shown to degrade heme to biliverdin.[16] It should also be noted that the enzymatic inefficiency W66F MhuD compared to WT can be clearly observed. Therefore, the decrease in ruffling completely

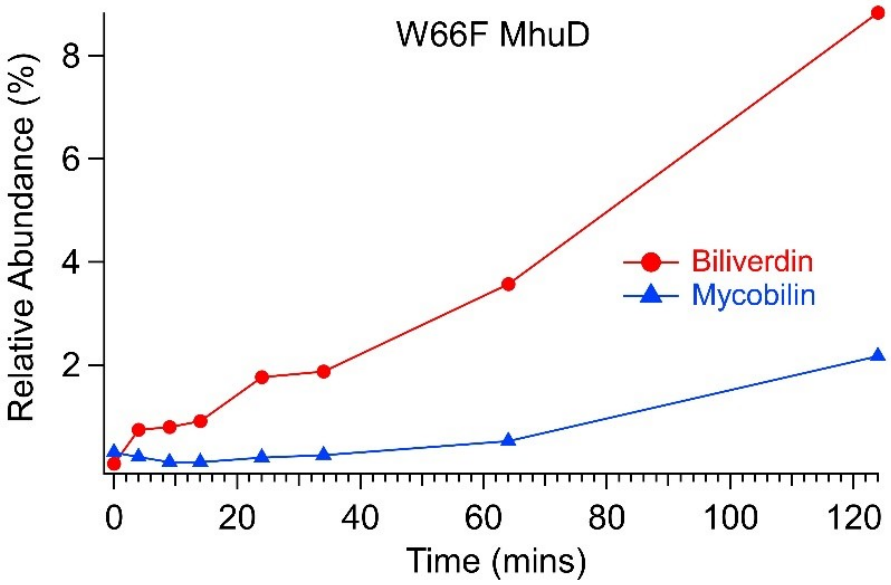

Figure 3. 7. Time-resolved ESI-MS study on heme degradation by W66F MhuD. Formation of mycobilin and biliverdin is plotted as relative abundance (%) against heme as a function of time. Sample at each time-point has 4 mins delay taken up by thawing and injecting process. Thus, 0 min time-point sample is 50 μM W66F MhuD–heme (50 mM KPi pH 6.0, 37ºC).

altered the product identity, and biliverdin is observed as the major product for W66F MhuD.

Second-sphere substitutions alter biliverdin isomer. Tandem LC-MS on the 120 min sample of heme degradation by WT MhuD was performed to identify the biliverdin isomers. Careful inspection of the Mass Ion Chromatogram (MIS) for m/z 583 (biliverdin) in all the runs revealed that multiple peaks correlating to m/z 583 was present. Optimized ESI-MS run revealed four peaks corresponding to m/z 583 eluted at 38.7, 39.0, 39.4 and 40.2 mins for WT MhuD (Figure B.11). Tandem LC-MS performed on all the four m/z 583 peaks showed distinct fragmentation pattern (Figure 3.8). The fragment ions typical for α, β and δ-biliverdin is m/z 297, 343 and 402 respectively, and the fragment ions corresponding to each of the biliverdin isomers except γ-biliverdin has previously been assigned.[17, 18] Therefore, the m/z 583 peak having the major MS/MS fragment ion of m/z 555 was assigned to γ-biliverdin (Figure 3.9). By identifying the major MS/MS fragment ions of each peak, the biliverdin isomers for the eluted peaks were assigned in the following order: α, δ, β and γ (Figure 3.8, Figure B.11). Also, the elution order for the biliverdin isomers remained same as observed in previous studies. The presence of all the biliverdin isomers as the minor product during heme degradation by WT MhuD is very interesting, and thus, similar tandem LC-MS study was performed to identify the biliverdin isomers formed during heme degradation by F23W and W66F MhuD.

Tandem LC-MS on the heme degradation sample at 120 min by F23W MhuD was performed. Using the similar analysis performed for WT MhuD, the largest observed fragment ions were matched with their corresponding biliverdin isomer. Thus, β, δ and α-

biliverdin isomers were identified and labeled (Figure B.12). Unlike WT MhuD, γ-biliverdin isomers was not observed. The mutation of Phe23 to Trp may sterically hinder the oxygenation at the γ-*meso*-carbon. Therefore, the lack of regioselectivity observed for the formation of the biliverdin isomers by WT and F23W MhuD questions whether this reaction is proceeding enzymatically.

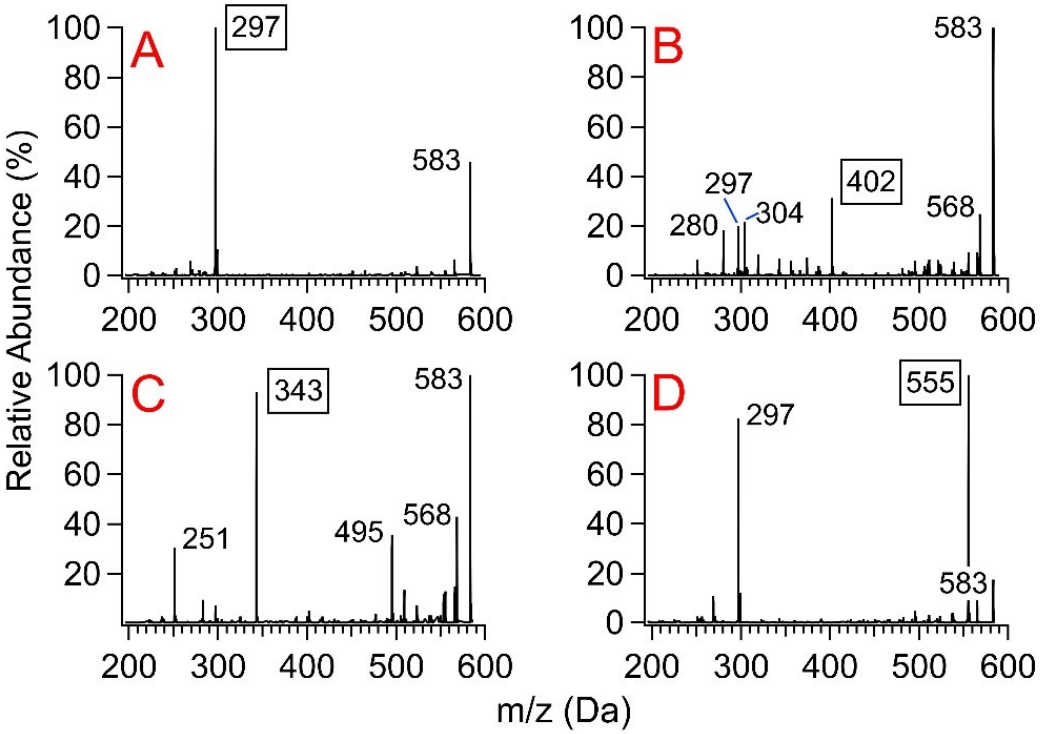

Figure 3. 8. MS/MS spectra of each chromatographic peak corresponding to m/z 583 ran for 120 min heme degradation sample by WT MhuD. Spectra A-C were assigned as α, δ and β-biliverdin respectively, based on their assignment from previous studies.[17, 18] Spectra D has major fragments (m/z 555 and m/z 297) that hasn't been assigned before and is assigned to γ-biliverdin. Spectra A-D is put here according to their elution order (Figure B.11).

Finally, the heme degradation sample at 120 min by W66F MhuD was analyzed using tandem LC-MS. It should be noted that the retention time observed for the ESI-MS chromatogram involving biliverdin isomers did not stay consistent between WT, F23W and W66F runs. However, this would not affect the identity of biliverdin isomers as they were identified using the fragment ions from tandem LC-MS run. Tandem LC-MS reveled that W66F MhuD degrades heme to α-biliverdin predominantly (Figure B.12), with a very small amount of β-biliverdin. To date, this is the second MhuD variant after R26S to have been able to degrade heme to α-biliverdin. Also, the presence of predominantly one biliverdin isomer suggests that the formation of biliverdin by W66F MhuD is regioselective and is formed enzymatically.

Second-sphere amino acid substitution effect the rate of heme degradation. A kinetic study was done due to the observed 620 nm peak during the Abs-monitored heme degradation by F23W MhuD (Figure 3.2). This was performed to extract the rate constant of the monooxygenation of heme by monitoring the Soret band, and of the dioxygenation of *meso*-hydroxyheme by monitoring the 620 nm peak, at RT. The decreased Soret band monitored as a function of time was fit to a pseudo-first order kinetic model using equation (3.1) (Figure B.13). A heme monooxygenation rate constant (k_1) of 0.0253 ± 0.0002 min^{-1} was extracted from the fit with a R^2 value of 0.9931. Next, the increase of the Q-band at 620 nm was monitored as a function of time and fit to a kinetic model described by equation (3.2) to extract the rate constant for the dioxygenation reaction. The dioxygenation rate constant (k_2) was extracted to be vanishingly small with R^2 of 0.9950 (Figure 3.9). Comparing the two rate constants, the initial monooxygenation is observed to be 13 orders of magnitude faster process than the dioxygenation.

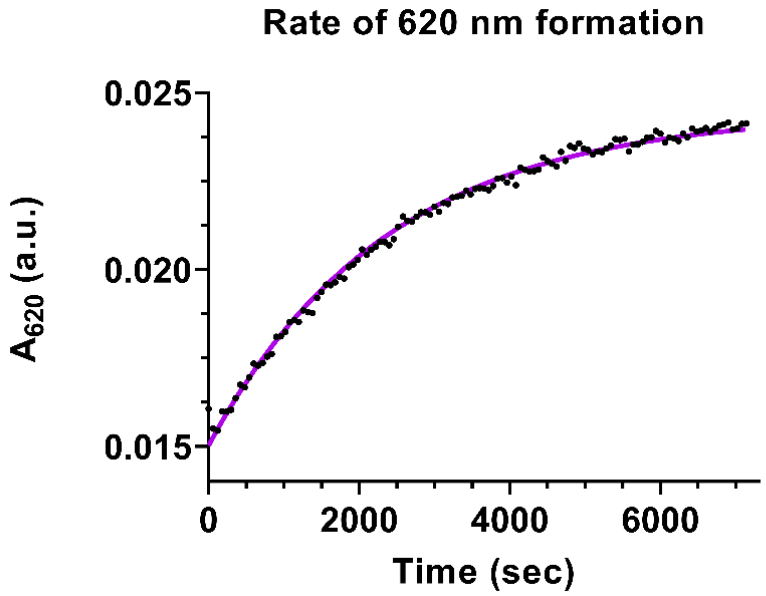

Figure 3. 97. 620 nm peak was monitored during the heme degradation by F23W MhuD as a function of time and fitted using a kinetic model described in equation (3.2). The fitting gave a rate of 1.645 x 10^{-15} ± 3.618 x 10^{-7} min^{-1} for dioxygenation reaction (k_2), with a R^2 of 0.9950. Black dots represent the experimental data and the purple line represents the fitted data.

To further understand the impact of heme ruffling on the heme monooxygenation, kinetic analysis was performed to extract the rate of heme monooxygenation by WT, W66F and F23W MhuD at 37ºC. The data was analyzed using equation (3.1) by monitoring the disappearance of the Soret band of each variants. The rate of heme monooxygenation observed for W66F is much slower than observed for WT and F23W MhuD (Figure B.14, Table 2.1). It is 16 times slower than WT and 31 times slower than F23W MhuD.

Next, the observed rate of heme monooxygenation by F23W is twice as observed for WT MhuD. However, the kinetic fitting graph (Figure B.14) shows that the

disappearance of the Soret band in F23W is not as efficient as observed in WT MhuD. This may be explained by the difference between the Abs intensity of the mycobilin bound vs the *meso*-hydroxyheme bound MhuD.

Table 3. 1. The pseudo first order rate of monooxygenation by WT, F23W and W66F MhuD extracted by monitoring the decrease of Soret band as a function of time at 37°C. The data was fit into equation (3.1), the resulting rate with standard error and R^2 is shown below.

Variant	Rate with standard error (min^{-1})	R^2
W66F	0.00481 ± 0.00362	0.9889
WT	0.07956 ± 0.00520	0.9937
F23W	0.15072 ± 0.01882	0.9661

3.4 DISCUSSION

Implication of heme conformation on product formation. The significance of heme conformations on the enzymatic mechanism by MhuD is poorly understood. The spectroscopic investigation revealed that MhuD has a ruffled ground state, and thermally accessible planar excited state. Planar heme conformation is observed in the active site of the canonical HO, such as HO-1[19] and *C. diphtheriae*-HO,[20] whereas, IsdI from *Staphylococcus aureus* induces one of the largest ruffling deformations known in the biochemical literature (PDB ID 3QGP).[21] The magnitude of heme ruffling induced by MhuD can be tuned by the F23W and W66F substitutions because these residues act like a vice on the heme substrate (Figure 1). Thus, F23W MhuD has increased population of the ruffled comformation[7] compared to wild-type (WT) enzyme, and W66F MhuD[5] has

increased population of planar conformation compared to WT enzyme. UV/Vis and MS studies on heme degradation by MhuD variants presented here suggested that the second-sphere substitution influences the enzymatic mechanism. ESI-MS and tandem LC-MS study provided insights on the role of heme conformation on the formation of the final product by variants of MhuD. Decreased heme ruffling in W66F MhuD completely altered the product identity to α-biliverdin. This would mean that W66F MhuD alters the heme degradation mechanism in a way to afford biliverdin formation. On the other hand, increased heme ruffling did not change the product identity, as mycobilin was identified as the major product for F23W-mediated heme degradation. However, the presence of highly ruffled heme significantly altered the dioxygenation pathway, evidenced by the *meso*-hydroxyheme observation.

Kinetics study was performed by monitoring the Soret and the 620 nm peak to gain insights into the rate of heme monooxygenation and the rate of *meso*-hydroxyheme dioxygenation by F23W MhuD. The 620 nm peak suggests formation of *meso*-hydroxyheme intermediate. Thus, the ruffled heme may have influenced the heme degradation pathway of F23W MhuD to afford the observation of an intermediate. The rate of heme monooxygenation (k_1) was extracted using a pseudo first order kinetic model (equation 3.1) and then was added into the derived kinetic model (equation 3.2) to calculate the rate of dioxygenation of *meso*-hydroxyheme (k_2). The extracted k_2 value is considerably slower than the k_1 value, which means that the formation of heme to *meso*-hydroxyheme is a much faster process than the formation of *meso*-hydroxyheme to mycobilin. Thus, the increased heme ruffling induced by the substitution to bulkier Trp residue at the 23 position seem to slow the dioxygenation reaction. Therefore, these data

would strongly suggest that the heme conformation can play a role in altering the heme degradation mechanism and can also tune the final product formation.

ESI-MS and tandem-MS study identified all the biliverdin isomers as a minor product for WT, whereas, α, β and δ-biliverdin isomers was identified as a minor product for F23W MhuD. This would suggest that there is lack of regioselectivity on biliverdin formation by WT and F23W MhuD. Since miniscule amount of β-biliverdin is observed, the oxygenation reactions seem to be regioselective to α-meso carbons for W66F MhuD and is proceeding enzymatically. All the isomers of biliverdin are observed when heme is degraded through a coupled oxidation pathway in the presence of O_2 and a reductant.[22, 23] In the presence of catalase, the coupled oxidation of myoglobin was inhibited, leading authors to conclude that exogenous peroxide is required for coupled oxidation of myoglobin. However, this study was performed in the presence of catalase and superoxide dismutase. Thus, it is unlikely that MhuD heme degradation reaction produces exogenous peroxide or superoxide. However, it is likely that the reactive oxygen species (ROS) being produced in the active site of MhuD may be causing the coupled oxidation of heme to biliverdin isomers. Therefore, biliverdin formation by WT and F23W MhuD may be proceeding via a non-enzymatic pathway, however, α-biliverdin is being produced enzymatically by W66F MhuD.

Importance of dynamic heme in the conversion of heme to mycobilin. MhuD houses a dynamic heme in its active site, which may be essential for its catalytic activity. UV/Vis and ESI-MS assay suggested that the heme conformation plays a role its degradation mechanism by MhuD. It can be clearly observed that when heme is tuned into a single conformation (ruffled or planar) by the second-sphere amino acid

substitution, the enzymatic activity of MhuD is altered. Thus, to investigate these changes in the enzymatic activity, the rate of change in Soret peak was monitored and fit using a pseudo first order kinetic model (equation 3.1). Surprisingly, the rate of change in Soret peak for F23W is twice as fast compared to WT MhuD. But the decrease in Soret band is more pronounced in WT compared to F23W MhuD (Figure B.14). As mentioned previously, the Soret peak observed for MhuD-*meso*-hydroxyheme complex is much intense than for MhuD-mycobilin complex.[9] Thus, these observations suggest that F23W MhuD is producing *meso*-hydroxyheme instead of degrading heme fully to mycobilin. This result is consistent with the above kinetic study performed for F23W MhuD (Figure 3.10.). On the other hand, W66F is observed to degrade heme very slowly compared to F23W and WT MhuD. The slower rate observed may be due to the decreased heme ruffling induced by the active site of W66F MhuD. The decreased ruffling is altering the enzymatic pathway of W66F MhuD to afford biliverdin formation, and thus it is not surprising that the rate of heme oxidation is slowed down significantly. These observations strongly suggest that the initially ruffled heme may be necessary for the conversion of heme to β/δ-*meso*-hydroxyheme by MhuD. Finally, the inefficient enzymatic pathway that was observed in the absence of either of the heme conformations would strongly suggest that dynamic heme is essential for an efficient conversion of heme to mycobilin by MhuD.

Possible heme degradation mechanism by W66F MhuD. Formation of α-biliverdin proceeds via α-*meso*-hydroxyheme intermediate in the heme degradation mechanism by canonical HO.[10] The initial oxygenation happens at the α-*meso*-carbon through a ferric-hydroperoxo intermediate.[24-26] The ordered hydrogen bonding network is

proposed to act like a OH radical trap and help guide it to the α-meso carbon.[27] This is followed by a subsequent conversion of α-*meso*-hydroxyheme to α-verdoheme intermediate.[28-30] The final oxygenation and the ultimate ring cleavage to form biliverdin is proposed to be initiated by binding of either O_2 or H_2O_2 to ferrous verdoheme.[31-33] However, MhuD does not have the water cluster present in its active site as the canonical HOs, which can guide the initial oxygenation to occur at the α-*meso*-carbon. Thus, it is likely that the heme degradation may proceed via a distinct mechanism. It is possible that it may follow a similar mechanism as proposed for R26S MhuD,[16] to proceed via a diol intermediate.[34] Thus, identifying the C1 product of W66F MhuD-mediated heme degradation would help elucidate the mechanism. But, the enzymatic activity in W66F is not as efficient as compared to R26S MhuD (Chapter 4) and may pose difficulties in identifying the C1 product. Therefore, a comprehensive study to characterize the C1 product of W66F MhuD is warranted.

3.5 CONCLUSION

In conclusion, Abs and MS study suggest that heme degradation by MhuD depends on the heme distortions induced by the active site. Highly ruffled heme altered the mechanism by affording a *meso*-hydroxyheme intermediate, and the kinetics study confirmed that the conversion of *meso*-hydroxyheme to mycobilin is very inefficient. Increased ruffling was observed to enhance the initial monooxygenation of heme to *meso*-hydroxyheme. In contrast, planar heme slowed down the degradation of heme by MhuD and completely changed the mechanism to afford biliverdin as the major product. Therefore, dynamic heme substrate is required for the heme degradation by MhuD.

3.6 CHAPTER 3 REFERENCES

1. Bandarian, V.; Ludwig, M. L.; Matthews, R. G., Factors modulating conformational equilibria in large modular proteins: a case study with cobalamin-dependent methionine synthase. *Proc. Natl. Acad. Sci.*, 2003, *100* (14), 8156-63.

2. Perutz, M. F., Stereochemistry of cooperative effects in haemoglobin. *Nature*, 1970, *228* (5273), 726-39.

3. John A. Shelnutt, X.-Z. S., Jian-Guo Ma, Song-Ling Jia, Walter Jentzen, Craig J. Medforth, Craig J. Medforth Nonplanar porphyrins and their significance in proteins. *Chem. Soc. Rev.*, 1998, *27*, 31-41.

4. Jentzen, W.; Song, X. Z.; Shelnutt, J. A., Structural characterization of synthetic and protein-bound porphyrins in terms of the lowest-frequency normal coordinates of the macrocycle. *J. Phys. Chem. B*, 1997, *101* (9), 1684-1699.

5. Graves, A. B.; Horak, E. H.; Liptak, M. D., Dynamic ruffling distortion of the heme substrate in non-canonical heme oxygenase enzymes. *Dalton Trans.*, 2016, *45* (24), 10058-67.

6. Graves, A. B.; Morse, R. P.; Chao, A.; Iniguez, A.; Goulding, C. W.; Liptak, M. D., Crystallographic and spectroscopic insights into heme degradation by Mycobacterium tuberculosis MhuD. *Inorg. Chem.*, 2014, *53* (12), 5931-40.

7. Graves, A. B.; Graves, M. T.; Liptak, M. D., Measurement of Heme Ruffling Changes in MhuD Using UV-vis Spectroscopy. *J. Phys. Chem. B*, 2016, *120* (16), 3844-53.

8. Nambu, S.; Matsui, T.; Goulding, C. W.; Takahashi, S.; Ikeda-Saito, M., A new way to degrade heme: the Mycobacterium tuberculosis enzyme MhuD catalyzes heme degradation without generating CO. *J. Biol. Chem.*, 2013, *288* (14), 10101-9.

9. Matsui, T.; Nambu, S.; Goulding, C. W.; Takahashi, S.; Fujii, H.; Ikeda-Saito, M., Unique coupling of mono- and dioxygenase chemistries in a single active site promotes heme degradation. *Proc. Natl. Acad. Sci.*, 2016, *113* (14), 3779-84.

10. Matsui, T.; Unno, M.; Ikeda-Saito, M., Heme oxygenase reveals its strategy for catalyzing three successive oxygenation reactions. *Acc. Chem. Res.*, 2010, *43* (2), 240-7.

11. Chim, N.; Iniguez, A.; Nguyen, T. Q.; Goulding, C. W., Unusual diheme conformation of the heme-degrading protein from Mycobacterium tuberculosis. *J. Mol. Bio.*, 2010, *395* (3), 595-608.

12. Thakuri, B.; Graves, A. B.; Chao, A.; Johansen, S. L.; Goulding, C. W.; Liptak, M. D., The affinity of MhuD for heme is consistent with a heme degrading function in vivo. *Metallomics*, 2018, *10* (11), 1560-1563.

13. Berry, E. A.; Trumpower, B. L., Simultaneous determination of hemes a, b, and c from pyridine hemochrome spectra. *Anal. Biochem.*, 1987, *161* (1), 1-15.

14. Zhu, W.; Wilks, A.; Stojiljkovic, I., Degradation of heme in gram-negative bacteria: the product of the hemO gene of Neisseriae is a heme oxygenase. *J. Bacteriol.*, 2000, *182* (23), 6783-90.

15. Tenhunen, R.; Marver, H. S.; Schmid, R., Microsomal heme oxygenase. Characterization of the enzyme. *J. Biol. Chem.*, 1969, *244* (23), 6388-94.

16. Chao, A.; Goulding, C. W., A Single Mutation in the Mycobacterium tuberculosis Heme-Degrading Protein, MhuD, Results in Different Products. *Biochemistry*, 2019, *58* (6), 489-492.

17. O'Neill, M. J.; Wilks, A., The P. aeruginosa Heme Binding Protein PhuS Is a Heme Oxygenase Titratable Regulator of Heme Uptake. *ACS Chem. Biol.*, 2013, *8* (8), 1794-1802.

18. Barker, K. D.; Barkovits, K.; Wilks, A., Metabolic Flux of Extracellular Heme Uptake in Pseudomonas aeruginosa Is Driven by the Iron-regulated Heme Oxygenase (HemO). *J. Biol. Chem.*, 2012, *287* (22), 18342-18350.

19. Schuller, D. J.; Wilks, A.; Ortiz de Montellano, P. R.; Poulos, T. L., Crystal structure of human heme oxygenase-1. *Nat. Struct. Biol.*, 1999, *6* (9), 860-7.

20. Unno, M.; Matsui, T.; Chu, G. C.; Couture, M.; Yoshida, T.; Rousseau, D. L.; Olson, J. S.; Ikeda-Saito, M., Crystal structure of the dioxygen-bound heme oxygenase from Corynebacterium diphtheriae: implications for heme oxygenase function. *J. Biol. Chem.*, 2004, *279* (20), 21055-61.

21. Takayama, S. J.; Ukpabi, G.; Murphy, M. E.; Mauk, A. G., Electronic properties of the highly ruffled heme bound to the heme degrading enzyme IsdI. *Proc. Natl. Acad. Sci.*, 2011, *108* (32), 13071-6.

22. Petryka, Z.; Nicholson, D. C.; Gray, C. H., Isomeric bile pigments as products of the in vitro fission of haemin. *Nature*, 1962, *194*, 1047-8.

23. Murphy, R. F.; OhEocha, C.; P, O. C., The formation of verdohaemochrome from pyridine protohaemichrome by extracts of red algae and of liver. *Biochem. J.*, 1967, *104* (1), 6C-8C.

24. Denisov, I. G.; Ikeda-Saito, M.; Yoshida, T.; Sligar, S. G., Cryogenic absorption spectra of hydroperoxo-ferric heme oxygenase, the active intermediate of enzymatic heme oxygenation. *FEBS Lett.*, 2002, *532* (1-2), 203-6.

25. Davydov, R.; Kofman, V.; Fujii, H.; Yoshida, T.; Ikeda-Saito, M.; Hoffman, B. M., Catalytic mechanism of heme oxygenase through EPR and ENDOR of cryoreduced oxy-heme oxygenase and its Asp 140 mutants. *J. Am. Chem. Soc.*, 2002, *124* (8), 1798-1808.

26. Davydov, R. M.; Yoshida, T.; Ikeda-Saito, M.; Hoffman, B. M., Hydroperoxy-heme oxygenase generated by cryoreduction catalyzes the formation of alpha-meso-hydroxyheme as detected by EPR and ENDOR. *J. Am. Chem. Soc.*, 1999, *121* (45), 10656-10657.

27. Chen, H.; Moreau, Y.; Derat, E.; Shaik, S., Quantum mechanical/molecular mechanical study of mechanisms of heme degradation by the enzyme heme oxygenase: the strategic function of the water cluster. *J. Am. Chem. Soc.*, 2008, *130* (6), 1953-65.

28. Sakamoto, H.; Omata, Y.; Palmer, G.; Noguchi, M., Ferric alpha-hydroxyheme bound to heme oxygenase can be converted to verdoheme by dioxygen in the absence of added reducing equivalents. *J. Biol. Chem.*, 1999, *274* (26), 18196-18200.

29. Matera, K. M.; Takahashi, S.; Fujii, H.; Zhou, H.; Ishikawa, K.; Yoshimura, T.; Rousseau, D. L.; Yoshida, T.; IkedaSaito, M., Oxygen and one reducing equivalent are both required for the conversion of alpha-hydroxyhemin to verdoheme in heme oxygenase. *J. Biol. Chem.*, 1996, *271* (12), 6618-6624.

30. Migita, C. T.; Fujii, H.; Mansfield Matera, K.; Takahashi, S.; Zhou, H.; Yoshida, T., Molecular oxygen oxidizes the porphyrin ring of the ferric alpha-hydroxyheme in heme oxygenase in the absence of reducing equivalent. *Biochim. Biophys. Acta*, 1999, *1432* (2), 203-13.

31. Sano, S.; Sano, T.; Morishima, I.; Shiro, Y.; Maeda, Y., On the mechanism of the chemical and enzymic oxygenations of alpha-oxyprotohemin IX to Fe.biliverdin IX alpha. *Proc. Natl. Acad. Sci.*, 1986, *83* (3), 531-5.

32. Matsui, T.; Nakajima, A.; Fujii, H.; Matera, K. M.; Migita, C. T.; Yoshida, T.; Ikeda-Saito, M., O-2- and H2O2-dependent verdoheme degradation by heme oxygenase - Reaction mechanisms and potential physiological roles of the dual pathway degradation. *J. Biol. Chem.*, 2005, *280* (44), 36833-36840.

33. Matsui, T.; Iwasaki, M.; Sugiyama, R.; Unno, M.; Ikeda-Saito, M., Dioxygen Activation for the Self-Degradation of Heme: Reaction Mechanism and Regulation of Heme Oxygenase. *Inorg. Chem.*, 2010, *49* (8), 3602-3609.

34. Wang, J.; Niemevz, F.; Lad, L.; Huang, L.; Alvarez, D. E.; Buldain, G.; Poulos, T. L.; de Montellano, P. R., Human heme oxygenase oxidation of 5- and 15-phenylhemes. *J. Biol. Chem.*, 2004, *279* (41), 42593-604.

CHAPTER 4: INVESTIGATING THE ELECTRONIC STRUCTURE OF THE HEME SUBSTRATE INDUCED BY R26S SUBSTITUTION IN *MYCOBACTERIUM TUBERCULOSIS* MHUD.

4.2 INTRODUCTION

Heme oxygenases (HO) are a group of protein that are responsible for the degradation of heme to release non-heme iron, and produce biliverdin and carbon monoxide (CO) as a side product.[10, 15] This heme degradation process plays an essential role in various organisms, such as: iron homeostasis, cell signaling and protection against oxidative stress.[35-37] The HO enzymes in the bacterial pathogens degrade heme as a source of iron for their growth, survival and pathogenicity, and predominantly produce biliverdin and CO.[14, 38] However, some bacterial pathogens have evolved the heme degradation pathways to produce different heme degradation products.[11, 39, 40] *Staphylococcus aureus* heme degrading enzyme, IsdG and IsdI has been studied to catabolize heme to produce non-heme iron, formaldehyde and staphylobilin isomers.[41, 42] On the other hand, Mycobacterium heme utilization degrader (MhuD) is a heme degrading enzyme from *Mycobacterium Tuberculosis*, that has been shown to degrade heme to release non-heme iron and mycobilin as an organic byproduct.[8, 9] The unique degradation product by MhuD means that it degrades heme through a mechanistically different pathway than the canonical HO.

The regiochemistry of the first oxygenation step for forming meso-hydroxyheme intermediate during the heme degradation by the canonical HO differs from the non-canonical HO. Canonical HOs from bacteria to mammals have similar alpha helical fold, where the heme is sandwiched in between.[19, 43, 44] They also contain ordered hydrogen bonding network responsible for guiding the transient OH radical to regioselectivity attack the α-meso position of the porphyrin ring.[27] This hydrogen bonding network is absent in non-canonical HOs such as IsdG/I and MhuD.[6, 21, 45, 46] The heme in the active

site of such enzymes is significantly distorted or ruffled compared to canonical HOs. Crystal structure of MhuD-heme-CN (PDB: 4NL5) shows that the heme is ruffled in the active site of MhuD in such a way that α and γ–*meso* carbons are more accessible to reactive radical oxygen species to attack.[6] However, recent study suggests that formation of mycobilin proceeds via α-oxygenation of β or δ-hydroxyheme.[9] This would mean that significant electronic contribution is very likely for the regioselectivity of heme cleavage by MhuD. Ruffling has been suggested to stabilize $^2B_{2g}$ electronic state which puts significant spin density into the *meso* carbon positions,[21, 47, 48] and this makes iron-dioxygen attack more favorable. WT MhuD has been suggested to stabilize $^2B_{2g}$ [$(d_{xz}, d_{yz})^4 (d_{xy})^1$] ground electronic state with thermally accessible ^2E_g [$(d_{xz}, d_{yz})^3 (d_{xy})^2$] excited electronic state.[6] Since, the β or δ-meso carbon positions are ruffled away from the distal position, there may be an electronic driving force responsible for initial oxygenation at the β or δ-meso carbon positions.

Recent study on R26S MhuD has shown that the mutation causes changes in the product identity upon heme degradation, resulting in formation of α-biliverdin with the release of non-heme iron and formaldehyde (Figure 4.1).[16] Arg26 in the active site of MhuD is hydrogen bonded with one of the propionates of heme (between δ and γ-*meso* carbons). Therefore, Arg26 was initially proposed to play a role in orienting the heme at the active site of MhuD. It is well known that MhuD can bind two heme per monomer in its active site.[11] Thus, MhuD has two distinct binding sites for each heme molecule. Based on the crystal structure of MhuD–diheme (PDB: 3HX9), Arg26 is involved in forming a salt bridge with the propionate group (between δ and γ *meso* carbons) of the solvent exposed heme but has no interaction with the solvent protected heme. Thus,

Arg26 may also be important in orienting the heme in this distinct solvent exposed binding pocket. The formation of biliverdin is similar to canonical HO, however a different C1 product suggest unique heme degradation mechanism. In addition, ~24% of the product observed during the heme degradation by R26S MhuD is mycobilin. Thus, the R26S substitution might have altered the active site in a way to accommodate different heme degradation pathways to produce biliverdin and mycobilin, and the formation of these products may proceed via different electronic structure of the heme substrate.

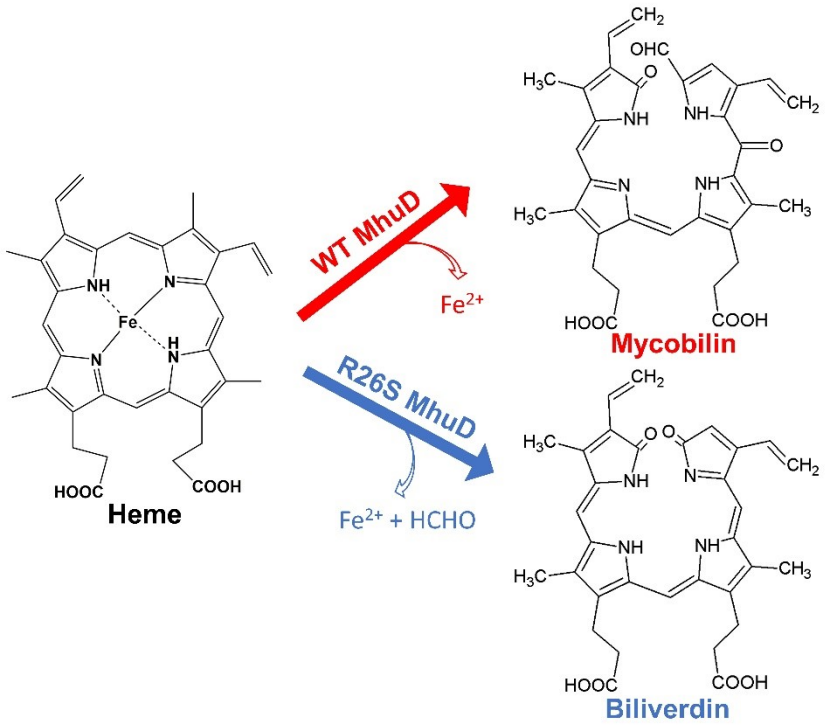

Figure 4. 1 WT MhuD degrades heme to mycobilin and releases non-heme iron. R26S MhuD has been shown to degrade heme to biliverdin while releasing non-heme iron and formaldehyde.[16]

In this study, the change in electronic structure of heme and its reactivity induced by the R26S substitution in MhuD, as well as the possible of role of Arg26 is investigated

using various spectroscopic techniques. UV-Vis absorbance spectroscopy was used to observe if substitution of Arginine 26 to Serine changes the ruffling of heme in the active site of MhuD. Cryogenic Magnetic Circular Dichroism (MCD) and Variable Field Variable Temperature (VTVH) MCD spectroscopic techniques were used to provide insights on the ground electronic states of cyanide inhibited R26S MhuD–heme. Other spectroscopic techniques such as, ^{1}H NMR and temperature dependent ^{1}H NMR were utilized to investigate the electronic states of the cyanide inhibited R26S MhuD–heme–CN at room temperature. Temperature dependent ^{1}H NMR was used to investigate the presence of more than one electronic state with the use of Curie plot. Finally, LC-MS was utilized to monitor the heme degradation activity by R26S MhuD. The results of these techniques are reported here in the results section and their implications has been discussed in the discussion section.

4.2 EXPERIMENTAL

Unless otherwise noted, all materials in this work were purchased from Fisher Scientific and used without further purification.

Protein Expression and Purification: A gene encoding R26S MhuD on a pET22a vector was transformed into BL21 gold cells. DNA sequencing at Vermont Cancer Center (VCC) confirmed the sequence of R26S MhuD gene (Table C.1). Expression of R26S MhuD was performed as previously described for WT MhuD.[11] R26S MhuD was purified using an Äkta pure 25 L fast protein liquid chromatography (FPLC) system (GE Healthcare) as previously described.[16] Fractions containing purified R26S MhuD were pooled and the sample volume was reduced to 10 mL using Amicon stirred cells with 10 kDa ultrafiltration membranes. Following overnight dialysis against 50 mM Tris, 50 mM

NaCl pH 7.4, 10 mg/L of >99% pure MhuD were obtained as assessed using a Bradford assay and SDS-PAGE (Figure C.1 and C.2).

Spectroscopic Characterization: Absorbance spectra at room temperature were acquired for R26S MhuD–heme and R26S MhuD–heme–CN in 50 mM Tris pH 7.4, 50 mM NaCl, by scanning from 900 to 200 nm at 600nm/min with a 1.0 nm data interval and 0.1 s integration time using Cary 100 Bio spectrophotometer. Preparation of heme-bound R26S MhuD has been described previously.[6] R26S MhuD–heme and R26S MhuD–heme–CN extinction coefficient for the Soret band was determined to be 66.9 mM^{-1} cm^{-1} and 85.6 mM^{-1} cm^{-1} respectively using the pyridine hemechrome assay as described previously.[49]

^{1}H NMR spectra was acquired on cyanide inhibited R26S MhuD–heme–CN in 50 mM Tris pH 7.4, 50 mM NaCl as previously described for WT MhuD.[6] Buffer was exchanged into 20mM NaPi pH 7.4 using a PD-10 column. Volume of R26S MhuD–heme–CN was reduced to 615 µL using Amicon stirred cells with 10 kDa ultrafiltration membranes. This was followed by lyophilization of the R26S MhuD–heme–CN for at least 24 hrs on a VirTis lyophilizer. The powder was dissolved using 615 µL of 100% D_2O, to give final concentration of 1 mM R26S MhuD–heme–CN . ^{1}H NMR Spectra of R26S MhuD–heme–CN were acquired using Super Water Eliminating Fourier Transform (Super-WEFT) pulse sequence technique as previously described.[6, 50] ^{1}H NMR super WEFT spectra at 11, 25, 35 and 42 ºC were collected on a Varian Unity Inova 500 MHz NMR spectrometer using 50 ms τ-delay and 50 ms acquisition time. The NMR data was analyzed and processed using MestreNova 14.0.4.

Cryogenic Magnetic Circular Dichroism (MCD) were acquired for 10 μM R26S MhuD–heme–CN in 50 mM KP_i pH 7.4, 50 mM NaCl, 60% (v/v) glycerol using Jasco J-815 spectropolarimeter and an Oxford SM4000-8T Spectromag controlled by a Mercury iTC temperature controller and a Mercury iPS power supply. Spectral data were acquired with a 1.0 nm bandwidth, 0.25 s integration time, 0.5 nm data pitch, and 200 nm/min scanning speed. The MCD spectra was processed by removing the CD contribution from the final MCD spectrum. This was done by subtracting the negative field data from the positive field data and dividing by 2. Variable Field Variable Temperature (VTVH) MCD saturation magnetization curve were acquired at 2, 5 and 10 K for the Soret band at 422 nm by ramping the magnetic field at 0.7 T/min, with a 1.0 nm bandwidth, 0.25 s integration time, and a data pitch of 0.5 nm. Simulations for Model 2 and Model 3 were used as previously described.[6]

Heme Degradation Assay. Heme catalyzed reaction by R26S MhuD were analyzed. Degradation of 50 uM R26S MhuD–heme in 50 mM KPi pH 6.0, 150 mM NaCl at 37^{o}C was performed in the presence of 5 mM ascorbate, 10 mM EDTA, 840 U/mL of catalase and 167 U/mL of Superoxide Dismutase (SOD). Liquid Chromatography-Mass Spectrometry (LC-MS) was used to determine the composition of products formed as a function of time. LC-MS was performed on Shimadzu Prominence HPLC system coupled to an AB Sciex 4000 QTrap Pro hybrid triple-quadrupole/linear ion trap liquid chromatograph-mass spectrometer operated in position ion mode. Heme degradation samples of R26S MhuD at 0, 5, 10, 20, 30, 60 and 120 mins we injected on the LC-MS equilibrated with 2 % Acetonitrile (MeCN) with 0.1% formic acid (v/v) in water (v/v). The m/z 583, 611 and 616 peaks eluted with a linear gradient from 2% MeCN to 98%

with 0.1% formic acid (v/v) in water (v/v) over 50 mins using 1 mm C18 LC column scanning from m/z 600-1500. Ion chromatograms (EIC) of the target ions (m/z 583, 611 and 616) were extracted from the total ion chromatogram from each ESI-MS run using BioAnalyst 1.5. The averaged background spectra from the baseline of the chromatogram preceding each chromatographic peak in each EIC were subtracted from the averaged spectra of the chromatographic peak to produce background subtracted spectra for each target ion. The background subtracted spectra of each target ion was then integrated to get the peak area, which was used to calculate the relative abundances of the target ions for each time-point.

4.3 RESULTS

Spectroscopic Characterization: Using UV/Vis absorption spectroscopy, ruffling of R26S MhuD–heme–CN was assessed. Previous study has demonstrated that up to 1.0 Å ruffling there is no change in energy in the Q band region whereas the Soret band energy is blue shifted.[7] However, beyond 1.0 Å ruffling, both Q-band and Soret band are red-shifted. Q band feature of the Cyanite inhibited R26S MhuD–heme did not change (18,000 cm^{-1}) but the Soret band blue shifted from 23,900 cm^{-1} to 24,000 cm^{-1} (Figure 4.2) compared to WT MhuD–heme–CN. However, since 100 cm^{-1} is about the experimental error of the UV-Vis spectrophotometer that we use, this suggests that the substitution of arginine 26 to serine does not significantly affect the ruffling of the heme in the MhuD's active site.

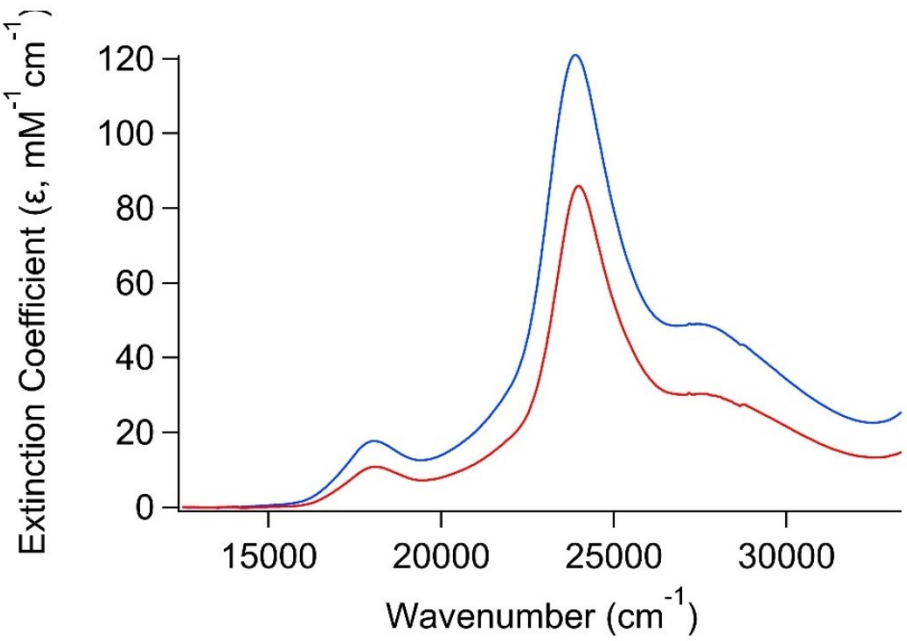

Figure 4. 2. UV/Vis absorption spectra of WT (*blue*) and R26S (*red*) MhuD–heme–CN in 50 mM Tris pH 7.4, 50 mM NaCl. The Q-band did not change but the Soret band blue-shifted by 100 cm^{-1}

Previous studies via MCD spectroscopy have provided insights on the electronic structures of MhuD–heme–CN species. Correlation between the population of the ^2E_g electronic state and the area under the of the Soret band has been previously established.[7] For the ^2E_g [$(d_{xz}, d_{yz})^3$ $(d_{xy})^2$] electronic ground state, spin-orbit coupling exists between ground state and low lying excited state.[51] This would lead to increased C- term MCD intensity as compared to $^2B_{2g}$ [$(d_{xz}, d_{yz})^4$ $(d_{xy})^1$] electronic ground state, where the spin-orbit coupling may not exist or is not as strong. MCD spectra of R26S MhuD– heme–CN was collected and compared to F23W and WT MhuD–heme–CN. The area

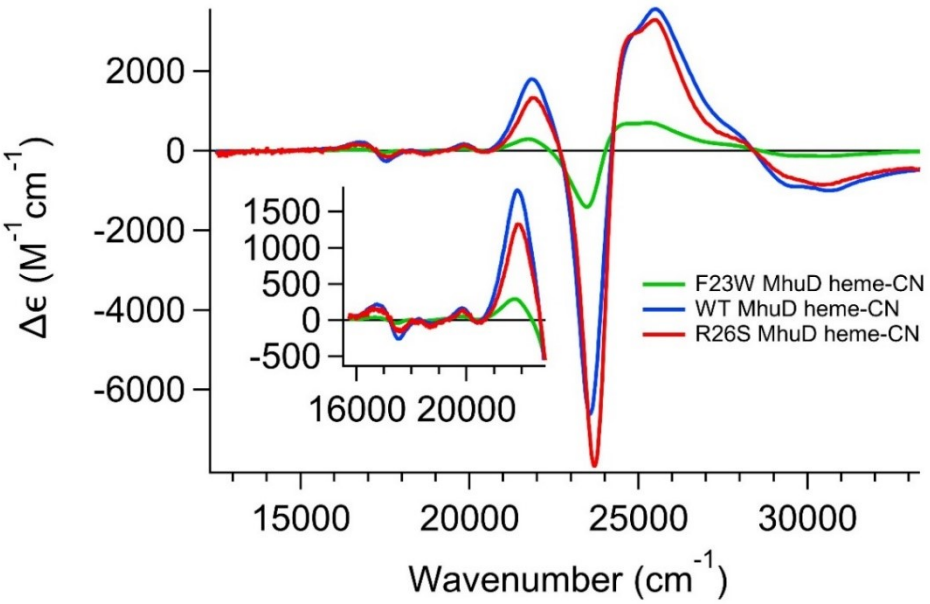

Figure 4. 3. 5K, 7T MCD spectra of R26S MhuD–heme–CN (*dotted red*), WT MhuD–heme–CN (*solid purple*), F23W MhuD–heme–CN (*dotted blue*). **Inset:** Magnified MCD spectra from 500-650 nm.

under the curve for the Soret band observed for R26S is larger than WT and F23W MhuD–heme–CN (Figure 4.3, Table C.2). Previous study has suggested that the state populations are proportional to the area under the curve, as such that, higher area under the curve means higher ^2E_g electronic state population. Therefore, MCD spectra suggests that the more population of ^2E_g electronic state is observed for R26S MhuD–heme–CN compared to F23W and WT MhuD–heme–CN.

VTVH MCD spectroscopy was performed to identify the ground state of R26S MhuD–heme–CN. Analysis of the VTVH MCD saturation magnetization curves for the Soret band of R26S MhuD–heme–CN revealed that the slope of the curves increases with increasing temperature. In other words, nesting is being observed because of the presence of a thermally accessible excited state. Comparison of the saturation magnetization curve

of R26S MhuD–heme–CN was made to the model complexes known to have pure ^2E_g and $^2B_{2g}$ electronic ground states (Figure 4.4). This suggested that R26S MhuD–heme–CN has a $^2B_{2g}$ [$(d_{xz}, d_{yz})^4 (d_{xy})^1$] electronic ground state and with increasing temperature,

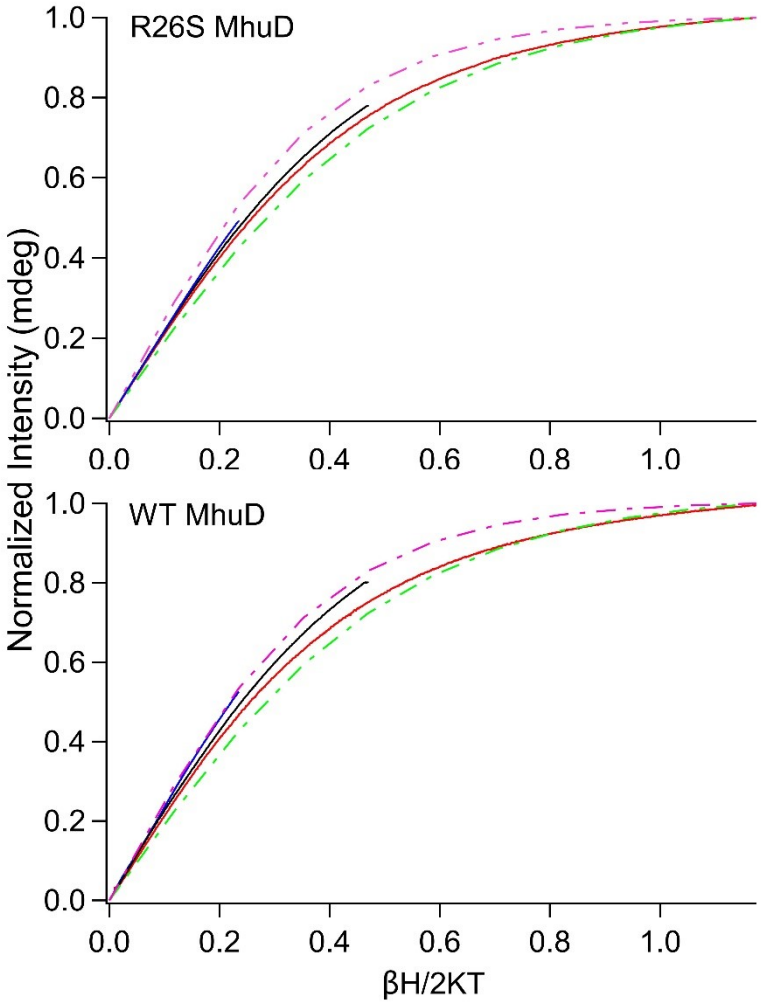

Figure 4. 4. VTVH MCD saturation magnetization curve for R26S MhuD–heme–CN (*top*) in 50 mM KP_i, pH 7.4, 50 mM NaCl, 60% (*v/v*) glycerol at 2 (*red*), 5 (*black*) and 10 K (*blue*). VTVH MCD saturation magnetization curve for WT MhuD–heme–CN is adapted from ref 22 and shows the curve at 2 (red), 5 (*black*) and 10 K (*blue*). The simulated magnetization curves for the ferric heme model complexes with ^2E_g (*dashed purple*) and $^2B_{2g}$ (*dashed green*) electronic ground states are used for comparisons.

^2E_g [$(d_{xz}, d_{yz})^3 (d_{xy})^2$] electronic state is populated (Figure 4.4). However, the saturation magnetization curves of R26S is less nested when compared to WT MhuD–heme–CN (Figure 4.4)[6]. Decreased nesting observed R26S MhuD–heme–CN can be attributed to the increased energy gap between ^2E_g and $^2B_{2g}$ for compared to WT MhuD–heme–CN. This implies that heme in the active site of the R26S MhuD may be less dynamic than in the native enzyme (WT). Interestingly, VTVH and MCD data may suggest that there may be a mixture of two species of R26S MhuD–heme–CN with different electronic states present in the solution. These spectroscopies along with UV/Vis cannot distinguish between the species, as the data collected from them will be due to the equilibrium mixture of these states.

Next, ^{1}H NMR experiments were employed to further investigate and identify the electronic states influenced by R26S substitution in MhuD–heme–CN. Previous studies have suggested ^2E_g electronic states of cyanide inhibited heme oxygenase are associated with downfield hyperfine-shifted ^{1}H resonances[52] and $^2B_{2g}$ electronic states are associated with upfield hyperfine-shifted ^{1}H resonances.[21] Downfield hyperfine shifted resonances are retained in ^{1}H NMR spectra of R26S substituted MhuD–heme–CN , and the furthest is observed at 20.0 ppm (Figure 4.5), suggesting that ^2E_g electronic state is populated at room temperature. Upfield hyperfine- shifted resonances are also observed for R26S-MhuD–heme–CN , and the furthest one is observed at -16.2 ppm, which suggest the presence of a $^2B_{2g}$ electronic state as well. However, the upfield resonances are less paramagnetically shifted than F23W and WT MhuD–heme–CN.[53] This suggests that less

populated $^2B_{2g}$ electronic state is observed for R26S compared to F23W and WT MhuD. It seems that at room temperature, ^2E_g is more populated than $^2B_{2g}$ electronic state for

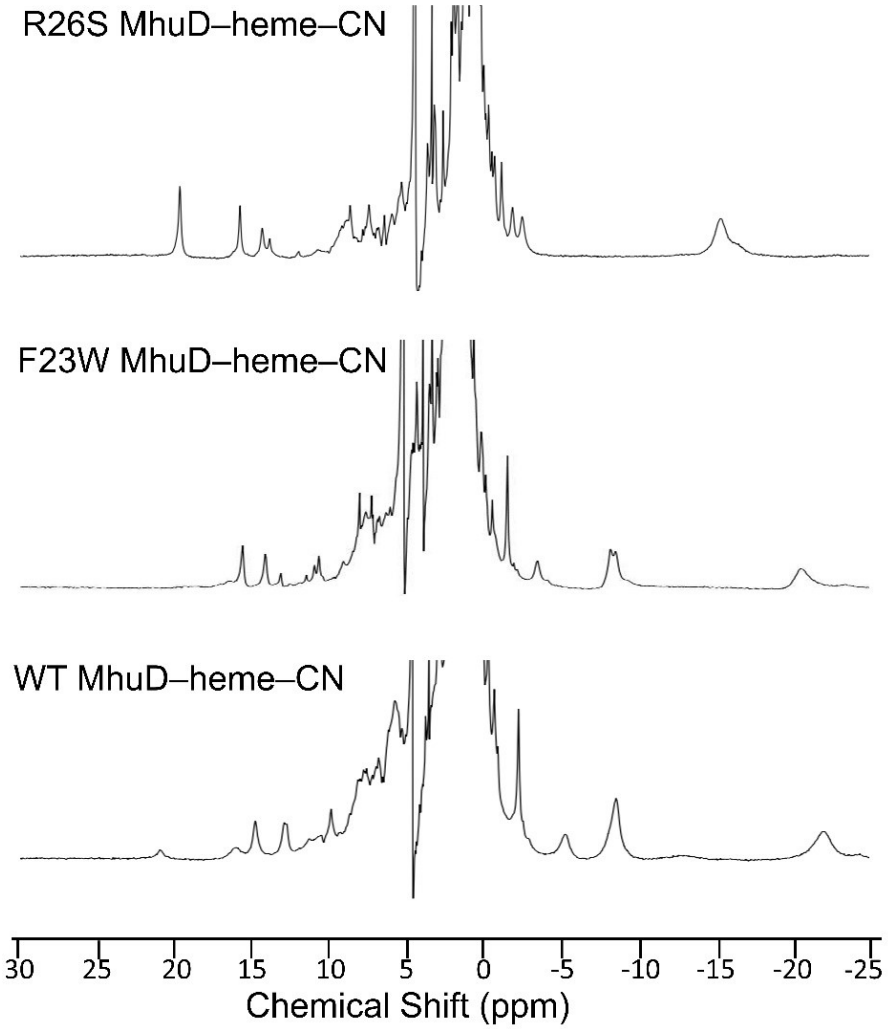

Figure 4. 5. ^{1}H NMR spectra of 1mM R26S MhuD–heme–CN (*top*), F23W MhuD–heme–CN (*middle*) and WT MhuD–heme–CN (*bottom*) in 20mM NaPi pH 7.4, 50mM NaCl (100% D_2O) at 25 ºC. ^{1}H NMR spectra of F23W MhuD–heme–CN and WT MhuD–heme–CN adapted from ref 5 and 6 respectively.

R26S MhuD–heme–CN. To further study the presence of more than one *S*=½ electronic states, temperature dependent NMR study was performed.

^{1}H NMR super-WEFT spectra of R26S MhuD–heme–CN was acquired at 11, 25, 35 and 42 ºC (Figure 4.6). The chemical shifts of resonances from A-G are monitored

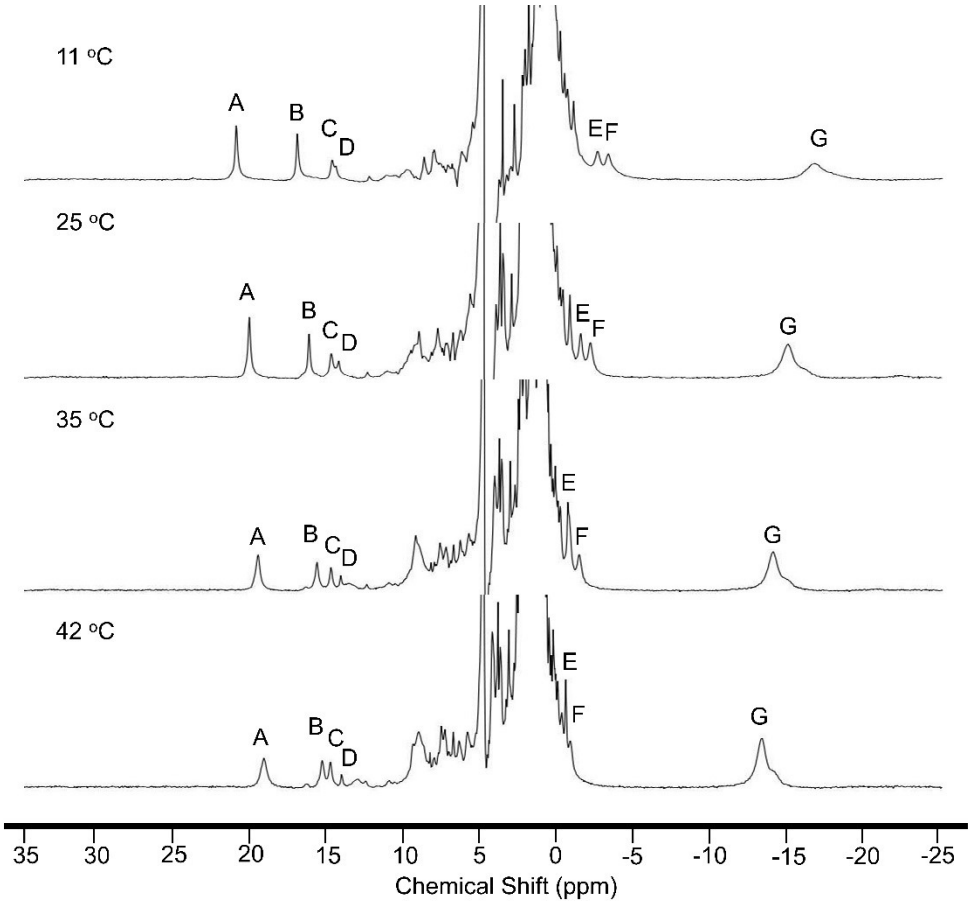

Figure 4. 6. ^{1}H NMR super-WEFT spectra of 1mM MhuD–heme–CN in 20mM NaPi, 50mM NaCl pH 7.4 at 11 ºC, 25 ºC, 35 ºC and 42 ºC as labeled above. The chemical shifts of resonances A-G are labeled and monitored as a function of temperature.

and reported as a function of temperature. These resonances are then plotted and fitted to the Curie Law as a function of inverse temperature (1/T in K-1) (Figure 4.7). Two of the four downfield shifted resonances (A-B) have linear dependence close to the typical 0-10 ppm range and hence exhibit Curie behavior.[54] However other resonances (C-G) does not show linear dependence with increasing temperature, exhibiting a non-Curie behavior.

This means that the downfield shifted resonances showing Curie behavior suggest the presence of pure ^2E_g electronic state, indicating a planar heme in the active site. On the other hand, the paramagnetically shifted resonances from C-G does not exhibit Curie behavior as the temperature approaches infinity, implying that a mixture of two different S=½ electronic states are present. This would suggest presence of two different species

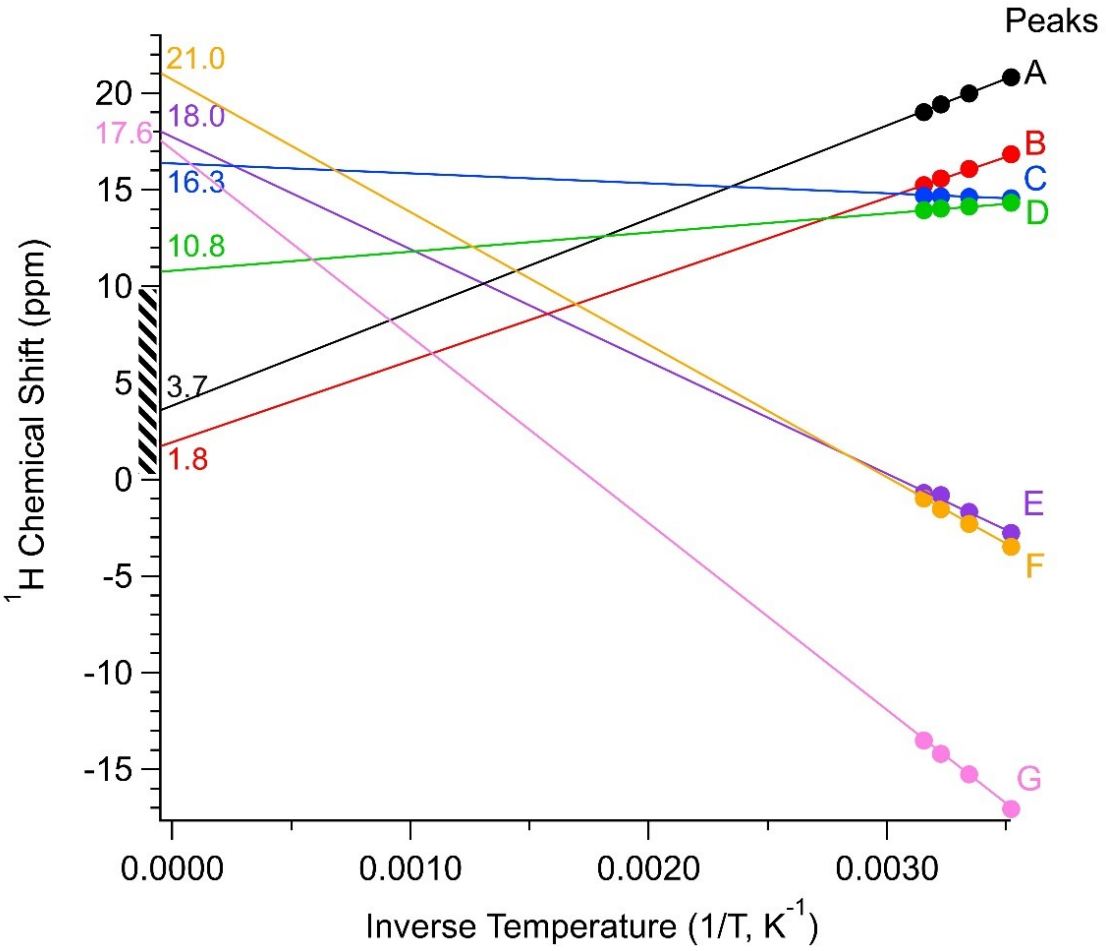

Figure 4. 7. Curie plot of ^{1}H resonance from A-G of R26S MhuD–heme–CN . Solid circles represent the experimental data at 11, 25, 35 and 42 ºC. The lines are the fit to the Curie law drawn linearly with increasing temperature.

of R26S MhuD–heme–CN in solution. MCD, VTVH and Abs studies cannot distinguish between these species, as the spectra collected will be due to the equilibrium mixture between these states in solution. However, temperature dependent ^{1}H NMR spectroscopy can and was able to identify these species.

Heme degradation Assay. Time-resolved MS study on heme degradation by R26S MhuD showed biliverdin as the major product and mycobilin as the minor product (Figure 4.7). With the increasing time, it becomes clearer that the heme degradation

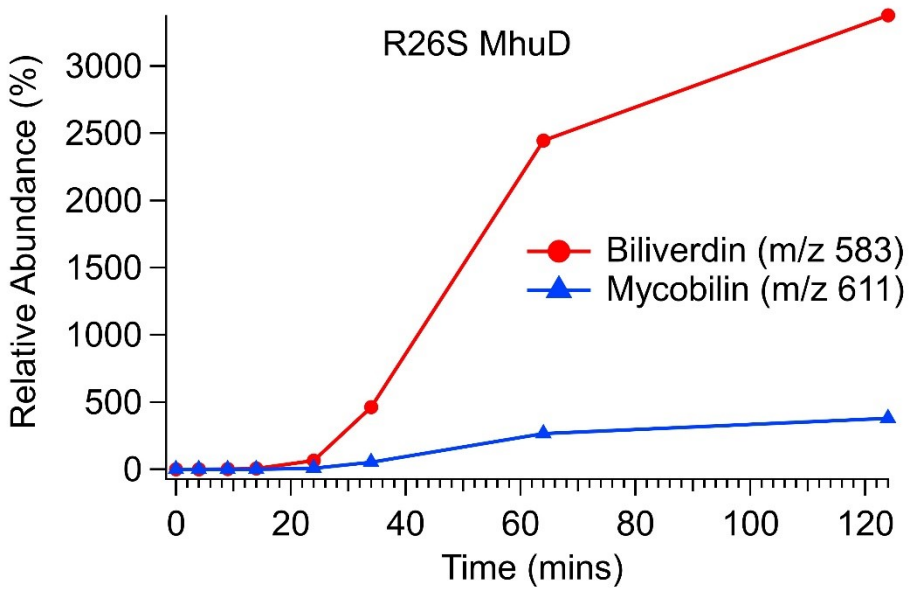

Figure 4. 8. Time-resolved LC-MS study on heme degradation by R26S MhuD. Formation of mycobilin and biliverdin is plotted as relative abundance (%) against heme as a function of time. Sample at each time-point has 4 mins delay taken up by thawing and injecting process. Thus, 0 min time-point sample is 50 μM R26S MhuD–heme (50 mM KPi pH 6.0, 150 mM NaCl, 37°C).

by R26S MhuD yields biliverdin as the major product. This is in line with the results published by Goulding and co-workers, where they observed α-biliverdin as the major product and very small amount of mycobilin isomers as the minor product.[16]

4.4 DISCUSSION

Electronic structure of R26S MhuD–heme–CN : ^{1}H NMR spectra of R26S MhuD–heme–CN showed the presence of two different electronic states as WT MhuD–heme–CN,[6] but ^{1}H NMR alone cannot distinguish between the presence of two different species. Thus, the temperature dependence of the paramagnetically shifted resonances were investigated through a temperature dependent ^{1}H NMR study (Figure 4.6). This study revealed the likelihood of two species of R26S MhuD–heme with different electronic states. The Curie plot (Figure 4.7) suggested that a single electronic state is populated by resonances having a linear dependence with temperature ($^{2}E_{g}$), and mixture of two electronic states ($^{2}E_{g}$ and $^{2}B_{2g}$) are present for the resonances having non-linear dependence with temperature.

The MCD, VTVH and Abs spectra arises from the equilibrium mixture between the two species in solution. Due to the nature of these techniques, they cannot distinguish between these species ($^{2}E_{g}$ and mixture of $^{2}E_{g}$ and $^{2}B_{2g}$). Thus, a conclusive statement cannot be made from the Abs data in order to understand the effect of Arg26 substitution on heme ruffling. As for the MCD spectra, it is dominated by the C-term intensity ($^{2}E_{g}$). Hence, it is almost impossible to analyze the data in order to extract information on $^{2}B_{2g}$ electronic state or distinguish between the two species. However, the VTVH curve for R26S MhuD–heme–CN suggested a $^{2}B_{2g}$ electronic ground state with $^{2}E_{g}$ excited state.

Based on the temperature dependent ^{1}H NMR and the cryogenic VTVH data, the $^{2}B_{2g}$ electronic ground state can be assigned for the species with a mixture of $^{2}E_{g}$ and $^{2}B_{2g}$ electronic states.

Interestingly, these observations could be explained by a mixture two species with varied heme conformations that is present in active site of R26S MhuD. One species has a planar heme conformation ($^{2}E_{g}$) and the other species have a ruffled heme conformation ($^{2}B_{2g}$ and $^{2}E_{g}$) with $^{2}B_{2g}$ ground state. The presence of the two different species of R26S MhuD–heme–CN with different electronic structure will certainly have implications on the reactivity of MhuD by Arg26 substitution. This is further supported by a recent study where biliverdin is observed as the major and mycobilin as the minor product of heme degradation by R26S MhuD.[16] The implication of this is further discussed in detail below.

Implication of the electronic structure on heme degradation by R26S MhuD. Recent studies have highlighted α-biliverdin as the product of heme degradation by R26S MhuD.[16, 55] The C1 product of the heme degradation by R26S MhuD is also different from WT MhuD, as formaldehyde is released instead of CO.[16] This suggest that heme degradation might be proceeding through a pathway different from that of canonical HO. Time-dependent MS study on the heme degradation by R26S MhuD showed biliverdin as the major product. The spectroscopic data collected illustrated the possibility of two different species of R26S MhuD–heme–CN. One housing planar heme in the active site and the other housing more ruffled heme in the active site. Thus, we propose that the R26S MhuD with planar heme having $^{2}E_{g}$ electronic ground state may be responsible for degrading heme to biliverdin. In addition, R26S MhuD with dynamic heme having a

mixture of $^2B_{2g}$ and ^2E_g electronic states may be responsible for degrading heme to mycobilin.

Role of Arginine 26. Since R26S MhuD degrades heme with a different mechanism than canonical HO and WT MhuD, a recent study proposes that the role of Arg26 is more than just properly orienting heme within the active site.[16] A recent computational study on heme degradation by R26S MhuD suggested that after the mutation, the salt bridge formed between Arg26 and one of the propionate group (between δ and γ-*meso* carbons) is broken, which allowed for that propionate group to form hydrogen bond with Asn7 instead.[56] It is then proposed that this allows the hydroxyl radical to attack α-*meso* position since β and δ-*meso* positions are ruffled towards the proximal His75, and γ-*meso* position is sterically hindered by the Ile9. This would mean the salt bridge between Arg26 and the propionate needs to be stabilized for Asn7 to guide the hydroxyl radical to β or δ-*meso* carbon positions, suggesting that Asn7 may play a role in regioselective oxygenation during the first step. This may explain the formation of biliverdin but formation of mycobilin (~24%) during the heme degradation by R26S MhuD challenges this proposal.[16]

Since the presence of two different species of R26S MhuD–heme–CN with varied electronic structure may explain the formation of biliverdin and mycobilin during the heme degradation by R26S MhuD, it is reasonable to suggest that Arg26 not only stabilizes the heme orientation but may also stabilize the heme conformation in the active site of MhuD. The salt bridge interaction between the Arg26 and the propionate group of the heme substrate allows for placing the heme in a prime location where it can attain the required conformation induced by second sphere amino acids interaction. In addition,

MhuD has two distinct binding sites for heme in its active site, where Arg26 forms a salt bridge interaction with the solvent exposed heme molecule. Without such interaction, we can speculate that the heme in the active site of R26S MhuD will not be locked into a position, and the large active site pocket of MhuD along with the presence of two distinct binding sites may allow for some flexibility on heme binding. This would mean that R26S MhuD loses its control on guiding heme towards the correct binding pocket, allowing heme to bind to either of the binding site. Presence of two different conformation of heme in the active site of R26S MhuD, as suggested in this spectroscopic study, may be the result of binding of heme at two different binding sites. However, it is worth noting that current study is insufficient in understanding how different conformation of heme is controlled in the active site of R26S MhuD. Therefore, further investigation regarding this hypothesis is necessary.

4.5 CONCLUSION

In summary, a single mutation of Arginine 26 to Serine in MhuD induced a drastic change in its electronic structure. Through the spectroscopic investigations performed in this study, the possibility for the presence of a pure ^2E_g and a mixture of $^2B_{2g}$ and ^2E_g electronic states is proposed. This would then suggest that more than one conformation of heme may be present in the active site of R26S MhuD. These conformations may be thus be responsible for formation of biliverdin as the major product and mycobilin as a very minor product. However, additional spectroscopic characterization may be necessary to fully elucidate the role of R26 and the electronic structure induced by its substitution.

4.6 CHAPTER 4 REFERENCES

1. Bandarian, V.; Ludwig, M. L.; Matthews, R. G., Factors modulating conformational equilibria in large modular proteins: a case study with cobalamin-dependent methionine synthase. *Proc. Natl. Acad. Sci.*, 2003, *100* (14), 8156-63.

2. Perutz, M. F., Stereochemistry of cooperative effects in haemoglobin. *Nature*, 1970, *228* (5273), 726-39.

3. John A. Shelnutt, X.-Z. S., Jian-Guo Ma, Song-Ling Jia, Walter Jentzen, Craig J. Medforth, Craig J. Medforth Nonplanar porphyrins and their significance in proteins. *Chem. Soc. Rev.*, 1998, *27*, 31-41.

4. Jentzen, W.; Song, X. Z.; Shelnutt, J. A., Structural characterization of synthetic and protein-bound porphyrins in terms of the lowest-frequency normal coordinates of the macrocycle. *J. Phys. Chem. B*, 1997, *101* (9), 1684-1699.

5. Graves, A. B.; Horak, E. H.; Liptak, M. D., Dynamic ruffling distortion of the heme substrate in non-canonical heme oxygenase enzymes. *Dalton Trans.*, 2016, *45* (24), 10058-67.

6. Graves, A. B.; Morse, R. P.; Chao, A.; Iniguez, A.; Goulding, C. W.; Liptak, M. D., Crystallographic and spectroscopic insights into heme degradation by Mycobacterium tuberculosis MhuD. *Inorg. Chem.*, 2014, *53* (12), 5931-40.

7. Graves, A. B.; Graves, M. T.; Liptak, M. D., Measurement of Heme Ruffling Changes in MhuD Using UV-vis Spectroscopy. *J. Phys. Chem. B*, 2016, *120* (16), 3844-53.

8. Nambu, S.; Matsui, T.; Goulding, C. W.; Takahashi, S.; Ikeda-Saito, M., A new way to degrade heme: the Mycobacterium tuberculosis enzyme MhuD catalyzes heme degradation without generating CO. *J. Biol. Chem.*, 2013, *288* (14), 10101-9.

9. Matsui, T.; Nambu, S.; Goulding, C. W.; Takahashi, S.; Fujii, H.; Ikeda-Saito, M., Unique coupling of mono- and dioxygenase chemistries in a single active site promotes heme degradation. *Proc. Natl. Acad. Sci.*, 2016, *113* (14), 3779-84.

10. Matsui, T.; Unno, M.; Ikeda-Saito, M., Heme oxygenase reveals its strategy for catalyzing three successive oxygenation reactions. *Acc. Chem. Res.*, 2010, *43* (2), 240-7.

11. Chim, N.; Iniguez, A.; Nguyen, T. Q.; Goulding, C. W., Unusual diheme conformation of the heme-degrading protein from Mycobacterium tuberculosis. *J. Mol. Bio.*, 2010, *395* (3), 595-608.

12. Thakuri, B.; Graves, A. B.; Chao, A.; Johansen, S. L.; Goulding, C. W.; Liptak, M. D., The affinity of MhuD for heme is consistent with a heme degrading function in vivo. *Metallomics*, 2018, *10* (11), 1560-1563.

13. Berry, E. A.; Trumpower, B. L., Simultaneous determination of hemes a, b, and c from pyridine hemochrome spectra. *Anal. Biochem.*, 1987, *161* (1), 1-15.

14. Zhu, W.; Wilks, A.; Stojiljkovic, I., Degradation of heme in gram-negative bacteria: the product of the hemO gene of Neisseriae is a heme oxygenase. *J. Bacteriol.*, 2000, *182* (23), 6783-90.

15. Tenhunen, R.; Marver, H. S.; Schmid, R., Microsomal heme oxygenase. Characterization of the enzyme. *J. Biol. Chem.*, 1969, *244* (23), 6388-94.

16. Chao, A.; Goulding, C. W., A Single Mutation in the Mycobacterium tuberculosis Heme-Degrading Protein, MhuD, Results in Different Products. *Biochemistry*, 2019, *58* (6), 489-492.

17. O'Neill, M. J.; Wilks, A., The P. aeruginosa Heme Binding Protein PhuS Is a Heme Oxygenase Titratable Regulator of Heme Uptake. *ACS Chem. Biol.*, 2013, *8* (8), 1794-1802.

18. Barker, K. D.; Barkovits, K.; Wilks, A., Metabolic Flux of Extracellular Heme Uptake in Pseudomonas aeruginosa Is Driven by the Iron-regulated Heme Oxygenase (HemO). *J. Biol. Chem.*, 2012, *287* (22), 18342-18350.

19. Schuller, D. J.; Wilks, A.; Ortiz de Montellano, P. R.; Poulos, T. L., Crystal structure of human heme oxygenase-1. *Nat. Struct. Biol.*, 1999, *6* (9), 860-7.

20. Unno, M.; Matsui, T.; Chu, G. C.; Couture, M.; Yoshida, T.; Rousseau, D. L.; Olson, J. S.; Ikeda-Saito, M., Crystal structure of the dioxygen-bound heme oxygenase from Corynebacterium diphtheriae: implications for heme oxygenase function. *J. Biol. Chem.*, 2004, *279* (20), 21055-61.

21. Takayama, S. J.; Ukpabi, G.; Murphy, M. E.; Mauk, A. G., Electronic properties of the highly ruffled heme bound to the heme degrading enzyme IsdI. *Proc. Natl. Acad. Sci.*, 2011, *108* (32), 13071-6.

22. Petryka, Z.; Nicholson, D. C.; Gray, C. H., Isomeric bile pigments as products of the in vitro fission of haemin. *Nature*, 1962, *194*, 1047-8.

23. Murphy, R. F.; OhEocha, C.; P, O. C., The formation of verdohaemochrome from pyridine protohaemichrome by extracts of red algae and of liver. *Biochem. J.*, 1967, *104* (1), 6C-8C.

24. Denisov, I. G.; Ikeda-Saito, M.; Yoshida, T.; Sligar, S. G., Cryogenic absorption spectra of hydroperoxo-ferric heme oxygenase, the active intermediate of enzymatic heme oxygenation. *FEBS Lett.*, 2002, *532* (1-2), 203-6.

25. Davydov, R.; Kofman, V.; Fujii, H.; Yoshida, T.; Ikeda-Saito, M.; Hoffman, B. M., Catalytic mechanism of heme oxygenase through EPR and ENDOR of cryoreduced oxy-heme oxygenase and its Asp 140 mutants. *J. Am. Chem. Soc.*, 2002, *124* (8), 1798-1808.

26. Davydov, R. M.; Yoshida, T.; Ikeda-Saito, M.; Hoffman, B. M., Hydroperoxy-heme oxygenase generated by cryoreduction catalyzes the formation of alpha-meso-hydroxyheme as detected by EPR and ENDOR. *J. Am. Chem. Soc.*, 1999, *121* (45), 10656-10657.

27. Chen, H.; Moreau, Y.; Derat, E.; Shaik, S., Quantum mechanical/molecular mechanical study of mechanisms of heme degradation by the enzyme heme oxygenase: the strategic function of the water cluster. *J. Am. Chem. Soc.*, 2008, *130* (6), 1953-65.

28. Sakamoto, H.; Omata, Y.; Palmer, G.; Noguchi, M., Ferric alpha-hydroxyheme bound to heme oxygenase can be converted to verdoheme by dioxygen in the absence of added reducing equivalents. *J. Biol. Chem.*, 1999, *274* (26), 18196-18200.

29. Matera, K. M.; Takahashi, S.; Fujii, H.; Zhou, H.; Ishikawa, K.; Yoshimura, T.; Rousseau, D. L.; Yoshida, T.; IkedaSaito, M., Oxygen and one reducing equivalent are both required for the conversion of alpha-hydroxyhemin to verdoheme in heme oxygenase. *J. Biol. Chem.*, 1996, *271* (12), 6618-6624.

30. Migita, C. T.; Fujii, H.; Mansfield Matera, K.; Takahashi, S.; Zhou, H.; Yoshida, T., Molecular oxygen oxidizes the porphyrin ring of the ferric alpha-hydroxyheme in heme oxygenase in the absence of reducing equivalent. *Biochim. Biophys. Acta*, 1999, *1432* (2), 203-13.

31. Sano, S.; Sano, T.; Morishima, I.; Shiro, Y.; Maeda, Y., On the mechanism of the chemical and enzymic oxygenations of alpha-oxyprotohemin IX to Fe.biliverdin IX alpha. *Proc. Natl. Acad. Sci.*, 1986, *83* (3), 531-5.

32. Matsui, T.; Nakajima, A.; Fujii, H.; Matera, K. M.; Migita, C. T.; Yoshida, T.; Ikeda-Saito, M., O-2- and H2O2-dependent verdoheme degradation by heme oxygenase - Reaction mechanisms and potential physiological roles of the dual pathway degradation. *J. Biol. Chem.*, 2005, *280* (44), 36833-36840.

33. Matsui, T.; Iwasaki, M.; Sugiyama, R.; Unno, M.; Ikeda-Saito, M., Dioxygen Activation for the Self-Degradation of Heme: Reaction Mechanism and Regulation of Heme Oxygenase. *Inorg. Chem.*, 2010, *49* (8), 3602-3609.

34. Wang, J.; Niemevz, F.; Lad, L.; Huang, L.; Alvarez, D. E.; Buldain, G.; Poulos, T. L.; de Montellano, P. R., Human heme oxygenase oxidation of 5- and 15-phenylhemes. *J. Biol. Chem.*, 2004, *279* (41), 42593-604.

35. Ferris, C. D.; Jaffrey, S. R.; Sawa, A.; Takahashi, M.; Brady, S. D.; Barrow, R. K.; Tysoe, S. A.; Wolosker, H.; Baranano, D. E.; Dore, S.; Poss, K. D.; Snyder, S. H., Haem oxygenase-1 prevents cell death by regulating cellular iron. *Nat. Cell Biol.*, 1999, *1* (3), 152-7.

36. Brouard, S.; Otterbein, L. E.; Anrather, J.; Tobiasch, E.; Bach, F. H.; Choi, A. M.; Soares, M. P., Carbon monoxide generated by heme oxygenase 1 suppresses endothelial cell apoptosis. *J. Exp. Med.*, 2000, *192* (7), 1015-26.

37. Dore, S.; Takahashi, M.; Ferris, C. D.; Zakhary, R.; Hester, L. D.; Guastella, D.; Snyder, S. H., Bilirubin, formed by activation of heme oxygenase-2, protects neurons against oxidative stress injury. *Proc. Natl. Acad. Sci.*, 1999, *96* (5), 2445-50.

38. Schmitt, M. P., Utilization of host iron sources by Corynebacterium diphtheriae: identification of a gene whose product is homologous to eukaryotic heme oxygenases and is required for acquisition of iron from heme and hemoglobin. *J. Bacteriol.*, 1997, *179* (3), 838-45.

39. Skaar, E. P.; Gaspar, A. H.; Schneewind, O., IsdG and IsdI, heme-degrading enzymes in the cytoplasm of Staphylococcus aureus. *J. Biol. Chem.*, 2004, *279* (1), 436-43.

40. LaMattina, J. W.; Nix, D. B.; Lanzilotta, W. N., Radical new paradigm for heme degradation in Escherichia coli O157:H7. *Proc. Natl. Acad. Sci.*, 2016, *113* (43), 12138-12143.

41. Reniere, M. L.; Ukpabi, G. N.; Harry, S. R.; Stec, D. F.; Krull, R.; Wright, D. W.; Bachmann, B. O.; Murphy, M. E.; Skaar, E. P., The IsdG-family of haem oxygenases degrades haem to a novel chromophore. *Mol. Microbiol.*, 2010, *75* (6), 1529-38.

42. Matsui, T.; Nambu, S.; Ono, Y.; Goulding, C. W.; Tsumoto, K.; Ikeda-Saito, M., Heme degradation by Staphylococcus aureus IsdG and IsdI liberates formaldehyde rather than carbon monoxide. *Biochemistry*, 2013, *52* (18), 3025-7.

43. Hirotsu, S.; Chu, G. C.; Unno, M.; Lee, D. S.; Yoshida, T.; Park, S. Y.; Shiro, Y.; Ikeda-Saito, M., The crystal structures of the ferric and ferrous forms of the heme complex of HmuO, a heme oxygenase of Corynebacterium diphtheriae. *J. Biol. Chem.*, 2004, *279* (12), 11937-47.

44. Friedman, J.; Lad, L.; Li, H.; Wilks, A.; Poulos, T. L., Structural basis for novel delta-regioselective heme oxygenation in the opportunistic pathogen Pseudomonas aeruginosa. *Biochemistry*, 2004, *43* (18), 5239-45.

45. Lee, W. C.; Reniere, M. L.; Skaar, E. P.; Murphy, M. E., Ruffling of metalloporphyrins bound to IsdG and IsdI, two heme-degrading enzymes in Staphylococcus aureus. *J. Biol. Chem.*, 2008, *283* (45), 30957-63.

46. Ukpabi, G.; Takayama, S. J.; Mauk, A. G.; Murphy, M. E., Inactivation of the heme degrading enzyme IsdI by an active site substitution that diminishes heme ruffling. *J. Biol. Chem.*, 2012, *287* (41), 34179-88.

47. Safo, M. K.; Walker, F. A.; Raitsimring, A. M.; Walters, W. P.; Dolata, D. P.; Debrunner, P. G.; Scheidt, W. R., Axial Ligand Orientation in Iron(Iii) Porphyrinates - Effect of Axial Pi-Accepters - Characterization of the Low-Spin Complex [Fe(Tpp)(4-Cnpy)(2)]Clo4. *J. Am. Chem. Soc.*, 1994, *116* (17), 7760-7770.

48. Rivera, M.; Caignan, G. A.; Astashkin, A. V.; Raitsimring, A. M.; Shokhireva, T.; Walker, F. A., Models of the low-spin iron(III) hydroperoxide intermediate of heme oxygenase: magnetic resonance evidence for thermodynamic stabilization of the d(xy) electronic state at ambient temperatures. *J. Am. Chem. Soc.*, 2002, *124* (21), 6077-89.

49. Berry, E. A.; Trumpower, B. L., Simultaneous Determination of Hemes-a, Hemes-B, and Hemes-C from Pyridine Hemochrome Spectra. *Anal Biochem*, 1987, *161* (1), 1-15.

50. Inubushi, T.; Becker, E. D., Efficient Detection of Paramagnetically Shifted Nmr Resonances by Optimizing the Weft Pulse Sequence. *J Magn Reson*, 1983, *51* (1), 128-133.

51. Lehnert, N., Elucidating second coordination sphere effects in heme proteins using low-temperature magnetic circular dichroism spectroscopy. *J. Inorg. Biochem.*, 2012, *110*, 83-93.

52. Li, Y.; Syvitski, R. T.; Chu, G. C.; Ikeda-Saito, M.; Mar, G. N., Solution 1H NMR investigation of the active site molecular and electronic structures of substrate-bound, cyanide-inhibited HmuO, a bacterial heme oxygenase from Corynebacterium diphtheriae. *J. Biol. Chem.*, 2003, *278* (9), 6651-63.

53. Graves, A. B.; Horak, E. H.; Liptak, M. D., Dynamic ruffling distortion of the heme substrate in non-canonical heme oxygenase enzymes. *Dalton Transactions*, 2016, *45* (24), 10058-10067.

54. Shokhirev, N. V.; Walker, F. A., Analysis of the temperature dependence of the H-1 contact shifts in low-spin Fe(III) model hemes and heme proteins: Explanation of "Curie" and "anti-Curie" behavior within the same molecule. *J. Phys. Chem.*, 1995, *99* (50), 17795-17804.

55. Chao, A.; Burley, K. H.; Sieminski, P. J.; de Miranda, R.; Chen, X.; Mobley, D. L.; Goulding, C. W., Structure of a Mycobacterium tuberculosis Heme-Degrading Protein, MhuD, Variant in Complex with Its Product. *Biochemistry*, 2019, *58* (46), 4610-4620.

56. Yuan, C.; Zhang, Y.; Tan, H.; Li, X.; Chen, G.; Jia, Z., ONIOM investigations of the heme degradation mechanism by MhuD: the critical function of heme ruffling. *Phys. Chem. Chem. Phys.*, 2020, *22* (16), 8817-8826.

CHAPTER 5: INVESTIGATING THE EFFECT ON HEME RUFFLING AND DEGRADATION BY F23W SUBSTITUTION IN *STAPHYLOCOCCUS AUREUS* ISDG.

5.1 INTRODUCTION

Staphylococcus aureus is a Gram-positive pathogen involved with staph infections. People with chronic conditions such as diabetes, cancer etc., are at greater risk from this infection. The drug resistant strain such as Methicillin-Resistant *S. aureus* (MRSA) has a high mortality rate[1] and according to CDC, the untreated MRSA can become severe and cause sepsis. The rates of MRSA related infections compared to other developed countries is higher in the United States.[2] Due to increased infection, the clinical researches are being done to treat the conditions caused by MRSA, such as Pneumonia, Osteomyelitis, etc.[3] However, the mortality rate has stayed high even with the antibiotics in the market that are effective against MRSA. In addition, the vaccine development has also been unsatisfactory.[3] Therefore, more extensive research on discovering better insights between the host and the *S. aureus* pathogen is necessary.

Like most organisms, *S. aureus* also needs iron to grow and survive inside the human host. However, most of the iron in human body is in the form of heme and it is also the preferred iron source for *S. aureus* during the early infection period.[4] The heme acquisition from the host by *S. aureus* utilizes the iron-regulated surface determinant (Isd) system, where several Isd proteins and enzymes are involved in the iron acquisition.[5-8] IsdG and IsdI enzymes in the Isd system are involved in cleaving the heme to release iron, formaldehyde and an organic byproduct called staphylobilin.[9-11] These enzymes are a viable drug target for the future development of therapeutic strategies against *S. aureus* and thus, understanding the mechanism behind the cleavage of heme by IsdG/I to sequester iron is essential.

Similar to IsdG/I, our body also have heme degrading enzymes known as human heme oxygenase (hHO), which falls within canonical heme oxygenase (HO) family. Like all the canonical HO, the hHO degrades heme to release iron, carbon monoxide (CO) and biliverdin.[12, 13] Bacterial pathogens consisting of similar heme degrading enzyme predominantly degrades heme to produce biliverdin and CO.[14, 15] The ordered hydrogen bonding network present in the active site of these enzyme has been proposed to be responsible for guiding the OH radical to selectively attack α-meso position of heme substrate.[16, 17] Such water cluster is absent in active site of non-canonical HO such as

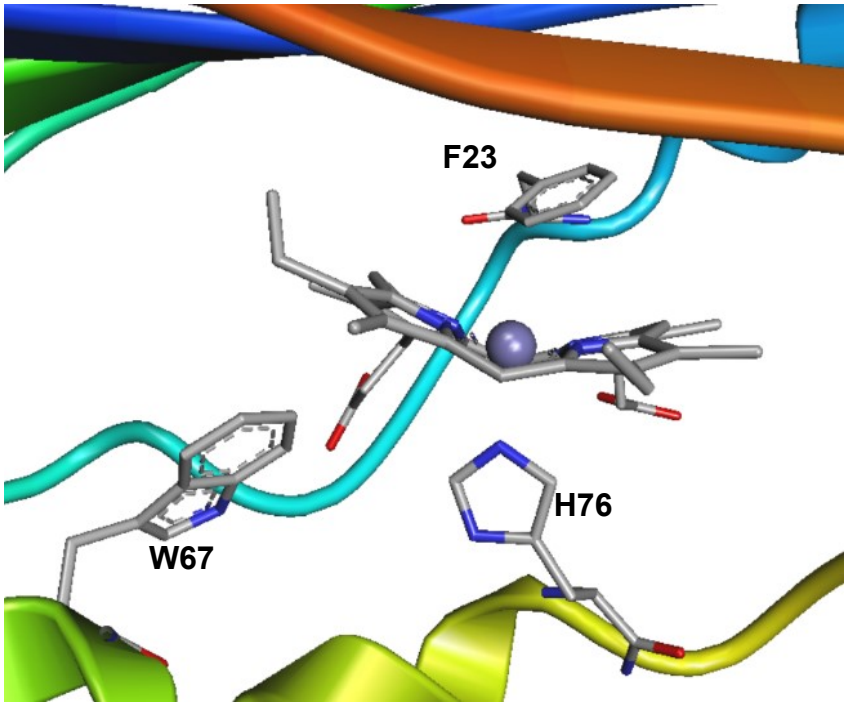

Figure 5. 1. Active site of heme bound N7A IsdG is shown to have hydrophobic interaction with secondary sphere amino acids F23 and W67. Substitution of W67 to Ala completely stopped the IsdG-mediated heme degradation. While F23A substitution did not alter the heme degradation by IsdG.[18]

Mycobacterium tuberculosis MhuD and *Staphylococcus aureus* IsdG/I.[19-22] Both IsdG/I and MhuD has been shown to degrade ruffled heme in the active site, which is proposed to be one of the reasons for their distinct enzymatic mechanism.[18, 19, 21, 23, 24] The IsdG-catalyzed heme degradation has been proposed to go through a bridged transition state with concerted O-O bond cleavage and C-O bond formation, resulting in oxygenation at the β/δ-*meso* carbons to form β/δ-*meso*-hydroxyheme intermediate on its way to towards staphylobilin formation.[25]

The heme substrate in the active site of IsdG hydrophobically interacts with several amino acid residues such as Leu9, Phe23, Trp67, Val80 etc.[19] (His76, Phe23 and W67 is shown in Figure 5.1). Roles of second-sphere amino acids in the IsdG/I catalyzed heme degradation has been studied in the past.[18, 25, 26] Most specifically the roles of Asn7 and Trp67 in the heme degradation mechanism seems to be important. The Asn7 is responsible for rotating the hydrogen bonded hydroperoxo ligand towards β- and δ-*meso* carbons, and the hydrophobic interaction between heme and the Trp67 leads to the pushing of β- and δ-*meso* carbons towards the distal hydroperoxo ligand.[20, 24, 25] Also, recent study has proposed that Asn7 and Trp67 work together towards a unique heme degradation chemistry by IsdG.[26]

Another residue that makes hydrophobic interaction with the substrate is Phe23. Surprisingly, the role of Phe23 has not been widely studied. Previous study on this residue on Phe23 substitution to Ala, showed that the heme degradation mechanism was not affected.[18] Conversely, the conserved Phe23 residue in MhuD has been shown to alter the electronic structure of heme, thereby affecting the enzymatic activity of F23W MhuD.[23] The F23W variant showed increased heme substrate ruffling compared to WT

MhuD. The Phe23 in IsdG makes steric contact on the distal side of heme and thus its substitution to a bulkier Trp amino acid is hypothesized to alter the heme ruffling and consequently its electronic structure and the enzymatic activity.

In this study, Phe23 was substituted to Trp to gain insights on its role in the enzymatic pathway by *S. aureus* IsdG. Circular Dichroism (CD) spectroscopy was utilized to analyze the secondary structure of the F23W variant. UV/Vis (Abs) spectroscopy was utilized to gain information on the F23W induced heme ruffling. The activity assay by this variant was studied using Abs spectroscopy and Liquid Chromatography-Mass Spectrometry (LC-MS). The results for this study are reported and their implication has been discussed below.

5.2 EXPERIMENTAL

Unless otherwise noted, all materials in this work were purchased from Fisher Scientific and used without further purification.

Protein Expression and Purification: The cloning of WT IsdG from pET-15b (Amp^r, Novagen)[9, 25-27] and S219V tobacco etch virus (TEV)[28] protease from PRK793 (Amp^r), have been previously described. A short-linker F23W variant of IsdG was prepared by site-directed mutagenesis using the QuickChange Lightning Kit (Agilent). The DNA primers to be used for mutagenesis were purchased from Midland Certified Reagent Company (Table D.1). DNA sequencing performed at the Vermont Integrative Genomics Resource at the University of Vermont confirmed the mutation of Phe23 to Trp (Table D.2). Plasmids encoding F23W IsdG were transformed in BL21-GOLD (DE3) cells (Stratagene).

Short-linker F23W IsdG was expressed as described previously for WT IsdG.[27] The purification of F23W IsdG was performed as previously described for WT IsdG with some modifications.[9, 25, 27] Cell pellets from 1 L of cell growth were lysed as previously described.[26] This was performed two more times and the filtered lysate were pooled before loading onto a 5 mL, nickel(II)-charged HiTrap Chelating HP column (GE Healthcare) equilibrated with 50 mM Tris pH 7.4, 150 mM NaCl using an ÄKTA Pure 25 L fast protein liquid chromatography (FPLC) system (GE Healthcare). After loading the filtered lysate onto the nickel(II)-charged HiTrap Chelating HP column, the column was washed with a 1.3 mM/mL linear gradient from 0 – 80 mM imidazole in 50 mM Tris pH 7.4, 150 mM NaCl at a flow rate of 5.0 mL/min. Pure, uncleaved F23W IsdG eluted during a subsequent 2.2 mM/mL linear gradient from 80 mM – 300 mM imidazole in 50 mM Tris pH 7.4, 150 mM NaCl at a flow rate of 5.0 mL/min (Figure D.1). FPLC fractions containing pure uncleaved F23W IsdG were assessed by SDS-PAGE gel electrophoresis (Figure D.2). The N-terminal His_6 tag was removed as previously described for WT IsdI.[23, 27, 29] The purity of the resulting pure untagged, short-linked F23W IsdG was >99%, as assessed by SDS-PAGE gel electrophoresis (Figure D.2).

Circular Dichroism(CD) spectroscopy. CD spectroscopy was utilized to analyze the secondary structure of short-linker F23W IsdG. F23W IsdG was exchanged onto 10 mM potassium phosphate (KP_i) pH 7.4 buffer using PD-10 desalting columns (GE Healthcare) and loaded onto 2mm path length quartz cuvettes (Starna). CD spectra were acquired from 260 – 185 nm with a scan speed of 20 nm/min, 1.0 nm bandwidth, 0.5 nm data pitch and a digital integration time of 8s using a Jasco J-1500 spectropolarimeter. A total of 6

spectra were collected and averaged, then subtracted from the CD spectra of blank buffer (10 mM KP_i pH 7.4) to get the final CD spectrum of F23W IsdG.

Electrospray Ionization Mass Spectrometry (ESI-MS). ESI-MS was used to assess His_6 tagged and untagged F23W IsdG. 25-uM samples of His_6 tagged and untagged F23W IsdG in 50 mM Tris pH 7.4, 150 mM NaCl were loaded onto C18 guard columns equilibrated with 2% acetonitrile with 0.1% formic acid (v/v) in water (v/v) using a QTRAP 4000 LCMS/MS system (Sciex) with an M/z from 600-2000. The samples were run on a linear gradient from 2 to 98% acetonitrile with 0.1% formic acid (v/v) in water (v/v) at a flow rate of 100 µL/min. The spectrum was deconvoluted using BioAnalyst 1.5 software. The observed molecular weights of His_6 tagged and untagged F23W IsdG are consistent with their calculated molecular weights (Figure D.3 and D.4)

Abs Spectroscopy. Short-linker heme-bound F23W IsdG (F23W IsdG–heme) and cyanide-inhibited F23W IsdG (F23W IsdG–heme–CN) were prepared as described previously for long-linker WT IsdG.[25, 27] The molar extinction coefficients were assessed for both of these species using the pyridine hemochrome method.[30] The molar extinction coefficients for F23W IsdG–heme and F23W IsdG–heme–CN were calculated as ε_{412} = 92.6 mM^{-1} cm^{-1} and ε_{420} = 90.3 mM^{-1} cm^{-1} respectively.

Room temperature Abs spectroscopy was used to assess heme ruffling byF23W IsdG. Abs spectra were collected for F23W IsdG–heme–CN samples in 50 mM Tris pH 7.4, 150 mM NaCl. The Abs spectra was collected on a Cary 100 Bio spectrophotometer from 800 – 200 nm with a scan rate of 600 nm/min, 0.1 s digital integration time, 2 nm bandwidth, and 1.0 nm data interval.

Abs Assay. The activity of heme catalyzed by F23W IsdG were analyzed by Abs spectroscopy. Degradation of 25 μM of F23W IsdG–heme in 50 mM Tris pH 7.4, 150 mM NaCl was performed in the presence of 2.5 mM ascorbate, 1 mM Ethylenediaminetetraacetic acid (EDTA), 1 K units of bovine liver catalase (Sigma Aldrich). Assays were run at room temperature and the Abs spectra of the reaction mixture were acquired every 2.5 mins between 800 – 200 nm for 60 mins with a scan rate of 600 nm/min, 0.1 s digital integration time, 2 nm bandwidth, and 1.0 nm data interval.

Liquid Chromatography-Mass Spectrometry (LC-MS) Assay. Using the same reaction condition as above, LC-MS was used to determine the composition of products formed as a function of time for the degradation of heme by F23W IsdG. LC-MS was performed on a system composed of a Shimadzu Prominence HPLC system coupled to an ABI Sciex 4000 QTrap Pro hybrid triple-quadrupole mass spectrometer operated in positive ion mode. Heme degradation sample of F23W IsdG at 10 and 60 mins were injected onto the LC-MS equilibrated with 2% acetonitrile with 0.1% formic acid (v/v) in water (v/v). The m/z 599, 611 and 616 peaks eluted with a linear gradient from 2 to 98% acetonitrile with 0.1% formic acid (v/v) in water (v/v) over 50 mins using a C4 LC column in a positive ESI scanning from m/z 600-1500. Ion chromatogram (EIC) of the target ions (m/z 599, 611 and 616) were extracted from the total ion chromatogram (TIC) from each LC-MS run.

5.3 RESULTS

CD Spectroscopy. CD spectroscopy was used to gain insights into the secondary structures of apo IsdG due to the F23W substitution. Fitted CD spectra of F23W IsdG

gave 10% α-helices and 35% β-sheets (Figure D.5 and Table D.3).[31-34] This is close to the observed secondary structure of WT IsdG (9% α-helices and 35% β-sheets) by CD spectroscopy (Figure 5.2, Table D.3). Comparing these values, there isn't significant change in the secondary structure of IsdG induced by F23W mutation. Therefore, any changes in the spectroscopic data moving forward can be attributed to the change in the interactions within the enzyme active site.

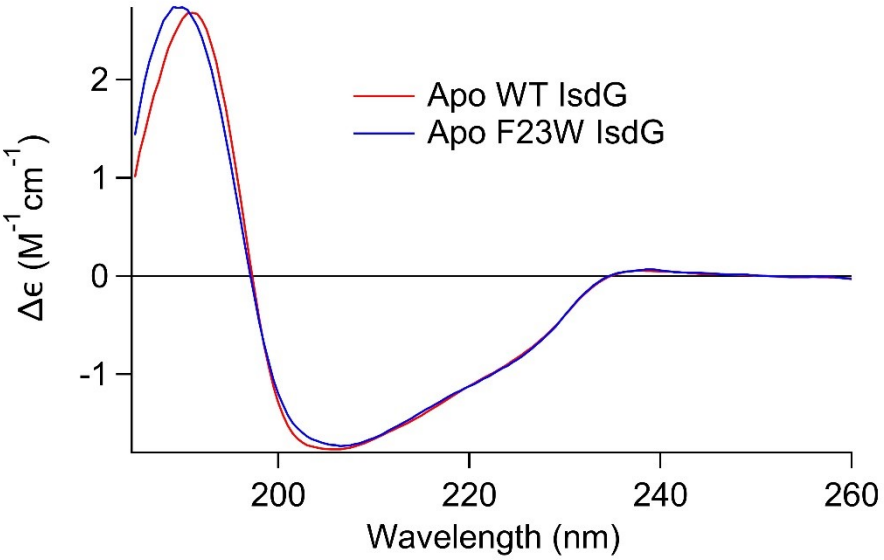

Figure 5. 2. UV CD spectra of the short-linker apo F23W IsdG (*solid blue*) in 10 mM potassium phosphate (KP_i) pH 7.4 was compared to that of WT IsdG[35] (*solid red*) (Figure D.5 and Table D.3).

Abs Spectroscopy Characterization: Using Abs spectroscopy, ruffling of the heme substrate within F23W MhuD–heme–CN was assessed. In the previously reported Abs spectrum of cyanide inhibited WT IsdG–heme, the lower energy Q-band is observed at 18,000 cm^{-1} and the higher energy Soret band is observed at 23,800 cm^{-1}. As compared to WT, there is no change in the the Q-band and the Soret band energy in the Abs

spectrum of F23W IsdG–heme–CN (Figure 5.3). The absorbance spectrum of porphyrin arises from the transition between two HOMOs (a_{1u} and a_{2u}) and two LUMOs (two e_g*), which give rise to two excited states.[36] Mixing of these states create a higher and a lower energy states corresponding to the Soret and the Q-bands, respectively. Effect of the second-sphere amino acid residue substitution on the heme macrocycle distortion has been studied in the past for *M. tuberculosis* MhuD[23, 37] and IsdG.[35] This can alter the

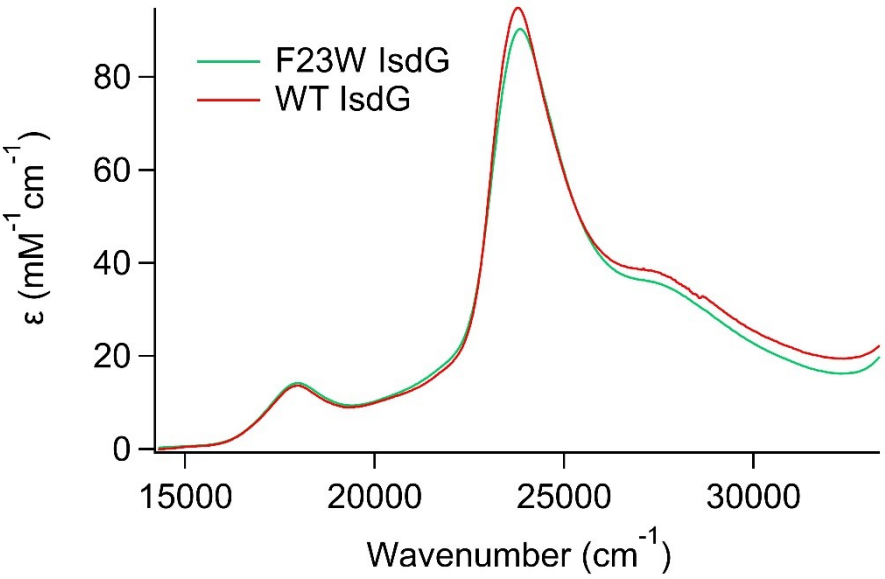

Figure 5. 3. UV/Vis absorption spectra of F23W IsdG–heme–CN (*solid green*) compared to that of WT IsdG–heme–CN (*solid red*).[35] The Soret and the Q-band energy remain unchanged after F23W substitution at 23,800 cm^{-1} and 18,000 cm^{-1} respectively.

Abs spectra of the heme bound enzyme by altering the energy gap between the filled a_{1u}/a_{2u} orbitals and the unoccupied e_g* orbitals. Previous DFT study has demonstrated that up to 1.0 Å ruffling of heme, there is no change in energy in the Q-band region, which then undergoes a red shift with increasing ruffling distortion.[37] However, up to 1.0 Å ruffling, the Soret band energy is blue shifted, and then red-shifts with larger degrees

of ruffling.[37] Since both the Soret and the Q-band energy did not change from WT to F23W, the mutation to bulkier Trp residue did not affect the heme ruffling, meaning that the filled a_{1u}/a_{2u} orbitals and the unoccupied e_g* orbitals stayed the same. This would also suggest that the heme is ruffled by ~2.04 Å in F23W IsdG–heme–CN, as observed for WT.[26]

Abs Assay. The heme degradation by F23W IsdG was monitored using Abs spectroscopy to understand the influence of Phe23 on the enzymatic efficiency (Figure 5.4). Previous studies have shown that Trp67 substitution to Ala completely stops the heme degradation activity by IsdG.[18] However, Trp67 substitution by less bulkier Phe in IsdG retained a decreased heme degradation activity compared to the WT enzyme.[35] On the other hand, effect of Phe23 substitution on the IsdG-mediated heme degradation has been studied previously by mutating Phe23 to smaller Ala residue.[18] The influence of Phe23 substitution to bulkier Trp residue is investigated here. Since heme can be degraded to biliverdin through the coupled oxidation pathway in the presence of hydrogen peroxide and a reductant, the heme degradation reaction by F23W

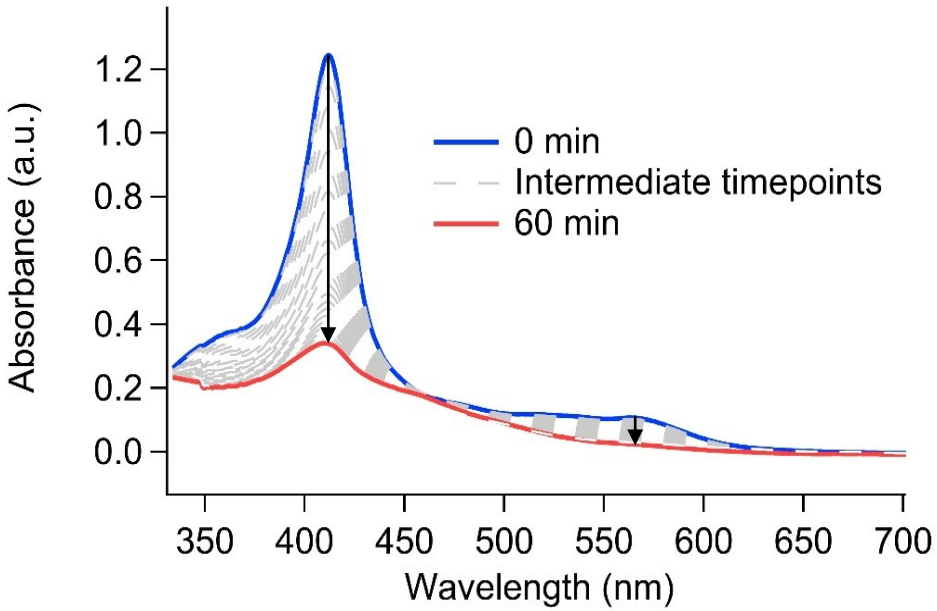

Figure 5. 4. UV/Vis monitored heme degradation by F23W IsdG (25 μM F23W IsdG–heme, 50 mM Tris pH 7.4, 150 mM NaCl) monitored every 2.5 mins for 60 mins at room temperature. Abs spectra at 0 min (*blue trace*), 2.5 – 57.5 mins (*Dashed grey*), and 60 mins (*solid red*) are shown. Vertical downward arrow at the Soret (412 nm) and the Q-band (563 nm) shows the direction of spectral change as a function of time.

IsdG was performed in the presence of catalase to avoid the degradation of heme through the coupled oxidation pathway.[38, 39] As a result, Abs monitored heme degradation spectral change would be due to the enzymatic heme degradation by F23W IsdG. Abs monitored activity assay by F23W IsdG showed decreased of the Soret band and the Q-band intensity at 412 nm and 563 nm respectively, as a function of time. This suggests that the degradation of heme is being carried out by F23W IsdG, which means that Phe23 substitution to bulkier Trp residue does not affect the enzymatic activity of IsdG. This observation agrees with the previous study, where the F23A substitution did not alter the heme degradation activity of IsdG.[18] However, previous study monitored the degradation

of heme but not the formation of products. Thus, in this study, the product identity of the heme degradation by F23W IsdG was monitored by LC-MS.

LC-MS assay. LC-MS was used to determine the composition of the products formed during the heme degradation reaction catalyzed by F23W IsdG. The F23W substitution does not seem to affect the enzymatic activity of IsdG, as demonstrated by the Abs monitored activity assay. Thus, to investigate if the heme degradation by IsdG is proceeding through similar mechanism after the Phe23 substitution to Trp, LC-MS was utilized. Like the Abs activity assay above, the heme degradation assay utilizing LC-MS was performed in the presence of catalase, to identify the products formed through the enzymatic degradation of heme by F23W IsdG. The heme degradation by F23W IsdG was monitored at two different time-points (10 and 60 mins) to understand the evolution of products being formed with time (Figure 5.5). At the initial 10 mins time-point, the MS spectra revealed three peaks of m/z 599, 611 and 616. These peaks correspond

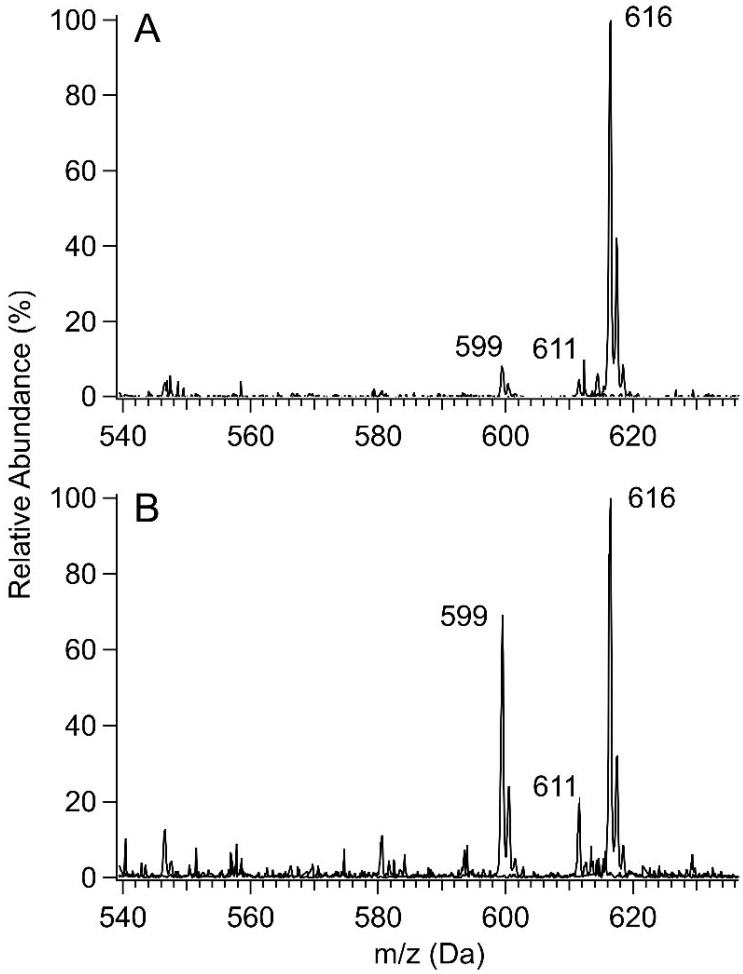

Figure 5. 5. LC-MS spectra of heme degradation by F23W IsdG at 10 mins (*A, top*) and 60 mins (*B, bottom*). Three peaks of m/z 599, 611 and 616 is observed at both time-points with different relative intensity. These peaks correspond to staphylobilin, formyl-oxo-bilin and heme, respectively.

with molar mass of staphylobilin, formyl-oxo-bilin, and heme, respectively.[40] The m/z 616 peak has the highest intensity compared to other peaks, which is expected as the heme degradation reaction is in its initial time-point. LC-MS performed at 60 min time-point again revealed the same three peaks, but their relative intensity changed as a function of time. As expected, m/z 599 peak at 60 mins has a higher intensity than at 10

mins. The peak intensity of m/z 611 also noticeably increased during the same time interval. As the heme degradation reaction proceeds forward, heme is degraded to form the final product staphylobilin along with the intermediate formyl-oxo-bilin. Formyl-oxo-bilin has been observed in the past as an intermediate on the way towards formation of staphylobilin during the heme degradation by IsdG.[40] The LC-MS data for the heme degradation by F23W IsdG suggests that the Phe23 substitution to larger amino acid does not significantly alter the enzymatic mechanism of IsdG. The heme degradation by WT IsdG is proposed to proceed via $^2B_{2g}$ electronic ground state where the heme substrate is observed to be more ruffled than in MhuD.[19, 21, 25] Therefore, this lack of change in the enzymatic mechanism is consistent with the Abs data that suggested lack of observed structural changes in heme due to F23W substitution.

5.4 DISCUSSION

Implication of F23W substitution on heme ruffling. The F23W substitution induced effect on heme ruffling of IsdG was accessed using Abs spectroscopy. The heme substrate in the active site of IsdG/I enzymes are more ruffled (1.9 – 2.3 Å)[19, 21] compared to that of MhuD.[21] Ruffling has been shown to change the electronic ground state from ^2E_g [$(d_{xy})^2$ $(d_{xz}, d_{yz})^3$] to $^2B_{2g}$ [$(d_{xz}, d_{yz})^4$ $(d_{xy})^1$]. Less ruffled heme is observed for the canonical HO, however, more ruffled heme in the active site of non-canonical HO is observed and is proposed to be important for their enzymatic activity. Substitution of Phe23 to larger Trp residue was hypothesized to alter the amount of ruffling onto the heme macrocycle through the hydrophobic steric interaction. However, the Abs data of cyanide inhibited F23W IsdG–heme is unchanged when compared to the Abs spectrum of WT IsdG–heme–CN. This would suggest a minimal effect on the heme ruffling by F23W

substitution. In addition, a previous computational study has shown that the energy cost related to ruffling of increases rapidly for ruffling above 1.8 Å.[23] Thus, it is possible that the ruffling distortion ceiling might have already been reached for the heme bound IsdG, and that increasing the steric bulk at the second-sphere amino acid residues such as F23W, does not increase heme ruffling. This is because the energy cost becomes very high to attain a higher degree of ruffling. Therefore, we can speculate this as the reason behind lack of spectral change observed for F23W IsdG–heme–CN compared to WT IsdG–heme–CN. Based upon this Abs data, it is likely that the electronic structure of F23W IsdG–heme–CN remained unchanged from the WT variant.

Implication of F23W substitution on heme degradation. Heme degradation reaction mediated by F23W substitution in IsdG does not seem to significantly alter the enzymatic activity of the mechanism. The Abs monitored heme degradation by F23W MhuD showed a constant decrease of Soret and Q-band features as a function of time. The LC-MS data showed the formation of formyl-oxo-bilin and staphylobilin consistent with this Abs study and a previous heme degradation study[40], suggesting that the enzymatic mechanism of IsdG remained unchanged with the F23W substitution. This further implies that the increasing steric bulk at the residue 23 does not affect the heme degradation mechanism of IsdG and is consistent with the lack of structural change of heme substrate by the F23W substitution. This result is different from the heme degradation study performed for MhuD where the conserved Phe23 residue was mutated to Trp (Chapter 2).[23] In the study, it was observed that the increased steric bulk significantly altered the enzymatic mechanism of MhuD. The heme degradation became less efficient, which gave rise to an observation of the *meso*-hydroxyheme intermediate,

as investigated by Abs study (Chapter 3). This would suggest that the role of Phe23 in heme degradation mechanism for IsdG/I may be distinct, and that the dioxygenation mechanism by IsdG/I may be fundamentally different than that of MhuD.

Role of Phe23 in IsdG. The heme substrate makes extensive hydrophobic interactions with Leu9, Phe23, Phe64, Trp67, Leu68 and Val80 in IsdG. It has been suggested that Phe23 located on the distal side of the heme along with proximal Trp67 may induce observed heme ruffling in heme bound IsdG.[19] However, increasing the steric bulk of Phe23 did not significantly alter the heme ruffling or the heme degradation mechanism by IsdG. Similar to this study, substitution of Phe23 to Ala did not significantly alter the heme degradation by IsdG as well.[18] The Phe23 substitution resulted in change in the heme conformation and the enzymatic activity in MhuD, but not in IsdG. Therefore, it is interesting to point out that the role of conserved Phe23 residue in MhuD and IsdG are very different. The data collected from this study point towards the fact that Phe23 doesn't change the IsdG or the heme substrate structure, and thus, does not play a significant role in enzymatic mechanism of IsdG/I.

5.5 CONCLUSION

In conclusion, the effect of F23W substitution on heme ruffling and heme degradation of *Staphylococcus aureus* IsdG is investigated using Abs spectroscopy and LC-MS. The heme ruffling study performed using Abs spectroscopy also showed no change in ruffling of heme by F23W substitution. The Abs and LC-MS study on the enzymatic activity of F23W IsdG suggested that the F23W substitution did not significantly affect the heme degradation mechanism. The observation from these studies

are consistent with the fact that Phe23 may not play a significant role in heme degradation mechanism by IsdG.

5.6 CHAPTER 4 REFERENCES

1. van Hal, S. J.; Jensen, S. O.; Vaska, V. L.; Espedido, B. A.; Paterson, D. L.; Gosbell, I. B., Predictors of Mortality in Staphylococcus aureus Bacteremia. *Clin. Microbiol. Rev.*, 2012, *25* (2), 362-386.

2. Klein, E. Y.; Mojica, N.; Jiang, W. D.; Cosgrove, S. E.; Septimus, E.; Morgan, D. J.; Laxminarayan, R., Trends in Methicillin-Resistant Staphylococcus aureus Hospitalizations in the United States, 2010-2014. *Clin. Infect. Dis.*, 2017, *65* (11), 1921-1923.

3. Turner, N. A.; Sharma-Kuinkel, B. K.; Maskarinec, S. A.; Eichenberger, E. M.; Shah, P. P.; Carugati, M.; Holland, T. L.; Fowler, V. G., Methicillin-resistant Staphylococcus aureus: an overview of basic and clinical research. *Nat. Rev. Microbiol.*, 2019, *17* (4), 203-218.

4. Skaar, E. P.; Humayun, M.; Bae, T.; DeBord, K. L.; Schneewind, O., Iron-source preference of Staphylococcus aureus infections. *Science*, 2004, *305* (5690), 1626-1628.

5. Mazmanian, S. K.; Skaar, E. P.; Gaspar, A. H.; Humayun, M.; Gornicki, P.; Jelenska, J.; Joachmiak, A.; Missiakas, D. M.; Schneewind, O., Passage of heme-iron across the envelope of Staphylococcus aureus. *Science*, 2003, *299* (5608), 906-909.

6. Grigg, J. C.; Vermeiren, C. L.; Heinrichs, D. E.; Murphy, M. E. P., Haem recognition by a Staphylococcus aureus NEAT domain. *Mol. Microbiol.*, 2007, *63* (1), 139-149.

7. Torres, V. J.; Pishchany, G.; Humayun, M.; Schneewind, O.; Skaar, E. P., Staphylococcus aureus IsdB is a hemoglobin receptor required for heme iron utilization. *J. Bacteriol.*, 2006, *188* (24), 8421-8429.

8. Tiedemann, M. T.; Muryoi, N.; Heinrichs, D. E.; Stillman, M. J., Iron acquisition by the haem-binding Isd proteins in Staphylococcus aureus: studies of the mechanism using magnetic circular dichroism. *Biochem. Soc. Trans.*, 2008, *36*, 1138-1143.

9. Skaar, E. P.; Gaspar, A. H.; Schneewind, O., IsdG and IsdI, heme-degrading enzymes in the cytoplasm of Staphylococcus aureus. *J. Biol. Chem.*, 2004, *279* (1), 436-43.

10. Matsui, T.; Nambu, S.; Ono, Y.; Goulding, C. W.; Tsumoto, K.; Ikeda-Saito, M., Heme degradation by Staphylococcus aureus IsdG and IsdI liberates formaldehyde rather than carbon monoxide. *Biochemistry*, 2013, *52* (18), 3025-7.

11. Reniere, M. L.; Ukpabi, G. N.; Harry, S. R.; Stec, D. F.; Krull, R.; Wright, D. W.; Bachmann, B. O.; Murphy, M. E.; Skaar, E. P., The IsdG-family of haem oxygenases degrades haem to a novel chromophore. *Mol. Microbiol.*, 2010, *75* (6), 1529-38.

12. Tenhunen, R.; Marver, H. S.; Schmid, R., Microsomal heme oxygenase. Characterization of the enzyme. *J. Biol. Chem.*, 1969, *244* (23), 6388-94.

13. Matsui, T.; Unno, M.; Ikeda-Saito, M., Heme oxygenase reveals its strategy for catalyzing three successive oxygenation reactions. *Acc. Chem. Res.*, 2010, *43* (2), 240-7.

14. Schmitt, M. P., Utilization of host iron sources by Corynebacterium diphtheriae: identification of a gene whose product is homologous to eukaryotic heme oxygenases and is required for acquisition of iron from heme and hemoglobin. *J. Bacteriol.*, 1997, *179* (3), 838-45.

15. Zhu, W.; Wilks, A.; Stojiljkovic, I., Degradation of heme in gram-negative bacteria: the product of the hemO gene of Neisseriae is a heme oxygenase. *J. Bacteriol.*, 2000, *182* (23), 6783-90.

16. Chen, H.; Moreau, Y.; Derat, E.; Shaik, S., Quantum mechanical/molecular mechanical study of mechanisms of heme degradation by the enzyme heme

oxygenase: the strategic function of the water cluster. *J. Am. Chem. Soc.*, 2008, *130* (6), 1953-65.

17. Wilks, A.; Heinzl, G., Heme oxygenation and the widening paradigm of heme degradation. *Arch. Biochem. Biophys.*, 2014, *544*, 87-95.

18. Wu, R. Y.; Skaar, E. P.; Zhang, R. G.; Joachimiak, G.; Gornicki, P.; Schneewind, O.; Joachimiak, A., Staphylococcus aureus IsdG and IsdI, heme-degrading enzymes with structural similarity to monooxygenases. *J. Biol. Chem.*, 2005, *280* (4), 2840-2846.

19. Lee, W. C.; Reniere, M. L.; Skaar, E. P.; Murphy, M. E., Ruffling of metalloporphyrins bound to IsdG and IsdI, two heme-degrading enzymes in Staphylococcus aureus. *J. Biol. Chem.*, 2008, *283* (45), 30957-63.

20. Takayama, S. J.; Ukpabi, G.; Murphy, M. E.; Mauk, A. G., Electronic properties of the highly ruffled heme bound to the heme degrading enzyme IsdI. *Proc. Natl. Acad. Sci.*, 2011, *108* (32), 13071-6.

21. Graves, A. B.; Morse, R. P.; Chao, A.; Iniguez, A.; Goulding, C. W.; Liptak, M. D., Crystallographic and spectroscopic insights into heme degradation by Mycobacterium tuberculosis MhuD. *Inorg. Chem.*, 2014, *53* (12), 5931-40.

22. Chim, N.; Iniguez, A.; Nguyen, T. Q.; Goulding, C. W., Unusual diheme conformation of the heme-degrading protein from Mycobacterium tuberculosis. *J. Mol. Bio.*, 2010, *395* (3), 595-608.

23. Graves, A. B.; Horak, E. H.; Liptak, M. D., Dynamic ruffling distortion of the heme substrate in non-canonical heme oxygenase enzymes. *Dalton Trans.*, 2016, *45* (24), 10058-67.

24. Ukpabi, G.; Takayama, S. J.; Mauk, A. G.; Murphy, M. E., Inactivation of the heme degrading enzyme IsdI by an active site substitution that diminishes heme ruffling. *J. Biol. Chem.*, 2012, *287* (41), 34179-88.

25. Lockhart, C. L.; Conger, M. A.; Pittman, D. S.; Liptak, M. D., Hydrogen bond donation to the heme distal ligand of Staphylococcus aureus IsdG tunes the electronic structure. *J. Biol. Inorg. Chem.*, 2015, *20* (5), 757-70.

26. Conger, M. A.; Cornetta, A. R.; Liptak, M. D., Spectroscopic Evidence for Electronic Control of Heme Hydroxylation by IsdG. *Inorg. Chem.*, 2019, *58* (22), 15455-15465.

27. Conger, M. A.; Pokhrel, D.; Liptak, M. D., Tight binding of heme to Staphylococcus aureus IsdG and IsdI precludes design of a competitive inhibitor. *Metallomics*, 2017, *9* (5), 556-563.

28. Kapust, R. B.; Tozser, J.; Fox, J. D.; Anderson, D. E.; Cherry, S.; Copeland, T. D.; Waugh, D. S., Tobacco etch virus protease: mechanism of autolysis and rational design of stable mutants with wild-type catalytic proficiency. *Protein Eng*, 2001, *14* (12), 993-1000.

29. Nallamsetty, S.; Kapust, R. B.; Tozser, J.; Cherry, S.; Tropea, J. E.; Copeland, T. D.; Waugh, D. S., Efficient site-specific processing of fusion proteins by tobacco vein mottling virus protease in vivo and in vitro. *Protein Expression Purif.*, 2004, *38* (1), 108-15.

30. Berry, E. A.; Trumpower, B. L., Simultaneous determination of hemes a, b, and c from pyridine hemochrome spectra. *Anal. Biochem.*, 1987, *161* (1), 1-15.

31. Lobley, A.; Whitmore, L.; Wallace, B. A., DICHROWEB: an interactive website for the analysis of protein secondary structure from circular dichroism spectra. *Bioinformatics*, 2002, *18* (1), 211-2.

32. Whitmore, L.; Wallace, B. A., DICHROWEB, an online server for protein secondary structure analyses from circular dichroism spectroscopic data. *Nucleic Acids Res.*, 2004, *32* (Web Server issue), W668-73.

33. Compton, L. A.; Johnson, W. C., Jr., Analysis of protein circular dichroism spectra for secondary structure using a simple matrix multiplication. *Anal. Biochem.*, 1986, *155* (1), 155-67.

34. Sreerama, N.; Woody, R. W., Estimation of protein secondary structure from circular dichroism spectra: comparison of CONTIN, SELCON, and CDSSTR methods with an expanded reference set. *Anal. Biochem.*, 2000, *287* (2), 252-60.

35. Schuelke-Sanchez, A. E. Spectroscopic Study of the Formation and Degradation of Metalated Tetrapyrroles by the Enzymes CfbA, IsdG, and MhuD. Dissertation and Theses, University of Vermont, 2019.

36. Gouterman, M., Study of the Effects of Substitution on the Absorption Spectra of Porphin. *J. Chem. Phys.*, 1959, *30*, 1139 - 1161.

37. Graves, A. B.; Graves, M. T.; Liptak, M. D., Measurement of Heme Ruffling Changes in MhuD Using UV-vis Spectroscopy. *J. Phys. Chem. B*, 2016, *120* (16), 3844-53.

38. Falk, J. E., *Porphyrins and Metalloporphyrins*. Elsevier Publishing Co. : Amsterdam, 1964.

39. Jones, P.; Prudhoe, K.; Robson, T., Oxidation of deuteroferrihaem by hydrogen peroxide. *Biochem. J.*, 1973, *135* (2), 361-5.

40. Streit, B. R.; Kant, R.; Tokmina-Lukaszewska, M.; Celis, A. I.; Machovina, M. M.; Skaar, E. P.; Bothner, B.; DuBois, J. L., Time-resolved Studies of IsdG Protein Identify Molecular Signposts along the Non-canonical Heme Oxygenase Pathway. *J. Biol. Chem.*, 2016, *291* (2), 862-871.

CHAPTER 6: SYNTHESIS OF *MESO*–HYDROXYHEME: TO UNDERSTAND THE ENZYMATIC MECHANISM OF MHUD FOR CONVERSION OF β/δ-*MESO*–HYDROXYHEME TO MYCOBILIN.

6.1 INTRODUCTION

Heme oxygenases (HOs) are a family of enzymes found in mammals, bacteria and plants, that are involved in the biological process of heme degradation, where heme is oxidatively cleaved to form biliverdin, with the release of carbon monoxide (CO) and free iron.[1-3] During the heme degradation by HO, heme is first hydroxylated at the α-*meso* position to form α-*meso*-hydroxyheme.[4] Next, α-*meso*-hydroxyheme is converted to form verdoheme, by the release of *meso*-carbon as CO.[4, 5] Finally, verdoheme is converted to biliverdin through the oxidative cleavage at the α-*meso* position and the iron is released (Figure 6.1).[6, 7]

In bacterial pathogens, HO predominantly catalyzes heme to produce biliverdin,[8, 9] however, several bacterial pathogens such as *Mycobacterium tuberculosis* and

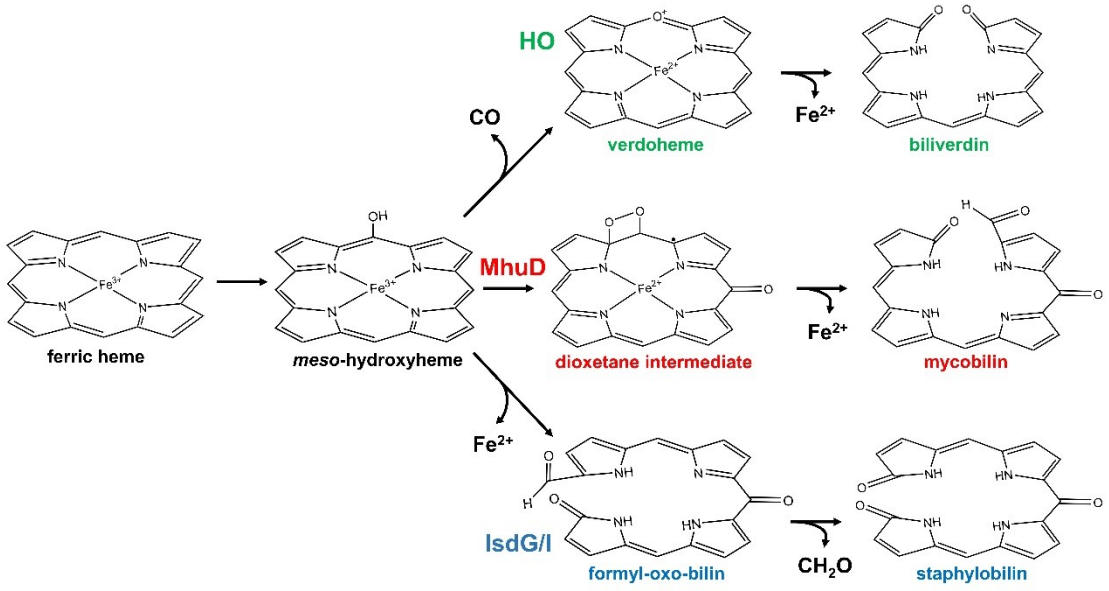

Figure 6. 1. Proposed heme degradation mechanism by HO, MhuD and IsdG/I. The first monooxygenation step on forming *meso*-hydroxyheme is common for all three. The subsequent degradation by HO (*top*), MhuD (*middle*) and IsdG/I (*bottom*) produces different side and final products by releasing iron.

In bacterial pathogens, HO predominantly catalyzes heme to produce biliverdin,[8, 9] however, several bacterial pathogens such as *Mycobacterium tuberculosis* and *Staphylococcus aureus* consists of non-canonical HO that degrades heme to produce different organic byproducts than biliverdin.[10-12] *M. tuberculosis* MhuD has been shown to degrade heme to mycobilin, with the release of free iron and the *meso*-carbon is retained as an aldehyde group.[11] On the other hand, *S. aureus* IsdG/I catalyzes heme to produce staphylobilin, with the release of free iron and formaldehyde (Figure 6.1).[10] Like canonical HO, the heme degradation by IsdG/I and MhuD has been proposed to go through a *meso*-hydroxyheme intermediate,[13, 14] and this is also where the similarities end between them. Moreover, unlike the canonical HO, the initial hydroxylation by IsdG/I and MhuD has been shown to happen at the β/δ-*meso* position (Figure 6.1).[10, 13, 14] Thus, these non-canonical HO follow distinct heme degradation mechanism than what has been known for canonical HO.

Previous studies have synthesized α-*meso*-hydroxyheme to help understand the nature of the α-*meso*-hydroxyheme-HO complex, as well as to help understand the underlying mechanism behind the conversion of α-*meso*-hydroxyheme to verdoheme[5, 7, 15, 16] because the reactive *meso*-hydroxyheme intermediate is hard to isolate and characterize. The *meso*-hydroxyheme is proposed to exist in a resonance structure of a keto form, a phenolate form, and a ferrous neutral radical form.[15] The spectroscopic study on the α-*meso*-hydroxyheme-HO complex has helped to understand its coordination chemistry.[15] More importantly, the verdoheme formation from α-*meso*-hydroxyheme-HO was suggested to go through either Fe(III) and Fe(II) state.[15] An Electron Paramagnetic Resonance study later revealed that an equilibrium between a Fe(III) and a Fe(II) with an

organic radical exists for α-*meso*-hydroxyheme-HO complex.[4] The studies involving the need of an oxygen and an electron for the conversion of α-*meso*-hydroxyheme to verdoheme using a synthetic *meso*-hydroxyheme has been controversial.[5, 15, 16] Nevertheless, a kinetic study has suggested that the more favorable path involves conversion of Fe(III) α-*meso*-hydroxyheme to Fe(III) verdoheme, which then gets reduced to Fe(II) verdoheme.[17]

Similarly, artificially synthesized *meso*-hydroxyheme can be complexed to MhuD in order to investigate the nature of *meso*-hydroxyheme-MhuD via spectroscopy, and to understand the mechanism on conversion of β/δ-*meso*-hydroxyheme to mycobilin. Previous study using artificial *meso*-hydroxyheme has showed that heme degradation by MhuD proceeds via β/δ-*meso*-hydroxyheme.[13] In addition, it also revealed that β/δ-*meso*-hydroxyheme gets converted to a dioxetane intermediate on the way to mycobilin formation (Figure 6.1).[13] Likewise, other spectroscopic techniques such as Magnetic Circular Dichroism can be utilized to understand the electronic ground state of the *meso*-hydroxyheme-MhuD, similar to what has been studied for MhuD–heme complex.[18-20] This can help understand any electronic driving force behind the dioxygenation reaction of β/δ-*meso*-hydroxyheme to mycobilin. Similarly, the synthetic *meso*-hydroxyheme can be complexed to R26S and W66F variants of MhuD in understanding the mechanism behind their role in formation of biliverdin instead of mycobilin (Chapter 3).[21] Therefore, the synthesis of *meso*-hydroxyheme will help answer lot of the questions regarding the second step of the heme degradation by MhuD (Figure 6.1).

The full synthetic steps on formation of *meso*-hydroxyheme from heme is shown in the Figure 6.2. However, in this study, synthesis of *meso*-benzoyloxyprotoporphyrin IX dimethyl ester from heme, using previously described methods is performed. Next step on the conversion of *meso*-benzoyloxyprotoporphyrin IX dimethyl ester to *meso*-

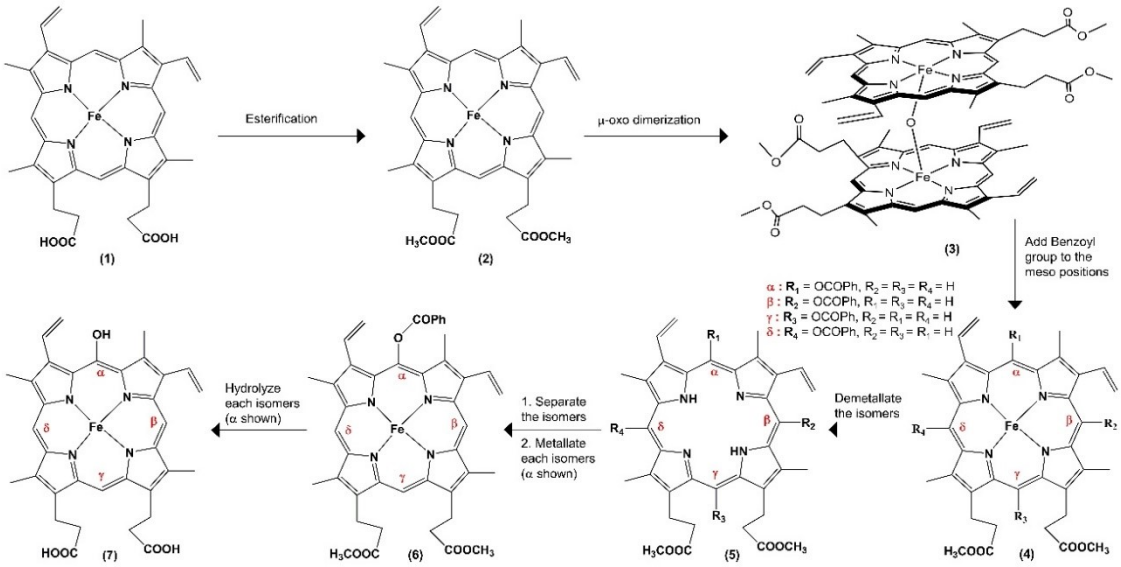

Figure 6. 2. Synthetic steps on formation of *meso*-hydroxyheme from heme.The products at each synthetic step are labelled from (1) to (7). They correspond to: heme (1), heme dimethyl ester (2), u-oxo-bis(heme dimethyl ester) (3), *meso*-benzoyloxy heme dimethyl ester isomers (4), *meso*-benzoyloxyprotoporphyrin IX dimethyl ester isomers (5), α-benzoyloxyprotoporphyrin IX dimethyl ester (6) and α-*meso*-hydroxyheme (7).

hydroxyheme is describe in the following chapter (Chapter 7). For the synthesis, previous methods were slightly modified, and are described below. The UV/Vis absorbance (Abs) spectroscopy along with the Mass Spectrometry (MS) were used to characterize the products at various synthetic steps. The results and some interesting observations during the synthesis has been reported and discussed in detail below.

6.2 EXPERIMENTAL

Unless otherwise noted, all materials in this work were purchased from Fisher Scientific and used without further purification.

Conversion of heme to heme dimethyl ester (hDME). The process of esterifying the acid groups of heme is well known and has been described previously.[22, 23] However, the method was adjusted slightly and described as follows. 0.5 g of hemin chloride was esterified using 50 mL sulfuric acid/methanol (5%, v/v) acid at room temperature while stirring overnight (~20 hrs). The resulting reaction mixture was washed with diethyl ether and hydrochloric acid/water (5%, w/v). The middle precipitate layer (hDME) was collected, filtered through a filter paper, and dried. The final yield was ~99%.

Conversion of hDME to μ-oxo-bis(heme dimethyl ester) [μ-oxo-bis(hDME)]. The dimerization reactions of hDME to μ-oxo-bis(hDME) has been previously been described.[24, 25] A modification was made during the alumina chromatography, where the dimer band was eluted with acetonitrile/chloroform (5%, v/v). Also, the crystallization of μ-oxo-bis(hDME) was modified using hexane-chloroform mixture. The final yield was ~25%.

Addition of *meso*-benzoyloxo group and demetallation to prepare isomeric mixture of *meso*-benzoyloxyprotoporphyrin IX dimethyl ester (*meso*-bPPIX-DME). The preparation of isomeric mixture of *meso*-benzoyloxyheme dimethyl ester and *meso*-bPPIX-DME was performed as described previously with some modifications.[7] The elution of isomeric mixture of *meso*-benzoyloxyheme dimethyl ester using alumina

chromatography was performed using chloroform/methanol (100:1, v/v). Likewise, after the demetallation, the elution of the isomeric mixture of *meso*-bPPIX-DME using alumina chromatography was performed using a mixture of acetonitrile/chloroform (5%, v/v).

Spectral Characterization. UV/Vis Absorbance (Abs) spectroscopy was utilized to analyze the spectra of hDME, μ-oxo-bis(hDME) and *meso*-bPPIX-DME in chloroform. The Abs spectra was collected on a Cary 100 Bio spectrophotometer with a scan rate of 600 nm/min, 0.1 s digital integration time, 2 nm bandwidth, and 1.0 nm data interval.

Mass Spectrometry (MS). Two different ionization techniques were utilized: Electrospray ionization (ESI-MS) and Atmospheric pressure chemical ionization (APCI-MS) for the sample analysis using ABI Sciex 4000 QTrap Pro hybrid triple-quadrupole mass spectrometer. Sample of hDME and μ-oxo-bis(hDME) was injected into the MS using ESI, equilibrated with 98% acetonitrile with 0.1% formic acid (v/v) in water (v/v). In addition, APCI was also used to inject the μ-oxo-bis(hDME) sample into the MS, equilibrated with 100% acetonitrile as the mobile phase. MS Data was analyzed using BioAnalyst 1.5.

6.3 RESULTS AND DISCUSSION

Spectral Characterization of hDME: The Abs spectra of the esterified product in chloroform was taken to make sure the esterification reaction was successful (Figure 6.3). The Abs spectrum of the esterified product in chloroform had a Soret band at 387 nm and Q-bands at 510, 541, and 641 nm. This is similar to the Abs spectrum reported

for the heme dimethyl ester in previous study.[26] Next, ESI-MS was also performed on the esterified product to confirm this result. During the extraction procedure, three different layers were observed in the separatory funnel. The top was an organic layer, middle was a precipitate, and the bottom layer was an aqueous mixture. Using ESI-MS organic, and

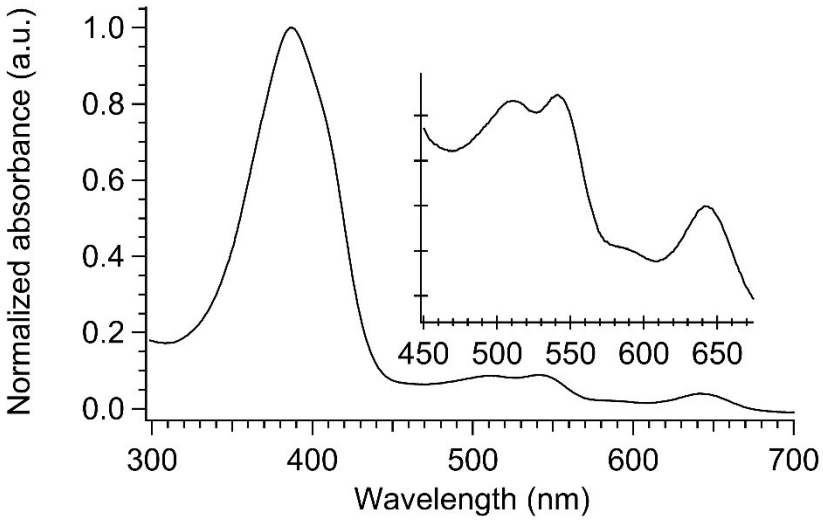

Figure 6. 3. Abs spectrum of esterified product in chloroform with Soret band at 387 nm and Q-bands at 510, 541, and 641 nm. It matches the Abs spectra of hDME. Inset: the zoomed in Abs spectrum from 450 to 675 nm.

the precipitate layer was analyzed to identify the formation of hDME. ESI-MS spectra of the precipitate dissolved in chloroform showed a defined peak of m/z 644.3 (Figure 6.4). This matches the theoretical mass of hDME (644.5 g/mol). However, the MS of the organic layer suggests that it may be a mixture of hDME and other impurities (Figure E.1). Qualitatively, the esterified heme is dark reddish in color when dissolved in chloroform. Therefore, Abs and MS data suggests that the esterification of heme was successful.

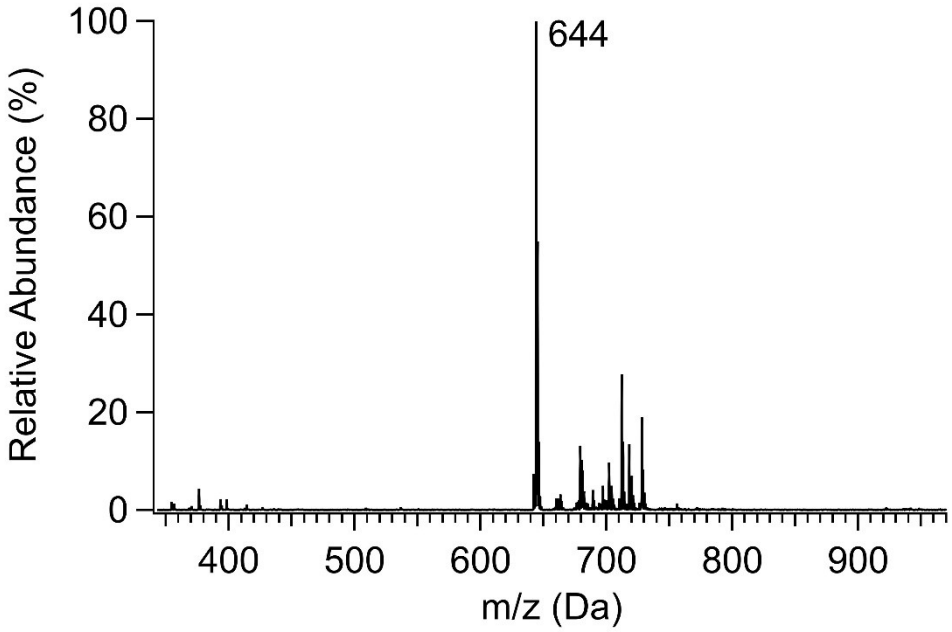

Figure 6. 4. ESI-MS spectrum of the esterified product (extracted precipitate). The m/z 644.3 is consistent with the theoretical mass of hDME (644.2 g/mol).

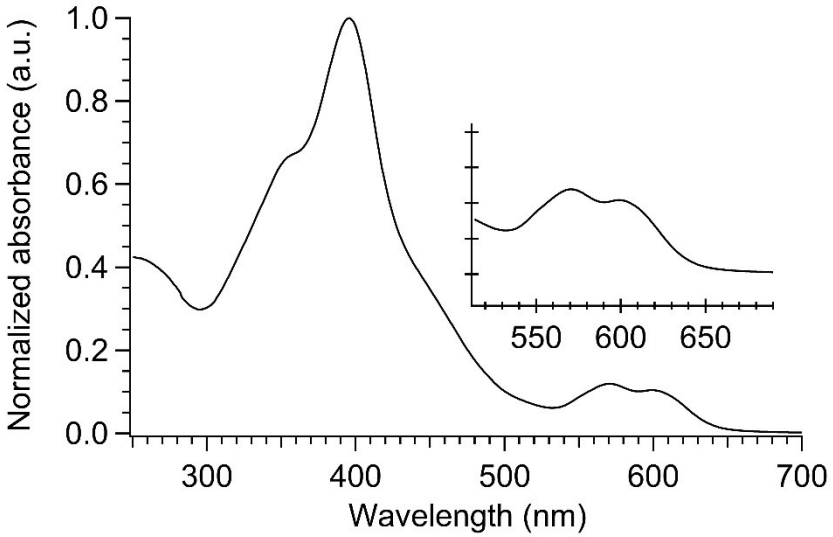

Figure 6. 5. Abs spectrum of dimerized product of the esterified heme (hDME) in chloroform with Soret band at 396 nm and Q-bands at 571 and 599 nm. Inset: the zoomed in Abs spectrum from 520 to 690 nm.

Spectral Characterization of μ-oxo-bis(hDME). After the dimerization, Abs spectra was taken to confirm the formation of μ-oxo-bis(hDME). The Abs spectrum is a match to the previously reported μ-oxo-bis(hDME),[27] with a Soret band at 396 nm and the Q-bands at 571 and 599 nm (Figure 6.5). Qualitatively, after the dimerization reaction, a change from reddish to a distinct green solution is observed. But the ESI-MS taken on the dimerized product revealed m/z of 644.3 (data no shown). Careful observations during the dimer synthesis pointed out that the dimer was not very stable in the acidic environment or in an organic solvent with a proton source. In the previous studies involving μ-oxo-bis(Fe(III)porphyrin) polymer[28, 29] and μ-oxo-bis(Fe(III)TPP)[30], the presence of Bronsted acid readily broke the μ-oxo bridge to give their respective monomers. This is shown to be a reversible phenomenon, where it reverts to μ-oxo bridged dimer upon addition of a base. Thus, the dimer formation seems to be acid-base controlled. Another study has determined that the dimerization of Iron(III) protoporphyrin IX is controlled by solvent identity.[31]The study revealed that the μ-oxo dimer does not form in the presence of a protic solvent. Instead π–π dimerization or monomer formation was observed when methanol, ethanol, 2-propanol, etc., was used.[31]

Thus, it is plausible that the ESI-MS process that is used to identify the μ-oxo-bis(hDME) in this study is breaking apart the μ-oxo bridge, because a small amount of formic acid [98% acetonitrile with 0.1% formic acid (v/v) in water (v/v)] is being used as a mobile phase (Figure E.2). Therefore, the mobile phase was changed to 100% acetonitrile and the ESI-MS was performed on the dimerized product (Figure E.3). Removing the proton source resulted in a peak at m/z 1343.7 and m/z 718.4. These peaks may be arising from the presence of potassium adduct ions (+K, m/z 38 for m/z 1343.7

peak and +2K-H, m/z 76 for m/z 718.4 peak). Changing the ionization source from ESI to APCI may get rid of the metal adduct ion problem. Unlike, ESI where the ionization occurs in the liquid-phase[32], the ionization in APCI occurs in the gas-phase[33]. Thus, the metal ions such as sodium and potassium cannot be easily vaporized as ions, consequently their corresponding adduct ions would be absent when APCI is used as an ionization source. APCI-MS of the dimerized sample showed a peak at m/z 1305.6 and m/z 644.2 (Figure E.4), corresponding to μ-oxo-bis(hDME) and hDME, respectively. Since APCI-MS is used for identification purposes only, it is impossible to quantify the amount of dimer species in solution because the ionization efficiency of the μ-oxo-bis(hDME) and hDME is not known. This data does, however, show that the dimerization reaction was successful. Thus, the crystallized dimer was used as a starting material for the next step in synthesis.

Spectral Characterization of *meso*-bPPIX-DME. During the alumina chromatography of the demetallated *meso*-benzoyloxyheme dimethyl ester, two distinct bands were observed; green top band and bright red bottom band. The bright red band was eluted using acetonitrile/chloroform (5%, v/v), while the green band did not travel. The green band may be the unreacted *meso*-benzoyloxyheme dimethyl ester. Abs spectra

for the bright red band in chloroform was taken (Figure 6.6). The Abs spectra of the bright red solution has a Soret band at 408 nm and the Q-bands at 506, 540, 578 and 630

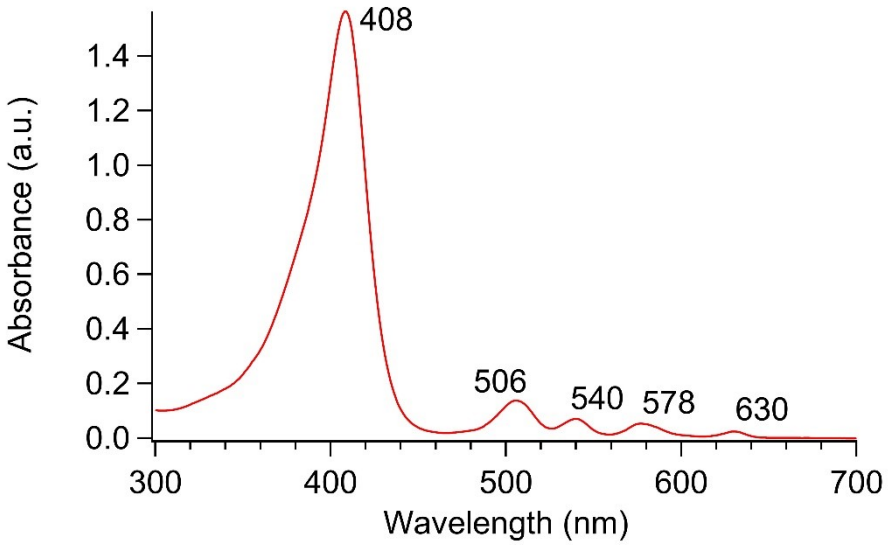

Figure 6. 6. UV/Vis absorbance spectra alumina eluted bright red band (*solid red*). The Soret band is observed at 408 nm and the Q-bands are observed at 506, 540, 578 and 630 nm. This is like the Abs spectra reported for *meso*-benzoyloxyprotoporphyrin IX dimethyl ester.[7, 34]

nm. This is consistent with the Abs spectra of α-benzoyloxoprotoporphyrin IX dimethyl ester[7, 34], however the Abs spectra for other *meso*-bPPIX-DME isomers (β, γ and δ) are also very similar[34]. Also, without the separation of these isomers, it is likely that the resulting Abs spectra is due to the combination of all four isomers in solution. Nonetheless, this suggests that *meso*-bPPIX-DME isomers were successfully synthesized. Several attempts to separate the isomers using a High Pressure Liquid Chromatography (HPLC) method as described previously, has been unsuccessful.[35] Careful qualitative inspection suggested that the color of the isomeric mixture of *meso*-bPPIX-DME was changing with time. Abs spectra was taken to check the changes in the color (Figure E.5).

In the old sample, a new peak at 666 nm is observed compared to the fresh sample. This may be due to the photooxidation of the *meso*-bPPIX-DME isomers. Previous studies have shown that photooxidation of protoporphyrin IX dimethyl ester in an aprotic solvent yielded a mixture of hydroxyaldehydes (photoprotoporphyrins), which is evidenced by the growth of a band at 670 nm.[36] Thus, it is likely that the *meso*-bPPIX-DME isomers has been photooxidized. The eluted isomeric mixture of *meso*-bPPIX-DME was not protected from light while performing HPLC separation. Along with mixtures of *meso*-bPPIX-DME isomers, photooxidized mixtures of these isomers could also be present in the solution, which can make HPLC separation quite difficult. Thus, the separation must be performed in the absence of light. Even though the separation of the isomers weren't completed, the data shows that the formation of the *meso*-bPPIX-DME isomers from μ-oxo-bis(hDME) was successful. It is worth noting that the Abs spectra of protoporphyrin IX dimethyl ester in chloroform is also very similar to the spectra of *meso*-bPPIX-DME isomers (Figure 6.3).[37] However, this seems unlikely and the ^{1}H NMR spectra on the separated *meso*-bPPIX-DME isomers can provide evidence regarding this issue.

6.4 CONCLUSION

In conclusion, hemin chloride has been successfully esterified to heme dimethyl ester and confirmed with Abs spectroscopy. Next, the ester was dimerized to form μ-oxo-bis(heme dimethyl ester) and confirmed with Abs spectroscopy and Mass Spectrometry. Finally, the addition of benzoyl-oxo protecting group onto the *meso* carbons of the dimer, followed by its demetallation, resulted in the formation of *meso*-henzoyloxyprotoporphyrin IX dimethyl ester isomers. The formation *meso*-bPPIX-DME was suggested by the Abs spectroscopy, however, more work needs to be done to confirm

this. The final goal for this project is to synthesize *meso*-hydroxyheme, thus its future directions are discussed in the following chapter (Chapter 7).

6.5 CHAPTER 6 REFERENCES

1. Tenhunen, R.; Marver, H. S.; Schmid, R., Microsomal heme oxygenase. Characterization of the enzyme. *J. Biol. Chem.*, 1969, *244* (23), 6388-94.

2. Matsui, T.; Unno, M.; Ikeda-Saito, M., Heme oxygenase reveals its strategy for catalyzing three successive oxygenation reactions. *Acc. Chem. Res.*, 2010, *43* (2), 240-7.

3. Yoshida, T.; Kikuchi, G., Features of the reaction of heme degradation catalyzed by the reconstituted microsomal heme oxygenase system. *J. Biol. Chem.*, 1978, *253* (12), 4230-6.

4. Liu, Y.; Moenne-Loccoz, P.; Loehr, T. M.; Ortiz de Montellano, P. R., Heme oxygenase-1, intermediates in verdoheme formation and the requirement for reduction equivalents. *J. Biol. Chem.*, 1997, *272* (11), 6909-17.

5. Sakamoto, H.; Omata, Y.; Palmer, G.; Noguchi, M., Ferric alpha-hydroxyheme bound to heme oxygenase can be converted to verdoheme by dioxygen in the absence of added reducing equivalents. *J. Biol. Chem.*, 1999, *274* (26), 18196-18200.

6. Yoshinaga, T.; Sudo, Y.; Sano, S., Enzymatic Conversion of Alpha-Oxyprotohaem-Ix into Biliverdin-Ix-Alpha by Heme Oxygenase. *Biochem. J.*, 1990, *270* (3), 659-664.

7. Sano, S.; Sano, T.; Morishima, I.; Shiro, Y.; Maeda, Y., On the mechanism of the chemical and enzymic oxygenations of alpha-oxyprotohemin IX to Fe.biliverdin IX alpha. *Proc. Natl. Acad. Sci.*, 1986, *83* (3), 531-5.

8. Schmitt, M. P., Utilization of host iron sources by Corynebacterium diphtheriae: identification of a gene whose product is homologous to eukaryotic heme

oxygenases and is required for acquisition of iron from heme and hemoglobin. *J. Bacteriol.*, 1997, *179* (3), 838-45.

9. Zhu, W.; Wilks, A.; Stojiljkovic, I., Degradation of heme in gram-negative bacteria: the product of the hemO gene of Neisseriae is a heme oxygenase. *J. Bacteriol.*, 2000, *182* (23), 6783-90.

10. Reniere, M. L.; Ukpabi, G. N.; Harry, S. R.; Stec, D. F.; Krull, R.; Wright, D. W.; Bachmann, B. O.; Murphy, M. E.; Skaar, E. P., The IsdG-family of haem oxygenases degrades haem to a novel chromophore. *Mol. Microbiol.*, 2010, *75* (6), 1529-38.

11. Nambu, S.; Matsui, T.; Goulding, C. W.; Takahashi, S.; Ikeda-Saito, M., A new way to degrade heme: the Mycobacterium tuberculosis enzyme MhuD catalyzes heme degradation without generating CO. *J. Biol. Chem.*, 2013, *288* (14), 10101-9.

12. Matsui, T.; Nambu, S.; Ono, Y.; Goulding, C. W.; Tsumoto, K.; Ikeda-Saito, M., Heme degradation by Staphylococcus aureus IsdG and IsdI liberates formaldehyde rather than carbon monoxide. *Biochemistry*, 2013, *52* (18), 3025-7.

13. Matsui, T.; Nambu, S.; Goulding, C. W.; Takahashi, S.; Fujii, H.; Ikeda-Saito, M., Unique coupling of mono- and dioxygenase chemistries in a single active site promotes heme degradation. *Proc. Natl. Acad. Sci.*, 2016, *113* (14), 3779-84.

14. Streit, B. R.; Kant, R.; Tokmina-Lukaszewska, M.; Celis, A. I.; Machovina, M. M.; Skaar, E. P.; Bothner, B.; DuBois, J. L., Time-resolved Studies of IsdG Protein Identify Molecular Signposts along the Non-canonical Heme Oxygenase Pathway. *J. Biol. Chem.*, 2016, *291* (2), 862-871.

15. Matera, K. M.; Takahashi, S.; Fujii, H.; Zhou, H.; Ishikawa, K.; Yoshimura, T.; Rousseau, D. L.; Yoshida, T.; IkedaSaito, M., Oxygen and one reducing equivalent are both required for the conversion of alpha-hydroxyhemin to verdoheme in heme oxygenase. *J. Biol. Chem.*, 1996, *271* (12), 6618-6624.

16. Migita, C. T.; Fujii, H.; Mansfield Matera, K.; Takahashi, S.; Zhou, H.; Yoshida, T., Molecular oxygen oxidizes the porphyrin ring of the ferric alpha-hydroxyheme in heme oxygenase in the absence of reducing equivalent. *Biochim. Biophys. Acta*, 1999, *1432* (2), 203-13.

17. Sakamoto, H.; Takahashi, K.; Higashimoto, Y.; Harada, S.; Palmer, G.; Noguchi, M., A kinetic study of the mechanism of conversion of alpha-hydroxyheme to verdoheme while bound to heme oxygenase. *Biochem. Biophys. Res. Commun.*, 2005, *338* (1), 578-83.

18. Graves, A. B.; Morse, R. P.; Chao, A.; Iniguez, A.; Goulding, C. W.; Liptak, M. D., Crystallographic and spectroscopic insights into heme degradation by Mycobacterium tuberculosis MhuD. *Inorg. Chem.*, 2014, *53* (12), 5931-40.

19. Graves, A. B.; Horak, E. H.; Liptak, M. D., Dynamic ruffling distortion of the heme substrate in non-canonical heme oxygenase enzymes. *Dalton Trans.*, 2016, *45* (24), 10058-67.

20. Graves, A. B.; Graves, M. T.; Liptak, M. D., Measurement of Heme Ruffling Changes in MhuD Using UV-vis Spectroscopy. *J. Phys. Chem. B*, 2016, *120* (16), 3844-53.

21. Chao, A.; Goulding, C. W., A Single Mutation in the Mycobacterium tuberculosis Heme-Degrading Protein, MhuD, Results in Different Products. *Biochemistry*, 2019, *58* (6), 489-492.

22. Clezy, P. S.; Morell, D. B., A spectroscopic study of haematin compounds in the Soret region. *Biochim. Biophys. Acta*, 1963, *71*, 165-71.

23. Falk, J. E.; Dresel, E. I.; Benson, A.; Knight, B. C., Studies on the biosynthesis of blood pigments. 4. The nature of the porphyrins formed on incubation of chicken erythrocyte preparations with glycine, delta-aminolaevulic acid or porphobilinogen. *Biochem. J.*, 1956, *63* (1), 87-94.

24. Fleischer, E. B., Srivastava, T. S., Structure and properties of .mu.-oxobis(tetraphenylporphineiron(III). *J. Am. Chem. Soc.*, 1969, *91* (9), 2403-2405.

25. Wicholas, M.; Mustacich, R.; Jayne, D., Proton nuclear magnetic resonance contact shifts of binuclear oxo-bridged iron (3) porphyrins. *J. Am. Chem. Soc.*, 1972, *94* (13), 4518-22.

26. Tetsuhiko, Y., Tomio, O., Equilibria of Imidazole Derivatives with (Protoporphyrin IX dimethyl ester)iron(III) Chloride. *Bulletin of the Chemical Society of Japan* 1979, *52* (8), 2268-2275.

27. O'Keeffe, D. H.; Barlow, C. H.; Smythe, G. A.; Fuchsman, W. H.; Moss, T. H.; Lilienthal, H. R.; Caughey, W. S., Magnetic and spectroscopic probes for FeOFe linkages in hemin systems. *Bioinorg. Chem.*, 1975, *5* (2), 125-47.

28. Schappacher, M.; Deffieux, A., Reversible Switching between Linear and Ring Polystyrenes Bearing Porphyrin End Groups. *J. Am. Chem. Soc.*, 2011, *133* (6), 1630-1633.

29. Schappacher, M.; Deffieux, A., Reversible Switching between Linear and Ring Poly(EO)s Bearing Iron Tetraphenylporphyrin Ends Triggered by Solvent, pH, or Redox Stimuli. *Macromolecules*, 2011, *44* (11), 4503-4510.

30. Ghosh, S. K.; Patra, R.; Rath, S. P., Synthesis, structure and photocatalytic activity of a remarkably bent, cofacial ethene-linked diiron (III) mu-oxobisporphyrin. *Inorg. Chim. Acta*, 2010, *363* (12), 2791-2799.

31. Asher, C.; de Villiers, K. A.; Egan, T. J., Speciation of Ferri protoporphyrin IX in Aqueous and Mixed Aqueous Solution Is Controlled by Solvent Identity, pH, and Salt Concentration. *Inorg. Chem.*, 2009, *48* (16), 7994-8003.

32. Ho, C. S.; Lam, C. W.; Chan, M. H.; Cheung, R. C.; Law, L. K.; Lit, L. C.; Ng, K. F.; Suen, M. W.; Tai, H. L., Electrospray ionisation mass spectrometry: principles and clinical applications. *Clin. Biochem. Rev.*, 2003, *24* (1), 3-12.

33. Bruins, A. P., Atmospheric-Pressure-Ionization Mass-Spectrometry .1. Instrumentation and Ionization Techniques. *TrAC, Trends Anal. Chem.*, 1994, *13* (1), 37-43.

34. Jackson, A. H.; Rao, K. R. N.; Wilkins, M., Synthetic and Biosynthetic-Studies of Porphyrins .11. The Synthesis of Meso Oxygenated Protoporphyrins. *J. Chem. Soc., Perkin Trans. 1*, 1987, (2), 307-312.

35. Hackson, A. H., Nagaraja Rao, K. R., Wilkins, M., Synthesis of the Four meso-Oxyprotoporphyrin Isomers. *J. Chem. Soc., Chem. Commun.*, 1982, (14), 794-796.

36. Cox, G. S., Whitten, D. G., Mechanisms for the photooxidation of protoporphyrin IX in solution. *J. Am. Chem. Soc.*, 1982, *102* (2), 516-521.

37. Falk, J. E., *Porphyrins and Metalloporphyrins*. Elsevier Publishing Co. : Amsterdam, 1964.

CHAPTER 7: CONCLUSIONS AND FUTURE DIRECTIONS

7.1 CONCLUSIONS

A spectroscopic and chromatographic study of MhuD and its variants has provided insights into the heme binding and degradation by MhuD. Also, a spectroscopic investigation of the F23W variant of IsdG provided detailed understanding on the role of Phe23 residue in the heme degradation mechanism. Heme binding affinity studied using fluorescence spectroscopy showed that MhuD binds the first heme with nanomolar dissociation constant, making it a competent HO *in vivo*. An Abs assay was developed to investigate the second dissociation constant. The micromolar binding affinity was extracted from the fitted Abs data for binding of a second heme by MhuD. This led us to propose that MhuD–diheme is a preferred state in a heme replete condition, and to speculate that MhuD may have a secondary function of heme storage or a regulatory protein. Next, the influence of second-sphere amino acids on the heme degradation mechanism was studied.

An Abs and MS study of WT, F23W and W66F MhuD was performed to investigate the role of active site induced heme ruffling on the heme degradation mechanism by MhuD. The heme substrate is more ruffled in F23W MhuD,[1] and less ruffled in W66F compared to WT MhuD.[2] Abs and MS monitored heme degradation by F23W MhuD showed decreased heme degradation activity. Furthermore, tandem LC-MS and Abs spectra identified the presence of a *meso*-hydroxyheme intermediate. Thus, the Abs monitored assay was used to determine the rate formation and destruction of the *meso*-hydroxyheme. The data suggested that the rate of formation of the intermediate is considerably faster than its rate of conversion to the final product. Thus, increased heme ruffling seems to alter the heme degradation pathway by slowing down the second step of

the mechanism. This would also suggest that planar heme conformation may be important for the conversion of *meso*-hydroxyheme to mycobilin. On the other hand, heme degradation by W66F MhuD was studied as a function of time using Abs and MS. The study confirmed the alteration of the product identity, as α–biliverdin is observed as the major product of heme degradation by W66F MhuD. This suggests that the active site of MhuD incorporating less ruffled heme dramatically changes the heme degradation mechanism in a way to accommodate different organic byproduct. These data suggest that the heme substrate ruffling deformation induced by the active site of MhuD is responsible for the unique heme degradation products. Therefore, it is important to have a dynamic heme in the active site of MhuD for its activity, because the absence of either of the heme conformation (planar or ruffled) completely alters the heme degradation mechanism.

A combination of Abs, NMR and MCD spectroscopy was utilized to study cyanide inhibited R26S MhuD–heme–CN to understand the role of Arg26 in heme degradation mechanism of MhuD. A recent study has shown that R26S MhuD degrades heme to biliverdin by the release of formaldehyde.[3] NMR spectroscopy confirmed the presence of two different species: one with ^2E_g [$(d_{xz}, d_{yz})^3 (d_{xy})^2$] electronic ground state (planar heme) and another with a mixture of ^2E_g and $^2B_{2g}$ [$(d_{xz}, d_{yz})^4 (d_{xy})^1$] electronic states (dynamic heme). The Abs spectrum of R26S showed lack of change in the Soret and the Q-band compared to WT MhuD–heme–CN, however, it is likely that the Abs spectroscopy may not be sensitive enough to distinguish between the two species. Moreover, VTVH MCD spectroscopy showed $^2B_{2g}$ as the electronic ground state of the dynamic species. Based on the crystal structure of MhuD–heme–CN[4] and MhuD–

diheme,[5] Arg26 forms a salt bridge interaction with a propionate group of heme in MhuD–heme, and with a propionate group of the solvent exposed heme in MhuD–diheme structure. Thus, losing this interaction would lead to lack of control on guiding heme into the correct binding pocket, which may result in binding of heme at different binding site inducing separate heme conformations. A heme degradation study performed using MS and a previous study[3] has shown that biliverdin and mycobilin are formed as the major and the minor product, respectively. Previous studies have shown, MhuD degrades dynamic heme in its active site to mycobilin and canonical HO degrades planar heme in its active site to biliverdin.[4, 6, 7] Thus, the presence of planar or dynamic heme in the active site may control the identity of heme degradation product by R26S MhuD. Therefore, these data led us to propose that the loss of Arg26 involved in stabilizing the monoheme binding site, changes the dynamics of the active site of R26S MhuD in a way to accommodate either planar or dynamic heme.

Besides MhuD, heme degradation of IsdG was also examined. Spectroscopic and chromatographic investigation on Phe23 substituted *Staphylococcus Aureus* IsdG was performed using a combination of Abs, CD and MS to gain insights on the role of Phe23 in the heme degradation mechanism by IsdG. CD spectroscopy showed a lack of structural changes in IsdG due to F23W substitution. Furthermore, the Abs spectrum of F23W IsdG confirmed that the bulkier amino acid substitution at the 23-residue position did not alter the heme conformation. The MS and the Abs monitored activity assays confirmed the presence of formyl-oxo-bilin and staphylobin, suggesting that the heme is being degraded efficiently by F23W IsdG. These data showed that the F23W substitution did not affect the heme degradation activity by IsdG, which is consistent with the CD and

the Abs data. Phe23 is a conserved residue in IsdG and MhuD, however, the data presented in this study strongly suggest that its role is distinct in each of these enzymes. Therefore, the Phe23 is not involved in the heme degradation mechanism by IsdG.

Finally, the synthesis of *meso*-hydroxyheme was initiated to investigate the electronic structure of the meso-hydroxyheme complexed with MhuD, and subsequently understand the mechanism behind the conversion *meso*-hydroxyheme to mycobilin. MS and Abs spectroscopy were utilized, which confirmed the identity of synthesized intermediates along the *meso*-hydroxyheme conversion process. Hemin chloride was used as a starting product and successfully converted to isomeric mixture of *meso*-benzoyloxoprotoporphyrin dimethyl ester (*meso*-bPPIX DME) using previously described methods with several modifications, as described in Chapter 6. However, the separation of these isomers along with their hydrolysis to form *meso*-hydroxyheme will be discussed below (Future direction).

7.2 FUTURE DIRECTIONS

A thorough investigation on heme degradation by F23W MhuD suggested that the second step of the heme degradation mechanism is significantly slowed down. This is the first instance where an intermediate; *meso*-hydroxyheme, has been observed during heme degradation by MhuD. The *meso*-hydroxyheme in canonical HO has been proposed to have a resonance structure of a ferric keto form, a ferric phenolate form, and a ferrous neutral radical form. Electron Paramagnetic Resonance (EPR) is a great tool to elucidate local environment, structure, and oxidation states of the paramagnetic center. Thus, EPR spectroscopy could be utilized to investigate *meso*-hydroxyheme. Previously, the reconstituted MhuD–β-*meso*-hydroxyheme study has identified the intermediate as a

ferrous neutral radical form using EPR spectroscopy.[8] However, past studies have shown that the experimentally observed *meso*-hydroxyheme complexed with the HO-1[9] had different structure than the one observed from the reconstituted HO1–β-*meso*-hydroxyheme.[10] Therefore, the intermediate observed during the heme degradation by F23W MhuD should be analyzed by EPR to characterize the intermediate.

Next, the *meso*-hydroxyheme synthesis can be completed from an isomeric mixture of *meso*-bPPIX DME. The separation of these isomers with Normal Phase HPLC has been unsuccessful. A previous method which uses 250 x 4 mm Hypersil 5 Silica column with Acetone :1,2-dichloroethane (1:99) as mobile phase has been successful in separating the isomers.[11] The method describes that the alumina chromatography for the collection of isomeric mixtures were performed in the dark and were collected in 50 mL batch and these batches were analyzed by HPLC at 400 nm. It should also be noted that the silica column is hygroscopic in nature and to maintain a consistent retention time and better separation, a 50% water-saturated mobile phase should be used.[12] Therefore, these changes can be done to the current HPLC method to separate the *meso*-bPPIX DME isomers. After the separation of the isomers, the separated *meso*-bPPIX DME can be metallated and hydrolyzed to give their respective *meso*-hydroxyheme isomer, as described previously.[13] It has been proposed that heme ruffling may alter the electronic structure and the reactivity of IsdG/I– and MhuD–*meso*-hydroxyheme complex, however, this remains untested experimentally. Therefore, Magnetic Circular Dichroism (MCD) spectroscopy can be used to characterize the electronic structure of MhuD–*meso*-hydroxyheme and the IsdG/I–*meso*-hydroxyheme complex.

7.3 CHAPTER 7 REREFENCES

1. Graves, A. B.; Horak, E. H.; Liptak, M. D., Dynamic ruffling distortion of the heme substrate in non-canonical heme oxygenase enzymes. *Dalton Trans.*, 2016, *45* (24), 10058-67.

2. Graves, A. B.; Graves, M. T.; Liptak, M. D., Measurement of Heme Ruffling Changes in MhuD Using UV-vis Spectroscopy. *J. Phys. Chem. B*, 2016, *120* (16), 3844-53.

3. Chao, A.; Goulding, C. W., A Single Mutation in the Mycobacterium tuberculosis Heme-Degrading Protein, MhuD, Results in Different Products. *Biochemistry*, 2019, *58* (6), 489-492.

4. Graves, A. B.; Morse, R. P.; Chao, A.; Iniguez, A.; Goulding, C. W.; Liptak, M. D., Crystallographic and spectroscopic insights into heme degradation by Mycobacterium tuberculosis MhuD. *Inorg. Chem.*, 2014, *53* (12), 5931-40.

5. Chim, N.; Iniguez, A.; Nguyen, T. Q.; Goulding, C. W., Unusual diheme conformation of the heme-degrading protein from Mycobacterium tuberculosis. *J. Mol. Bio.*, 2010, *395* (3), 595-608.

6. Sugishima, M.; Oda, K.; Ogura, T.; Sakamoto, H.; Noguchi, M.; Fukuyama, K., Alternative cyanide-binding modes to the haem iron in haem oxygenase. *Acta Crystallogr., Sect. F: Struct. Biol. Cryst. Commun.*, 2007, *63* (Pt 6), 471-4.

7. Tenhunen, R.; Marver, H. S.; Schmid, R., Microsomal heme oxygenase. Characterization of the enzyme. *J. Biol. Chem.*, 1969, *244* (23), 6388-94.

8. Matsui, T.; Nambu, S.; Goulding, C. W.; Takahashi, S.; Fujii, H.; Ikeda-Saito, M., Unique coupling of mono- and dioxygenase chemistries in a single active site promotes heme degradation. *Proc. Natl. Acad. Sci.*, 2016, *113* (14), 3779-84.

9. Liu, Y.; Moenne-Loccoz, P.; Loehr, T. M.; Ortiz de Montellano, P. R., Heme oxygenase-1, intermediates in verdoheme formation and the requirement for reduction equivalents. *J. Biol. Chem.*, 1997, *272* (11), 6909-17.

10. Matera, K. M.; Takahashi, S.; Fujii, H.; Zhou, H.; Ishikawa, K.; Yoshimura, T.; Rousseau, D. L.; Yoshida, T.; IkedaSaito, M., Oxygen and one reducing equivalent are both required for the conversion of alpha-hydroxyhemin to verdoheme in heme oxygenase. *J. Biol. Chem.*, 1996, *271* (12), 6618-6624.

11. Jackson, A. H.; Rao, K. R. N.; Wilkins, M., Synthetic and Biosynthetic-Studies of Porphyrins .11. The Synthesis of Meso Oxygenated Protoporphyrins. *J. Chem. Soc., Perkin Trans. 1*, 1987, (2), 307-312.

12. Bidlingmeyer, B. A., Liquid Chromatography Problem Solving and Troubleshooting. *J Chromatogr Sci*, 1996, *34* (11), 529.

13. Sano, S.; Sano, T.; Morishima, I.; Shiro, Y.; Maeda, Y., On the mechanism of the chemical and enzymic oxygenations of alpha-oxyprotohemin IX to Fe.biliverdin IX alpha. *Proc. Natl. Acad. Sci.*, 1986, *83* (3), 531-5.

COMPREHENSIVE BIBILIOGRAPHY

1. Anzaldi, L. L.; Skaar, E. P., Overcoming the heme paradox: heme toxicity and tolerance in bacterial pathogens. *Infect. Immun.*, 2010, *78* (12), 4977-89.

2. Aranda, R.; Worley, C. E.; Liu, M.; Bitto, E.; Cates, M. S.; Olson, J. S.; Lei, B.; Phillips, G. N., Bis-methionyl coordination in the crystal structure of the heme-binding domain of the streptococcal cell surface protein shp. *J. Mol. Bio.*, 2007, *374* (2), 374-383.

3. Asher, C.; de Villiers, K. A.; Egan, T. J., Speciation of Ferri protoporphyrin IX in Aqueous and Mixed Aqueous Solution Is Controlled by Solvent Identity, pH, and Salt Concentration. *Inorg. Chem.*, 2009, *48* (16), 7994-8003.

4. Bandarian, V.; Ludwig, M. L.; Matthews, R. G., Factors modulating conformational equilibria in large modular proteins: a case study with cobalamin-dependent methionine synthase. *Proc. Natl. Acad. Sci.*, 2003, *100* (14), 8156-63.

5. Barker, K. D.; Barkovits, K.; Wilks, A., Metabolic Flux of Extracellular Heme Uptake in Pseudomonas aeruginosa Is Driven by the Iron-regulated Heme Oxygenase (HemO). *J. Biol. Chem.*, 2012, *287* (22), 18342-18350.

6. Berry, E. A.; Trumpower, B. L., Simultaneous determination of hemes a, b, and c from pyridine hemochrome spectra. *Anal. Biochem.*, 1987, *161* (1), 1-15.

7. Berry, E. A.; Trumpower, B. L., Simultaneous Determination of Hemes-a, Hemes-B, and Hemes-C from Pyridine Hemochrome Spectra. *Anal Biochem*, 1987, *161* (1), 1-15.

8. Berry, E. A.; Trumpower, B. L., Simultaneous Determination of Hemes *a*, *b*, and *c* from Pyridine Hemochrome Spectra. *Anal. Biochem.*, 1987, *161* (1), 1-15.

9. Bidlingmeyer, B. A., Liquid Chromatography Problem Solving and Troubleshooting. *J. Chromatogr. Sci.*, 1996, *34* (11), 529.

10. Brouard, S.; Otterbein, L. E.; Anrather, J.; Tobiasch, E.; Bach, F. H.; Choi, A. M.; Soares, M. P., Carbon monoxide generated by heme oxygenase 1 suppresses endothelial cell apoptosis. *J. Exp. Med.*, 2000, *192* (7), 1015-26.

11. Bruins, A. P., Atmospheric-Pressure-Ionization Mass-Spectrometry .1. Instrumentation and Ionization Techniques. *TrAC, Trends Anal. Chem.*, 1994, *13* (1), 37-43.

12. Caignan, G. A.; Deshmukh, R.; Wilks, A.; Zeng, Y. H.; Huang, H. W.; Moenne-Loccoz, P.; Bunce, R. A.; Eastman, M. A.; Rivera, M., Oxidation of heme to beta- and delta-biliverdin by Pseudomonas aeruginosa heme oxygenase as a consequence of an unusual seating of the heme. *J. Am. Chem. Soc.*, 2002, *124* (50), 14879-14892.

13. Chan, A. C. K.; Lelj-Garolla, B.; Rosell, F. I.; Pedersen, K. A.; Mauk, A. G.; Murphy, M. E. P., Cofacial heme binding is linked to dimerization by a bacterial heme transport protein. *J. Mol. Bio.*, 2006, *362* (5), 1108-1119.

14. Chao, A.; Burley, K. H.; Sieminski, P. J.; de Miranda, R.; Chen, X.; Mobley, D. L.; Goulding, C. W., Structure of a Mycobacterium tuberculosis Heme-Degrading Protein, MhuD, Variant in Complex with Its Product. *Biochemistry*, 2019, *58* (46), 4610-4620.

15. Chao, A.; Sieminski, P. J.; Owens, C. P.; Goulding, C. W., Iron Acquisition in Mycobacterium tuberculosis. *Chem. Rev.*, 2019, *119* (2), 1193-1220.

16. Chao, A.; Goulding, C. W., A Single Mutation in the Mycobacterium tuberculosis Heme-Degrading Protein, MhuD, Results in Different Products. *Biochemistry*, 2019, *58* (6), 489-492.

17. Cheesman, M. R.; Greenwood, C.; Thomson, A. J., Magnetic Circular-Dichroism of Hemoproteins. *Adv. Inorg. Chem.*, 1991, *36*, 201-255.

18. Chen, H.; Moreau, Y.; Derat, E.; Shaik, S., Quantum mechanical/molecular mechanical study of mechanisms of heme degradation by the enzyme heme

oxygenase: the strategic function of the water cluster. *J. Am. Chem. Soc.*, 2008, *130* (6), 1953-65.

19. Chim, N.; Iniguez, A.; Nguyen, T. Q.; Goulding, C. W., Unusual diheme conformation of the heme-degrading protein from Mycobacterium tuberculosis. *J. Mol. Bio.*, 2010, *395* (3), 595-608.

20. Clezy, P. S.; Morell, D. B., A spectroscopic study of haematin compounds in the Soret region. *Biochim. Biophys. Acta*, 1963, *71*, 165-71.

21. Cole, S. T.; Eiglmeier, K.; Parkhill, J.; James, K. D.; Thomson, N. R.; Wheeler, P. R.; Honore, N.; Garnier, T.; Churcher, C.; Harris, D.; Mungall, K.; Basham, D.; Brown, D.; Chillingworth, T.; Connor, R.; Davies, R. M.; Devlin, K.; Duthoy, S.; Feltwell, T.; Fraser, A.; Hamlin, N.; Holroyd, S.; Hornsby, T.; Jagels, K.; Lacroix, C.; Maclean, J.; Moule, S.; Murphy, L.; Oliver, K.; Quail, M. A.; Rajandream, M. A.; Rutherford, K. M.; Rutter, S.; Seeger, K.; Simon, S.; Simmonds, M.; Skelton, J.; Squares, R.; Squares, S.; Stevens, K.; Taylor, K.; Whitehead, S.; Woodward, J. R.; Barrell, B. G., Massive gene decay in the leprosy bacillus. *Nature*, 2001, *409* (6823), 1007-11.

22. Compton, L. A.; Johnson, W. C., Jr., Analysis of protein circular dichroism spectra for secondary structure using a simple matrix multiplication. *Anal. Biochem.*, 1986, *155* (1), 155-67.

23. Conger, M. A.; Cornetta, A. R.; Liptak, M. D., Spectroscopic Evidence for Electronic Control of Heme Hydroxylation by IsdG. *Inorg. Chem.*, 2019, *58* (22), 15455-15465.

24. Conger, M. A.; Pokhrel, D.; Liptak, M. D., Tight binding of heme to Staphylococcus aureus IsdG and IsdI precludes design of a competitive inhibitor. *Metallomics*, 2017, *9* (5), 556-563.

25. Contreras, H.; Chim, N.; Credali, A.; Goulding, C. W., Heme uptake in bacterial pathogens. *Curr. Opin. Chem. Biol.*, 2014, *19*, 34-41.

26. Contreras, H.; Joens, M. S.; McMath, L. M.; Le, V. P.; Tullius, M. V.; Kimmey, J. M.; Bionghi, N.; Horwitz, M. A.; Fitzpatrick, J. A.; Goulding, C. W., Characterization of a Mycobacterium tuberculosis nanocompartment and its potential cargo proteins. *J. Biol. Chem.*, 2014, *289* (26), 18279-89.

27. Costa, D. L.; Namasivayam, S.; Amaral, E. P.; Arora, K.; Chao, A.; Mittereder, L. R.; Maiga, M.; Boshoff, H. I.; Barry, C. E., 3rd; Goulding, C. W.; Andrade, B. B.; Sher, A., Pharmacological Inhibition of Host Heme Oxygenase-1 Suppresses Mycobacterium tuberculosis Infection In Vivo by a Mechanism Dependent on T Lymphocytes. *Mbio*, 2016, *7* (5).

28. Cox, G. S., Whitten, D. G., Mechanisms for the photooxidation of protoporphyrin IX in solution. *J. Am. Chem. Soc.*, 1982, *102* (2), 516-521.

29. Dailey, H. A.; Gerdes, S.; Dailey, T. A.; Burch, J. S.; Phillips, J. D., Noncanonical coproporphyrin-dependent bacterial heme biosynthesis pathway that does not use protoporphyrin. *Proc. Natl. Acad. Sci.*, 2015, *112* (7), 2210-2215.

30. Davydov, R. M.; Yoshida, T.; Ikeda-Saito, M.; Hoffman, B. M., Hydroperoxy-heme oxygenase generated by cryoreduction catalyzes the formation of alpha-meso-hydroxyheme as detected by EPR and ENDOR. *J. Am. Chem. Soc.*, 1999, *121* (45), 10656-10657.

31. Davydov, R.; Kofman, V.; Fujii, H.; Yoshida, T.; Ikeda-Saito, M.; Hoffman, B. M., Catalytic mechanism of heme oxygenase through EPR and ENDOR of cryoreduced oxy-heme oxygenase and its Asp 140 mutants. *J. Am. Chem. Soc.*, 2002, *124* (8), 1798-1808.

32. De Voss, J. J.; Rutter, K.; Schroeder, B. G.; Barry, C. E., 3rd, Iron acquisition and metabolism by mycobacteria. *J. Bacteriol.*, 1999, *181* (15), 4443-51.

33. Denisov, I. G.; Ikeda-Saito, M.; Yoshida, T.; Sligar, S. G., Cryogenic absorption spectra of hydroperoxo-ferric heme oxygenase, the active intermediate of enzymatic heme oxygenation. *FEBS Lett.*, 2002, *532* (1-2), 203-6.

34. Dore, S.; Takahashi, M.; Ferris, C. D.; Zakhary, R.; Hester, L. D.; Guastella, D.; Snyder, S. H., Bilirubin, formed by activation of heme oxygenase-2, protects neurons against oxidative stress injury. *Proc. Natl. Acad. Sci.*, 1999, *96* (5), 2445-50.

35. Duong, T.; Park, K.; Kim, T.; Kang, S. W.; Hahn, M. J.; Hwang, H. Y.; Jang, I.; Oh, H. B.; Kim, K. K., Structural and functional characterization of an Isd-type haem-degradation enzyme from Listeria monocytogenes. *Acta Crystallogr., Sect. D: Biol. Crystallogr.*, 2014, *70* (Pt 3), 615-26.

36. Esson, W. H., V. A., On the laws of connexion between the condition of a chemical change and its amount. *Phil. Trans. Roy. Soc. (London)*, 1866, *156*.

37. Falk, J. E., *Porphyrins and Metalloporphyrins*. Elsevier Publishing Co. : Amsterdam, 1964.

38. Falk, J. E.; Dresel, E. I.; Benson, A.; Knight, B. C., Studies on the biosynthesis of blood pigments. 4. The nature of the porphyrins formed on incubation of chicken erythrocyte preparations with glycine, delta-aminolaevulic acid or porphobilinogen. *Biochem. J.*, 1956, *63* (1), 87-94.

39. Ferris, C. D.; Jaffrey, S. R.; Sawa, A.; Takahashi, M.; Brady, S. D.; Barrow, R. K.; Tysoe, S. A.; Wolosker, H.; Baranano, D. E.; Dore, S.; Poss, K. D.; Snyder, S. H., Haem oxygenase-1 prevents cell death by regulating cellular iron. *Nat. Cell Biol.*, 1999, *1* (3), 152-7.

40. Fleischer, E. B., Srivastava, T. S., Structure and properties of .mu.-oxobis(tetraphenylporphineiron(III). *J. Am. Chem. Soc.*, 1969, *91* (9), 2403-2405.

41. Fleischhacker, A. S.; Sharma, A.; Choi, M.; Spencer, A. M.; Bagai, I.; Hoffman, B. M.; Ragsdale, S. W., The C-Terminal Heme Regulatory Motifs of Heme Oxygenase-2 Are Redox-Regulated Heme Binding Sites. *Biochemistry*, 2015, *54* (17), 2709-2718.

42. Friedman, J.; Lad, L.; Li, H.; Wilks, A.; Poulos, T. L., Structural basis for novel delta-regioselective heme oxygenation in the opportunistic pathogen Pseudomonas aeruginosa. *Biochemistry*, 2004, *43* (18), 5239-45.

43. Ghosh, S. K.; Patra, R.; Rath, S. P., Synthesis, structure and photocatalytic activity of a remarkably bent, cofacial ethene-linked diiron (III) mu-oxobisporphyrin. *Inorg. Chim. Acta*, 2010, *363* (12), 2791-2799.

44. Gorst, C. M.; Wilks, A.; Yeh, D. C.; de Montellano, P. R. O.; La Mar, G. N., Solution H-1 NMR investigation of the molecular and electronic structure of the active site of substrate-bound human heme oxygenase: the nature of the distal hydrogen bond donor to bound ligands. *J. Am. Chem. Soc.*, 1998, *120* (34), 8875-8884.

45. Gouterman, M., Spectra of Porphyrins. *J. Mol. Spectrosc.*, 1961, *6*, 138-163.

46. Gouterman, M., Study of the Effects of Substitution on the Absorption Spectra of Porphin. *J. Chem. Phys.*, 1959, *30*, 1139 - 1161.

47. Graves, A. B.; Graves, M. T.; Liptak, M. D., Measurement of Heme Ruffling Changes in MhuD Using UV-vis Spectroscopy. *J. Phys. Chem. B*, 2016, *120* (16), 3844-53.

48. Graves, A. B.; Horak, E. H.; Liptak, M. D., Dynamic ruffling distortion of the heme substrate in non-canonical heme oxygenase enzymes. *Dalton Trans.*, 2016, *45* (24), 10058-67.

49. Graves, A. B.; Horak, E. H.; Liptak, M. D., Dynamic ruffling distortion of the heme substrate in non-canonical heme oxygenase enzymes. *Dalton Transactions*, 2016, *45* (24), 10058-10067.

50. Graves, A. B.; Morse, R. P.; Chao, A.; Iniguez, A.; Goulding, C. W.; Liptak, M. D., Crystallographic and spectroscopic insights into heme degradation by Mycobacterium tuberculosis MhuD. *Inorg. Chem.*, 2014, *53* (12), 5931-40.

51. Grigg, J. C.; Vermeiren, C. L.; Heinrichs, D. E.; Murphy, M. E. P., Haem recognition by a Staphylococcus aureus NEAT domain. *Mol. Microbiol.*, 2007, *63* (1), 139-149.

52. Grzegorzewicz, A. E.; Pham, H.; Gundi, V. A. K. B.; Scherman, M. S.; North, E. J.; Hess, T.; Jones, V.; Gruppo, V.; Born, S. E. M.; Kordulakova, J.; Chavadi, S. S.; Morisseau, C.; Lenaerts, A. J.; Lee, R. E.; McNeil, M. R.; Jackson, M., Inhibition of mycolic acid transport across the Mycobacterium tuberculosis plasma membrane. *Nat. Chem. Biol.*, 2012, *8* (4), 334-341.

53. Hackson, A. H., Nagaraja Rao, K. R., Wilkins, M., Synthesis of the Four meso-Oxyprotoporphyrin Isomers. *J. Chem. Soc., Chem. Commun.*, 1982, (14), 794-796.

54. Haley, K. P.; Janson, E. M.; Heilbronner, S.; Foster, T. J.; Skaar, E. P., Staphylococcus lugdunensis IsdG liberates iron from host heme. *J. Bacteriol.*, 2011, *193* (18), 4749-57.

55. Hanna, D. A.; Harvey, R. M.; Martinez-Guzman, O.; Yuan, X.; Chandrasekharan, B.; Raju, G.; Outten, F. W.; Hamza, I.; Reddi, A. R., Heme dynamics and trafficking factors revealed by genetically encoded fluorescent heme sensors. *Proc. Natl. Acad. Sci.*, 2016, *113* (27), 7539-44.

56. Hirotsu, S.; Chu, G. C.; Unno, M.; Lee, D. S.; Yoshida, T.; Park, S. Y.; Shiro, Y.; Ikeda-Saito, M., The crystal structures of the ferric and ferrous forms of the heme complex of HmuO, a heme oxygenase of Corynebacterium diphtheriae. *J. Biol. Chem.*, 2004, *279* (12), 11937-47.

57. Ho, C. S.; Lam, C. W.; Chan, M. H.; Cheung, R. C.; Law, L. K.; Lit, L. C.; Ng, K. F.; Suen, M. W.; Tai, H. L., Electrospray ionisation mass spectrometry: principles and clinical applications. *Clin. Biochem. Rev.*, 2003, *24* (1), 3-12.

58. Huang, X. Y.; Groves, J. T., Oxygen Activation and Radical Transformations in Heme Proteins and Metalloporphyrins. *Chem. Rev.*, 2018, *118* (5), 2491-2553.

59. Inubushi, T.; Becker, E. D., Efficient Detection of Paramagnetically Shifted Nmr Resonances by Optimizing the Weft Pulse Sequence. *J Magn Reson*, 1983, *51* (1), 128-133.

60. Jackson, A. H.; Rao, K. R. N.; Wilkins, M., Synthetic and Biosynthetic-Studies of Porphyrins .11. The Synthesis of Meso Oxygenated Protoporphyrins. *J. Chem. Soc., Perkin Trans. 1*, 1987, (2), 307-312.

61. Jentzen, W.; Song, X. Z.; Shelnutt, J. A., Structural characterization of synthetic and protein-bound porphyrins in terms of the lowest-frequency normal coordinates of the macrocycle. *J. Phys. Chem. B*, 1997, *101* (9), 1684-1699.

62. John A. Shelnutt, X.-Z. S., Jian-Guo Ma, Song-Ling Jia, Walter Jentzen, Craig J. Medforth, Craig J. Medforth Nonplanar porphyrins and their significance in proteins. *Chem. Soc. Rev.*, 1998, *27*, 31-41.

63. Jones, C. M.; Niederweis, M., Mycobacterium tuberculosis Can Utilize Heme as an Iron Source. *J. Bacteriol.*, 2011, *193* (7), 1767-1770.

64. Jones, P.; Prudhoe, K.; Robson, T., Oxidation of deuteroferrihaem by hydrogen peroxide. *Biochem. J.*, 1973, *135* (2), 361-5.

65. Kapust, R. B.; Tozser, J.; Fox, J. D.; Anderson, D. E.; Cherry, S.; Copeland, T. D.; Waugh, D. S., Tobacco etch virus protease: mechanism of autolysis and rational design of stable mutants with wild-type catalytic proficiency. *Protein Eng*, 2001, *14* (12), 993-1000.

66. King, D. W.; Kester, D. R., A General-Approach for Calculating Polyprotic Acid Speciation and Buffer Capacity. *J. Chem. Educ.*, 1990, *67* (11), 932-933.

67. Klein, E. Y.; Mojica, N.; Jiang, W. D.; Cosgrove, S. E.; Septimus, E.; Morgan, D. J.; Laxminarayan, R., Trends in Methicillin-Resistant Staphylococcus aureus Hospitalizations in the United States, 2010-2014. *Clin. Infect. Dis.*, 2017, *65* (11), 1921-1923.

68. Kleingardner, J. G.; Bowman, S. E.; Bren, K. L., The influence of heme ruffling on spin densities in ferricytochromes c probed by heme core 13C NMR. *Inorg. Chem.*, 2013, *52* (22), 12933-46.

69. Koga, S.; Yoshihara, S.; Bando, H.; Yamasaki, K.; Higashimoto, Y.; Noguchi, M.; Sueda, S.; Komatsu, H.; Sakamoto, H., Development of a heme sensor using fluorescently labeled heme oxygenase-1. *Anal. Biochem.*, 2013, *433* (1), 2-9.

70. Kuzmic, P., Dynafit-a Software Package for Enzymology. *Method Enzymol.*, 2009, *467*, 247-280.

71. Kuzmic, P., Program DYNAFIT for the analysis of enzyme kinetic data: Application to HIV proteinase. *Anal. Biochem.*, 1996, *237* (2), 260-273.

72. LaMattina, J. W.; Nix, D. B.; Lanzilotta, W. N., Radical new paradigm for heme degradation in Escherichia coli O157:H7. *Proc. Natl. Acad. Sci.*, 2016, *113* (43), 12138-12143.

73. Lawn, S. D.; Zumla, A. I., Tuberculosis. *Lancet*, 2011, *378* (9785), 57-72.

74. Lee, W. C.; Reniere, M. L.; Skaar, E. P.; Murphy, M. E., Ruffling of metalloporphyrins bound to IsdG and IsdI, two heme-degrading enzymes in Staphylococcus aureus. *J. Biol. Chem.*, 2008, *283* (45), 30957-63.

75. Lehnert, N., Elucidating second coordination sphere effects in heme proteins using low-temperature magnetic circular dichroism spectroscopy. *J. Inorg. Biochem.*, 2012, *110*, 83-93.

76. Li, Y.; Syvitski, R. T.; Chu, G. C.; Ikeda-Saito, M.; Mar, G. N., Solution 1H NMR investigation of the active site molecular and electronic structures of substrate-bound, cyanide-inhibited HmuO, a bacterial heme oxygenase from Corynebacterium diphtheriae. *J. Biol. Chem.*, 2003, *278* (9), 6651-63.

77. Liu, Y.; Moenne-Loccoz, P.; Loehr, T. M.; Ortiz de Montellano, P. R., Heme oxygenase-1, intermediates in verdoheme formation and the requirement for reduction equivalents. *J. Biol. Chem.*, 1997, *272* (11), 6909-17.

78. Lobley, A.; Whitmore, L.; Wallace, B. A., DICHROWEB: an interactive website for the analysis of protein secondary structure from circular dichroism spectra. *Bioinformatics*, 2002, *18* (1), 211-2.

79. Lockhart, C. L.; Conger, M. A.; Pittman, D. S.; Liptak, M. D., Hydrogen bond donation to the heme distal ligand of Staphylococcus aureus IsdG tunes the electronic structure. *J. Biol. Inorg. Chem.*, 2015, *20* (5), 757-70.

80. Lojek, L. J.; Farrand, A. J.; Wisecaver, J. H.; Blaby-Haas, C. E.; Michel, B. W.; Merchant, S. S.; Rokas, A.; Skaar, E. P., Chlamydomonas reinhardtii LFO1 Is an IsdG Family Heme Oxygenase. *Msphere*, 2017, *2* (4).

81. Mack, J.; Stillman, M. J.; Kobayashi, N., Application of MCD spectroscopy to porphyrinoids. *Coord. Chem. Rev.*, 2007, *251* (3-4), 429-453.

82. Matera, K. M.; Takahashi, S.; Fujii, H.; Zhou, H.; Ishikawa, K.; Yoshimura, T.; Rousseau, D. L.; Yoshida, T.; IkedaSaito, M., Oxygen and one reducing equivalent are both required for the conversion of alpha-hydroxyhemin to verdoheme in heme oxygenase. *J. Biol. Chem.*, 1996, *271* (12), 6618-6624.

83. Matsui, T.; Iwasaki, M.; Sugiyama, R.; Unno, M.; Ikeda-Saito, M., Dioxygen Activation for the Self-Degradation of Heme: Reaction Mechanism and Regulation of Heme Oxygenase. *Inorg. Chem.*, 2010, *49* (8), 3602-3609.

84. Matsui, T.; Nakajima, A.; Fujii, H.; Matera, K. M.; Migita, C. T.; Yoshida, T.; Ikeda-Saito, M., O-2- and H2O2-dependent verdoheme degradation by heme oxygenase - Reaction mechanisms and potential physiological roles of the dual pathway degradation. *J. Biol. Chem.*, 2005, *280* (44), 36833-36840.

85. Matsui, T.; Nambu, S.; Goulding, C. W.; Takahashi, S.; Fujii, H.; Ikeda-Saito, M., Unique coupling of mono- and dioxygenase chemistries in a single active site promotes heme degradation. *Proc. Natl. Acad. Sci.*, 2016, *113* (14), 3779-84.

86. Matsui, T.; Nambu, S.; Ono, Y.; Goulding, C. W.; Tsumoto, K.; Ikeda-Saito, M., Heme degradation by Staphylococcus aureus IsdG and IsdI liberates formaldehyde rather than carbon monoxide. *Biochemistry*, 2013, *52* (18), 3025-7.

87. Matsui, T.; Unno, M.; Ikeda-Saito, M., Heme oxygenase reveals its strategy for catalyzing three successive oxygenation reactions. *Acc. Chem. Res.*, 2010, *43* (2), 240-7.

88. Matthews, S.; Pacholarz, K. J.; France, A. P.; Jowitt, T. A.; Hay, S.; Barran, P.; Munro, A. W., MhuD from Mycobacterium tuberculosis: Probing a Dual Role in Heme Storage and Degradation. *ACS Infect. Dis.*, 2019, *5* (11), 1855-1866.

89. Mattle, D.; Zeltina, A.; Woo, J. S.; Goetz, B. A.; Locher, K. P., Two Stacked Heme Molecules in the Binding Pocket of the Periplasmic Heme-Binding Protein HmuT from Yersinia pestis. *J. Mol. Bio.*, 2010, *404* (2), 220-231.

90. Mazmanian, S. K.; Skaar, E. P.; Gaspar, A. H.; Humayun, M.; Gornicki, P.; Jelenska, J.; Joachmiak, A.; Missiakas, D. M.; Schneewind, O., Passage of heme-iron across the envelope of Staphylococcus aureus. *Science*, 2003, *299* (5608), 906-909.

91. McLean, K. J.; Munro, A. W., Drug targeting of heme proteins in Mycobacterium tuberculosis. *Drug Discovery Today*, 2017, *22* (3), 566-575.

92. Migita, C. T.; Fujii, H.; Mansfield Matera, K.; Takahashi, S.; Zhou, H.; Yoshida, T., Molecular oxygen oxidizes the porphyrin ring of the ferric alpha-hydroxyheme in heme oxygenase in the absence of reducing equivalent. *Biochim. Biophys. Acta*, 1999, *1432* (2), 203-13.

93. Moody, P. C. E.; Raven, E. L., The Nature and Reactivity of Ferryl Heme in Compounds I and II. *Acc. Chem. Res.*, 2018, *51* (2), 427-435.

94. Mourino, S.; Giardina, B. J.; Reyes-Caballero, H.; Wilks, A., Metabolite-driven Regulation of Heme Uptake by the Biliverdin IXbeta/delta-Selective Heme Oxygenase (HemO) of Pseudomonas aeruginosa. *J. Biol. Chem.*, 2016, *291* (39), 20503-15.

95. Murphy, R. F.; OhEocha, C.; P, O. C., The formation of verdohaemochrome from pyridine protohaemichrome by extracts of red algae and of liver. *Biochem. J.*, 1967, *104* (1), 6C-8C.

96. Nallamsetty, S.; Kapust, R. B.; Tozser, J.; Cherry, S.; Tropea, J. E.; Copeland, T. D.; Waugh, D. S., Efficient site-specific processing of fusion proteins by tobacco vein mottling virus protease in vivo and in vitro. *Protein Expression Purif.*, 2004, *38* (1), 108-15.

97. Nambu, S.; Matsui, T.; Goulding, C. W.; Takahashi, S.; Ikeda-Saito, M., A new way to degrade heme: the Mycobacterium tuberculosis enzyme MhuD catalyzes heme degradation without generating CO. *J. Biol. Chem.*, 2013, *288* (14), 10101-9.

98. Namuangruk, S.; Sirithip, K.; Rattanatwan, R.; Keawin, T.; Kungwan, N.; Sudyodsuk, T.; Promarak, V.; Surakhot, Y.; Jungsuttiwong, S., Theoretical investigation of the charge-transfer properties in different meso-linked zinc porphyrins for highly efficient dye-sensitized solar cells. *Dalton Trans.*, 2014, *43* (24), 9166-9176.

99. Naveh, D.; Yankilewitz, T.; Lagziel, A.; Sompolinsky, D., [Skin granulomata caused by a new microorganism (Mycobacterium haemophilum sp. nov.)]. *Harefuah*, 1978, *95* (1), 5-8.

100. Ogura, H.; Evans, J. P.; Peng, D. G.; Satterlee, J. D.; de Montellano, P. R. O.; La Mar, G. N., The Orbital Ground State of the Azide-Substrate Complex of Human Heme Oxygenase Is an Indicator of Distal H-Bonding: Implications for the Enzyme Mechanism. *Biochemistry*, 2009, *48* (14), 3127-3137.

101. O'Keeffe, D. H.; Barlow, C. H.; Smythe, G. A.; Fuchsman, W. H.; Moss, T. H.; Lilienthal, H. R.; Caughey, W. S., Magnetic and spectroscopic probes for FeOFe linkages in hemin systems. *Bioinorg. Chem.*, 1975, *5* (2), 125-47.

102. O'Neill, M. J.; Wilks, A., The P. aeruginosa Heme Binding Protein PhuS Is a Heme Oxygenase Titratable Regulator of Heme Uptake. *ACS Chem. Biol.*, 2013, *8* (8), 1794-1802.

103. Owens, C. P.; Chim, N.; Graves, A. B.; Harmston, C. A.; Iniguez, A.; Contreras, H.; Liptak, M. D.; Goulding, C. W., The Mycobacterium tuberculosis secreted protein Rv0203 transfers heme to membrane proteins MmpL3 and MmpL11. *J. Biol. Chem.*, 2013, *288* (30), 21714-28.

104. Owens, C. P.; Chim, N.; Goulding, C. W., Insights on how the Mycobacterium tuberculosis heme uptake pathway can be used as a drug target. *Future Med. Chem.*, 2013, *5* (12), 1391-1403.

105. Owens, C. P.; Du, J.; Dawson, J. H.; Goulding, C. W., Characterization of heme ligation properties of Rv0203, a secreted heme binding protein involved in Mycobacterium tuberculosis heme uptake. *Biochemistry*, 2012, *51* (7), 1518-31.

106. Pacheco, S. A.; Hsu, F. F.; Powers, K. M.; Purdy, G. E., MmpL11 Protein Transports Mycolic Acid-containing Lipids to the Mycobacterial Cell Wall and Contributes to Biofilm Formation in Mycobacterium smegmatis. *J. Biol. Chem.*, 2013, *288* (33), 24213-24222.

107. Perrin, C. L., Linear or Nonlinear Least-Squares Analysis of Kinetic Data? *J. Chem. Educ.*, 2017, *94* (6), 669-672.

108. Perutz, M. F., Stereochemistry of cooperative effects in haemoglobin. *Nature*, 1970, *228* (5273), 726-39.

109. Petryka, Z.; Nicholson, D. C.; Gray, C. H., Isomeric bile pigments as products of the in vitro fission of haemin. *Nature*, 1962, *194*, 1047-8.

110. Poulos, T. L., Heme Enzyme Structure and Function. *Chem. Rev.*, 2014, *114* (7), 3919-3962.

111. Puri, S.; O'Brian, M. R., The hmuQ and hmuD genes from Bradyrhizobium japonicum encode heme-degrading enzymes. *J. Bacteriol.*, 2006, *188* (18), 6476-82.

112. Ratledge, C.; Dover, L. G., Iron metabolism in pathogenic bacteria. *Annu. Rev. Microbiol.*, 2000, *54*, 881-941.

113. Reniere, M. L.; Ukpabi, G. N.; Harry, S. R.; Stec, D. F.; Krull, R.; Wright, D. W.; Bachmann, B. O.; Murphy, M. E.; Skaar, E. P., The IsdG-family of haem oxygenases degrades haem to a novel chromophore. *Mol. Microbiol.*, 2010, *75* (6), 1529-38.

114. Rivera, M.; Caignan, G. A.; Astashkin, A. V.; Raitsimring, A. M.; Shokhireva, T.; Walker, F. A., Models of the low-spin iron(III) hydroperoxide intermediate of heme oxygenase: magnetic resonance evidence for thermodynamic stabilization of the d(xy) electronic state at ambient temperatures. *J. Am. Chem. Soc.*, 2002, *124* (21), 6077-89.

115. Rodriguez, G. M.; Smith, I., Identification of an ABC transporter required for iron acquisition and virulence in Mycobacterium tuberculosis. *J. Bacteriol.*, 2006, *188* (2), 424-30.

116. Ryndak, M. B.; Wang, S.; Smith, I.; Rodriguez, G. M., The Mycobacterium tuberculosis high-affinity iron importer, IrtA, contains an FAD-binding domain. *J. Bacteriol.*, 2010, *192* (3), 861-9.

117. Safo, M. K.; Walker, F. A.; Raitsimring, A. M.; Walters, W. P.; Dolata, D. P.; Debrunner, P. G.; Scheidt, W. R., Axial Ligand Orientation in Iron(Iii) Porphyrinates - Effect of Axial Pi-Accepters - Characterization of the Low-Spin Complex [Fe(Tpp)(4-Cnpy)(2)]Clo4. *J. Am. Chem. Soc.*, 1994, *116* (17), 7760-7770.

118. Sakamoto, H.; Omata, Y.; Palmer, G.; Noguchi, M., Ferric alpha-hydroxyheme bound to heme oxygenase can be converted to verdoheme by dioxygen in the absence of added reducing equivalents. *J. Biol. Chem.*, 1999, *274* (26), 18196-18200.

119. Sakamoto, H.; Takahashi, K.; Higashimoto, Y.; Harada, S.; Palmer, G.; Noguchi, M., A kinetic study of the mechanism of conversion of alpha-hydroxyheme to verdoheme while bound to heme oxygenase. *Biochem. Biophys. Res. Commun.*, 2005, *338* (1), 578-83.

120. Sano, S.; Sano, T.; Morishima, I.; Shiro, Y.; Maeda, Y., On the mechanism of the chemical and enzymic oxygenations of alpha-oxyprotohemin IX to Fe.biliverdin IX alpha. *Proc. Natl. Acad. Sci.*, 1986, *83* (3), 531-5.

121. Schappacher, M.; Deffieux, A., Reversible Switching between Linear and Ring Poly(EO)s Bearing Iron Tetraphenylporphyrin Ends Triggered by Solvent, pH, or Redox Stimuli. *Macromolecules*, 2011, *44* (11), 4503-4510.

122. Schappacher, M.; Deffieux, A., Reversible Switching between Linear and Ring Polystyrenes Bearing Porphyrin End Groups. *J. Am. Chem. Soc.*, 2011, *133* (6), 1630-1633.

123. Schmitt, M. P., Utilization of host iron sources by Corynebacterium diphtheriae: identification of a gene whose product is homologous to eukaryotic heme oxygenases and is required for acquisition of iron from heme and hemoglobin. *J. Bacteriol.*, 1997, *179* (3), 838-45.

124. Schuelke-Sanchez, A. E. Spectroscopic Study of the Formation and Degradation of Metalated Tetrapyrroles by the Enzymes CfbA, IsdG, and MhuD. Dissertation and Theses, University of Vermont, 2019.

125. Schuller, D. J.; Wilks, A.; Ortiz de Montellano, P. R.; Poulos, T. L., Crystal structure of human heme oxygenase-1. *Nat. Struct. Biol.*, 1999, *6* (9), 860-7.

126. Shokhirev, N. V.; Walker, F. A., Analysis of the temperature dependence of the H-1 contact shifts in low-spin Fe(III) model hemes and heme proteins: Explanation of "Curie" and "anti-Curie" behavior within the same molecule. *J. Phys. Chem.*, 1995, *99* (50), 17795-17804.

127. Singh, P.; Benjak, A.; Schuenemann, V. J.; Herbig, A.; Avanzi, C.; Busso, P.; Nieselt, K.; Krause, J.; Vera-Cabrera, L.; Cole, S. T., Insight into the evolution and origin of leprosy bacilli from the genome sequence of Mycobacterium lepromatosis. *Proc. Natl. Acad. Sci.*, 2015, *112* (14), 4459-4464.

128. Skaar, E. P.; Gaspar, A. H.; Schneewind, O., Bacillus anthracis IsdG, a heme-degrading monooxygenase. *J. Bacteriol.*, 2006, *188* (3), 1071-80.

129. Skaar, E. P.; Gaspar, A. H.; Schneewind, O., IsdG and IsdI, heme-degrading enzymes in the cytoplasm of Staphylococcus aureus. *J. Biol. Chem.*, 2004, *279* (1), 436-43.

130. Skaar, E. P.; Humayun, M.; Bae, T.; DeBord, K. L.; Schneewind, O., Iron-source preference of Staphylococcus aureus infections. *Science*, 2004, *305* (5690), 1626-1628.

131. Solomon, E. I.; Pavel, E. G.; Loeb, K. E.; Campochiaro, C., Magnetic Circular-Dichroism Spectroscopy as a Probe of the Geometric and Electronic-Structure of Nonheme Ferrous Enzymes. *Coord. Chem. Rev.*, 1995, *144*, 369-460.

132. Song, Y.; Yang, M.; Wegner, S. V.; Zhao, J.; Zhu, R.; Wu, Y.; He, C.; Chen, P. R., A Genetically Encoded FRET Sensor for Intracellular Heme. *ACS Chem. Biol.*, 2015, *10* (7), 1610-5.

133. Sreerama, N.; Woody, R. W., Estimation of protein secondary structure from circular dichroism spectra: comparison of CONTIN, SELCON, and CDSSTR methods with an expanded reference set. *Anal. Biochem.*, 2000, *287* (2), 252-60.

134. Sreerama, N.; Woody, R. W., Estimation of protein secondary structure from circular dichroism spectra: Comparison of CONTIN, SELCON, and CDSSTR methods with an expanded reference set. *Anal. Biochem.*, 2000, *287* (2), 252-260.

135. Stojiljkovic, I.; Kumar, V.; Srinivasan, N., Non-iron metalloporphyrins: potent antibacterial compounds that exploit haem/Hb uptake systems of pathogenic bacteria. *Mol. Microbiol.*, 1999, *31* (2), 429-42.

136. Streit, B. R.; Kant, R.; Tokmina-Lukaszewska, M.; Celis, A. I.; Machovina, M. M.; Skaar, E. P.; Bothner, B.; DuBois, J. L., Time-resolved Studies of IsdG Protein Identify Molecular Signposts along the Non-canonical Heme Oxygenase Pathway. *J. Biol. Chem.*, 2016, *291* (2), 862-871.

137. Sugishima, M.; Oda, K.; Ogura, T.; Sakamoto, H.; Noguchi, M.; Fukuyama, K., Alternative cyanide-binding modes to the haem iron in haem oxygenase. *Acta Crystallogr., Sect. F: Struct. Biol. Cryst. Commun.*, 2007, *63* (Pt 6), 471-4.

138. Suzuki, K.; Akama, T.; Kawashima, A.; Yoshihara, A.; Yotsu, R. R.; Ishii, N., Current status of leprosy: Epidemiology, basic science and clinical perspectives. *J. Dermatol.*, 2012, *39* (2), 121-129.

139. Swain, C. G., The Kinetic Analysis of Consecutive Irreversible First Order Reactions. *J. Am. Chem. Soc.*, 1944, *66*, 1696-1700.

140. Takayama, S. J.; Ukpabi, G.; Murphy, M. E.; Mauk, A. G., Electronic properties of the highly ruffled heme bound to the heme degrading enzyme IsdI. *Proc. Natl. Acad. Sci.*, 2011, *108* (32), 13071-6.

141. Tenhunen, R.; Marver, H. S.; Schmid, R., Microsomal heme oxygenase. Characterization of the enzyme. *J. Biol. Chem.*, 1969, *244* (23), 6388-94.

142. Tetsuhiko, Y., Tomio, O., Equilibria of Imidazole Derivatives with (Protoporphyrin IX dimethyl ester)iron(III) Chloride. *Bulle of the Chemical Society of Japan* 1979, *52* (8), 2268-2275.

143. Thakuri, B.; Graves, A. B.; Chao, A.; Johansen, S. L.; Goulding, C. W.; Liptak, M. D., The affinity of MhuD for heme is consistent with a heme degrading function in vivo. *Metallomics*, 2018, *10* (11), 1560-1563.

144. Tiedemann, M. T.; Muryoi, N.; Heinrichs, D. E.; Stillman, M. J., Iron acquisition by the haem-binding Isd proteins in Staphylococcus aureus: studies of the mechanism using magnetic circular dichroism. *Biochem. Soc. Trans.*, 2008, *36*, 1138-1143.

145. Torres, V. J.; Pishchany, G.; Humayun, M.; Schneewind, O.; Skaar, E. P., Staphylococcus aureus IsdB is a hemoglobin receptor required for heme iron utilization. *J. Bacteriol.*, 2006, *188* (24), 8421-8429.

146. Tufariello, J. M.; Kerantzas, C. A.; Vilcheze, C.; Calder, R. B.; Nordberg, E. K.; Fischer, J. A.; Hartman, T. E.; Yang, E.; Driscoll, T.; Cole, L. E.; Sebra, R.; Maqbool, S. B.; Wattam, A. R.; Jacobs, W. R., The Complete Genome Sequence of the Emerging Pathogen Mycobacterium haemophilum Explains Its Unique Culture Requirements. *Mbio*, 2015, *6* (6).

147. Tullius, M. V.; Harmston, C. A.; Owens, C. P.; Chim, N.; Morse, R. P.; McMath, L. M.; Iniguez, A.; Kimmey, J. M.; Sawaya, M. R.; Whitelegge, J. P.; Horwitz, M. A.; Goulding, C. W., Discovery and characterization of a unique mycobacterial heme acquisition system. *Proc. Natl. Acad. Sci.*, 2011, *108* (12), 5051-5056.

148. Turner, N. A.; Sharma-Kuinkel, B. K.; Maskarinec, S. A.; Eichenberger, E. M.; Shah, P. P.; Carugati, M.; Holland, T. L.; Fowler, V. G., Methicillin-resistant Staphylococcus aureus: an overview of basic and clinical research. *Nat. Rev. Microbiol.*, 2019, *17* (4), 203-218.

149. Ukpabi, G.; Takayama, S. J.; Mauk, A. G.; Murphy, M. E., Inactivation of the heme degrading enzyme IsdI by an active site substitution that diminishes heme ruffling. *J. Biol. Chem.*, 2012, *287* (41), 34179-88.

150. Unno, M.; Matsui, T.; Chu, G. C.; Couture, M.; Yoshida, T.; Rousseau, D. L.; Olson, J. S.; Ikeda-Saito, M., Crystal structure of the dioxygen-bound heme oxygenase from Corynebacterium diphtheriae: implications for heme oxygenase function. *J. Biol. Chem.*, 2004, *279* (20), 21055-61.

151. van Hal, S. J.; Jensen, S. O.; Vaska, V. L.; Espedido, B. A.; Paterson, D. L.; Gosbell, I. B., Predictors of Mortality in Staphylococcus aureus Bacteremia. *Clin. Microbiol. Rev.*, 2012, *25* (2), 362-386.

152. Videira, M. A. M.; Lobo, S. A. L.; Silva, L. S. O.; Palmer, D. J.; Warren, M. J.; Prieto, M.; Coutinho, A.; Sousa, F. L.; Fernandes, F.; Saraiva, L. M., Staphylococcus aureus haem biosynthesis and acquisition pathways are linked through haem monooxygenase IsdG. *Mol. Microbiol.*, 2018, *109* (3), 385-400.

153. Wang, J.; Niemevz, F.; Lad, L.; Huang, L.; Alvarez, D. E.; Buldain, G.; Poulos, T. L.; de Montellano, P. R., Human heme oxygenase oxidation of 5- and 15-phenylhemes. *J. Biol. Chem.*, 2004, *279* (41), 42593-604.

154. Watanabe, M.; Tanaka, Y.; Suenaga, A.; Kuroda, M.; Yao, M.; Watanabe, N.; Arisaka, F.; Ohta, T.; Tanaka, I.; Tsumoto, K., Structural basis for multimeric heme complexation through a specific protein-heme interaction - The case of the third neat domain of IsdH from Staphylococcus aureus. *J. Biol. Chem.*, 2008, *283* (42), 28649-28659.

155. Weinberg, E. D., Iron and infection. *Microbiol. Rev.*, 1978, *42* (1), 45-66.

156. Weisstein, E. W. Cubic Formula. http://mathworld.wolfram.com/CubicFormula.html.

157. Whitmore, L.; Wallace, B. A., DICHROWEB, an online server for protein secondary structure analyses from circular dichroism spectroscopic data. *Nucleic Acids Res.*, 2004, *32* (Web Server issue), W668-73.

158. Wicholas, M.; Mustacich, R.; Jayne, D., Proton nuclear magnetic resonance contact shifts of binuclear oxo-bridged iron (3) porphyrins. *J. Am. Chem. Soc.*, 1972, *94* (13), 4518-22.

159. Wilks, A.; Heinzl, G., Heme oxygenation and the widening paradigm of heme degradation. *Arch. Biochem. Biophys.*, 2014, *544*, 87-95.

160. Wilks, A.; Ikeda-Saito, M., Heme Utilization by Pathogenic Bacteria: Not All Pathways Lead to Biliverdin. *Acc. Chem. Res.*, 2014, *47* (8), 2291-2298.

161. World Health Organization. Grobal Tuberculosis Report. 2019.

162. Wu, R. Y.; Skaar, E. P.; Zhang, R. G.; Joachimiak, G.; Gornicki, P.; Schneewind, O.; Joachimiak, A., Staphylococcus aureus IsdG and IsdI, heme-degrading enzymes with structural similarity to monooxygenases. *J. Biol. Chem.*, 2005, *280* (4), 2840-2846.

163. Xu, Z. J.; Meshcheryakov, V. A.; Poce, G.; Chng, S. S., MmpL3 is the flippase for mycolic acids in mycobacteria. *Proc. Natl. Acad. Sci.*, 2017, *114* (30), 7993-7998.

164. Yi, L.; Ragsdale, S. W., Evidence that the heme regulatory motifs in heme oxygenase-2 serve as a Thiol/Disulfide redox switch regulating heme binding. *J. Biol. Chem.*, 2007, *282* (29), 21056-21067.

165. Yoshida, T.; Kikuchi, G., Features of the reaction of heme degradation catalyzed by the reconstituted microsomal heme oxygenase system. *J. Biol. Chem.*, 1978, *253* (12), 4230-6.

166. Yoshinaga, T.; Sudo, Y.; Sano, S., Enzymatic Conversion of Alpha-Oxyprotohaem-Ix into Biliverdin-Ix-Alpha by Heme Oxygenase. *Biochem. J.*, 1990, *270* (3), 659-664.

167. Yuan, C.; Zhang, Y.; Tan, H.; Li, X.; Chen, G.; Jia, Z., ONIOM investigations of the heme degradation mechanism by MhuD: the critical function of heme ruffling. *Phys. Chem. Chem. Phys.*, 2020, *22* (16), 8817-8826.

168. Yuan, X.; Rietzschel, N.; Kwon, H.; Walter Nuno, A. B.; Hanna, D. A.; Phillips, J. D.; Raven, E. L.; Reddi, A. R.; Hamza, I., Regulation of intracellular heme trafficking revealed by subcellular reporters. *Proc. Natl. Acad. Sci.*, 2016, *113* (35), E5144-52.

169. Zhu, W.; Wilks, A.; Stojiljkovic, I., Degradation of heme in gram-negative bacteria: the product of the hemO gene of Neisseriae is a heme oxygenase. *J. Bacteriol.*, 2000, *182* (23), 6783-90.

APPENDIX A: SUPPORTING INFORMATION FOR CHAPTER 2

A.1 SUPPLEMENTAL EXPERIMENTAL

The fluorescence-detected titrations of heme into MhuD and $MhuD_{CH}$ were analyzed in order to determine K_{d1} for MhuD and $MhuD_{CH}$. The Trp66 fluorescence intensity for a mixture of MhuD, MhuD–heme, and heme depends upon equation (A.1):

$$F = \frac{([MhuD]_T+[heme]_T+K_{d1})-\sqrt{([MhuD]_T+[heme]_T+K_{d1})^2-4[MhuD]_T[heme]_T}}{2} \text{ X } \left(\frac{F_{min}-F_{max}}{[MhuD]_T}\right) + F_{max} \quad \text{(A.1)}$$

The Abs-detected titrations were analyzed to extract K_{d2} for MhuD and $MhuD_{CH}$. The Abs intensity at 410 nm for a mixture of MhuD, MhuD–diheme, MhuD–heme, and heme depends upon equation (A.2):

$$A_{410} = \frac{\varepsilon_{MhuD-diheme}[MhuD_T][heme]^2+\varepsilon_{MhuD-heme}K_{d2}[MhuD_T][heme]}{[heme]^2+K_{d2}[heme]+K_{d1}K_{d2}} + \frac{\varepsilon_{heme}([heme]^3+K_{d2}[heme]^2+K_{d1}K_{d2}[heme])}{[heme]^2+K_{d2}[heme]+K_{d1}K_{d2}} \quad \text{(A.2)}$$

where $\varepsilon_{MhuD–diheme}$, $\varepsilon_{MhuD–heme}$, and ε_{heme} are the molar extinction coefficients for MhuD–diheme, MhuD–heme, and heme, respectively, at 410 nm. The Abs-detected heme titrations intoWT MhuD were performed to extract the dissociation constant (K_{d2}) of binding for the second heme substrate. The Abs intensity at 410 nm for a mixture containing MhuD–diheme, MhuD–heme, MhuD and heme depends on equation (A.3):

$$A_{410} = \varepsilon_{MhuD-diheme}[MhuD-diheme] + \varepsilon_{MhuD-heme}[MhuD-heme] + \varepsilon_{heme}[heme] \quad \text{(A.3)}$$

where, $\varepsilon_{MhuD\text{-}diheme}$, $\varepsilon_{MhuD-heme,}$ and ε_{heme} are the extinction coefficients of these species at 410 nm. The K_{d1} for the first heme binding to MhuD is given by equation (A.4):

$$K_{d1} = \frac{[MhuD][Heme]}{[MhuD - heme]} \quad (A.4)$$

The K_{d2} for the second heme binding to MhuD is given by equation (A.5):

$$K_{d2} = \frac{[MhuD - heme][Heme]}{[MhuD - diheme]} \quad (A.5)$$

The total amount of MhuD ($MhuD_T$) is defined by equation (A.6):

$$[MhuD_T] = [MhuD] + [MhuD - diheme] + [MhuD - heme] \quad (A.6)$$

Rearranging equation (A.6):

$$[MhuD] = [MhuD_T] - [MhuD - diheme] - [MhuD - heme] \quad (A.7)$$

The total amount of heme ($heme_T$) is defined by equation (A.8):

$$[heme_T] = [heme] + 2[MhuD - diheme] + [MhuD - heme] \quad (A.8)$$

This equation can be rearranged to give equation (A.9)

$$[heme] = [heme_T] - 2[MhuD - diheme] - [MhuD - heme] \quad (A.9)$$

Next, we have introduced a dummy variable, α, which is given by equation (A.10) [1]

$$\text{Let } \alpha = \frac{[MhuD-diheme]}{[heme]^2} \quad (A.10)$$

By dividing [*MhuD–diheme*], [*MhuD–heme*] and [*MhuD*] by α, we get equations (A.11) - (A.13) respectively:

$$\frac{[MhuD - diheme]}{\alpha} = [heme]^2 \quad (A.11)$$

$$\frac{[MhuD - heme]}{\alpha} = K_{d2}[heme] \quad (A.12)$$

$$\frac{[MhuD]}{\alpha} = K_{d1}K_{d2} \qquad (A.13)$$

Dividing equation (A.6) by α using equations (A.11), (A.12) and (A.13) results in equation (A.14):

$$\frac{[MhuD_T]}{\alpha} = [heme]^2 + K_{d2}[heme] + K_{d1}K_{d2} \qquad (A.14)$$

Dividing equation (A.9) by α and substituting with equations (A.11) and (A.12) gives equation (A.15):

$$\frac{[heme_T]}{\alpha} = 2[heme]^2 + K_{d2}[heme] + \frac{[heme]}{\alpha} \qquad (A.15)$$

Dividing equation (A.13) by equation (A.14) gives equation (A.16):

$$[MhuD] = \frac{[MhuD_T]K_{d1}K_{d2}}{[heme]^2 + K_{d2}[heme] + K_{d1}K_{d2}} \qquad (A.16)$$

Dividing [*heme*] by α and using equation (A.10), we get equation (A.17):

$$\frac{[heme]}{\alpha} = \frac{[heme]^3}{[MhuD - diheme]} \qquad (A.17)$$

Multiplying equation (A.4) and (A.5), we get equation (A.18):

$$K_{d1}K_{d2} = \frac{[heme]^2[MhuD]}{[MhuD - diheme]} \qquad (A.18)$$

Rearranging equation (A.18) results in equation (A.19):

$$[MhuD - diheme] = \frac{[heme]^2[MhuD]}{K_{d1}K_{d2}} \qquad (A.19)$$

Substitution of equation (A.19) into equation (A.17) gives equation (A.20):

$$\frac{[heme]}{\alpha} = \frac{[heme]K_{d1}K_{d2}}{[MhuD]} \quad (A.20)$$

Substitution of equation (A.16) into equation (A.20) gives equation (A.21):

$$\frac{[heme]}{\alpha} = \frac{[heme]^3 + [heme]^2K_{d2} + [heme]K_{d1}K_{d2}}{[MhuD_T]} \quad (A.21)$$

Substitution of equation (A.21) in equation (A.15), gives equation (A.22)

$$\frac{[heme_T]}{\alpha} = \frac{2[MhuD_T][heme]^2 + [MhuD_T][heme]K_{d2} + [heme]^3 + [heme]^2K_{d2} + [heme]K_{d1}K_{d2}}{[MhuD_T]} \quad (A.22)$$

Dividing equation (A.22) by equation (A.14) and solving, gives cubic equation (A.23):

$$[heme]^3 + [heme]^2(2[MhuD_T] + K_{d2} - [heme_T]) + [heme]([MhuD_T]K_{d2} + K_{d1}K_{d2} - [heme_T]K_{d2}) - [heme_T]K_{d1}K_{d2} = 0 \quad (A.23)$$

The above equation (A.23) is in the form $x^3 + ax^2 + bx + c = 0$, where:

$a = 2[MhuD_T] + K_{d2} - [heme_T]$

$b = ([MhuD_T]K_{d2} + K_{d1}K_{d2} - [heme_T]K_{d2})$

$c = -[heme_T]K_{d1}K_{d2}$

$x = [heme]$

Solving and simplifying the cubic equation for x gives three real roots which is given by equation (A.24.a), (A.24.b) and (A.24.c).[2]

$$x = 2\sqrt{-Q}\cos\left(\frac{\emptyset}{3}\right) - \frac{a}{3} \qquad (A.24.a)$$

$$x = 2\sqrt{-Q}\cos\left(\frac{\emptyset}{3} + 120^o\right) - \frac{a}{3} \qquad (A.24.b)$$

$$x = 2\sqrt{-Q}\cos\left(\frac{\emptyset}{3} + 240^o\right) - \frac{a}{3} \qquad (A.24.c)$$

where,

$$Q = \frac{3b - a^2}{9} \qquad (A.25.a)$$

$$\emptyset = cos^{-1}\left(\frac{R}{\sqrt{-Q^3}}\right) \qquad (A.25.b)$$

$$R = \frac{9ab - 27c - 2a^3}{54} \qquad (A.25.c)$$

Equation (A.24.a) is the relevant solution of the cubic equation for this expreiment. Other solutions: (A.24.b) and (A.24.c) did not provide best fits for the experiment and hence would no

t be used to fit the data to calculate K_{d2}. Therefore, equation (A.24.a) will be used for rest of the analysis. Dividing equation (1) by α yields equation (A.26):

$$\frac{A_{410}}{\alpha} = \frac{\varepsilon_{MhuD-diheme}[MhuD - diheme]}{\alpha} + \frac{\varepsilon_{MhuD-heme}[MhuD - heme]}{\alpha} + \frac{\varepsilon_{heme}[heme]}{\alpha} \qquad (A.26)$$

Substituting the values from equation (A.11), (A.12) and (A.21) to equation (A.26) gives equation (A.27):

$$\frac{A_{410}}{\alpha} = \varepsilon_{MhuD-diheme}[heme]^2 + \varepsilon_{MhuD-heme}K_{d2}[heme] + \varepsilon_{heme}\left(\frac{[heme]^3 + [heme]^2K_{d2} + [heme]K_{d1}K_{d2}}{[MhuD_T]}\right) \quad \text{(A.27)}$$

Dividing equation (A.27) by equation (A.14) and solving for A_{410} gives equation (A.28):

$$A_{410} = \frac{[MhuD_T]\varepsilon_{MhuD-diheme}[heme]^2 + [MhuD_T]\varepsilon_{MhuD-heme}K_{d2}[heme]}{[heme]^2 + K_{d2}[heme] + K_{d1}K_{d2}} + \frac{\varepsilon_{heme}([heme]^3 + [heme]^2K_{d2} + [heme]K_{d1}K_{d2})}{[heme]^2 + K_{d2}[heme] + K_{d1}K_{d2}} \quad \text{(A. 28)}$$

Equation (A.28) and equation (A.24.a) was rewritten in Graph Pad Prism 7.0 to fit the data collected from UV/Vis spectrophotometer and extract K_{d2} as equation (A.29):

$$A = 2 * P + Kd2 - X$$

$$B = (P * Kd2) + (Kd1 * Kd2) - (X * Kd2)$$

$$C = -(X * Kd1 * Kd2)$$

$$Q = ((3 * B) - (A * A))/9$$

$$R = ((9 * A * B) - (27 * C) - (2 * A * A * A))/54$$

$$T = arccos\left(\frac{R}{sqrt\left(-(Q * Q * Q)\right)}\right)$$

$$H = ((2 * \left(sqrt(-Q)\right) * \cos\left(\frac{T}{3}\right))) - \left(\frac{A}{3}\right)$$

$$Y = \frac{(P * E * H * H) + (F * P * Kd2 * H) + \left(G * \left((H * H * H) + (Kd2 * H * H) + (H * Kd1 * Kd2)\right)\right)}{(H * H) + (Kd2 * H) + (Kd1 * Kd2)} \quad \text{(A.29)}$$

where, E, F and G are extinction coefficient of *MhuD–diheme, MhuD–heme* and *heme*, P is the total concentration of the protein. Abs data was used to plot abosrobance at 410 nm (A_{410}) as a function of total heme concentration ($heme_T$).

Table A. 1. $MhuD_{CH}$ gene sequence.

M-46	H-45	H-44	H-43	H-42	H-41	H-40	S-39	S-38	G-37	L-36	V-35
ATG	CAC	CAT	CAT	CAT	CAT	CAT	TCT	TCT	GGT	CTG	GTG
P-34	R-33	G-32	S-31	G-30	M-29	K-28	E-27	T-26	A-25	A-24	A-23
CCA	CGC	GGT	TCT	GGT	ATG	AAA	GAA	ACC	GCT	GCT	GCT
K-22	F-21	E-20	R-19	Q-18	H-17	M-16	D-15	S-14	P-13	D-12	L-11
AAA	TTC	GAA	CGC	CAG	CAC	ATG	GAC	AGC	CCA	GAT	CTG
G-10	T-9	D-8	D-7	D-6	D-5	K-4	A-3	M-2	A-1	P2	V3
GGT	ACC	GAC	GAC	GAC	GAC	AAG	GCC	ATG	GCC	CCA	GTG
V4	K5	I56	N7	A8	I9	E10	V11	P12	A13	G14	A15
GTG	AAG	ATC	AAC	GCA	ATC	GAG	GTG	CCC	GCC	GGC	GCT
G16	P17	E18	L19	E20	K21	R22	F23	A24	H25	R26	A27
GGC	CCC	GAG	CTG	GAG	AAG	CGG	TTC	GCT	CAC	CGC	GCG
H28	A29	V30	E31	N32	S33	P34	G35	F36	L37	G38	F39
CAC	GCG	GTC	GAG	AAC	TCC	CCG	GGT	TTC	CTC	GGC	TTT
Q40	L41	L42	R43	P44	V45	K46	G47	E48	E49	R50	Y51
CAG	CTG	TTA	CGT	CCG	GTC	AAG	GGT	GAA	GAA	CGC	TAC
F52	V53	V54	T55	H56	W57	E58	S59	D60	E61	A62	F63
TTC	GTG	GTG	ACA	CAC	TGG	GAG	TCC	GAT	GAA	GCA	TTC
Q64	A65	W66	A67	N68	G69	P70	A71	I72	A73	A74	H75
CAG	GCG	TGG	GCA	AAC	GGG	CCC	GCC	ATC	GCA	GCC	CAT
A76	G77	H78	R79	A80	N81	P82	V83	A84	T85	G86	A87
GCC	GGA	CAC	CGG	GCC	AAC	CCC	GTG	GCG	ACC	GGT	GCT
S88	L89	L90	E91	F92	E93	V94	V95	L96	D97	V98	G99
TCG	CTG	CTG	GAA	TTC	GAG	GTC	GTG	CTT	GAC	GTC	GGT
G100	T101	G102	K103	T104	A105						
GGG	ACC	GGC	AAG	ACT	GCA						

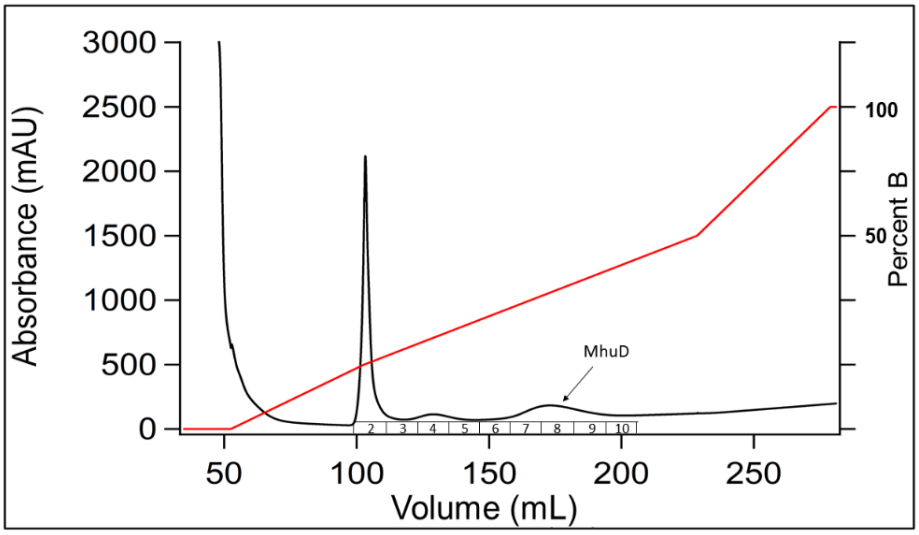

Figure A. 1. FPLC chromatograph for purification of MhuD. The 280 nm absorbance (*black trace*) and percentage of Buffer B (50 mM Tris, 350 mM NaCl, 500 mM Imidazole pH 7.8, *red trace*) are plotted as function of buffer run through the column. Numbers in boxes on top of the x-axis refer to fractions collected during FPLC.

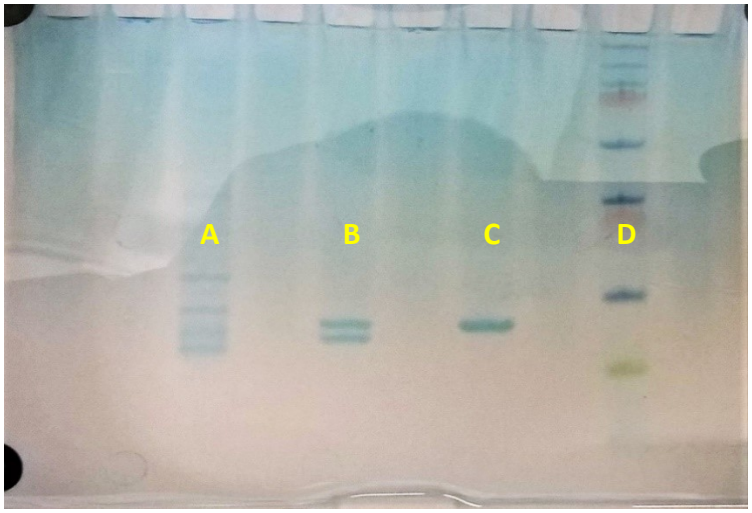

Figure A. 2. MhuD was obtained as assessed by SDS-PAGE gel electrophoresis. From left to right, the lanes correspond to: (A) FPLC fraction 2, (B) FPLC fraction 4, (C) FPLC fractions 7-9, and (D) PageRuler Plus prestained protein ladder (Pierce).

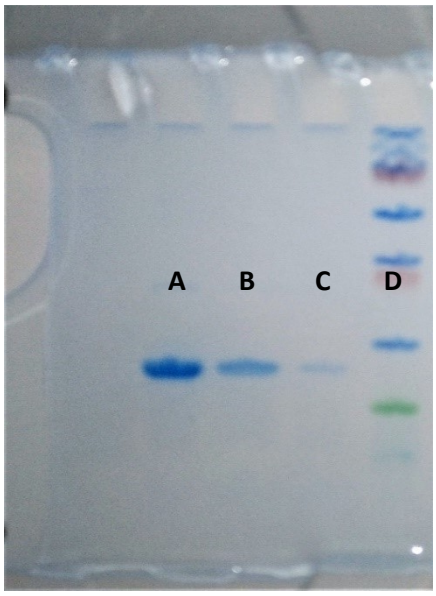

Figure A. 3. Purity of MhuD assessed by SDS-PAGE. (A) MhuD, (B) 1/10 dilution of MhuD, (C) 1/100, dilution of MhuD, and (D) PageRuler Plus prestained protein ladder (Pierce)

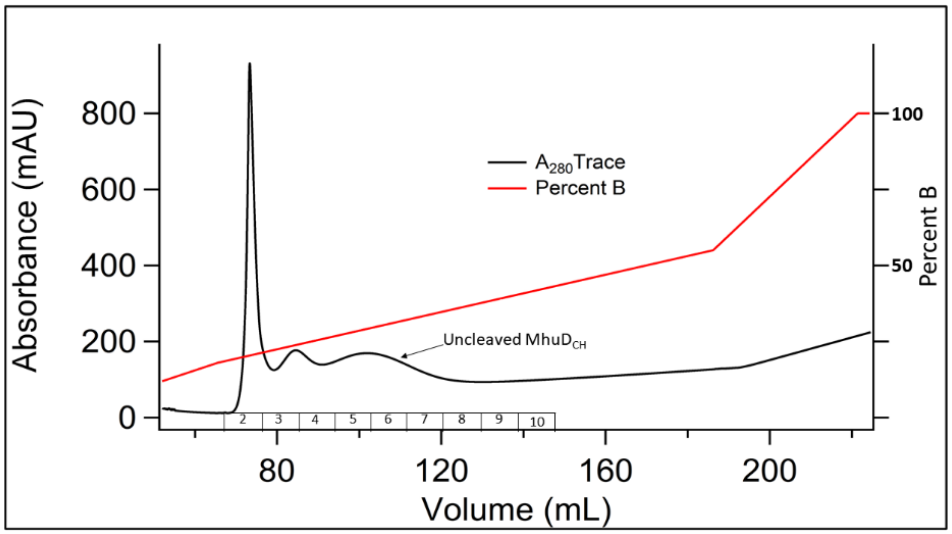

Figure A. 4. FPLC chromatograph for purification of uncleaved $MhuD_{CH}$. The 280 nm absorbance (*black trace*) and percentage of Buffer B (50 mM Tris, 350 mM NaCl, 500 mM Imidazole pH 7.8, *red trace*) are plotted as a function of buffer run through the column. Numbers in boxes on top of the x-axis refer to fractions collected during FPLC.

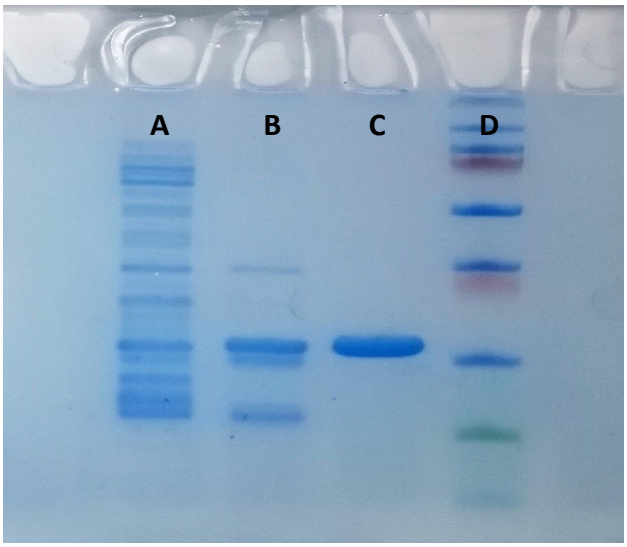

Figure A. 5. Uncleaved $MhuD_{CH}$ was obtained as assessed by SDS-PAGE gel electrophoresis. From left to right, the lanes represent: (A) FPLC fraction 2, (B) FPLC fraction 3, (C) FPLC fractions 5-7, and (D) PageRuler Plus prestained protein ladder (Pierce).

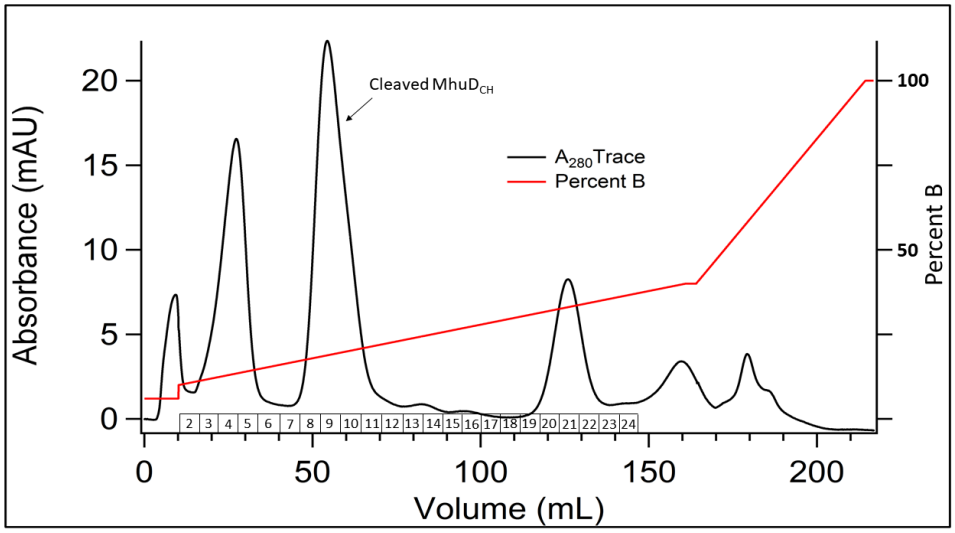

Figure A. 6. FPLC chromatograph for purification of cleaved $MhuD_{CH}$ (*Black Trace*). The 280 nm absorbance (black trace) and percentage buffer B (20 mM Tris, 500 mM NaCl pH 8.0, red trace). Numbers in boxes on top of the x-axis refer to fractions collected during FPLC.

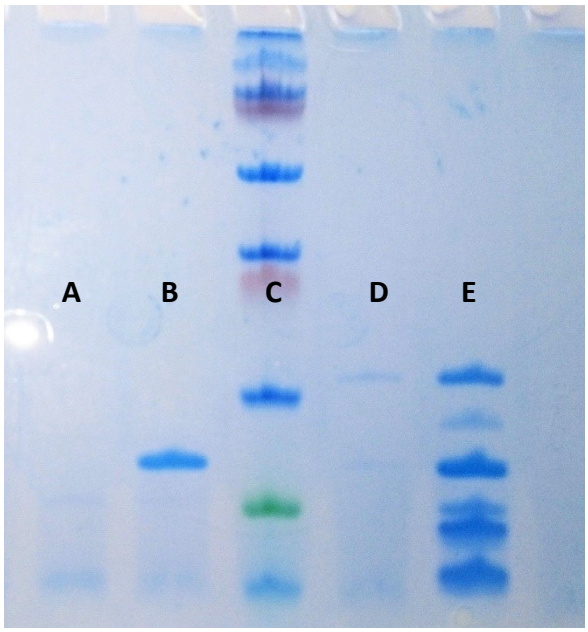

Figure A. 7. Cleaved $MhuD_{CH}$ was obtained as assessed by SDS-PAGE gel electrophoresis. From left to right, the lanes correspond to: (A) FPLC fractions 3-5, (B) FPLC fractions 8-11, (C) PageRuler Plus prestained protein ladder (Pierce), (D) FPLC fractions 20-22, and (E) $MhuD_{CH}$ enterokinase reaction mixture prior to anion-exchange chromatography.

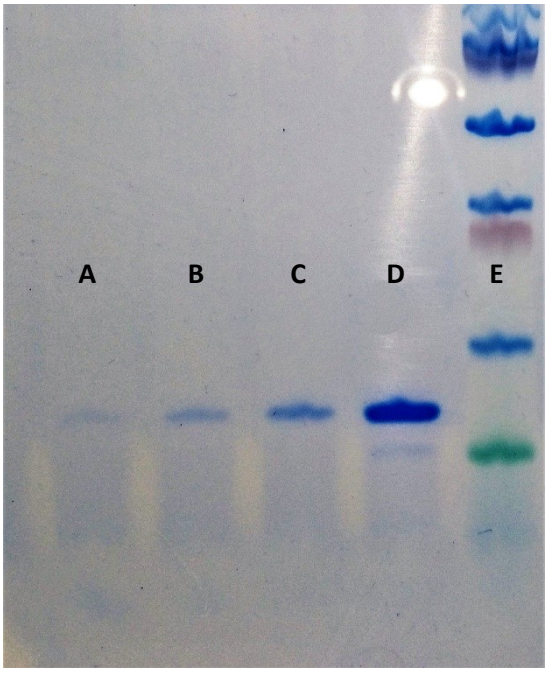

Figure A. 8. Purity of $MhuD_{CH}$ assessed by SDS-PAGE. (A) 1/100 dilultion of $MhuD_{CH}$, (B) 1/20 dilution of $MhuD_{CH}$, (C) 1/10 dilution of $MhuD_{CH}$, (D) Cleaved $MhuD_{CH}$, and (E) PageRuler Plus prestained protein ladder (Pierce)

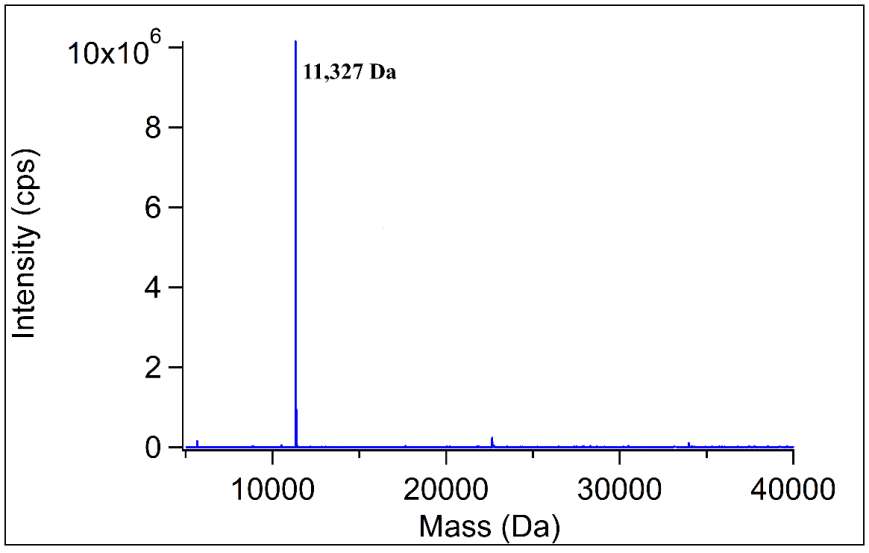

Figure A. 9. ESI-MS of 30 uM cleaved $MhuD_{CH}$ in 50 mM Tris pH 7.4, 150 mM NaCl. The observed molecular weight of 11,327 Da is in excellent aggrement with the expected molecular weight 11,327 Da.

Table A. 2. Soret band wavelength upon addition of 0.2, 1, 2 and 3 equivalents of heme to MhuD.

	Soret band, λ_{max} (nm)			
Heme Equivalents	**Trial 1**	**Trial 2**	**Trial 3**	**Average**
0.2	407	408	407	407
1	401	401	402	401
2	401	403	400	401
3	409	410	410	410

Table A. 3. Soret band wavelength upon addition of 0.2, 1, 2 and 3 equivalents of heme to $MhuD_{CH}$.

	Soret band, λ_{max} (nm)			
Heme Equivalents	**Trial 1**	**Trial 2**	**Trial 3**	**Average**
0.2	408	408	408	408
1	401	399	399	400
2	395	395	395	395
3	394	393	394	394

A.2 APPENDIX A REFERENCES

1. King, D. W.; Kester, D. R., A General-Approach for Calculating Polyprotic Acid Speciation and Buffer Capacity. *J. Chem. Educ.*, 1990, *67* (11), 932-933.

2. Weisstein, E. W. Cubic Formula.
http://mathworld.wolfram.com/CubicFormula.html.

APPENDIX B: SUPPORTING INFORMATION FOR CHAPTER 3

B.1 SUPPLEMENTAL EXPERIMENTAL

Spectral Analysis. The Abs-detected heme degradation by F23W MhuD was analyzed at 412 nm to extract the rate of breakdown of heme to meso-hydroxyheme (k_1) using equation (B.1):[1]

$$A_{Soret} = \left(A_{Soret,0} - A_{Soret,\infty}\right)e^{-k_1 t} + A_{Soret,\infty} \quad \text{(B.1)}$$

where, $A_{Soret,0}$ is the absorbance at 0 min, $A_{Soret,\infty}$ is the final absorbance intensity at at ∞ min and k_1 is the constant for heme monooxygenation. The decrease of the Soret band absorption intensity versus time was fit to equation B.1 using GraphPad Prism 8.0 in order to extract k_1 and its standard error for each MhuD variant. For F23W MhuD, the increase of 620 nm UV/Vis Abs feature was described by the following kinetic model:

$$A_{620} = A_{620,0} * \left[e^{-k_1 t} + \left(\frac{\varepsilon_{mh}}{\varepsilon_h}\right) * \left(\frac{k_1}{k_2 - k_1}\right) * \left(e^{-k_1 t} - e^{-k_2 t}\right)\right]$$

(B.2)

where $A_{620,0}$ is the absorbance at 0 min, k_1 is the rate constant for F23W MhuD-catalyze heme monooxygenation determined from fitting the Soret band decrease to equation 1, ε_{mh} is the molar extinction coefficient for meso-hydroxyheme, ε_h is the molar extinction coefficient for heme, and k_2 is the rate constant for heme dioxygenation. ε_h was determined based upon the pyridine hemochrome assay.[2] The change in absorbance at 620 nm versus time was fit to equation B.2 using GraphPad Prism 8.0 to extract k_2, ε_{mh},

and their standard errors. Complete derivations of equations B.1 and B.2 are shown below.

The heme degradation of heme to its final product can be given by equation (B.3):

$$Heme \overset{k_1}{\rightarrow} Meso-hydroxyheme \overset{k_2}{\rightarrow} Mycobilin \quad \text{(B.3)}$$

Simplifying equation (B.3) to express in terms of A, B and C, we get equation (B.4):

$$A \overset{k_1}{\rightarrow} B \overset{k_2}{\rightarrow} C \quad \text{(B.4)}$$

Derivation of equation (B.1). The rate of heme monoxygenation is given by a psuedo-first order kinetics, because the rate is only proportional to the heme concentration. The differential equation of A can be given by equation (B.5):

$$\frac{dA}{dt} = -k_1[A] \quad \text{(B.5)}$$

Equation (B.5) can be organized as equation (B.6):

$$\frac{dA}{[A]} = -k_1 dt \quad \text{(B.6)}$$

Upon integration and simplification, equation (B.6) becomes equation (B.7):

$$[A] = [A]_0 e^{-k_1 t} \quad \text{(B.7)}$$

where $[A]_0$ is the F23W MhuD-heme concentration at 0 min. As explained in the previous paper[1], in this situation, [A] does not react completely and does not reach zero, instead it approaches a nonzero baseline at an infinite time (∞). For this the concentration of A can be written as $[A]_\infty$. Thus equation (B.7) can be written as equation (B.8):

$$[A] - [A]_\infty = ([A]_0 - [A]_\infty)e^{-k_1 t} \quad \text{(B.8)}$$

Using Beer's law, equation (B.8) can be written in terms of Abs as given by equation (B.9):

$$A_{Soret} = \left(A_{Soret,0} - A_{Soret,\infty}\right)e^{-k_1 t} + A_{Soret,\infty} \quad \text{(B.9)}$$

Equation (B.9) was rewritten in GraphPad Prism 8.0 as equation (B.10) to fit the data collected from Abs monitored heme degradation assay to extract k_1.

$$\mathrm{Y} = ((\mathrm{I} - \mathrm{F}) * \exp(-\mathrm{k1} * \mathrm{X})) \; + \; \mathrm{F} \quad \text{(B.10)}$$

where I and F are the Soret absorbance at 0 and ∞ min. Abs data was used to plot absorbance at 412 nm (Y) as a function of time (X).

Derivation of equation (B.2). The differential equation for B from equation (B.4) can be also written as equation (B.11):

$$\frac{dB}{dt} = \; k_1 A - k_2 B \quad \text{(B.11)}$$

The concentration of B from equation (B.4) can then be expressed as shown in equation (B.12):[3, 4]

$$[B] = \frac{k_1[A_0]}{k_2 - k_1}(e^{-k_1 t} - e^{-k_2 t}) \quad \text{(B.12)}$$

Using the Beer's law, [B] and [A_o] can be expressed in terms of Abs as be given by equation (B.13) and (B.14):

$$[A] = \frac{A_{620,0}}{\varepsilon_h} \quad \text{(B.13)}$$

$$[B] = \frac{A_{620,B}}{\varepsilon_{mh}} \quad \text{(B.14)}$$

Pluggin (B.13) and (B.14) into equation gives equation (B.15):

$$A_{620,B} = A_{620,0}\left(\frac{\varepsilon_{mh}}{\varepsilon_h}\right)\left(\frac{k_1}{k_2-k_1}\right)(e^{-k_1 t} - e^{-k_2 t}) \quad \text{(B.15)}$$

Also, equation (B.7) can be written in terms of equation (B.16):

$$A_{620,A} = A_{620,0}\, e^{-k_1 t} \quad \text{(B.16)}$$

As the Abs spectra at 620 nm would have contribution from both A and B species, equation (B.15) and (B.16) can be written in terms of A_{620}, as given by equation (B.17):

$$A_{620} = A_{620,0}\left[e^{-k_1 t} + \left(\frac{\varepsilon_{mh}}{\varepsilon_h}\right)\left(\frac{k_1}{k_2-k_1}\right)(e^{-k_1 t} - e^{-k_2 t})\right] \quad \text{(B.17)}$$

Equation (B.17) was rewritten in GraphPad Prism 8.0 as equation (B.18) to fit the data collected from Abs monitored heme degradation assay to extract k_2 and ε_{mh}.

Y = A * (exp (-k1 * X)) + ((E / F) * (k1 / (k2 – k1)) * (exp (-k2 * X) – exp (-k2 * X)))) (B.18)

where, E and F are the molar extinction coefficients for F23W MhuD–meso-hydroxyheme and MhuD–heme at 620 nm respectively, and A is the initial Abs intensity at 620 nm. Abs data was used to plot absorbance at 620 nm (Y) as a function of time (X).

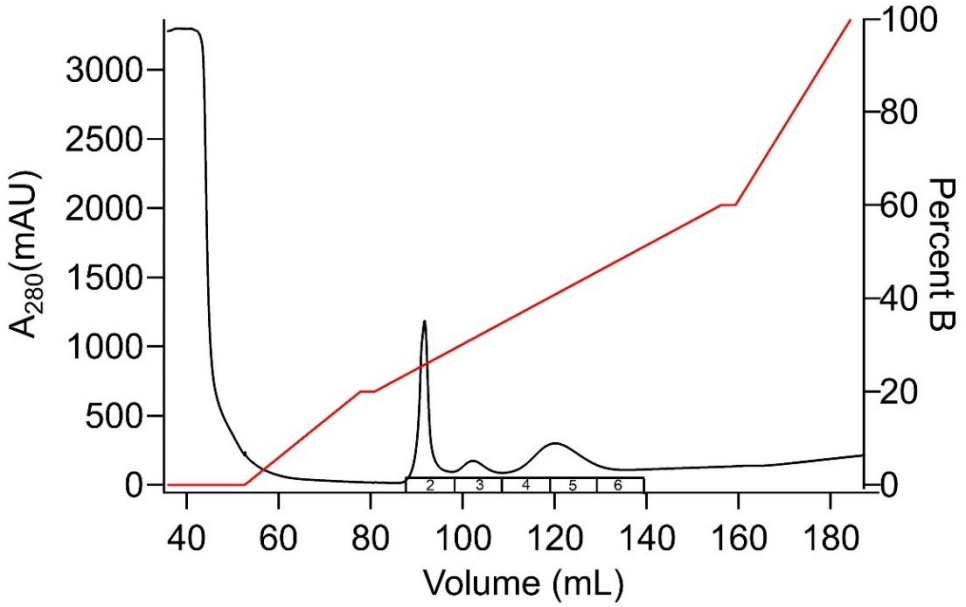

Figure B. 1. FPLC chromatograph for purification of F23W MhuD. The 280 nm absorbance (*black trace*) and percentage of Buffer B (50 mM Tris, 350 mM NaCl, 500 mM Imidazole pH 7.8, *red trace*) are plotted as a function of buffer run through the column. Numbers in boxes on top of the x-axis refer to fractions collected during FPLC.

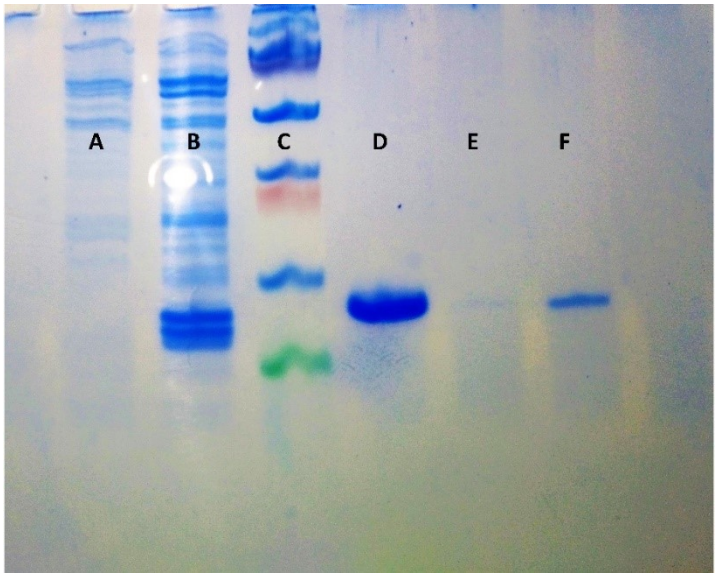

Figure B. 2. F23W MhuD assessed by SDS-PAGE gel electrophoresis. From left to right, the lanes represent: (A) FPLC fraction 2, (B) FPLC fraction 3, (C) PageRuler Plus prestained protein ladder (Pierce), (D) FPLC fractions 4-6, (E) 1/100 dilution of fractions 4-6, (F) 1/20 dilution of fractions 4-6.

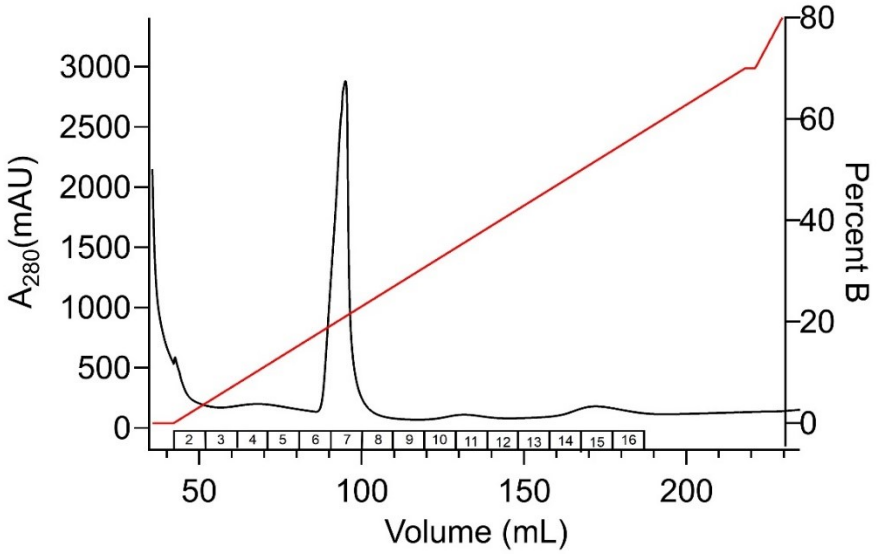

Figure B. 3. FPLC chromatograph for purification of W66F MhuD. The 280 nm absorbance (*black trace*) and percentage of Buffer B (50 mM Tris, 350 mM NaCl, 500 mM Imidazole pH 7.8, *red trace*) are plotted as a function of buffer run through the column. Numbers in boxes on top of the x-axis refer to fractions collected during FPLC.

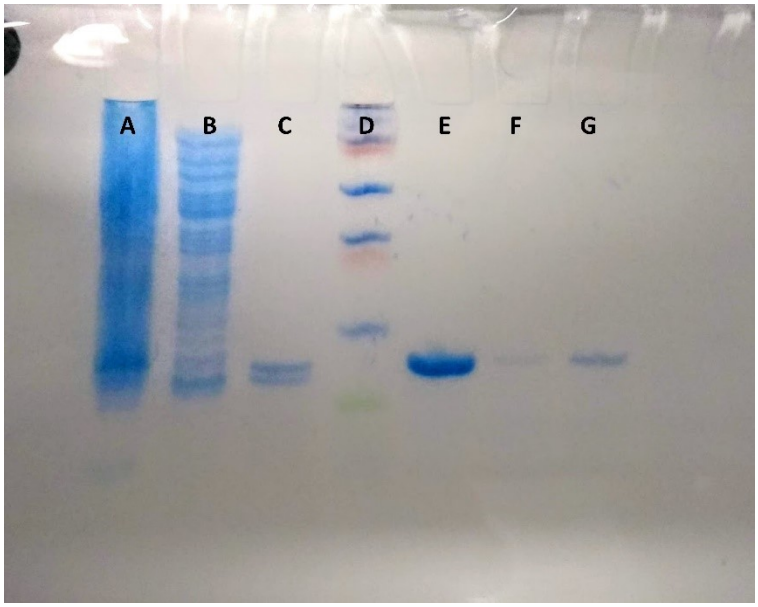

Figure B. 4. W66F MhuD assessed by SDS-PAGE gel electrophoresis. From left to right, the lanes represent: (A) Lysate, (B) FPLC fraction 7, (C) FPLC fraction 10-11, (D) PageRuler Plus prestained protein ladder (Pierce), (E) FPLC fractions 14-16, (E) 1/100 dilution of fractions 14-16, (F) 1/20 dilution of fractions 14-16.

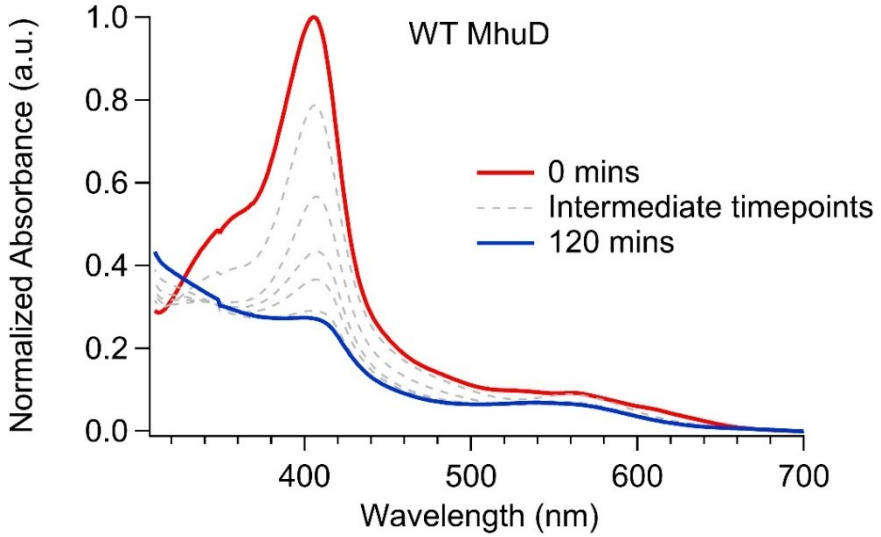

Figure B. 5. UV/Vis Assay of heme degradation by WT MhuD. Heme degradation by WT MhuD (50 μM WT MhuD–heme, 50 mM KPi pH 6.0, 37°C) monitored at 0 (red trace), 5 - 60 (Dotted gray) and 120 mins (blue trace).

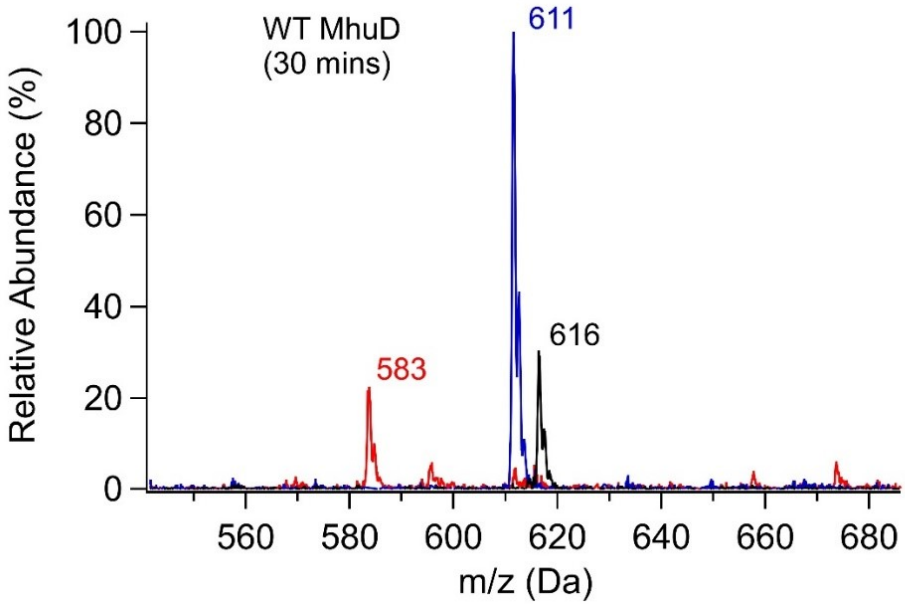

Figure B. 6. ESI-MS spectra of heme degradation by WT MhuD. Extracted Ion chromatogram of 30 min sample from heme degradation by WT MhuD (50 μM WT MhuD–heme, 50 mM Potassium Phosphate pH 6.0, 150 mM NaCl, 37°C). Peaks with m/z 583, 611 and 616 were observed, likely corresponding to formation of biliverdin, mycobilin and heme respectively.

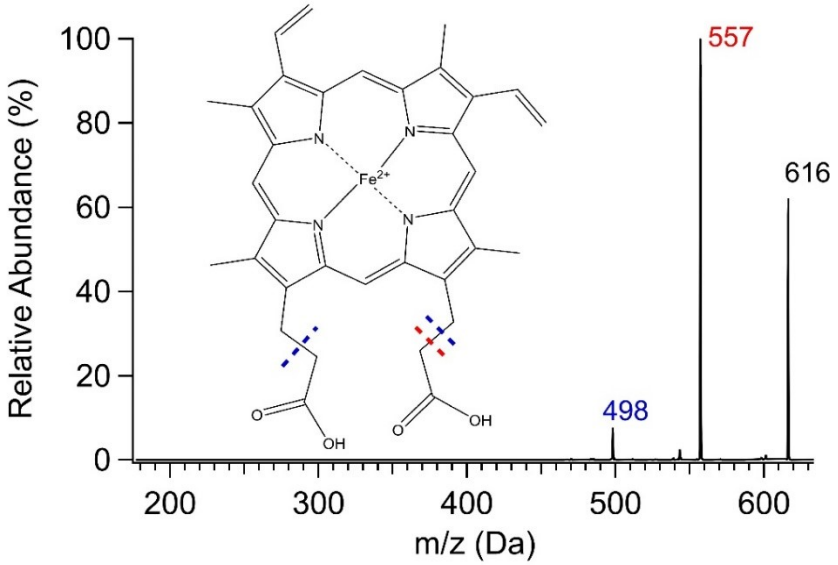

Figure B. 7. MS/MS spectrum of hemin chloride. Two major daughter fragments of m/z 557 and m/z 498 is observed corresponding to loss of CH_2COOH (red dotted line) and $(CH_2COOH)_2$ (blue dotted line) respectively.

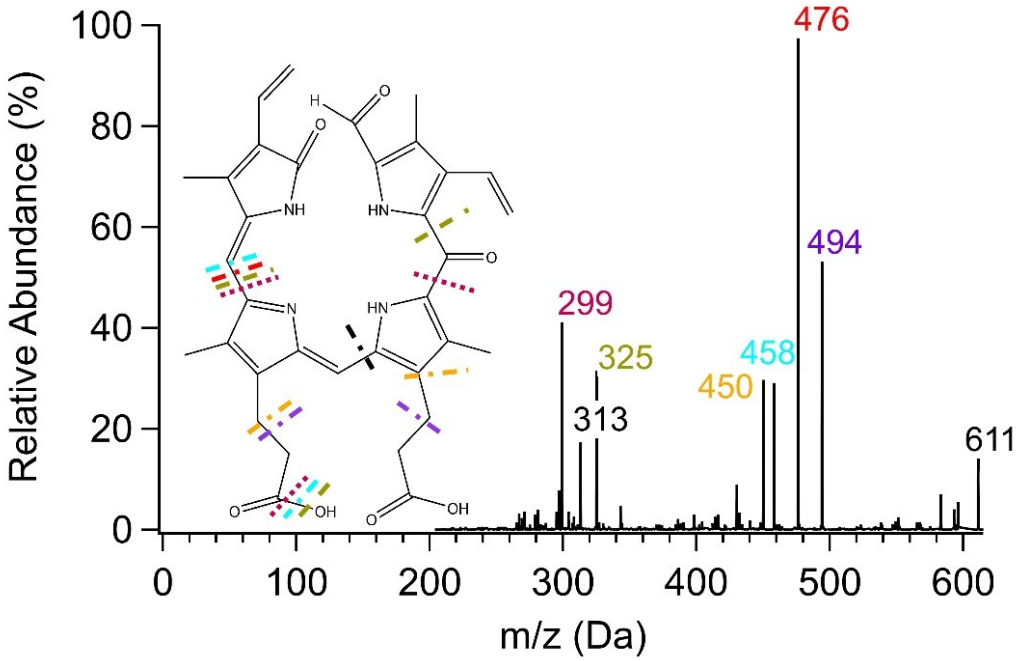

Figure B. 8. MS/MS spectrum of m/z 611 peak. The fragment ions observed during MS/MS of m/z 611 parent ion are color matched to their corresponding fragments and can be traced back to mycobilin.

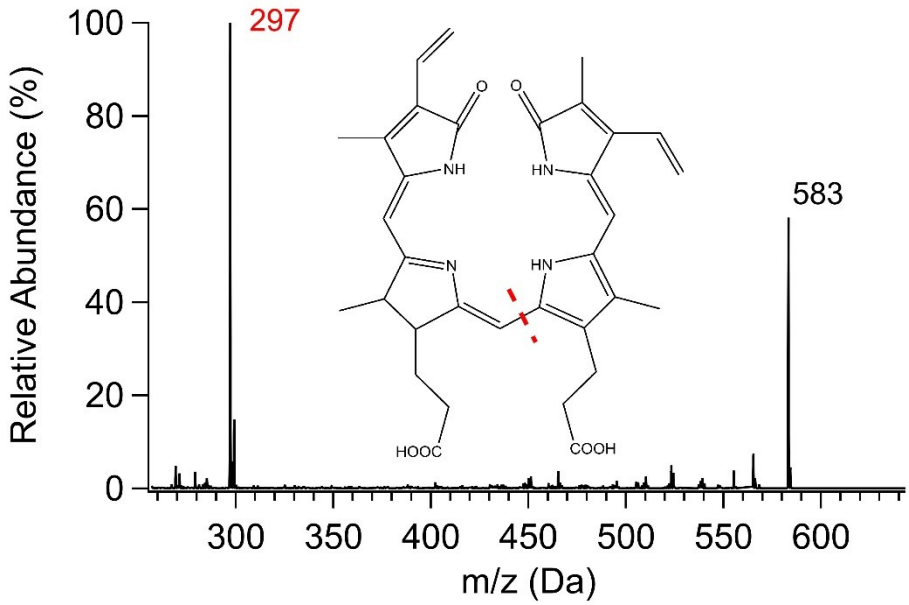

Figure B. 9. MS/MS spectrum of m/z 583 peak. The fragment ion of m/z 297 matches up with the loss of the fragment denoted by a red dotted line in the biliverdin structure above.

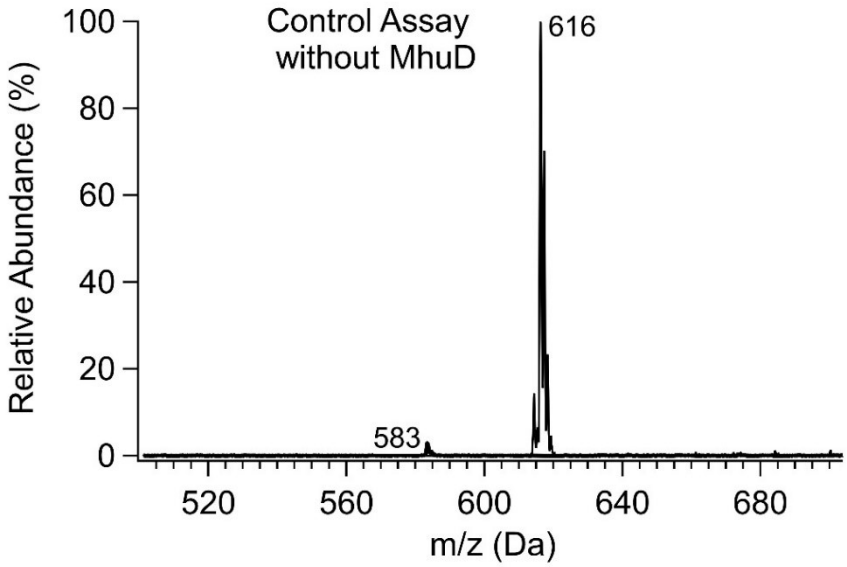

Figure B. 10. ESI-MS spectrum of hemin chloride degradation. Control assay of 50 μM hemin chloride, 50 mM Potassium Phosphate pH 6.0, 150 mM NaCl, 37ºC performed in the presence of 5 mM ascorbate, 10 mM EDTA, 840 U/mL of catalase and 167 U/mL of Superoxide Dismutase (SOD).

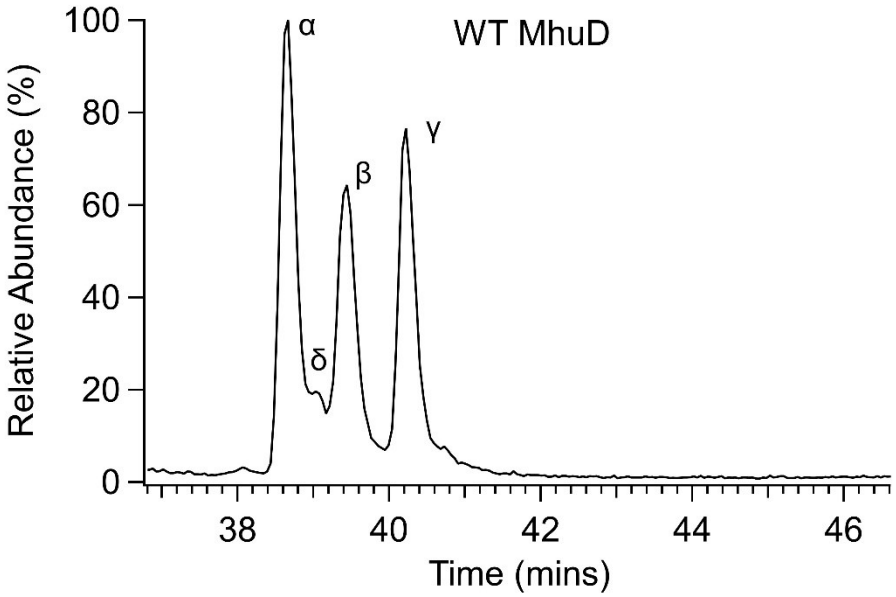

Figure B. 11. WT MhuD MS/MS chromatogram of m/z 583. Four peaks corresponding to parent ion of m/z 583 is observed when the heme degradation sample at 120 min by WT MhuD was analyzed by LC-MS/MS. MS^2 fragments (Figure 6) were used to identify each peak, where the isomers of biliverdin eluted in following order: α (38.7 min), δ (39.0 min), β (39.4 min) and γ (40.2 min) (as shown above).

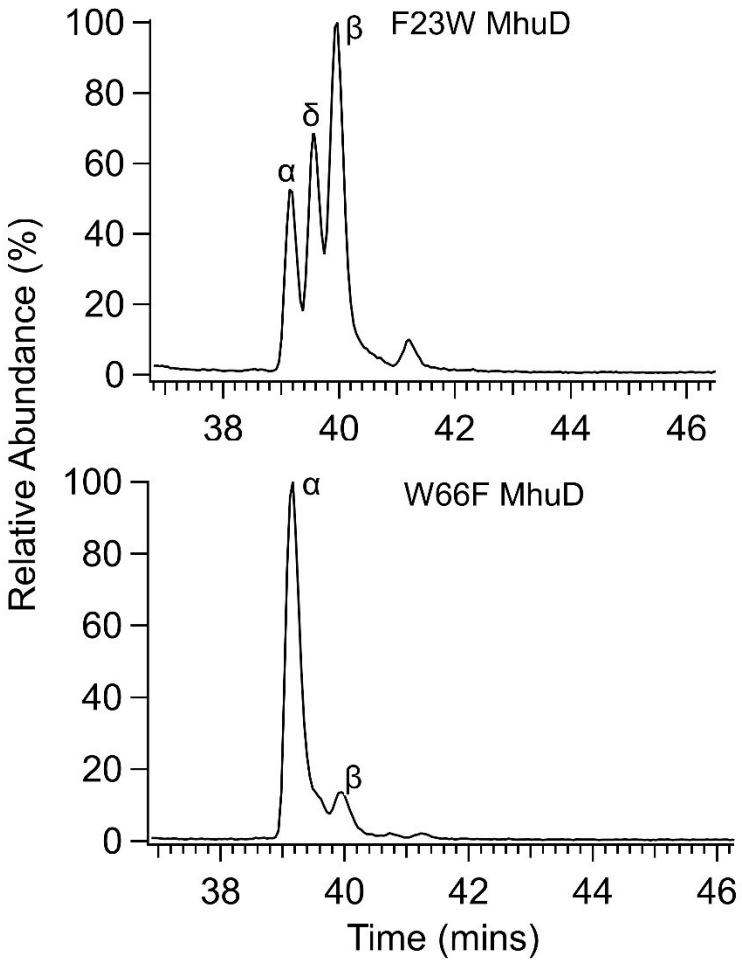

Figure B. 12. F23W and W66F MhuD MS/MS chromatogram of m/z 583. Peaks corresponding to parent ion of m/z 583 observed when heme degradation sample at 120 min by F23W (top) and W66F (bottom) MhuD were analyzed by LC-MS/MS. MS^2 fragments of m/z 583 were used to identify the peaks. α (39.2 min), δ (39.6 min) and β-biliverdin (40.0 min) isomers were identified for F23W MhuD, whereas, α (39.1 min) and β-biliverdin (39.9 min) isomers were identified for W66F MhuD.

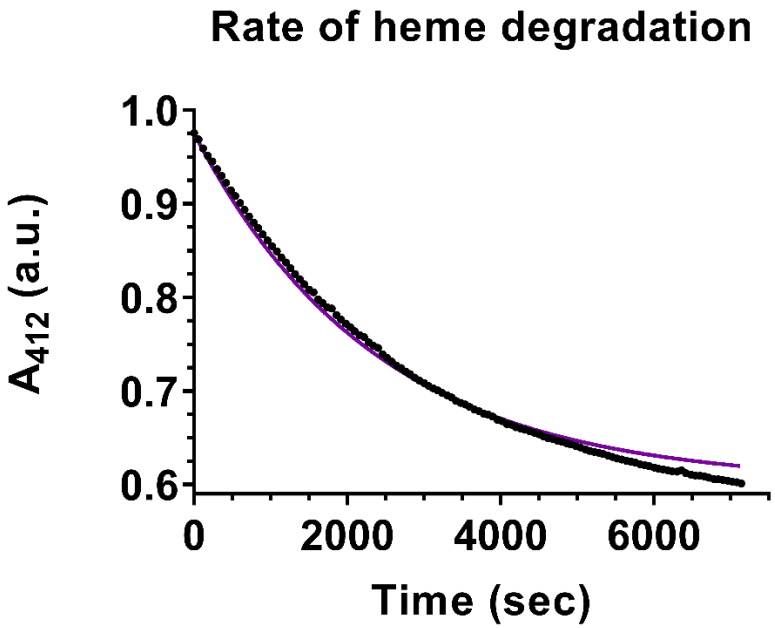

Figure B. 13. Rate of heme degradation by F23W MhuD. 412 nm peak was monitored during the heme degradation by F23W MhuD as a function of time and fitted using a pseudo first order kinetic model described in equation (1). The fitting gave a rate 0.0253 ± 0.0002 min^{-1} for heme monoxygenation reaction (k_1), with a R^2 of 0.9927. Black dots represent the experimental data and the purple line represents the fitted data.

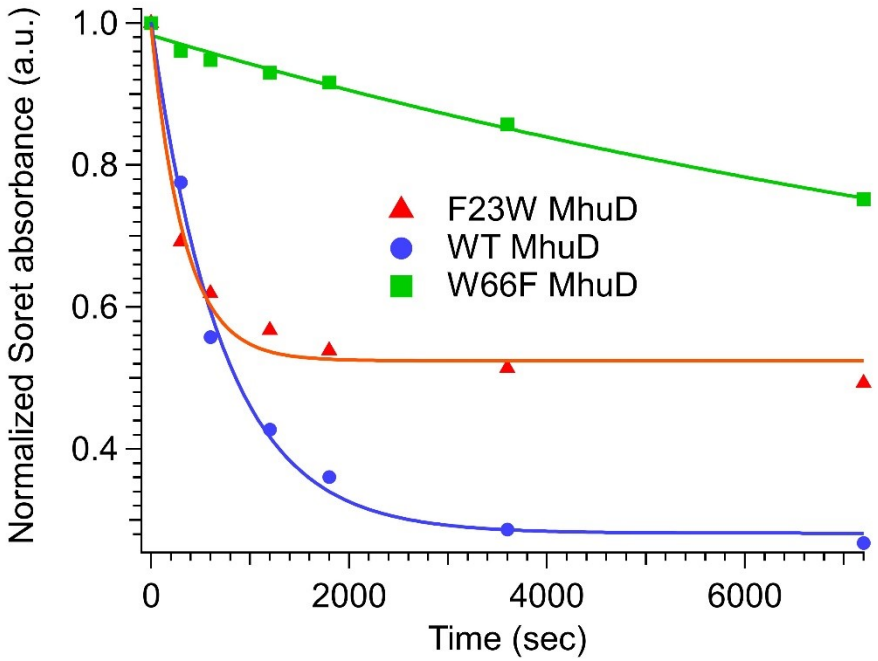

Figure B. 144. Rate of heme monooxygenation by F23W, WT and W66F MhuD. Decrease of Soret band at 37°C was monitored during the heme degradation by F23W, WT and W66F MhuD as a function of time and fitted using a pseudo first order kinetic model described in equation (1). The fitting gave a rate 0.15072 ± 0.01882 min^{-1} for F23W, 0.07956 ± 0.00520 min^{-1} for WT and 0.00481 ± 0.00362 min^{-1} for W66F MhuD (Table 2.1). The solid line represents the fitted data for the respective variants.

B.2 APPENDIX B REFERENCES

1. Perrin, C. L., Linear or Nonlinear Least-Squares Analysis of Kinetic Data? *J. Chem. Educ.*, 2017, *94* (6), 669-672.

2. Berry, E. A.; Trumpower, B. L., Simultaneous Determination of Hemes *a*, *b*, and *c* from Pyridine Hemochrome Spectra. *Anal. Biochem.*, 1987, *161* (1), 1-15.

3. Swain, C. G., The Kinetic Analysis of Consecutive Irreversible First Order Reactions. *J. Am. Chem. Soc.*, 1944, *66*, 1696-1700.

4. Esson, W. H., V. A., On the laws of connexion between the condition of a chemical change and its amount. *Phil. Trans. Roy. Soc. (London)*, 1866, *156*.

APPENDIX C: SUPPORTING INFORMATION FOR CHAPTER 4

C.1 SUPPLEMENTAL EXPERIMENTAL

Table C. 1. R26S MhuD gene sequence.

M1 ATG	P2 CCA	V3 GTG	V4 GTG	K5 AAG	I-6 ATC	N7 AAC	A8 GCA	I9 ATC	E10 GAG	V11 GTG	P12 CCC
A13 GCC	G14 GGC	A15 GCT	G16 GGC	P17 CCC	E18 GAG	L19 CTG	E20 GAG	K21 AAG	R22 CGG	F23 TTC	A24 GCT
H25 CAC	S26 AGC	A27 GCG	H28 CAC	A29 GCG	V30 GTC	E31 GAG	N32 AAC	S33 TCC	P34 CCG	G35 GGT	F36 TTC
L37 CTC	G38 GGC	F39 TTT	Q40 CAG	L41 CTG	L42 TTA	R43 CGT	P44 CCG	V45 GTC	K46 AAG	G47 GGT	E48 GAA
E49 GAA	R50 CGC	Y51 TAC	F52 TTC	V53 GTG	V54 GTG	T55 ACA	H56 CAC	W57 TGG	E58 GAG	S59 TCC	D60 GAT
E61 GAA	A62 GCA	F63 TTC	Q64 CAG	A65 GCG	W66 TGG	A67 GCA	N68 AAC	G69 GGG	P70 CCC	A71 GCC	I72 ATC
A73 GCA	A74 GCC	H75 CAT	A76 GCC	G77 GGA	H78 CAC	R79 CGG	A80 GCC	N81 AAC	P82 CCC	V83 GTG	A84 GCG
T85 ACC	G86 GGT	A87 GCT	S88 TCG	L89 CTG	L90 CTG	E91 GAA	F92 TTC	E93 GAG	V94 GTC	V95 GTG	L96 CTT
D97 GAC	V98 GTC	G99 GGT	G100 GGG	T101 ACC	G102 GGC	K103 AAG	T104 ACT	A105 GCA	TE106 TAA	G107 GGT	V108 GTA
P109 CCA	R110 CGA	G111 GGT	K112 AAG	L113 CTT	A114 GCG	A115 GCC	A116 GCA	L117 CTC	E118 GAG	H119 CAC	H120 CAC
H121 CAC	H122 CAC	H123 CAC	H124 CAC								

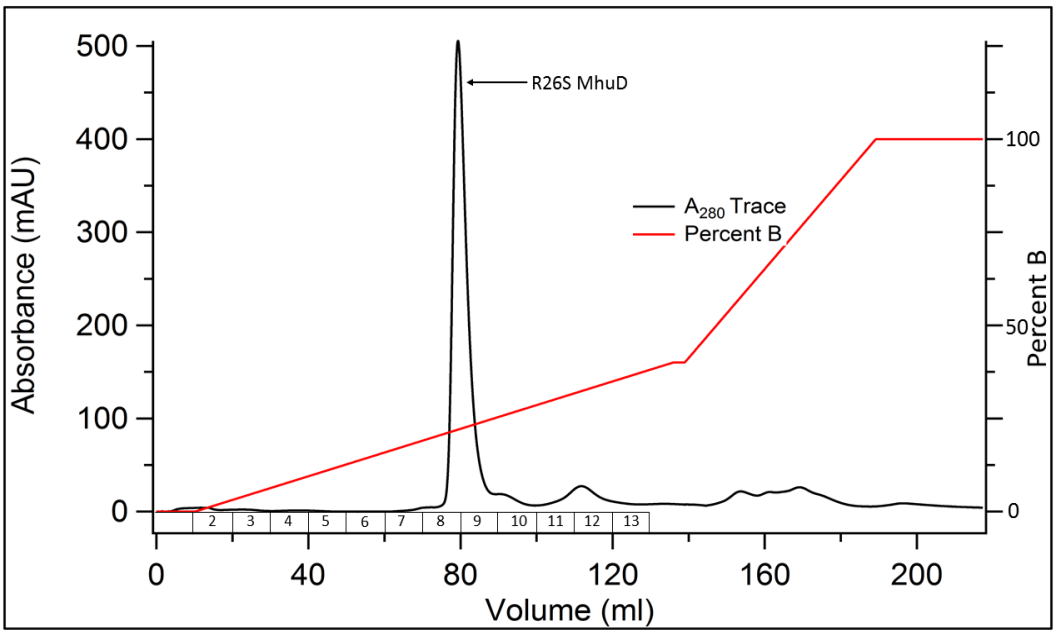

Figure C. 1. FPLC Chromatograph for purification of R26S MhuD. The 280 nm absorbance (*black trace)* and percentage of Buffer B (20 mM Tris, 200 mM NaCl pH 8.0, *red trace*) are plotted as function of buffer run through the column. Number in boxes on top of the x-axis refer to fractions collected during FPLC.

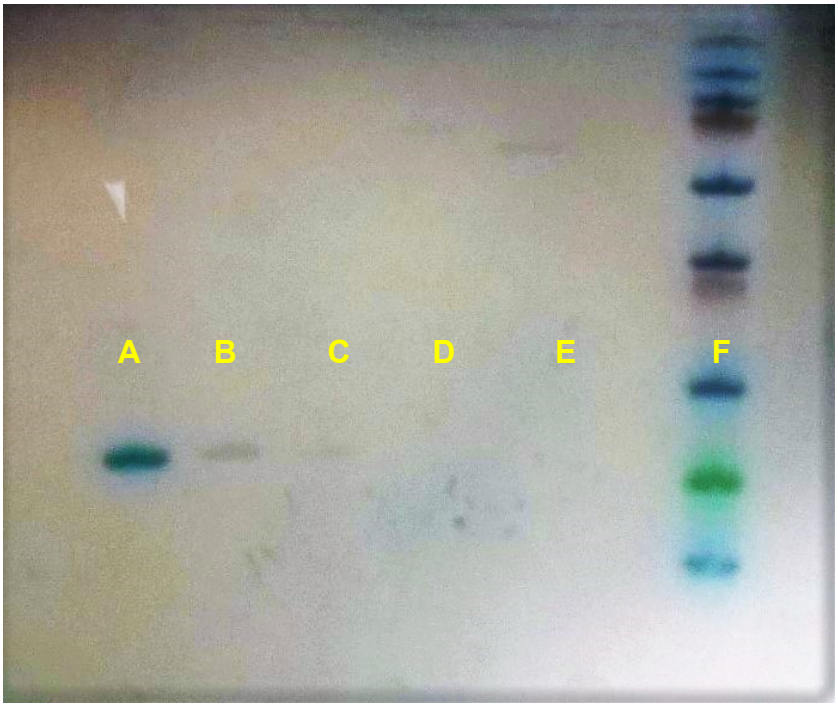

Figure C. 2. R26S MhuD was obtained as assessed by SDS-PAGE gel electrophoresis. From left to right, the lanes represent: (A) Fraction 8 and 9 pooled, (B) 1/10 dilution of R26S MhuD, (C) 1/100 dilution of R26S MhuD, (D) Fraction 10, (E) Fraction 12, (F) PageRuler Plus pre-stained protein ladder (Pierce).

Table C. 2. Gaussian fit results of the Soret band for WT, F23W, F23A and R26S MhuD-heme-CN.

Variant of MhuD	Area	Height (M^{-1} cm^{-1})		FWHM (cm^{-1})	
WT	-5.4015 x 10^6	-6650.91	+/- 0.06	763	+/- 50
F23W	-1.2902 x 10^6	-1486.93	+/- 0.06	820	+/- 50
R26S	-5.6514x 10^6	-8006.30	+/- 0.06	663	+/- 50

APPENDIX D: SUPPORTING INFORMATION FOR CHAPTER 5

D.1 SUPPLEMENTAL EXPERIMENTAL

Table D. 1. F23W IsdG primer sequence

Primer	**Sequence**
Forward	5'-aatcccatgtctcgtgtaccatcgttctataatatcttttgctgttcctttt-3'
Backward	5'-aaaaggaacagcaaaagatattatagaacgatggtacacgagacatgggatt-3'

Table D. 2. F23W IsdG gene sequence.

M-22	**G-21**	**H-20**	**H-19**	**H-18**	**H-17**	**H-16**	**H-15**	**D-14**	**Y-13**
ATG	GGT	CAT	CAT	CAT	CAT	CAT	CAC	GAT	TAC
D-12	**I-11**	**P-10**	**T-9**	**T-8**	**E-7**	**N-6**	**L-5**	**Y-4**	**F-3**
GAT	ATC	CCA	ACG	ACC	GAA	AAC	CTG	TAT	TTT
Q-2	**S-1**	**T-0**	**M1**	**K2**	**F3**	**M4**	**A5**	**E6**	**N7**
CAG	TCG	ACC	ATG	AAA	TTT	ATG	GCA	GAA	AAT
R8	**L9**	**T10**	**L11**	**T12**	**K13**	**G14**	**T15**	**A16**	**K17**
AGG	CTG	ACG	TTA	ACA	AAA	GGA	ACA	GCA	AAA
D18	**I19**	**I20**	**E21**	**R22**	**W23**	**Y24**	**T25**	**R26**	**H27**
GAT	ATT	ATA	GAA	CGA	TGG	TAC	ACG	AGA	CAT
G28	**I29**	**E30**	**T31**	**L32**	**E33**	**G34**	**F35**	**D36**	**G37**
GGG	ATT	GAA	ACA	TTA	GAA	GGC	TTT	GAT	GGC
M38	**F39**	**V40**	**T41**	**Q42**	**T43**	**L44**	**E45**	**Q46**	**E47**
ATG	TTT	GTT	ACA	CAA	ACT	TTA	GAA	CAA	GAA
D48	**F49**	**D50**	**E51**	**V52**	**K53**	**I54**	**L55**	**T56**	**V57**
GAT	TTT	GAT	GAA	GTG	AAA	ATT	TTA	ACA	GTT
W58	**K59**	**S60**	**K61**	**Q62**	**A63**	**F64**	**T65**	**D66**	**W67**
TGG	AAA	TCA	AAG	CAA	GCT	TTT	ACG	GAT	TGG
L68	**K69**	**S70**	**D71**	**V72**	**F73**	**K74**	**A75**	**A76**	**H77**
TTA	AAA	TCT	GAT	GTC	TTT	AAA	GCA	GCG	CAT
K78	**H79**	**V80**	**R81**	**S82**	**K83**	**N84**	**E85**	**D86**	**E87**
AAA	CAT	GTT	AGA	AGT	AAA	AAT	GAA	GAT	GAA
S88	**S89**	**P90**	**I91**	**I92**	**N93**	**N94**	**K95**	**V96**	**I97**
AGT	AGC	CCG	ATT	ATA	AAT	AAC	AAA	GTA	ATT
T98	**Y99**	**D100**	**I101**	**G102**	**Y103**	**S104**	**Y105**	**M106**	**K107**
ACA	TAT	GAT	ATA	GGC	TAT	AGT	TAC	ATG	AAA

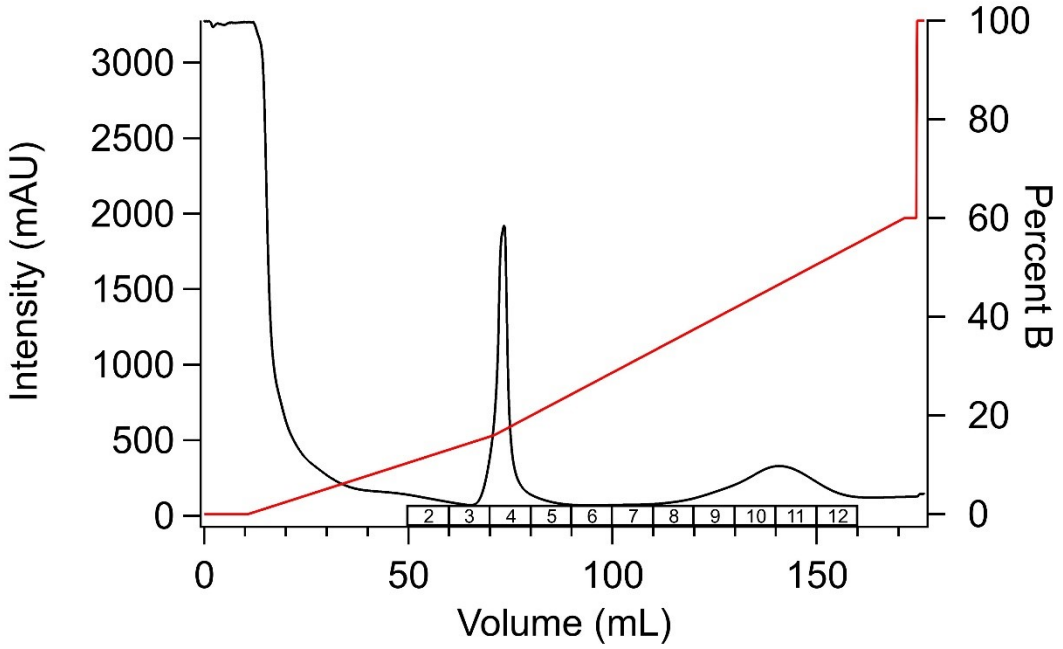

Figure D. 1. FPLC chromatograph for purification of F23W IsdG. The 280 nm absorbance (*black trace)* and percentage of Buffer B (50 mM Tris pH 7.4, 150 mM NaCl, 500 mM Imidazole, *red trace*) are plotted as function of buffer run through the column. Number in boxes on top of the x-axis refer to fractions collected during FPLC.

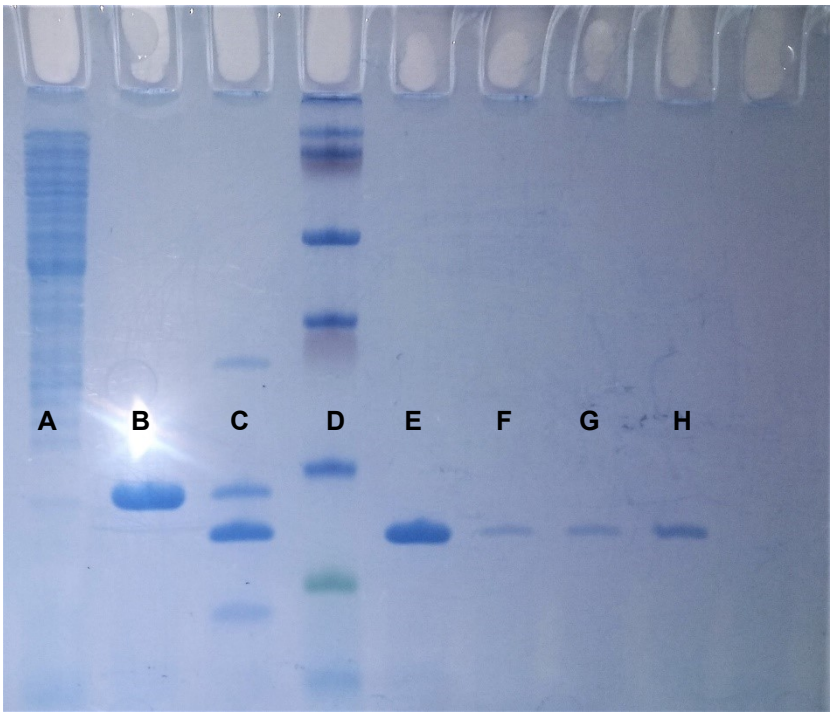

Figure D. 2. F23W IsdG was obtained as assessed by SDS-PAGE gel electrophoresis. From left to right, the lanes represent: (A) FPLC fractions 3-4, (B) FPLC fractions 9-12 (uncleaved F23W IsdG), (C) Cleavage reaction of uncleaved F23W IsdG with TEV, (D) PageRuler Plus pre-stained protein ladder (Pierce), (E) Cleaved F23W IsdG, (F) 1/100 dilution of E, (G) 5/100 dilution of E, (H) 1/10 dilution of E.

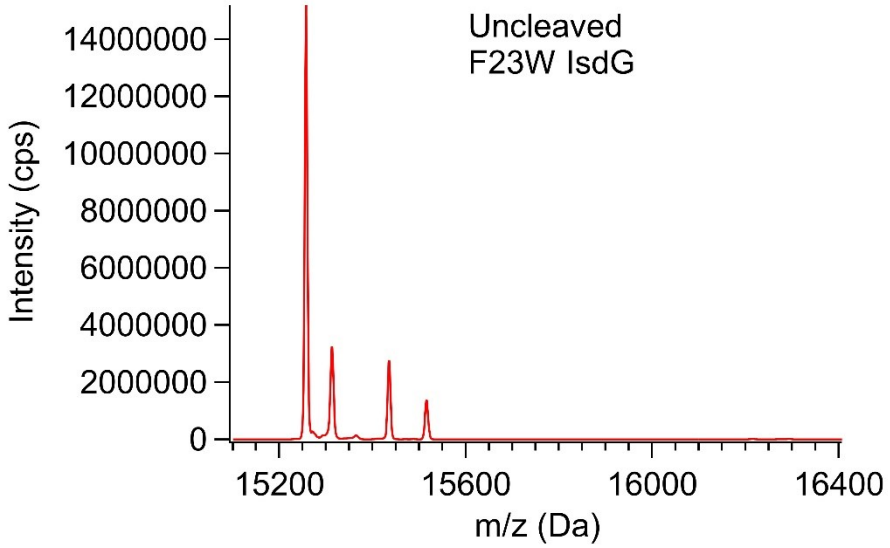

Figure D. 3. ESI-MS of uncleaved F23W IsdG in 50 mM Tris pH 7.4, 50 mM NaCl. The observed molecular weight of 15,258 g/mol is consisted with the calculated molecular weight of 15,257 g/mol.

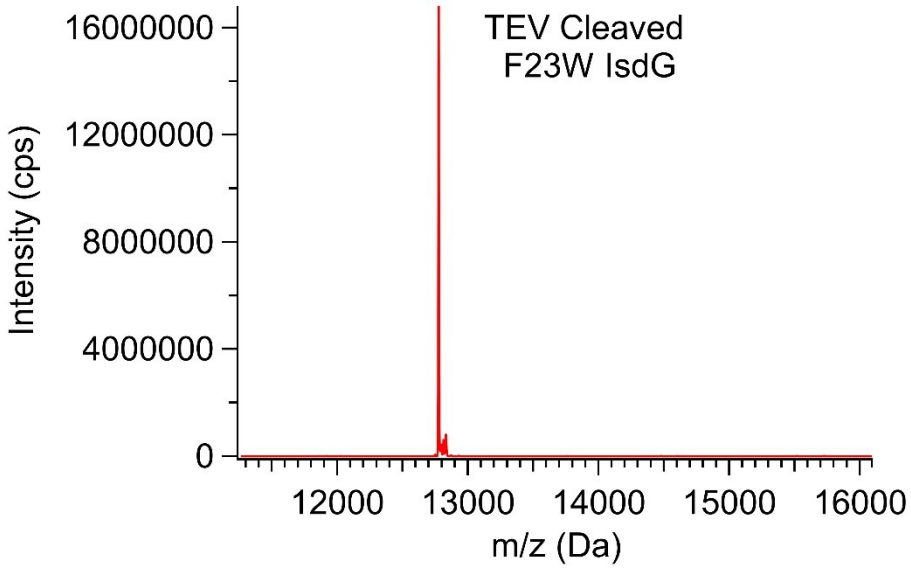

Figure D. 4. ESI-MS of cleaved F23W IsdG in 50 mM Tris pH 7.4, 50 mM NaCl. The observed molecular weight of 12776 g/mol for cleaved F23W IsdG is consistent the His_6 tag cleaved F23W IsdG.

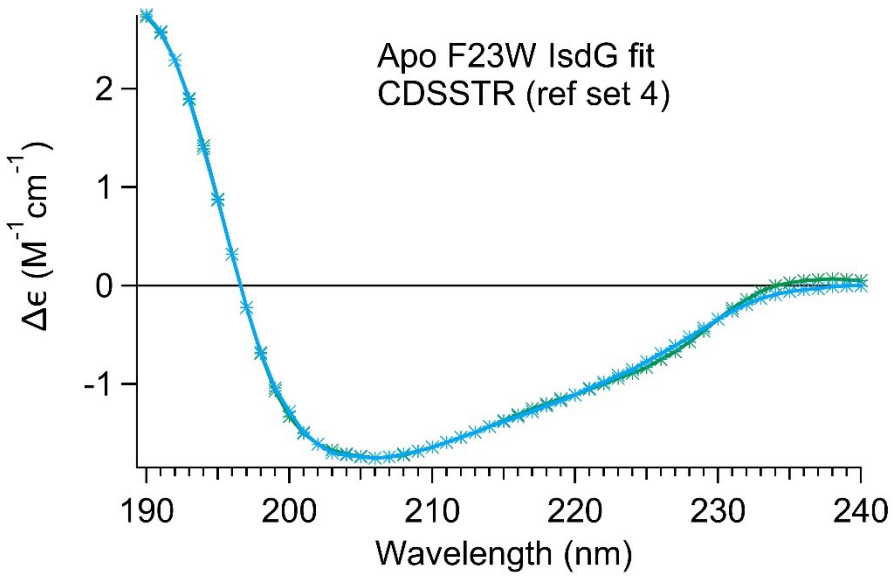

Figure D. 5. UV CD spectra of apo F23W IsdG (*solid green with star*) in 10 mM potassium phosphate buffer pH 7.4. The UV CD spectra of apo F23W IsdG is fitted using DichroWeb CDSSTR (reference set 4) algorithm.[1-4]

Table D. 3. Secondary structure analysis by UV CD for F23W IsdG using the fitting method in Figure D.5. and compared that to WT IsdG.

Species	**Percent α–helices**	**Percent β–sheets**
WT IsdG	9.0	35.0
F23W IsdG	10.0	35.0

D.2 APPENDIX D REFERENCES

1. Lobley, A.; Whitmore, L.; Wallace, B. A., DICHROWEB: an interactive website for the analysis of protein secondary structure from circular dichroism spectra. *Bioinformatics*, 2002, *18* (1), 211-2.

2. Whitmore, L.; Wallace, B. A., DICHROWEB, an online server for protein secondary structure analyses from circular dichroism spectroscopic data. *Nucleic Acids Res.*, 2004, *32* (Web Server issue), W668-73.

3. Compton, L. A.; Johnson, W. C., Jr., Analysis of protein circular dichroism spectra for secondary structure using a simple matrix multiplication. *Anal. Biochem.*, 1986, *155* (1), 155-67.

4. Sreerama, N.; Woody, R. W., Estimation of protein secondary structure from circular dichroism spectra: Comparison of CONTIN, SELCON, and CDSSTR methods with an expanded reference set. *Anal. Biochem.*, 2000, *287* (2), 252-260.

APPENDIX E: SUPPORTING INFORMATION FOR CHAPTER 6

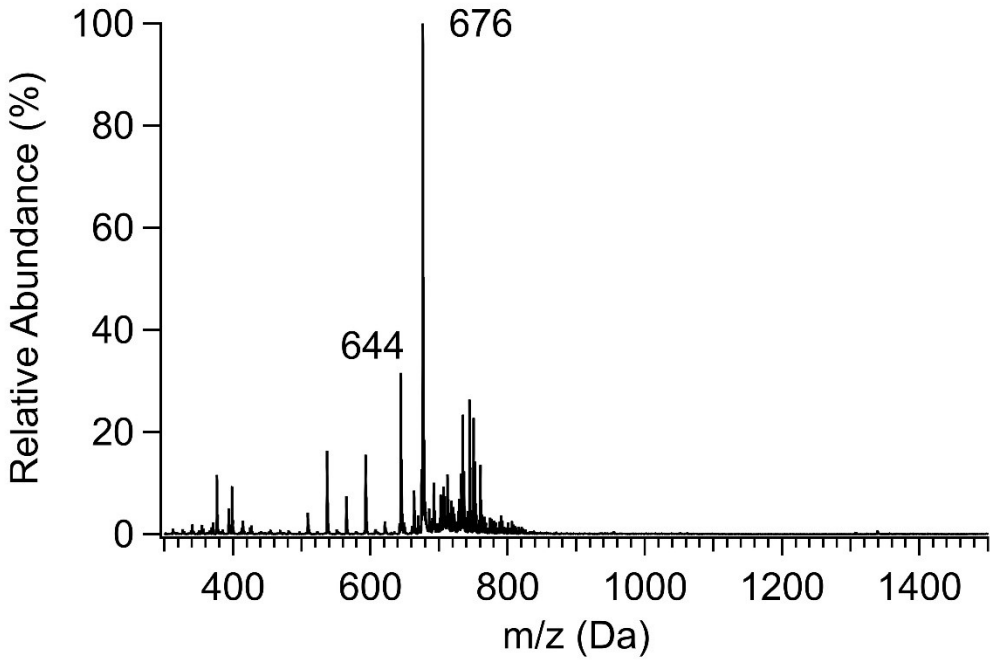

Figure E. 1. ESI-MS spectrum of the top organic layer. The m/z 644 (heme dimethyl ester) along with other impurities are observed.

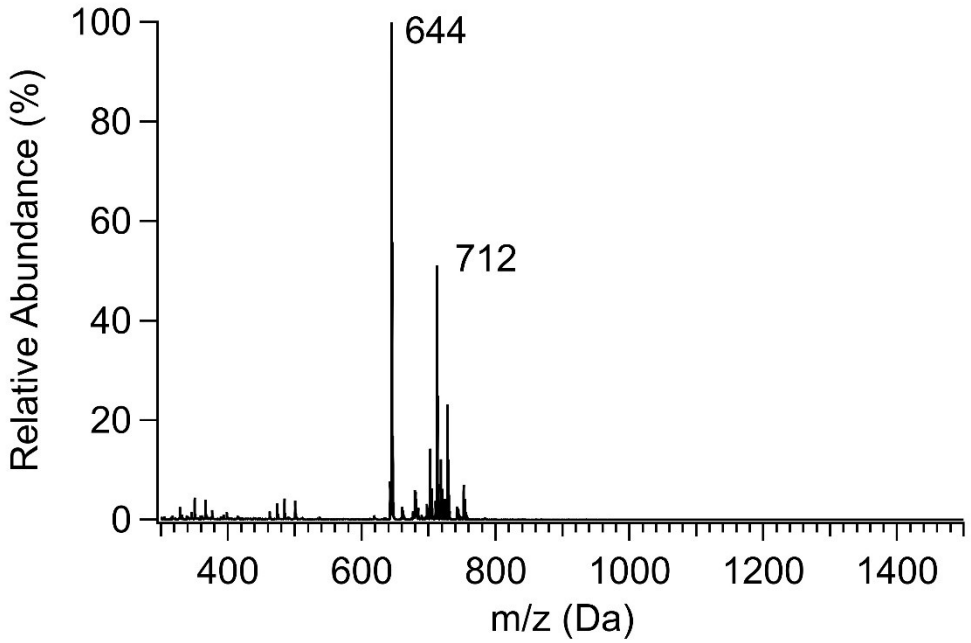

Figure E. 2. ESI-MS spectrum ESI-MS spectrum of the dimerized sample collected in the mobile phase of 98% acetonitrile with 0.1% formic acid (v/v) in water (v/v). The m/z 644.3 corresponding to heme dimethyl ester is observed, along with a possible adduct ion at m/z 712.3. But peak of m/z ~1305 corresponding to μ–oxo–bis(heme dimethyl ester) is missing.

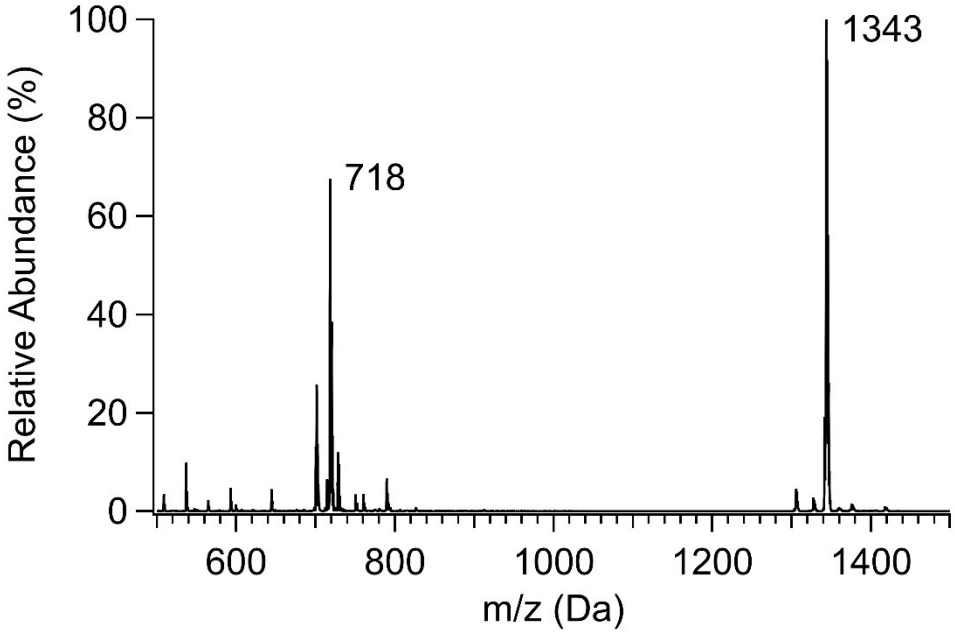

Figure E. 3. ESI-MS spectrum of dimerized sample with no proton source (100% acetonitrile used as a mobile phase). Peaks of m/z 1343 and m/z 718 are observed. The m/z 1343 may be the μ–oxo–bis(heme dimethyl ester) with a potassium adduct ion (+K, m/z 38) and the m/z 718 may be heme dimethyl ester with two potassium adduct ions (2K-H, m/z 76).

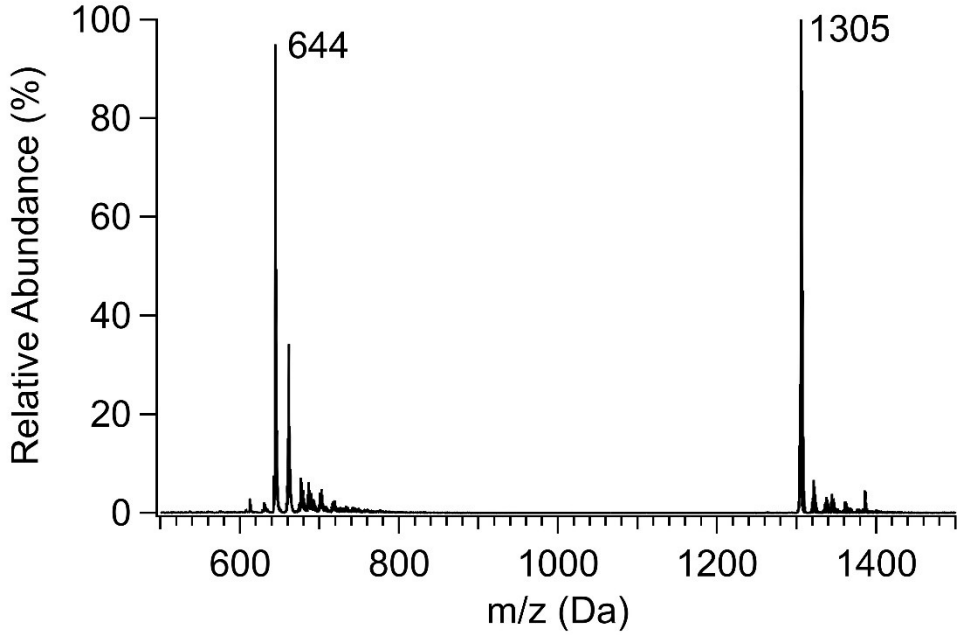

Figure E. 4. APCI-MS spectrum of dimerized sample with no proton source (100% acetonitrile used as a mobile phase). Peaks of m/z 1305.6 and m/z 644.2 are observed, corresponding to μ–oxo–bis(heme dimethyl ester) and heme dimethyl ester, respectively.

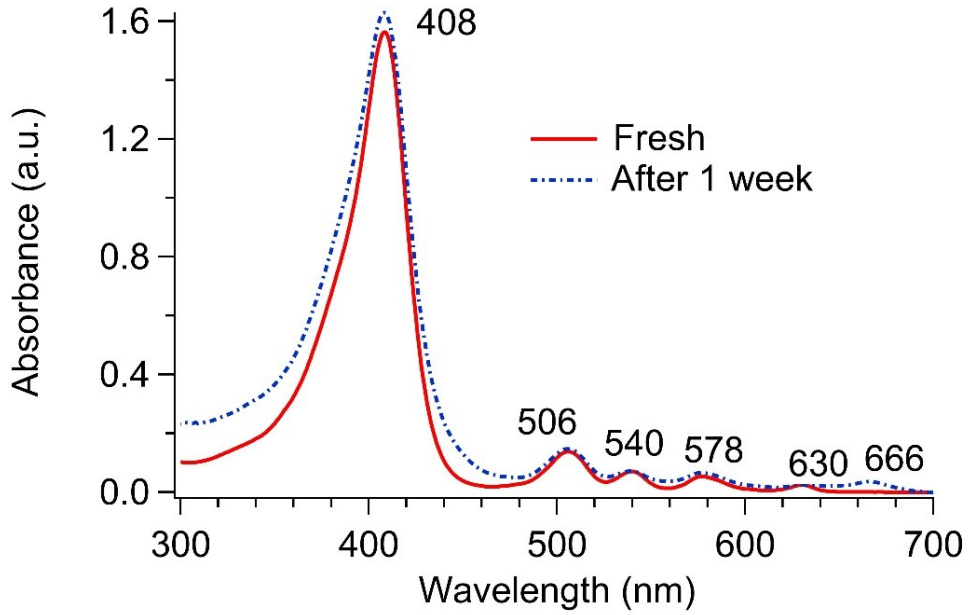

Figure E. 5. UV/Vis absorbance spectra of freshly eluted isomeric mixture of meso-benzoyloxyprotoporphyrin IX dimethyl ester (*solid red*) and a week old eluted isomeric mixture of meso-benzoyloxyprotoporphyrin IX dimethyl ester (*dashed blue*). Emergence of a peak at 666 nm is observed in the old sample.